Enhanced Dehydrogenation of Butane over Supported Pd & Pt Based Catalysts Prepared by Modified Electroless Deposition

Thesis

submitted in partial fulfillment of the requirements for the degree of

DOCTOR OF PHILOSOPHY

by

Rishabh Saxena

(146151012)

School of Energy Sciences and Engineering

Indian Institute of Technology Guwahati

January 2021

Dedicated

to

My Parents

School of Energy Sciences and Engineering

Indian Institute of Technology Guwahati

Guwahati – 781039, India

CERTIFICATE

This is to certify that the work contained in the thesis entitled **"Enhanced Dehydrogenation of Butane over Supported Pd & Pt Based Catalysts Prepared by Modified Electroless Deposition"** submitted by **Rishabh Saxena** (Roll No. 146151012) for award of the degree of Doctor of Philosophy, has been carried out under our supervision and this work has not been submitted elsewhere for award of any degree.

Mahuya De
Professor
Department of Chemical Engineering
Indian Institute of Technology Guwahati
Guwahati – 781039, India

Mohd. Qureshi
Professor
Department of Chemistry
Indian Institute of Technology Guwahati
Guwahati – 781039, India

ACKNOWLEDGEMENTS

First and foremost, praises and thanks to God, the Almighty, for showers of blessings throughout my Ph.D. tenure and giving strength and confidence to complete the research successfully. I extend my appreciation for the help and support to all the following persons who in one way or another have contributed in making this study and thesis possible.

First and foremost, I express my deepest gratitude and immeasurable appreciation to my supervisors ***Prof. Mahuya De*** and ***Prof. Mohd. Qureshi*** who have the attitude and the substance of a genius. They have continually and convincingly conveyed a spirit of adventure in regard to research and provided encouragement to make me learn. I am immensely thankful for their valuable suggestions, encouragement, indispensable support and guidance throughout my research work and being a source of constant motivation and knowledge.

I would also like to extend my sincere appreciation and gratitude to all the members of doctoral committee, ***Prof. Ramgopal V.S. Uppaluri***, ***Prof. Sharad Gokhale***, and ***Dr. Vairakannu Prabu*** who manifested their distinguished skills and talents of their own field and provided insightful suggestions for the constant improvisation of my thesis.

I am extremely grateful to the faculty and staff members of School of Energy Sciences and Engineering and Department of Chemical Engineering for their kind help and support. I am immensely thankful to Central Instruments Facilities (CIF) for providing facilities to carry out my research work. I am also thankful to the Indian Institute of Technology Guwahati for providing me with the infrastructure and facilities for advanced research.

In addition, a heartfelt thanks to my seniors *Dr. N. Vinothkumar, Dr. Ruhit J. Konwar, Dr. Sohan Bir Singh,* and research group members, *Saptarshi, Rahul, Nilesh, Ramanuj, Nayan, Phenecia, Syam* and *Anand* for all the worthy support and cooperation throughout the research tenure. I am highly thankful to my friends *Pawan* and *Satyam* for all the love and support. I am lucky to get excellent friends as *Ajeet, Harjeet* and *Prince* for their friendly gesture and timely assistance whenever needed. I am also fortunate enough to get a wonderful friend as *Rajneesh* who made my stay most enjoyable and unforgettable here in IIT Guwahati providing all care and support. Lastly, I would like to thank *Neha Singh* for being a pillar of strength to me and lending her constant support throughout my Ph.D. tenure, helping me in toughest times and motivating me to do better.

I am immensely thankful to my brother, *Mr. Suyash Saxena* for always loving and supporting me selflessly. At last but not the least, I acknowledge with deep sense of reverence, my gratitude towards my parents, *Mr. Sanjay Saxena* and *Mrs. Archana Saxena* for their unconditional love, care, and sacrifices and supporting me morally and spiritually throughout my life. I have always been inspired from my father who's never ending hard work make me realize every time that even sky is not the limit. My Ph.D. endeavor would not have been successful without my family. I dedicate this to you "*MOM*" and "*DAD*".

Rishabh Saxena

ABSTRACT

Butenes serve as the essential feedstock for production of many valuable chemicals such as poly-butene, styrene butadiene rubber, acrylonitrile butadiene styrene, 1,3 butadiene, methyl tertiary butyl ether, etc. Demand and market value of butenes have experienced a surge in recent years. Conventionally, butenes are produced by steam cracking of naphtha that operates at high temperatures and pressure generating large amount of coke and exhibiting low alkene selectivity. Catalytic dehydrogenation of butane is an economical and more selective route for production of butenes, operating at comparatively lower temperatures. Butane as feed is inexpensive and abundant, particularly after recent shale gas explorations. However, this process is also associated with thermodynamic limitation and coke formation at higher temperature. Hence, it is important to develop catalysts possessing higher activity, selectivity, yield and stability for butane dehydrogenation. The Pt based catalysts in combination with second metal such as with Sn, In, Pb, etc have been most widely investigated for butane dehydrogenation. However, the main challenge remains with the high cost of platinum and sintering at higher temperatures leading to deactivation over time. The Pd is less expensive than that of Pt, however for dehydrogenation application it remains largely unexplored, as the reported studies are very limited. Hence, there is a wide scope to study effectiveness of Pd. The impregnation, most commonly and widely used technique, is associated with low metal dispersion and weak metal-support interaction. Hence, preparation methodology that improves these properties of catalyst is expected to improve its performance. This study explored electroless deposition method to achieve uniform and high dispersion of metal over support.

The objectives of the thesis included preparation of alumina supported monometallic Pd and Pt catalysts by modified electroless deposition and optimization of preparation parameters. Comparison of the physicochemical properties and butane dehydrogenation performance of alumina supported monometallic Pd and Pt catalysts prepared by modified electroless deposition was done with that prepared by impregnation. The study investigated the effect of addition of surfactants during preparation of alumina supported Pd catalysts by electroless deposition, on their physicochemical properties and catalytic performance for butane dehydrogenation. The effect of addition of Ni, Cu and Ag as promoter in Pd based catalysts was also investigated. The Pd-Pt bimetallic catalysts were investigated for butane

dehydrogenation. The effects of variations in preparation, metal composition, metal deposition sequence, process parameters and addition of surfactant and promoter were studied.

In modified electroless deposition, the metal precursor and reducing agent solutions were passed through the porous support sequentially in cyclic steps. First cycle consisted of two steps; required volume of reducing agent (hydrazine) solution was passed through the aluminium oxide support followed by respective metal precursor solution. Same contact time was maintained for both the steps. This cycle was repeated twice to obtain the target deposition of metal on support. The deposited catalyst was dried overnight at 110 ^{o}C for 12 h. Various characterization techniques such as AAS, EDX, XRD, TEM, XPS, TPR, FT-IR and NH_3-TPD were used to determine the physicochemical properties of prepared catalysts. The catalytic performances of all the prepared catalysts were evaluated in terms of conversion, selectivity, yield and stability for butane dehydrogenation reaction at different temperatures from 100-600 ^{o}C under atmospheric pressure in a down-flow fixed bed reactor.

The modified electroless deposition method was successfully employed for the preparation of highly dispersed alumina supported platinum and palladium based catalysts. The preparation parameters, such as metal precursor concentration, reducing agent concentration, reducing agent type etc., had significant effect not only on the metal loading but also on metal cluster size and hence on metal dispersion. The platinum loading and average metal cluster size increased with the increase in metal precursor concentration. The use of 50% excess reducing agent was observed to be sufficient to facilitate reduction as well as considerable metal deposition. It was also observed that introducing reducing agent prior to the metal solution to alumina support gave better metal dispersion.

The physicochemical properties and catalytic performance of monometallic Pd and Pt catalysts prepared by deposition was compared with that of prepared by conventional impregnation method. The total metal loading was similar at 112.8 μmole per gram of catalyst for both the monometallic catalysts. This total metal loading was maintained for all subsequent studies. The Pt and Pd appeared to be clustered in catalysts prepared by impregnation, whereas, it was well dispersed in catalysts synthesized by deposition. For impregnated Pt/Al and Pd/Al monometallic catalysts, the average metal cluster size was 6 and 12 nm, respectively, but was lower at 3.4 and 4.6 nm, respectively, when prepared by modified deposition method at similar loadings. On comparing monometallic catalysts, it was observed that at lower temperature range alumina supported platinum catalyst, Pt/Al, showed the higher activity while, alumina

supported palladium catalyst, Pd/Al, was more active at temperature above 550 ^{o}C. Pt/Al exhibited 18.5% conversion at 550 ^{o}C that decreased to 16.3% on further raising the temperature to 600 ^{o}C, while, the conversion increased from 18 to 21% for Pd/Al catalyst. The impregnated Pt and Pd catalysts exhibited lower conversion of 14.5 and 13.5% at 550 ^{o}C and might be ascribed to lower metal dispersion. The deposited Pd/Al exhibited higher selectivity towards overall butene formation (>90%) compared to deposited Pt/Al (82%). In comparison to deposited catalysts, impregnated catalysts exhibited higher selectivity (40-50 %) towards C_1-C_3 product formation leading to their faster deactivation. Higher butene yield of 15 and 16% was obtained at 550 ^{o}C for deposited Pt and Pd catalysts, respectively, compared to corresponding impregnated catalysts (~7%). The on-stream stability of the catalyst was also improved by new deposition method. These results showed that Pd was equally effective as active metal for butane dehydrogenation and catalysts prepared by modified electroless deposition gave better results compared to the catalysts prepared by impregnation.

The addition of surfactant to alumina supported palladium catalyst affected its physicochemical properties and performance for butane dehydrogenation. The use of surfactant was observed to lower the average cluster size of deposited metal compared to that prepared in absence of surfactant. Depending on the type of surfactant, loading and morphology of deposited palladium varied. Both anionic (SDS) and non-ionic (Tween 20) surfactants were observed to be most effective in dispersing the metals on the support surface. Average Pd metal cluster size obtained for catalyst prepared by impregnation, deposition and SDS surfactant assisted deposition were 11.89, 4.6 and 1.18 nm, respectively. The catalysts prepared by surfactant assisted method showed improved activity, butene yield and stability. The butane conversion and butene selectivity were observed to be function of deposited metal cluster size. The catalyst, prepared in presence of anionic SDS surfactant with the highest metal dispersion and lowest metal size (1.2 nm), showed the best catalytic performance with a conversion of 33% and 99.7% selectivity towards butenes. It was followed by catalyst prepared in presence of non-ionic Tween 20 surfactant, showing 25% conversion and over 99% butene selectivity. The catalyst prepared by impregnation with the highest metal particle size (11.89 nm) exhibited the least activity and selectivity for butene.

The effect of addition of promoter metals (Ni, Cu, or Ag) to Pd catalysts was explored. The alumina supported Pd catalysts were co-deposited with 10 mol% of promoter metal keeping total metal loading same for all catalysts. The co-deposition of copper or silver with palladium increased activity and yield of butene. The copper promoted catalyst showed highest

conversion of 34% at 550 ^{o}C that further increased to 38% at higher temperature of 600 ^{o}C. The Ag promoted catalyst possessed highest selectivity towards butenes (>90% at 550 ^{o}C). The butene yield was highest for Pd-Cu/Al (29%) followed by Pd-Ag/Al (23%), Pd/Al (16%) and Pd-Ni/Al (13%), at 550 ^{o}C. Further, increase in copper content to 20 mol% Cu increased the yield of butene to 32% for Pd-Cu_{20}/Al. The palladium metal was in strong interaction with the promoter metals forming the alloys. Higher activity of these alloys enhanced performance of the promoted catalysts. The sintering tendency of nickel lowered the performance of Pd-Ni/Al. The stability of the catalysts was also enhanced by addition of promoters.

The effect of variation in relative amount of palladium and platinum in bimetallic Pd-Pt catalysts was studied using co-deposition and impregnation methods. The ratio of Pd to Pt was varied as 3:1, 1:1 and 1:3 on molar basis but total metal loading was kept similar. The varied metal ratio and preparation methods affected the morphology of deposited metals and hence the catalytic performance. Catalysts with higher palladium content exhibited lower acidity while higher platinum content led to improved metal dispersion. The deposited bimetallic catalysts, $1Pd1Pt_{ED}$, having equimolar palladium and platinum showed the highest butane conversion of 48.5% and butene yield of 42% at 550 °C. The same catalyst was also most stable showing only 15% deactivation after reaction time of 10 h. The $3Pd1Pt_{ED}$ catalyst, with higher palladium content, showed higher butene selectivity (91%) and stability (17% deactivation) in comparison to $1Pd3Pt_{ED}$ catalyst with higher platinum content (84.7% butene selectivity; 34% deactivation). The $3Pd1Pt_{ED}$ catalyst, having less acidic sites, suppressed C-C cleavage resulting in higher stability of catalyst. The catalysts prepared by electroless deposition gave higher butene yield and stability, compared to that prepared by conventional impregnation method. The overall order for butene yield was $1Pd1Pt_{ED}$ (42%) > $1Pd3Pt_{ED}$ (41%) > $3Pd1Pt_{ED}$ (40.3%) > $3Pd1Pt_{WI}$ (18.7%) > $1Pd3Pt_{WI}$ (18.4%) > $1Pd1Pt_{WI}$ (15.8%). Here, subscript ED stands for electroless deposition, while WI stands for impregnation.

The change in sequence of metal addition in bimetallic Pd-Pt catalyst prepared by modified deposition method also affected its properties and performance. The study was carried out for Pd:Pt mole ratio of 1:1 which showed better results as discussed in previous chapter. Catalysts with three sequence were studied: deposition of Pd followed by Pt, Pt followed by Pd and co-deposition. All the bimetallic Pd-Pt catalysts exhibited superior performance compared to that of either monometallic Pd or Pt catalysts that may be attributed to strong synergistic interaction between metals, stronger metal-support interaction and lower acidity of catalysts. The higher activity of bimetallic catalysts might had resulted by formation of Pd-Pt alloy. The lower

acidity of bimetallic catalysts resulted in their higher butene selectivity and stability by minimizing cracking and secondary reactions. The metal deposition order of bimetallic catalysts also affected their performance. The co-deposited catalyst with more uniform distribution of Pd and Pt metals showed better performance than bimetallic catalysts prepared by sequential deposition. The co-deposited Pd-Pt/Al catalyst showed the highest butane conversion of 50% at 600 ^{o}C and maintained a highest stability with only 15% deactivation after reaction time of 10 h. The same catalyst showed highest butene yield of 44% at 525 ^{o}C. Further, the effects of various process parameters on butane dehydrogenation reaction were investigated over best performing co-deposited Pd-Pt/Al catalyst**.** The activation energy for butane dehydrogenation reaction was determined to be 103 kJ/mol. This chapter also demonstrated the effect of addition of Tween 20 surfactant as dispersing agent and copper as promoter on the properties and performance of co-deposited bimetallic Pd-Pt/Al catalyst.

The present study established the superior performance of catalysts prepared by modified electroless deposition method. This deposition method resulted in better metal dispersion and higher metal-metal interaction on support surface in comparison to impregnation. Palladium proved to be equally active component for butane dehydrogenation with better stability and selectivity compared to Pt. Effectiveness of anionic and non-ionic surfactants in dispersing depositing metals and thereby increasing performance of catalysts was observed. Equimolar co-deposited Pd-Pt bimetallic evolved as most active catalyst by present study giving butene yield of 42%, higher or at per with that reported by many of the studies for dehydrogenation.

RESEARCH OUTPUTS

PUBLICATIONS

1. Saxena et al. Supported palladium nanoclusters: morphological modification towards enhancement of catalytic performance using surfactant-assisted metal deposition. *Applied Nanoscience* 10 (2020) 1793-1809.

2. Saxena et al. Enhanced performance of supported Pd-Pt bimetallic catalysts prepared by modified electroless deposition for butane dehydrogenation. *Applied Catalysis A: General* 610 (2021) 117933.

3. Saxena et al. Ni/Cu/Ag promoted Pd/Al_2O_3 catalysts prepared by electroless co-deposition for enhanced butane dehydrogenation. *Materials Chemistry and Physics* 261 (2021) 124236.

4. Saxena et al. Supported bimetallic Pd-Pt catalysts for butane dehydrogenation: Effect of composition and preparation. (Submitted)

5. Saxena et al. Preparation of alumina supported monometallic Pt & Pd catalysts by electroless deposition: Effect of synthesis parameters (Under preparation)

AWARDS

Best paper award for oral presentation in "Process and Product Development" at International Conference on New Frontiers in Chemical, Energy and Environmental Engineering held in February 2019 at NIT Warangal, India.

CONFERENCES

1. Saxena et al. **American Chemical Society Fall 2020 Virtual Meeting & Expo,** "Enhancement of catalytic performance of supported Pt catalysts using surfactant assisted electroless deposition method" (17 – 20 August, 2020).

2. Saxena et al. **International Conference on Sustainable Energy and Green Technology (SEGT-2019)**, "Development of highly dispersed supported palladium catalyst for butane dehydrogenation by modified electroless deposition" Bangkok, Thailand (10 – 14 December, 2019).

3. Saxena et al. **International Conference on New Frontiers in Chemical, Energy and Environmental Engineering (INCEEE - 2019**), "Effect of Process Parameters on Supported Pt Catalysts Synthesized by Electroless Deposition Method", NIT Warangal (15 – 16 February, 2019).

4. Saxena et al. **Asia Pacific Congress on Catalysis (APCAT-7),** "Development of Highly Dispersed Supported Noble Metal Catalysts by Electroless Deposition Method" (17 – 21 January, 2017).

5. Saxena R. **Intensive Course** on "Advances in Preparation and Characterization of Heterogeneous Catalysts" IIT-BHU Varanasi (8 – 20 June, 2015).

CONTENTS

LIST OF FIGURES

Chapter 3

Chapter 4

Chapter 5

LIST OF TABLES

भारतीय प्रौद्योगिकी संस्थान गुवाहाटी
Indian Institute of Technology Guwahati

LIST OF APPENDICES

भारतीय प्रौद्योगिकी संस्थान गुवाहाटी
Indian Institute of Technology Guwahati

Chapter 1

INTRODUCTION AND LITERATURE REVIEW

The first chapter introduces the topic and presents a literature review on the same. It further discusses the motivation of carrying out the presented study with specific objectives.

Keywords

Butenes; butane dehydrogenation; dehydrogenation catalysts; catalyst preparation; platinum; palladium

Chapter 1

1.1 Introduction

1.1.1 Importance of Butenes

Light olefins are essential raw materials widely used in various industrial applications [1]. Propene and butenes, are among the most commercially important starting chemicals, with a total reported demand of 260 million tons in 2016 [2]. Butene is an olefin with a chemical formula of C_4H_8. Butene can exist as different isomers such as iso-butene, 1-butene, and 2-butene (trans and cis). Because of presence of double bond, butenes are more reactive in comparison to butane. Butene is colourless, low-boiling, flammable, and highly volatile. Butene is traded commercially in three grades: polymer grade (PG) 99.5% or higher purity, chemical grade (CG) 90–96% purity, and refinery grade (RG) 50–70% purity.

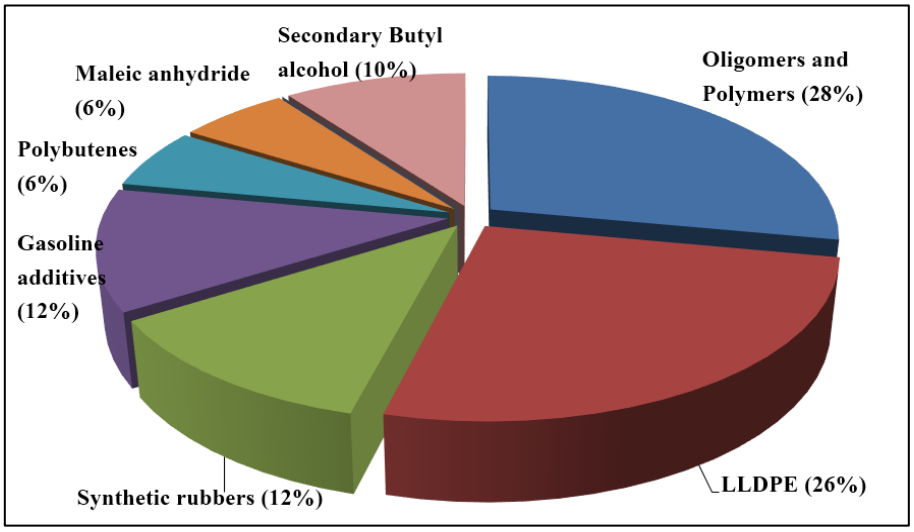

Figure 1.1. Various applications of butenes [2].

Butenes are used as raw materials to obtain poly-butene and synthetic resins such as linear low density polyethylene, which are used for food and non-food packaging such as bags and stretch wraps, toys, containers, pipes, etc. Butene is further used to obtain synthetic rubbers such as styrene butadiene rubber, polybutadiene rubber, and acrylonitrile butadiene styrene [3]. Butenes are also used in production of valeraldehyde, butylene oxide, maleic anhydride, secondary butyl alcohol and methyl ethyl ketone. In addition to this, 1-butene finds application as an intermediate for manufacturing of plasticizers, antioxidants, corrosion inhibitors, and as additives in hydraulic and lubricating oils [4]. Butenes also serve as the feedstock for the production of 1,3 butadiene and oxygenates such as methyl

tert-butyl ether and ethyl tert-butyl ether that are used as additives in gasoline for improving its octane number [5]. The major applications of butenes are shown in Figure 1.1.

1.1.2 Global market

The market for butenes has been growing steadily over the years. Strong demand has resulted from rising requirement of plastic for various applications. The growing demand for rubber from the automotive industry has also contributed to the growth in butene market. In Asia Pacific region, particularly in India and China, the increase in demand of these end products has caused huge rise in butene market value [6]. The butene market worldwide is estimated at USD 3.6 billion in 2020. It is projected to grow to USD 5.4 billion by 2027 (Figure 1.2) driven by a compounded growth of 5.9% [7].

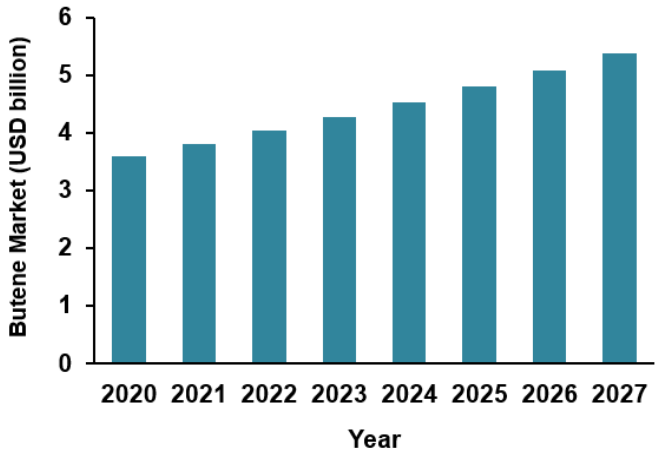

Figure 1.2. Growth predicted for butene market [7].

1.1.3 Production of butenes

Commercially butene is produced mainly as by-product during steam cracking and fluid catalytic cracking (FCC) of naphtha and gas oil [8,9]. However, typical product distribution from high-severity cracking process exhibits low selectivity to butenes, with formation of substantial quantities of methane and coke as co-products [10]. Also, these processes are operated at high temperature (~800 ^{o}C) requiring high energy and capital cost. The higher availability of relatively low cost natural gas and natural gas liquid, rich in ethane, has turned the focus on ethane cracking. Ethane cracking is increasingly replacing naphtha cracking in many refinery units. This has further decreased the supply of butene as cracking of ethane results in negligible formation of other olefins such as butenes, other than ethene.

Consequently, price of butene has increased sharply, creating opportunities for on-purpose catalytic technologies, such as the catalytic dehydrogenation of butane to butenes. Butane dehydrogenation is advantageous as it exclusively yields butenes instead of a mixture of products. Hence, butane dehydrogenation may be developed as more economical and selective route for the butene production.

1.1.4 Dehydrogenation of butane

The catalytic dehydrogenation of butane proceeds as follows:

$$C_4H_{10} \rightarrow C_4H_8 + H_2 \qquad [1.1]$$

It is an attractive alternative and more economical approach for butene production. The butane has become more easily and economically available after recent shale gas explorations, with butane being one of its constituents. Butane dehydrogenation also offers a more selective route for the butene production. The production of hydrogen as a co-product during butane dehydrogenation is also beneficial [10,11]. Another advantage of dehydrogenation process is its lower operating temperature (~600 ^{o}C) than naphtha cracking process.

At present, six butane dehydrogenation installations are in operation, with three other plants being planned [12]. The majority of these facilities are based in US and China and use either of the two technologies - the Catofin (Lummus) or the Oleflex (UOP) process [1]. The Catofin process is based on the Houdry Catadiene process, which originally was exclusively used for dehydrogenation of iso-butane to iso-butene. A Catofin plant generally consists of 5−8 parallel adiabatic fixed bed reactors containing a chromia−alumina catalyst. The reaction is conducted at temperatures of approximately 575 °C and pressures between 0.2 and 0.5 bar [13]. The Olefex process uses a fluidized bed reactor, a catalyst regeneration unit, and a product recovery section. The process use Pt−Sn based catalyst at pressures between 1 and 3 bar and temperatures ranging from 525 to 705 °C.

However, the dehydrogenation process is associated with some basic disadvantages such as (i) thermodynamic limitation in maximum yield of olefins (ii) high pressures operation (iii) endothermic process (e.g. for n-butane $\Delta H^{o} = \pm 125$ kJ mol^{-1}) requiring external source of heat (iv) use of high temperature leading to alkane cracking and fast coke formation causing fast catalyst deactivation (e.g. Cr–Al_2O_3 catalysts used in commercial process

require regeneration after every few minutes of operation) [14-16]. Hence, there still exists a huge scope for improvement in dehydrogenation catalysts, requiring the research to continue in this direction.

Recent studies on butane dehydrogenation mainly focus on two aspects: catalytic oxidative dehydrogenation (ODH) and catalytic dehydrogenation (DH). In ODH, oxygen is used as the oxidant, and water is formed as a by-product instead of hydrogen. Therefore, the reaction becomes exothermic and avoids the thermodynamic constraints of dehydrogenation process. Previous studies have shown that supported vanadia catalysts are the most active and selective for the oxidative dehydrogenation of butane [17,18]. However, the oxidative dehydrogenation of butane is not yet commercialized. The main reason is very low selectivity towards butenes at industrial level of butane conversion and the necessity to use pure oxygen during dehydrogenation reaction. Large-scale air separation to obtain oxygen is an expensive and energy-demanding technology [19].

For, dehydrogenation, the research is oriented towards finding new catalysts that will not only give high activity and butene selectivity but also high sustainability, requiring less frequent regeneration. This can be achieved by having more active sites that selectively activate C-H bond. Since dehydrogenation sites are different than the C-C bond activating sites, high olefin yields can be obtained by careful catalyst design. The high temperatures required to obtain high olefin yields are also favourable for the formation of coke. On increasing the temperature, the rates of both C−H and C−C cleavage reactions are increased. The formation of coke on the catalyst surface results in the progressive reduction of catalytic activity with time-on-stream and requires periodic regeneration to preserve sufficient activity [20]. The higher reactivity of butenes compared to that of butane, can further lead to unwanted side and secondary reactions. Developing catalyst that can prevent undesired secondary reactions of butene, even at higher temperature will lower the tendency of formation of C_1-C_3 hydrocarbons and prevent subsequent coke formation. This will enhance butene selectivity and the life cycle of catalysts.

1.2 Literature Review

The catalytic dehydrogenation of butane has been widely recognized as an alternative to steam cracking of naphtha for the production of butenes [11]. The most active catalyst

reported for butane dehydrogenation is platinum; however, in pure form it exhibits low butene selectivity and rapid coke deposition, which contributes to catalyst deactivation [21]. The majority of current research focuses on the Pt-based catalyst systems, due to the excellent C-H bond activation characteristic of Pt. However, some challenges still exist in formulating a selective and stable catalyst. Side reactions can often occur, which include hydrogenolysis and cracking. Hydrogenolysis involves the cleavage of a C-C or carbon-heteroatom bond by hydrogen [22]. Cracking can occur either thermally at high temperature and pressure or catalytically involving a Brønsted acid site that results in the formation of an alkene and an alkane, via a carbocation intermediate [23]. In addition to low selectivities, consequences of side reactions also include catalyst deactivation via carbon deposits on the catalyst surface, requiring regeneration of the catalyst by burning off the coke deposits [24]. The large Pt ensembles have been reported to have high activity for hydrogenolysis. Presence of any second element on the surface can act as a site diluent and increase the overall selectivity towards dehydrogenation [25]. Pt based promoted bimetallic catalysts have been investigated extensively as effective catalysts for butane dehydrogenation.

Previous works have focused on identifying the most effective second metal that can act as promoter and elucidating its role, both experimentally and theoretically. The addition of tin, indium, zinc or gallium to platinum has been found to be effective in increasing butene selectivity and suppressing coke formation [26-30]. Both geometric and electronic effects of the second metals have been proposed to explain their roles in modifying the catalyst surface and changing the surface chemistry involved in butane dehydrogenation [29,31,32].

Achieving high activity along with stability remains a challenge. The preparation methodology also plays an important role in catalytic performance. Most of the catalysts are prepared via impregnation of metal precursors onto a support, which are subsequently subjected to thermal treatment to be obtained in oxidized or reduced form. While such methods are simple and robust, they offer little control over particle composition and size. In a typical catalyst prepared in this way, the composition and size distribution of particles depend on the composition of metal precursors and also on the preparation procedure [34]. Moreover, most of the times secondary metal does not form an alloy with primary metal. All these contribute towards lowering of catalytic performance.

A brief overview of the available literature is presented in the following sub-sections.

1.2.1 Different dehydrogenation catalysts

Many materials have been explored as catalyst components for catalytic dehydrogenation. The two main formulations used are noble metal-based and metal oxide-based catalysts. Though, platinum is most extensively studied for dehydrogenation reaction, various other noble metals have also been successfully employed. The chromia based catalysts are most prominent among the metal oxides investigated and have been commercially used for butane dehydrogenation as mentioned earlier. However, these catalysts often showed low stability due to the coke formation, and needed frequent regeneration. Moreover, chromia based catalysts often brought severe pollution to environment. Consequently, most research has been devoted to develop platinum or modified platinum catalysts to increase dehydrogenation activity. Significant results have also been achieved through the use of gallium, indium, vanadium, zinc, and molybdenum oxides as promoters [35-39].

1.2.1.1 Platinum based catalysts

Generally, all noble metals are active for dehydrogenation in the metallic state [40]. Platinum has been established as the most efficient noble metal for the butane dehydrogenation. It has been extensively studied since it possesses greater C−H bond activation abilities than other noble metals. Accordingly, it was commercialized by Universal Oil Products (UOP) in Pacol process in 1968 and later in Oleflex in the early 1970s [41]. Platinum is a highly active catalytic element and is not required in large quantities to catalyse the reaction when it is dispersed on a high surface-area support.

Many authors have reported butane dehydrogenation over Pt catalysts doped on different support materials [11,21,31,32,38]. Though monometallic platinum catalysts are highly active but they are not selective to dehydrogenation. In addition, the monometallic Pt catalysts deactivate rapidly because of fouling by carbonaceous materials that form coke on catalyst and block active Pt sites [42]. It is believed that two processes cause the deactivation of monometallic Pt catalysts: (i) side reactions that lead to coverage of active sites with coke and (ii) high temperature regeneration triggering agglomeration or sintering of active metal [43]. Moreover, stronger interaction of platinum with olefins compared to that with paraffins also contribute to lowering of butene selectivity [44]. Further, other issues including catalyst poisoning, high cost of platinum, and poor reusability have encouraged to search for alternatives [45,46]. Thus, the promoters were employed along

with platinum that can weaken the platinum-olefin interaction selectively without affecting the platinum–paraffin interaction [47]. The probability of secondary reactions of olefins is thus decreased without affecting the paraffin dehydrogenation significantly. The promoters also improved the stability of the catalyst by decreasing coking by heavy carbonaceous materials.

Tin is by far the most studied promoter, the addition of which modifies both the platinum active phase and the support. Bocanegra et al. demonstrated that the presence of oxidized tin species in Pt–Sn/Al_2O_3 catalysts favoured the increase in n-butane conversion and butene selectivity along with decrease in coke deposition [48]. Lee et al. studied butane dehydrogenation over the Pt-Sn catalyst with low Pt content and reported that small amount of Sn addition improved the n-C_4 selectivity by blocking the cracking sites of Pt catalyst [42]. Also, the electronic and geometric effect of Pt-Sn alloy increased the stability. Nawaz et al. discussed the performance of Pt-Sn/slit-SAPO-34 novel catalyst for selective C_3–C_4 dehydrogenation [41]. The authors reported around 40% light alkane conversion with 92% n-butene selectivity over the catalyst. Nagaraja et al. reported that for n-butane dehydrogenation reaction, the bimetallic Pt-Sn/θ-Al_2O_3 catalyst improved the n-C_4^{2-} yield and the stability [5]. Deng et al. observed that the supported Pt–Sn bimetallic catalysts when directly reduced by H_2, were highly active for the dehydrogenation of n-butane [3]. It was demonstrated that direct reduction method induced more surface exposed Pt atoms from the Pt_3Sn alloy, which played an important role in the superior catalytic behaviours for n-butane dehydrogenation.

Although the beneficial effects of tin promotion are well-known and have been amply described in the literature, the working principles of the Pt−Sn system are still under debate. The issues such as metal sintering, neutralization of acidity of the support, etc. still remains a problem. Hence, other metals have also been studied as promoters for platinum in the dehydrogenation of butane. Most notably, zinc has been reported to prevent undesired side reactions such as coke formation and isomerization in a fashion similar to that of tin. Seo et al. prepared a series of Pt/Sn/M/γ-Al_2O_3 catalysts with different third metal (M = Zn, In, Y, Bi, and Ga) by a sequential impregnation method for n-butane dehydrogenation. The Pt/Sn/Zn/γ-Al_2O_3 catalyst showed the best catalytic performance [49]. Further, Lee et al. reported the use of Pt/Sn/Zn–K/Al_2O_3 catalyst for dehydrogenation of n-butane to n-

butenes [11]. Therein, the addition of zinc led to improvement in n-butane conversion and product yield.

Bocanegra et al. reported the use of trimetallic catalyst for butane dehydrogenation where support was initially impregnated with In, followed by a co-impregnation with Pt and Sn [50]. The geometric effects of In and Sn on Pt sites produced a dilution of the Pt surface and also led to alloy formation which positively influenced the catalytic performance. Nagaraja et al. used PtSn/θ–Al_2O_3 catalysts with different amount of potassium (0.4 - 1.45 wt%) introduced by an impregnation method, for n-butane dehydrogenation [51]. It was reported that the presence of small amount of potassium on bimetallic PtSn/θ-Al_2O_3 catalyst improved n-$C_4^=$ selectivity, but slightly decreased n-butane conversion. However, there was an overall increase of n-$C_4^=$ yield. The effect of potassium was caused by blocking the acid sites of Pt catalyst.

Similarly, GaO_x and InO_x dopants have also been used to hinder the side reactions by poisoning of surface Brønsted acid sites. The simultaneous formation of Pt−Ga and Pt−In alloys possessed a geometric and an electronic effect on the Pt nanoparticles, further decreasing the coke deposition [52]. Sun et al. demonstrated a novel approach for preparing Ga-promoted Pt particles that were found to suppress the coke formation and increase product selectivity [52]. Further, Wu et al. showed the positive effect of Indium addition on Pt catalysts [10]. They demonstrated that the performance of Pt/Mg(In)(Al)O for butane dehydrogenation was highly dependent on the bulk In/Pt ratio. The optimal ratio was found to be between 0.33 and 0.88, yielding >95% selectivity to butenes.

Another alloy that has been investigated was Pt−Ge, which was believed to function in a way analogous to that of Pt−Sn. Furukawa et al. showed that higher yields of butene were obtained over Pt-Ge/SiO_2 catalyst in comparison to Pt/SiO_2 and other intermetallic catalysts (Pt_3Zn, Pt_3Co, PtCo) [53]. Byron et al. proposed the use of boron additives to prevent coking on Pt catalysts [54]. The incorporation of boron improved the catalytic activity to approximately three times along with the enhancement in stability of Pt/SiO_2, which was attributed to the migration of alkyl groups from platinum catalytic centre to tetrahedrally coordinated boron sites.

In addition, Cu and Ag have also been employed as promoters for Pt based catalysts in dehydrogenation process. Ma et al. reported that the addition of Cu to Pt increased the

propene selectivity from 61 to 96% at 20% propane conversion [55]. Lee et al. demonstrated that Cu addition to Pt catalyst led to significant improvement in selectivity from 40 to 73% and decreasing catalyst deactivation, as copper addition reduced the acid sites as well as their intensity [56]. Kurokawa et al. reported that the presence of Ag as a promoter in the Pt/Al_2O_3 catalyst increased the conversion from 28 to 50% with enhancement in product selectivity to 78% during butane dehydrogenation [57]. The catalyst sintering is another factor contributing to stability and activity of catalysts and is affected by the interaction between Pt and the catalyst support. Nagai et al. reported that Pt on Al_2O_3 readily sintered after treatment in air at 800 °C, while Pt on CeO_2 remained stable due to the strong interaction between ceria and Pt [58]. Hence, scope still remains for further research with Pt based catalysts where these issues can be more effectively addressed.

1.2.1.2 Palladium based catalysts

Though, there is ample of literature on Pt based catalysts yet, studies reported on butane dehydrogenation over Pd based catalysts are still very limited. Pd based catalysts can be an attractive alternative to the more expensive Pt metal. The Pd has been reported to be a versatile metal to carry out hydrogenation as well as dehydrogenation reactions [59]. The catalytic potential of Pd metal has been investigated in various studies, where Pd along with second metal such as Sn, Cu, Zn, etc. exhibited significant activity for ethane, propane and butane dehydrogenation. Vallecillos et al. showed that the incorporation of Sn to Pd led to improvement in the initial selectivity during propane dehydrogenation from 15 to 61% as well as catalytic stability [60]. Rodriguez et al.–reported that the addition of Ga to Pd catalyst had a negative impact on the activity for butane dehydrogenation but led to an enhancement in the dehydrogenation selectivity [61]. Cao et al. studied the catalytic properties of the Pd-Cu single atom catalyst towards propane dehydrogenation [62]. They demonstrated that the presence of relatively inactive Cu surface was beneficial for the coupling and desorption of detached H atoms and helped in reducing side reactions such as deep dehydrogenation and C−C bond breaking. Similarly, Gallagher et al. investigated the role of intermetallic Pd-Zn catalysts for propane dehydrogenation [63]. Wu et al. reported the use of Pd and Pd-In catalysts for ethane dehydrogenation [64]. The authors demonstrated that addition of In to Pd catalysts increased TOR to 0.26 s^{-1} from 0.03 s^{-1} and selectivity to 100% from 53% achieved over monometallic Pd catalyst.

1.2.1.3 Other catalysts

Chromium oxide based catalysts for dehydrogenation was introduced by Frey and Huppke in the 1930s. Since 1940s, chromium supported on alumina was used for dehydrogenation of butane to butenes and butadiene that were used for various commercial applications. Nemykina et al. studied the states of chromium in both promoted and unpromoted alumina–chromium catalysts with various chromium contents [65]. Based on the experimental data, the authors suggested that highly disperse Cr^{3+} particles were responsible for the catalytic activity in isobutane dehydrogenation. Shee and Sayari reported light alkane dehydrogenation investigations over a series of mesoporous Cr_2O_3/Al_2O_3 catalysts containing 2–15 wt% chromia [66]. The alkane dehydrogenation activity increased with increasing chromia loading. Detailed characterization studies of spent and regenerated catalysts indicated that the formation of subsurface Cr(III) species during dehydrogenation may be the reason for the permanent lost in activity. Ajayi et al. studied the kinetics of *n*-butane dehydrogenation over CrO_xVO_x/MCM-41 catalyst [67]. Bekmukhamedov et al. reported the formation of silicon oxide structures in the composition of an alumina–chromium catalyst for the dehydrogenation of iso-butane [68]. The formation of silicon oxide structures on the catalyst surface was responsible for an increase in the concentration of Cr(III) ions and a decrease in the surface acidity, thereby increasing the catalytic activity. Recently, Nazimov et al. investigated a series of the chromia/alumina catalysts with the same surface Cr concentration of 4.4 ± 0.2 at. Cr/nm^2 and different potassium loadings (0–3.9 wt.%) for iso-butane dehydrogenation at 520−550 °C [69]. The results of the study showed that at potassium loadings up to 2 wt%, K preferably interacted with alumina and modified the average dispersion of $Cr^{3+}O_x$ species in the reduced catalysts, leading to a steady growth of conversion and selectivity.

Recently some studies explored the activity of metals other than platinum and chromium as the primary agent for dehydrogenation reactions. Wang et al. reported the use of Sn/SiO_2 catalyst for catalytic dehydrogenation of propane [46]. Sn was demonstrated to play a leading role in dehydrogenation as a highly active component. Further, to address the deactivation problem of Sn/SiO_2 catalyst due to coke deposition and mobility of Sn species during a long-term run, Pd was introduced into the catalyst and its effect was also validated. Otroshchenko et al. investigated non-oxidative dehydrogenation of propane, n-butane, and isobutene over bare ZrO_2 and binary $MZrO_x$ (M=Li, Ca, Mg, Y, Sm or La) materials [70].

The intrinsic activity of Zr^{4+} sites and/or their concentration was observed to depend on the kind of dopant for ZrO_2. The dopant was also established to inhibit side reactions especially those leading to coke due to reducing concentration of strong acidic sites. All binary catalysts exhibited low activity for secondary reactions of the target olefins; the desired selectivity was higher than 85% at alkane conversion of ~30%. Zhu et al. compared iso-butane dehydrogenation and n-butane dehydrogenation over Ni-Sn/SiO_2 catalyst [71]. They reported that the conversion was higher for n-butane dehydrogenation, however, the Ni catalyst deactivated rapidly with time. They also observed that the secondary reactions of butene over Ni and generation of coke were responsible for the reduced butene selectivity.

1.2.2 Effect of catalyst preparation

Preparation technique plays a pivotal role in deciding the properties and performance of any catalyst. It determines the distribution of metals cluster on the support surface as well as their interaction with the support, which in turn affects the overall performance of the catalyst. The nano metal particles have tendency to undergo agglomeration and form clusters, thereby decreasing the catalytic activity. Hence, bulk metals alone cannot be deployed for enhanced catalysis applications [72,73]. Enhanced catalysis can be achieved by allowing implantation of metal nano particles on high surface area supports that possess high temperature stability [74,75]. The fabrication of a catalyst that bears high activity, high selectivity, low poisoning and low cost is highly challenging due to associated problems such as sintering of metals, pore mouth blockage, clustered deposition and dead zones in the porous structure of the support materials. All these factors are detrimental to achieve high catalytic performance.

Most of the work reported on butane dehydrogenation involves catalyst preparation by impregnation method. Other reported methods include chemical vapour deposition [76], physical vapour deposition such as sputter deposition [77], and ion exchange [78]. Among these, from the perspective of cost effectiveness and scalability, only impregnation and ion exchange qualify to be relevant for supported catalyst fabrication. Though impregnation is a simple and efficient method, it is associated with major limitations in terms of low metal dispersion and weak interaction of metal with the support [79]. Also, this method has limitation regarding control of surface morphology at a nanoscale. Recent advancements in the field of nanoscience has allowed the fabrication of metal nanoparticles in a more controlled manner in terms of shape and size. Many studies have reported possibilities of

enhancing catalytic performance by moderating the morphology of deposited metals on surface of catalysts [80,81].

The development of supported metal catalysts by employing an economical and improved preparation method in order to achieve highly dispersed active metal sites over high surface area supports can prove beneficial in achieving higher catalytic activity. To achieve the same, several authors have studied the influence of preparation method on catalytic properties and their performance. Ballarini et al. studied the n-butane dehydrogenation reaction over PtSn and PtGe supported on γ-Al_2O_3. The catalysts were prepared by deposition of metal on sphere shaped α-Al_2O_3 using wash coating method [82]. Ballarini et al. also studied the deposition conditions of thin layers of γ-Al_2O_3 by dip-coating on a spherical substrate of α-Al_2O_3 spheres [83]. Better metallic dispersion and catalytic performance for n-butane dehydrogenation reaction was reported for these catalysts in comparison to other conventional catalytic system.

Hakuli et al. reported atomic layer epitaxy (ALE) technique for the preparation of CrO_x/Al_2O_3 catalysts using Cr vapor and air as source materials for CrO_x . They claimed that Cr^{6+} surface sites were in stronger interaction with Al_2O_3 and more uniformly distributed in the catalysts prepared by ALE than by impregnation [84]. Further, Kikuchi et al. investigated *n*-butane dehydrogenation over alumina-supported Pt catalysts modified with Sn [85]. Here, SnO_2-Al_2O_3 was prepared by the sol-gel method. This procedure was reported to have multiple advantages: (i) prevention of the loss of Sn at calcination step, (ii) attainment of highly dispersed tin oxides on the support surface and retarding side reactions and (iii) formation of Sn-rich $PtSn_2$ particles exhibiting high catalytic activity.

Electroless deposition is a catalytic or auto-catalytic process that proceeds by the activation of a substrate surface by seeding of metal nucleation sites [86]. It involves the reduction of metal precursor salt by a chemical reducing agent onto specific sites of catalyst surface that can be either an active or inert substrate seeded with a catalytic active metal [87]. The deposition of metal in its reduced state eliminates the requirement of an energy intensive reduction process. Conventional electroless plating method involved contacting of activated support with a solution consisting of targeted metal precursor, stabilizer and a reducing agent at elevated temperatures. Sodium citrate and sodium EDTA are some of the commonly employed dispersing agents whereas hydrazine is used as the reducing agent.

Electroless plating process is mainly reported for membrane preparation [86,88]. However, limited studies are available for catalyst preparation. Beard et al. used conventional electroless method to prepare carbon supported bimetallic PEM fuel cell catalysts [87]. Rhenium precursor was impregnated to the support which acted as seeds for deposition of platinum. Platinum cluster sizes were reported to be in the size range of 3.2-6.9 nm in the presence of a second metal, Rh. When Pd and Pt were used for seeding instead of Rh, slightly lower bimetallic cluster size was obtained [89]. Shaal et al. conducted hydrogenation studies with Ag-Pt/SiO_2 and Cu-Pd/SiO_2 catalysts prepared by conventional ELP in his two separate works [90,91]. Wongkaew et al. deployed conventional ELP to synthesize Pt-Pd bimetallic catalyst from a commercial Pd monometallic catalyst using bath composition and method similar to that followed by Beard et al. [92]. The authors reported an average particle size of 4.5 nm.

a) Role of support material

For supported catalysts, the choice of the appropriate support plays an important role. The nature of support is important not only because it governs the mechanical properties of the catalyst, but also because the interaction of the support with the active phase can have a profound impact on catalyst activity and selectivity. Effective supports for dehydrogenation of butane have to be thermally stable due to exposure to high reaction temperatures. Also, for an optimal distribution and dispersion of the metallic particles, a relatively large surface area and uniform pore size distribution are preferred [1]. The catalytic reaction rate is limited by the intra-particle mass transfer rate. If the mass transfer rate is relatively slow, both activity and selectivity are lowered. As a result, the support must have a low pore diffusional resistance. Thus, an appropriate pore structure must be determined for the support to achieve optimal catalytic performance.

Among many high surface area materials, alumina is one of the most stable support available. High surface area γ-alumina is the classical support employed in dehydrogenation catalysts due to its high thermal stability, mechanical strength, and its exceptional ability of maintaining high metal dispersion. Another advantage of the alumina support is its simple preparation method and low cost of precursor. Alumina can be easily prepared by precipitation method with controlled pore structure [93].

Many authors have investigated butane dehydrogenation over Pt based catalysts preferentially supported on alumina [5,11,44,56]. Lemonidou et al. investigated oxidative dehydrogenation of propane using vanadia catalysts supported on Al_2O_3, ZrO_2, TiO_2 and MgO. It was reported that V_2O_5 supported on Al_2O_3 exhibited the highest selectivity [18]. Xu et al. investigated dehydrogenation of propane over different supported gallium oxide catalysts. Ga_2O_3 supported on Al_2O_3 and ZrO_2 exhibited higher activity due to abundant presence of medium-strong acid sites on the catalyst surface, while those supported on SiO_2 and MgO were ineffective for propane dehydrogenation [94]. Chen et al. studied the effect of support in In_2O_3/MO_x (M = Al, Si, Zr) catalysts for propane dehydrogenation. It was demonstrated that dispersion of In_2O_3 species depended on type of support. The maximum metal dispersion and propylene yield was achieved for In_2O_3 supported on Al_2O_3 [95].

b) Role of surfactants

Surfactants are materials that can affect the interfacial surface tension. This ability enables them to act as effective dispersant. The use of surfactants helps in the synthesis of tailor made catalysts. Multiple works have been reported regarding synthesis of structured nano metal particles in presence of various surfactants using their shape directing and size limiting properties [96-99]. Sukonket et al. synthesized a series of ceria-zirconia mixed oxide supports by two different routes - surfactant-assisted route and a co-precipitation route [96]. The activity results indicated superior nature of the catalysts obtained by the surfactant-assisted route over the other. Chu et al. prepared $Cu/ZnO/Al_2O_3$ catalysts with the assistance of surfactant, tetraethylammonium hydroxide, and evaluated in methanol synthesis from syngas [97]. The catalyst prepared with addition of 2 wt.% surfactant exhibited better catalytic performance compared to that prepared without using surfactant. The better performance was attributed to smaller crystallite size of Cu and higher Cu surface area obtained in presence of surfactant. Sun et al. prepared CuO/CeO_2 catalyst by surfactant-assisted impregnation method, which showed better catalytic activity for low temperature CO oxidation compared to that showed by catalyst prepared by conventional impregnation method [98]. The results suggested that the surfactant addition into the impregnation solution improved the dispersion of CuO species, facilitating incorporation of Cu^{2+} into CeO_2 lattice. Thereby, the synergistic effects between CuO and CeO_2 was strengthened making the lattice oxygen more active, and resulting in enhanced activity for CO oxidation.

Shen et al. prepared a series of mesoporous SBA-15 supported CuO–CeO_2 catalysts by a surfactant-assisted impregnation method with PEG 200 as the surfactant [99]. The results showed that the surfactant had a substantial effect on the distribution and dispersion of Cu species. The synergetic effect between copper and ceria was enhanced by increased dispersion of copper and led to enhanced catalytic performance. Hajimirzaee et al. synthesized hydroxyapatite (HAP) in the presence of surfactants and tested it as a catalyst in CO oxidation [100]. The activity of HAP was increased when prepared in presence of surfactants such as polysorbate 20, polyethylene glycol and poly vinyl alcohol. The enhanced activity was due to higher BET surface areas and acid site densities in the surfactant-modified catalysts. Lei et al. used the Mn-based oxides and Cu-based oxides as active components that were supported on the honeycomb ceramic cordierite carrier modified by the double palm carboxyethylhydroxyethylmethyl sulfateammonium salt (TEP) surfactant [101]. The results indicated that addition of TEP increased the impregnation of the catalyst and made the dispersion of metal oxide more uniform that led to an increase in the de-nitration performance of the catalyst.

Summary

The dehydrogenation being an endothermic reaction, requires high temperatures. At such high temperatures, the rate of C-C cleavage also increases resulting in gradual loss of catalytic activity, and thus affecting the overall product yield. From literature survey, the best catalyst for butane dehydrogenation seems to be $(PtSn)_{1.5}/Al_2O_3$ catalyst reported by Nagaraja et al. (2014). The authors obtained a butane conversion of 43.6% at a reaction temperature of 550 °C with the butene yield of 37.7%. Though, the reported catalyst exhibited a considerable yield, the catalyst suffered ~7% deactivation after 3 h of time on stream. With the employment of conventional preparation technique of impregnation, it is difficult to gain control over metal particle size and achieve strong metal-support interaction. This adversely affects the metal dispersion over the support. The large metal ensembles in impregnated catalysts are reported to possess greater affinity for hydrogenolysis and cracking reactions that might result in catalyst deactivation. Furthermore, catalyst preparation by impregnation also requires energy intensive calcination process and hydrogen reduction at elevated temperatures prior to application in dehydrogenation reaction, that can be avoided in catalysts prepared by electroless deposition.

1.3 Motivation for present work

The literature shows that the platinum dominates the catalytic research of developing effective catalyst for butane dehydrogenation. Palladium, another metal of the same group as Pt, is expected to exhibit similar properties to that of Pt, thus bearing same chemical activity or reacting tendency. The intrinsic catalytic properties of Pd metal originate from the fundamental electronic configuration of its constituent element ($4d_{10}5s_0$). The higher reduction potential of palladium helps in enhancing its interaction with incoming hydrocarbon reactant and activating easier hydrogen abstraction. Also, palladium is less expensive alternative to platinum. Though palladium has wide potential as dehydrogenation catalysts, reported work on palladium as dehydrogenation catalysts is limited. Hence, this study explored the effectiveness of Pd based catalyst for butane dehydrogenation. Palladium can be explored for butane dehydrogenation as the lone active metal or in combination with platinum or other metals associated with dehydrogenation reactions. The literature reviews also showed how the catalyst preparation affects the properties of the catalysts and their catalytic performance. Particularly for supported metal catalysts dispersion of metal is an important factor that controls the overall performance. The impregnation method, the most widely used technique for catalyst preparation, is associated with limitations such as low metal dispersion and weak metal-support interaction. Hence, preparation methodology that improves these properties of catalyst is expected to improve its performance. The electroless plating has the potential of deposition of active metal on support with in-situ reduction and higher dispersion. However, in conventional form it is not suitable for preparation of supported metal catalyst. The modification of the conventional method will help to design catalysts with better performance. Hence, exploring Pd based catalysts in association with Pt and other metals for butane dehydrogenation prepared by electroless deposition seemed to be worthwhile.

1.4 Objectives of the thesis

The primary objective of this work was to develop highly active, selective and stable catalyst for butane dehydrogenation. Palladium was explored as the active metal in combination with Pt and other metals reported as having effective promotional effect for dehydrogenation. Alumina was used as the support for preparation of the catalysts. The electroless plating process was modified and made suitable for powder catalyst. The

catalysts prepared by modified electroless deposition method were compared with the catalysts prepared by conventional impregnation method. The specific objectives of the thesis are given below:

a) Preparation of alumina supported monometallic Pd and Pt catalysts by electroless deposition. Study and optimization of preparation parameters.

b) Comparison of the physicochemical properties and butane dehydrogenation performance of alumina supported monometallic Pd and Pt catalysts prepared by modified electroless deposition with that prepared by impregnation.

c) Study the effect of addition of surfactants during preparation of alumina supported Pd catalysts by electroless deposition, on their physicochemical properties and catalytic performance for butane dehydrogenation.

d) Study the effect of addition of Ni, Cu and Ag as promoter in Pd based catalysts on their physicochemical properties and catalytic performance for butane dehydrogenation.

e) Investigation of the Pd-Pt bimetallic catalysts for butane dehydrogenation. Study the effect of variations in preparation, metal composition, metal deposition sequence, process parameters and addition of surfactant and promoter.

1.5 Organization of the thesis

The thesis has been organized in 7 chapters as described below.

In **Chapter 1**, the topic has been introduced and literature review has been included. It also elaborates on motivation of the work and objectives.

The **Chapter 2** discusses the effect of preparation on properties of monometallic Pt and Pd catalysts has been discussed. The physicochemical properties and butane dehydrogenation performance of catalysts prepared by deposition were compared with that prepared by impregnation. For electroless deposition, effect of synthesis parameters has been discussed.

The **Chapter 3** discusses the effect of addition of different surfactants during Pd catalyst preparation by electroless deposition method. The performance of surfactant modified

catalysts has been evaluated for butane dehydrogenation and compared with that of unmodified and impregnated Pd catalysts.

The **Chapter 4** elaborates on the role of nickel, copper and silver as the promoter metals in Pd based catalysts. Further, the effect of copper content has been discussed.

The **Chapter 5** discusses the effect of metal composition in supported Pd-Pt bimetallic catalysts. The ratio of Pd to Pt was varied as 3:1, 1:1 and 1:3. Additionally, the effect of preparation methodology was also explored.

The **Chapter 6** discusses the effect of change in sequence of metal addition in Pd-Pt bimetallic catalysts prepared by deposition method. The effects of various process parameters on butane dehydrogenation reaction was also investigated. It also addresses the effect of surfactant and promoter in Pd-Pt bimetallic catalysts.

The **Chapter 7** summarizes the important findings and conclusions from this research work. The chapter also presents a brief overview on the recommendations for the future research in the related field.

References

[1] J.J.H.B. Sattler, J. Ruiz-Martinez, E. Santillan-Jimenez, B.M. Weckhuysen, Catalytic dehydrogenation of light alkanes on metals and metal oxides, Chem. Rev. 114 (2014) 10613–10653.

[2] Nexant Industry Report – Independent Market Report on the Global and Indonesian Petrochemicals Industry (2011), http://www.chandra-asri.com/UserFiles/201105151926340. Nexant Industry Report 2011. pdf (accessed September 20, 2020).

[3] L. Deng, H. Miura, T. Ohkubo, T. Shishido, Z. Wang, S. Hosokawa, K. Teramura, T. Tanaka, The importance of direct reduction in the synthesis of highly active Pt-Sn/SBA-15 for: n-butane dehydrogenation, Catal. Sci. Technol. 9 (2019) 947–956.

[4] https://www.transparencymarketresearch.com/asia-pacific-butene1-market.html

[5] B.M. Nagaraja, H. Jung, D.R. Yang, K.D. Jung, Effect of potassium addition on bimetallic PtSn supported θ-Al_2O_3 catalyst for n-butane dehydrogenation to olefins, Catal. Today. 232 (2014) 40–52.

[6] https://www.grandviewresearch.com/press-release/global-isobutene-market

[7] https://www.reportlinker.com/p05820653/Global-Butene-1Industry.html?utm_source=GNW

[8] U. Rodemerck, S. Sokolov, M. Stoyanova, U. Bentrup, D. Linke, E. V. Kondratenko, Influence of support and kind of VO_x species on isobutene selectivity and coke deposition in non-oxidative dehydrogenation of isobutane, J. Catal. 338 (2016) 174–183.

[9] J. Lu, Z. Zhao, C. Xu, A. Duan, P. Zhang, CrHZSM-5 zeolites - Highly efficient catalysts for catalytic cracking of isobutane to produce light olefins, Catal. Letters. 109 (2006) 65–70.

[10] J. Wu, Z. Peng, P. Sun, A.T. Bell, n-Butane dehydrogenation over Pt/Mg(In)(Al)O, Appl. Catal. A Gen. 470 (2014) 208–214.

[11] J.K. Lee, H. Seo, J.K. Kim, H. Seo, H.R. Cho, J. Lee, H. Chang, I.K. Song, Direct dehydrogenation of n-butane over Pt/Sn/Zn-K/Al_2O_3 catalyst: Effect of hydrogen in the feed, J. Nanosci. Nanotechnol. 16 (2016) 4580–4586.

[12] Ondrey, G. UOP's C_3 Oleflex process selected for propylene plant in the U.S. Gulf Coast, http://www.che.com/only_on_che/latest_news/UOPs-C3-Oleflex-process-selected-for-propylene-plantin-the-U-S-Gulf-Coast_10539.html (accessed Oct 23, 2020).
[13] M.M. Bhasin, J.H. McCain, B. V. Vora, T. Imai, P.R. Pujadó, Dehydrogenation and oxydehydrogenation of paraffins to olefins, Appl. Catal. A Gen. 221 (2001) 397–419.
[14] L.M. Madeira, Catalytic oxidative dehydrogenation of n-butane, Catal. Rev. - Sci. Eng. 44 (2002) 247–286.
[15] G. Tanimu, B.R. Jermy, S. Asaoka, S. Al-Khattaf, Composition effect of metal species in (Ni, Fe, Co)-Bi-O/gamma-Al_2O_3 catalyst on oxidative dehydrogenation of n-butane to butadiene, J. Ind. Eng. Chem. 45 (2017) 111–120.
[16] M. Setnička, P. Čičmanec, E. Tvarůžková, R. Bulánek, Combined oxidative and non-oxidative dehydrogenation of n-butane over VO_x species supported on HMS, Top. Catal. 56 (2013) 662–671.
[17] H. Dai, A.T. Bell, E. Iglesia, Effects of molybdena on the catalytic properties of vanadia domains supported on alumina for oxidative dehydrogenation of propane, J. Catal. 221 (2004) 491–499.
[18] A.A. Lemonidou, L. Nalbandian, I.A. Vasalos, Oxidative dehydrogenation of propane over vanadium oxide based catalysts. Effect of support and alkali promoter, Catal. Today. 61 (2000) 333–341.
[19] T. Otroshchenko, G. Jiang, V.A. Kondratenko, U. Rodemerck, E. V. Kondratenko, Current status and perspectives in oxidative, non-oxidative and CO_2-mediated dehydrogenation of propane and isobutane over metal oxide catalysts , Chem. Soc. Rev. (2020).
[20] M.P. Lobera, C. Téllez, J. Herguido, M. Menéndez, Transient kinetic modelling of propane dehydrogenation over a Pt-Sn-K/Al_2O_3 catalyst, Appl. Catal. A Gen. 349 (2008) 156–164.
[21] S.R. de Miguel, I.M.J. Vilella, P. Zgolicz, S.A. Bocanegra, Bimetallic catalysts supported on novel spherical $MgAl_2O_4$-coated supports for dehydrogenation processes, Appl. Catal. A Gen. 567 (2018) 36–44.
[22] J.H. Sinfelt, Hydrogenolysis of ethane over supported platinum, J. Phys. Chem. 68 (1964) 344–346.
[23] A. Corma, J. Planelles, J. Sánchez-Marín, F. Tomás, The role of different types of acid site in the cracking of alkanes on zeolite catalysts, J. Catal. 93 (1985) 30–37.
[24] J. Barbier, E. Churin, P. Marecot, J.C. Menezo, Deactivation by Coking of Platinum/Alumina Catalysts. Effects of Operating Temperature and Pressure, Appl. Catal. 36 (1988) 277–285.
[25] R.M. Rioux, H. Song, J.D. Hoefelmeyer, P. Yang, G.A. Somorjai, High-surface-area catalyst design: Synthesis, characterization, and reaction studies of platinum nanoparticles in mesoporous SBA-15 silica, J. Phys. Chem. B. 109 (2005) 2192–2202.
[26] S.A. Kanniappan, U.B.R. Ragula, Effect of reduction of Pt–Sn/α-Al_2O_3 on catalytic dehydrogenation of mixed-paraffin feed, Catalysts. 10 (2020) 113.
[27] K. Searles, K.W. Chan, J.A. Mendes Burak, D. Zemlyanov, O. Safonova, C. Copéret, Highly Productive Propane Dehydrogenation Catalyst Using Silica-Supported Ga-Pt Nanoparticles Generated from Single-Sites, J. Am. Chem. Soc. 140 (2018) 11674–11679.
[28] S. Rimaz, L. Chen, S. Kawi, A. Borgna, Promoting effect of Ge on Pt-based catalysts for dehydrogenation of propane to propylene, Appl. Catal. A Gen. 588 (2019) 117266.
[29] V.J. Cybulskis, B.C. Bukowski, H.T. Tseng, J.R. Gallagher, Z. Wu, E. Wegener, A.J. Kropf, B. Ravel, F.H. Ribeiro, J. Greeley, J.T. Miller, Zinc Promotion of Platinum for Catalytic Light Alkane Dehydrogenation: Insights into Geometric and Electronic Effects, ACS Catal. 7 (2017) 4173–4181.
[30] A. Perechodjuk, E. V. Kondratenko, Nonoxidative Dehydrogenation of Isobutane over $MZrO_x$(M = La or Y) with Supported Ir, Pt, Rh, or Ru: Effects of Promoters and Supported Metals, Ind. Eng. Chem. Res. 59 (2020) 21729-21735.
[31] A.D. Ballarini, C.G. Ricci, S.R. de Miguel, O.A. Scelza, Use of Al_2O_3-SnO_2 as a support of Pt for selective dehydrogenation of light paraffins, Catal. Today. 133–135 (2008) 28–34.
[32] L. Deng, H. Miura, T. Shishido, Z. Wang, S. Hosokawa, K. Teramura, T. Tanaka, Elucidating strong metal-support interactions in Pt–Sn/SiO_2 catalyst and its consequences for dehydrogenation of lower alkanes, J. Catal. 365 (2018) 277–291.
[33] A.P. Ferreira, S. Capela, P. Da Costa, C. Henriques, M.F. Ribeiro, F.R. Ribeiro, CH_4-SCR of NO over Co and Pd ferrierite catalysts: Effect of preparation on catalytic performance, Catal. Today. 119 (2007) 156–165.
[34] D.G. Araiza, D.G. Arcos, A. Gómez-Cortés, G. Díaz, Dry reforming of methane over Pt-Ni/CeO_2 catalysts: Effect of the metal composition on the stability, Catal. Today. 360 (2019) 46–54.
[35] M.S. Pereira, A.M. Da Silva, M.A.C. Nascimento, Effect of the zeolite cavity on the mechanism of dehydrogenation of light alkanes over gallium-containing zeolites, J. Phys. Chem. C. 115 (2011) 10104–10113.
[36] J. Liu, W. Zhou, D. Jiang, W. Wu, C. Miao, Y. Wang, X. Ma, Isobutane Dehydrogenation over InPtSn/$ZnAl_2O_4$ Catalysts: Effect of Indium Promoter, Ind. Eng. Chem. Res. 57 (2018) 11265–11270.

[37] X. sheng Wang, G. lin Zhou, Z. wei Chen, Q. Li, H. jun Zhou, C. ming Xu, Enhancing the vanadium dispersion on V-MCM-41 by boron modification for efficient iso-butane dehydrogenation, Appl. Catal. A Gen. 555 (2018) 171–177.

[38] J. Camacho-Bunquin, M.S. Ferrandon, H. Sohn, A.J. Kropf, C. Yang, J. Wen, R.A. Hackler, C. Liu, G. Celik, C.L. Marshall, P.C. Stair, M. Delferro, Atomically Precise Strategy to a PtZn Alloy Nanocluster Catalyst for the Deep Dehydrogenation of n -Butane to 1,3-Butadiene, ACS Catal. 8 (2018) 10058–10063.

[39] R. Yao, J.E. Herrera, L. Chen, Y.H.C. Chin, Generalized Mechanistic Framework for Ethane Dehydrogenation and Oxidative Dehydrogenation on Molybdenum Oxide Catalysts, ACS Catal. 10 (2020) 6952–6968.

[40] A.N. Matveyeva, S.O. Omarov, D.A. Sladkovskiy, D.Y. Murzin, Experimental studies and kinetic regularities of isobutane dehydrogenation over Ga_2O_3/Al_2O_3, Chem. Eng. J. 372 (2019) 1194–1204.

[41] Z. Nawaz, F. Baksh, J. Zhu, F. Wei, Dehydrogenation of C_3-C_4 paraffin's to corresponding olefins over slit-SAPO-34 supported Pt-Sn-based novel catalyst, J. Ind. Eng. Chem. 19 (2013) 540–546.

[42] M.H. Lee, B.M. Nagaraja, K.Y. Lee, K.D. Jung, Dehydrogenation of alkane to light olefin over PtSn/θ-Al_2O_3 catalyst: Effects of Sn loading, Catal. Today. 232 (2014) 53–62.

[43] Z. Han, S. Li, F. Jiang, T. Wang, X. Ma, J. Gong, Propane dehydrogenation over Pt-Cu bimetallic catalysts: The nature of coke deposition and the role of copper, Nanoscale. 6 (2014) 10000–10008.

[44] J.W. Jung, W. Il Kim, J.R. Kim, K. Oh, H.L. Koh, Effect of direct reduction treatment on Pt–Sn/Al_2O_3 catalyst for propane dehydrogenation, Catalysts. 9 (2019) 1–13.

[45] Y.P. Tian, P. Bai, S.M. Liu, X.M. Liu, Z.F. Yan, VO_x-K_2O/γ-Al_2O_3 catalyst for nonoxidative dehydrogenation of isobutane, Fuel Process. Technol. 151 (2016) 31–39.

[46] G. Wang, H. Zhang, H. Wang, Q. Zhu, C. Li, H. Shan, The role of metallic Sn species in catalytic dehydrogenation of propane: Active component rather than only promoter, J. Catal. 344 (2016) 606–608.

[47] J.K. Lee, H. Seo, U.G. Hong, G. Park, Y. Yoo, J. Lee, H. Chang, I.K. Song, Platinum-tin nano-catalysts supported on alumina for direct dehydrogenation of n-butane, J. Nanosci. Nanotechnol. 15 (2015) 8305–8310.

[48] S.A. Bocanegra, S.R. de Miguel, I. Borbath, J.L. Margitfalvi, O.A. Scelza, Behavior of bimetallic PtSn/Al_2O_3 catalysts prepared by controlled surface reactions in the selective dehydrogenation of butane, J. Mol. Catal. A Chem. 301 (2009) 52–60.

[49] H. Seo, J.K. Lee, U.G. Hong, G. Park, Y. Yoo, J. Lee, H. Chang, I.K. Song, Direct dehydrogenation of n-butane over Pt/Sn/M/γ-Al_2O_3 catalysts: Effect of third metal (M) addition, Catal. Commun. 47 (2014) 22–27.

[50] S.A. Bocanegra, A.A. Castro, O.A. Scelza, S.R. de Miguel, Characterization and catalytic behavior in the n-butane dehydrogenation of trimetallic InPtSn/$MgAl_2O_4$ catalysts, Appl. Catal. A Gen. 333 (2007) 49–56.

[51] B.M. Nagaraja, H. Jung, D.R. Yang, K.D. Jung, Effect of potassium addition on bimetallic PtSn supported θ-Al_2O_3 catalyst for n-butane dehydrogenation to olefins, Catal. Today. 232 (2014) 40–52.

[52] P. Sun, G. Siddiqi, M. Chi, A.T. Bell, Synthesis and characterization of a new catalyst Pt/Mg(Ga)(Al)O for alkane dehydrogenation, J. Catal. 274 (2010) 192–199.

[53] S. Furukawa, A. Tamura, K. Ozawa, T. Komatsu, Catalytic properties of Pt-based intermetallic compounds in dehydrogenation of cyclohexane and n-butane, Appl. Catal. A Gen. 469 (2014) 300–305.

[54] C. Byron, S. Bai, G. Celik, M.S. Ferrandon, C. Liu, C. Ni, A. Mehdad, M. Delferro, R.F. Lobo, A. V. Teplyakov, Role of boron in enhancing the catalytic performance of supported platinum catalysts for the nonoxidative dehydrogenation of n-butane, ACS Catal. 10 (2020) 1500–1510.

[55] Z. Ma, Z. Wu, J.T. Miller, Effect of Cu content on the bimetallic Pt–Cu catalysts for propane dehydrogenation, Catal. Struct. React. 3 (2017) 43–53.

[56] H. Lee, W. Il Kim, K.D. Jung, H.L. Koh, Effect of Cu promoter and alumina phases on Pt/Al_2O_3 for propane dehydrogenation, Korean J. Chem. Eng. 34 (2017) 1337–1345.

[57] H. Kurokawa, H. Namoto, A. Horinouchi, M. Sato, M. Usui, H. Ogihara, H. Miura, Dehydrogenation of n-butane to butenes and 1,3-butadiene over PtAg/Al_2O_3 catalysts in the presence of H_2, J. Mater. Sci. Chem. Eng. 06 (2018) 16–24.

[58] Y. Nagai, T. Hirabayashi, K. Dohmae, N. Takagi, T. Minami, H. Shinjoh, S. Matsumoto, Sintering inhibition mechanism of platinum supported on ceria-based oxide and Pt-oxide-support interaction, J. Catal. 242 (2006) 103–109.

[59] X.F. Guo, D.Y. Jang, H.G. Jang, G.J. Kim, Hydrogenation and dehydrogenation reactions catalyzed by CNTs supported palladium catalysts, Catal. Today. 186 (2012) 109–114.

[60] J. Valecillos, D. Rodnguez, J. Méndez, R. Solano, C. González, T. Acosta, J. Sánchez, G. Arteaga,

Propane dehydrogenation over alumina-supported palladium and palladium-tin catalysts, Ciencia (Special Number on Adsorption and Catalysis) 14 (2006) 125–134.
[61] L. Rodríguez, D. Romero, D. Rodríguez, J. Sánchez, F. Domínguez, G. Arteaga, Dehydrogenation of n-butane over Pd-Ga/Al_2O_3 catalysts, Appl. Catal. A Gen. 373 (2010) 66–70.
[62] X. Cao, Y. Ji, Y. Luo, Dehydrogenation of propane to propylene by a Pd/Cu single-atom catalyst: Insight from first-principles calculations, J. Phys. Chem. C. 119 (2015) 1016–1023.
[63] J.R. Gallagher, D.J. Childers, H. Zhao, R.E. Winans, R.J. Meyer, J.T. Miller, Structural evolution of an intermetallic Pd-Zn catalyst selective for propane dehydrogenation, Phys. Chem. Chem. Phys. 17 (2015) 28144–28153.
[64] Z. Wu, E.C. Wegener, H.T. Tseng, J.R. Gallagher, J.W. Harris, R.E. Diaz, Y. Ren, F.H. Ribeiro, J.T. Miller, Pd-In intermetallic alloy nanoparticles: Highly selective ethane dehydrogenation catalysts, Catal. Sci. Technol. 6 (2016) 6965–6976.
[65] E.I. Nemykina, N.A. Pakhomov, V. V. Danilevich, V.A. Rogov, V.I. Zaikovskii, T. V. Larina, V. V. Molchanov, Effect of chromium content on the properties of a microspherical alumina-chromium catalyst for isobutane dehydrogenation prepared with the use of a centrifugal thermal activation product of gibbsite, Kinet. Catal. 51 (2010) 898–906.
[66] D. Shee, A. Sayari, Light alkane dehydrogenation over mesoporous Cr_2O_3/Al_2O_3 catalysts, Appl. Catal. A Gen. 389 (2010) 155–164.
[67] B.P. Ajayi, B. Abussaud, R. Jermy, S. Al Khattaf, Kinetic modelling of n-butane dehydrogenation over CrO_xVO_x/MCM-41 catalyst in a fixed bed reactor, Prog. React. Kinet. Mech. 39 (2014) 341–353.
[68] G.E. Bekmukhamedov, S.R. Egorova, A.A. Lamberov, Effect of the nature of silicon oxide structures on the activity of an alumina-chromium catalyst in the reaction of iso-butane dehydrogenation, Catal. Ind. 6 (2014) 44–52.
[69] D.A. Nazimov, O. V. Klimov, A. V. Saiko, S.N. Trukhan, T.S. Glazneva, I.P. Prosvirin, S. V. Cherepanova, A.S. Noskov, Effect of the K loading on effective activation energy of isobutane dehydrogenation over chromia/alumina catalysts, Catal. Today. (2020) 1–9.
[70] T.P. Otroshchenko, V.A. Kondratenko, U. Rodemerck, D. Linke, E. V. Kondratenko, Non-oxidative dehydrogenation of propane, n-butane, and isobutane over bulk ZrO_2-based catalysts: Effect of dopant on the active site and pathways of product formation, Catal. Sci. Technol. 7 (2017) 4499–4510.
[71] Q. Zhu, G. Wang, H. Zhang, X. Zhu, C. Li, n-Butane dehydrogenation over Ni-Sn/SiO_2: Adsorption modes and reaction paths of n-butane and 1-butene, Appl. Catal. A Gen. 566 (2018) 113–120.
[72] J.H. Shim, B.J. Lee, Y.W. Cho, Thermal stability of unsupported gold nanoparticle: A molecular dynamics study, Surf. Sci. 512 (2002) 262–268.
[73] T.W. Hansen, A.T. Delariva, S.R. Challa, A.K. Datye, Sintering of catalytic nanoparticles: Particle migration or ostwald ripening?, Acc. Chem. Res. 46 (2013) 1720–1730.
[74] C.T. Campbell, S.C. Parker, D.E. Starr, The effect of size-dependent nanoparticle energetics on catalyst sintering, Science 298 (2002) 811–814.
[75] G.M. Veith, A.R. Lupini, S. Rashkeev, S.J. Pennycook, D.R. Mullins, V. Schwartz, C.A. Bridges, N.J. Dudney, Thermal stability and catalytic activity of gold nanoparticles supported on silica, J. Catal. 262 (2009) 92–101.
[76] P. Serp, P. Kalck, R. Feurer, Chemical vapor deposition methods for the controlled preparation of supported catalytic materials, Chem. Rev. 102 (2002) 3085–3128.
[77] H.Y. Park, I. Jang, N. Jung, Y.H. Chung, J.Y. Ryu, I.Y. Cha, H.J. Kim, J.H. Jang, S.J. Yoo, Green synthesis of carbon-supported nanoparticle catalysts by physical vapor deposition on soluble powder substrates, Sci. Rep. 5 (2015) 1–8.
[78] Q. Wang, S.Y. Park, J.S. Choi, J.S. Chung, Co/$K_xTi_2O_5$ catalysts prepared by ion exchange method for NO oxidation to NO_2, Appl. Catal. B Environ. 79 (2008) 101–107.
[79] F.W. Chang, W.Y. Kuo, H.C. Yang, Preparation of Cr_2O_3-promoted copper catalysts on rice husk ash by incipient wetness impregnation, Appl. Catal. A Gen. 288 (2005) 53–61.
[80] M. Ghorbanloo, V. Safarifard, A. Morsali, Heterogeneous catalysis with a coordination modulation synthesized MOF: Morphology-dependent catalytic activity, New J. Chem. 41 (2017) 3957–3965.
[81] S.X. Liang, Q. Zhang, Z. Jia, W. Zhang, W. Wang, L.C. Zhang, Tailoring surface morphology of heterostructured iron-based Fenton catalyst for highly improved catalytic activity, J. Colloid Interface Sci. 581 (2021) 860–873.
[82] A.D. Ballarini, P. Zgolicz, I.M.J. Vilella, S.R. de Miguel, A.A. Castro, O.A. Scelza, n-Butane dehydrogenation on Pt, PtSn and PtGe supported on γ-Al_2O_3 deposited on spheres of α-Al_2O_3 by washcoating, Appl. Catal. A Gen. 381 (2010) 83–91.
[83] A. Ballarini, S. Bocanegra, S. de Miguel, P. Zgolicz, Synthesis of spherical structured catalysts by dip-coating: Application to n-butane dehydrogenation, Can. J. Chem. Eng. 96 (2018) 696–703.
[84] A. Hakuli, A. Kytökivi, A.O.I. Krause, Dehydrogenation of i-butane on CrO_x/Al_2O_3 catalysts prepared

by ALE and impregnation techniques, Appl. Catal. A Gen. 190 (2000) 219–232.
[85] I. Kikuchi, M.A. Ohshima, H. Kurokawa, H. Miura, Effect of Sn addition on n-butane dehydrogenation over alumina-supported Pt catalysts prepared by co-impregnation and sol-gel methods, J. Japan Pet. Inst. 55 (2012) 206–213.
[86] D.A. Pacheco Tanaka, M.A. Llosa Tanco, S.I. Niwa, Y. Wakui, F. Mizukami, T. Namba, T.M. Suzuki, Preparation of palladium and silver alloy membrane on a porous α-alumina tube via simultaneous electroless plating, J. Memb. Sci. 247 (2005) 21–27.
[87] S. Haag, M. Burgard, B. Ernst, Pure nickel coating on a mesoporous alumina membrane: Preparation by electroless plating and characterization, Surf. Coatings Technol. 201 (2006) 2166–2173.
[88] K.D. Beard, M.T. Schaal, J.W. Van Zee, J.R. Monnier, Preparation of highly dispersed PEM fuel cell catalysts using electroless deposition methods, Appl. Catal. B Environ. 72 (2007) 262–271.
[89] K.D. Beard, J.W. Van Zee, J.R. Monnier, Preparation of carbon-supported Pt-Pd electrocatalysts with improved physical properties using electroless deposition methods, Appl. Catal. B Environ. 88 (2009) 185–193.
[90] M.T. Schaal, A.Y. Metcalf, J.H. Montoya, J.P. Wilkinson, C.C. Stork, C.T. Williams, J.R. Monnier, Hydrogenation of 3,4-epoxy-1-butene over Cu-Pd/SiO_2 catalysts prepared by electroless deposition, Catal. Today. 123 (2007) 142–150.
[91] M.T. Schaal, A.C. Pickerell, C.T. Williams, J.R. Monnier, Characterization and evaluation of Ag-Pt/SiO_2 catalysts prepared by electroless deposition, J. Catal. 254 (2008) 131–143.
[92] A. Wongkaew, Y. Zhang, J.M.M. Tengco, D.A. Blom, P.K. Sivasubramanian, P.T. Fanson, J.R. Regalbuto, J.R. Monnier, Characterization and evaluation of Pt-Pd electrocatalysts prepared by electroless deposition, Appl. Catal. B Environ. 188 (2016) 367–375.
[93] C. Kumar Patel, P. Jyoti Sarma, M. De, Comparative parametric study on development of porous structure of aluminium oxide in presence of anionic and cationic surfactants, Ceram. Int. 41 (2015) 3578–3588.
[94] B. Xu, B. Zheng, W. Hua, Y. Yue, Z. Gao, Support effect in dehydrogenation of propane in the presence of CO_2 over supported gallium oxide catalysts, J. Catal. 239 (2006) 470–477.
[95] M. Chen, J.L. Wu, Y.M. Liu, Y. Cao, L. Guo, H.Y. He, K.N. Fan, Study in support effect of In_2O_3/MO_x (M=Al, Si, Zr) catalysts for dehydrogenation of propane in the presence of CO_2, Appl.Catal. A Gen. 407 (2011) 20–28.
[96] T. Sukonket, A. Khan, B. Saha, H. Ibrahim, S. Tantayanon, P. Kumar, R. Idem, Influence of the Catalyst Preparation Method, Surfactant Amount, and Steam on CO_2 Reforming of CH_4 over $5Ni/Ce_{0.6}Zr_{0.4}O_2$ Catalysts, Energy and Fuels. 25 (2011) 864–877.
[97] Z. Chu, H. Chen, Y. Yu, Q. Wang, D. Fang, Surfactant-assisted preparation of Cu/ZnO/Al_2O_3 catalyst for methanol synthesis from syngas, J. Mol. Catal. A Chem. 366 (2013) 48–53.
[98] S. Sun, D. Mao, J. Yu, Enhanced CO oxidation activity of CuO/CeO_2 catalyst prepared by surfactant-assisted impregnation method, J. Rare Earths. 33 (2015) 1268–1274.
[99] W. Shen, D. Mao, Z. Luo, J. Yu, CO oxidation on mesoporous SBA-15 supported CuO-CeO_2 catalyst prepared by a surfactant-assisted impregnation method, RSC Adv. 7 (2017) 27689–27698.
[100] S. Hajimirzaee, S. Chansai, C. Hardacre, C.E. Banks, A.M. Doyle, Effects of surfactant on morphology, chemical properties and catalytic activity of hydroxyapatite, J. Solid State Chem. 276 (2019) 345–351.
[101] Z. Lei, J. Yang, S. Hao, W. Xin, L. Min, W. Yusu, X. Dan, Application of surfactant-modified cordierite-based catalysts in denitration process, Fuel. 268 (2020) 117242.

Chapter 1

भारतीय प्रौद्योगिकी संस्थान गुवाहाटी
Indian Institute of Technology Guwahati

Chapter 2

SUPPORTED MONOMETALLIC CATALYSTS: EFFECT OF PREPARATION METHODS

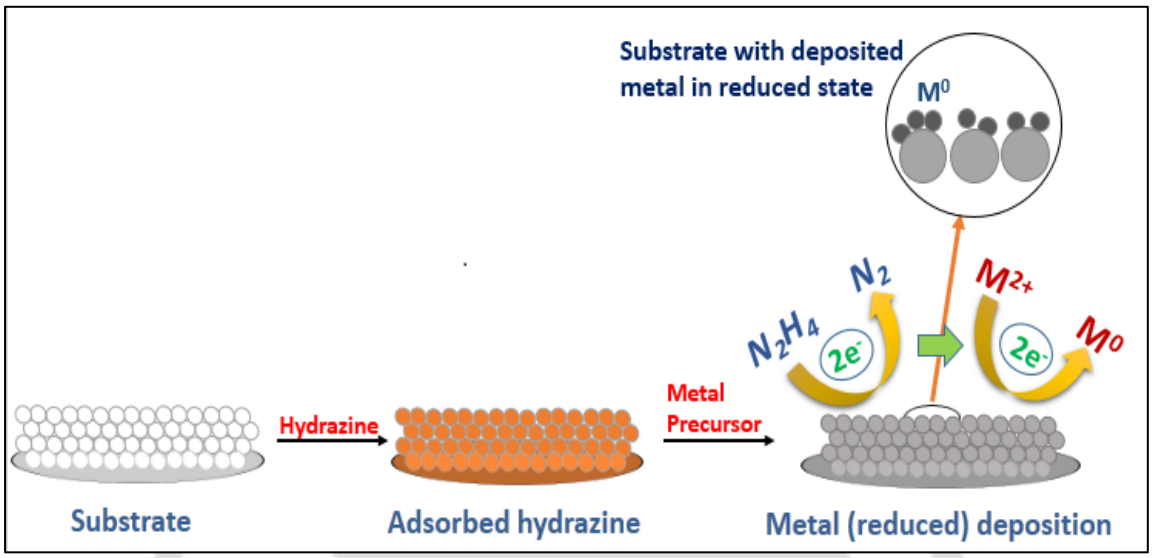

In this chapter, electroless deposition method was investigated for the preparation of supported monometallic catalysts. The effects of synthesis parameters such as concentration of metal precursor, concentration and type of reducing agents, sequence of addition of metal precursor and reducing agent were investigated on the extent of metal loading and nature of metal particles on the support. Their physicochemical properties and efficiency for butane dehydrogenation reaction were determined and compared with that prepared by conventional impregnation method.

Keywords

Catalyst preparation; electroless deposition; impregnation; palladium; platinum

Chapter 2

2.1 Introduction

Electroless plating has been reported as a potential method for deposition of metals on support surface, as discussed in Chapter 1. Conventional electroless method was used to prepare carbon supported bimetallic Pt/Rh and Pd/Pt catalysts to demonstrate the feasibility of such process as a novel technique for catalyst preparation [1]. Through deposition method, metal clusters were obtained in the range of 3 – 8 nm [2]. Similarly, for Ag-Pt/SiO_2 and Cu-Pd/SiO_2 catalysts, enhanced catalytic performance was observed for hydrogenation studies for the catalysts prepared by conventional ELP in comparison to those prepared by incipient impregnation [3,4].

In this study, the conventional electroless plating process was modified to overcome the problems associated with bath stability and unrestricted crystal growth on the surface and to achieve higher dispersion for similar metal loading and deposition time. Such a modification allowed carrying out the deposition on powdered catalyst with minimal loss of product and ensuring uniform deposition of the metal on the support. A sequential mode of deposition was designed for this purpose. The modified method is referred hereafter as Electroless Deposition (ED) method and can be used for depositing metals on commonly used support materials in powder form. The metal deposition in reduced state eliminates the requirement of an energy intensive reduction process prior to catalysis application. Since the metal deposition and reduction occurs simultaneously on the support surface, strong interactions are expected between metal and support.

In deposition method, both metal precursor solution and reducing agent solution were passed through the alumina substrate in a cyclic form. This chapter discusses the effects of various synthesis parameters such as metal precursor concentration, reducing agent concentration, type of reducing agent, etc. on the metal loading and morphology of catalysts. It further compares the supported monometallic Pd with Pt catalysts prepared by electroless deposition. The physicochemical properties of the catalysts were characterized by Atomic Absoprtion Spectroscopy (AAS), Energy dispersive X-ray spectroscopy (EDX), X-Ray diffraction analysis (XRD), Transmission Electron Microscopy (TEM), X-ray photon spectroscopy (XPS) and Temperature Programmed Reduction (TPR). The properties and butane dehydrogenation activity of the catalysts prepared by deposition method was compared to that prepared by impregnation at same metal loadings.

2.2 Experimental

2.2.1 Materials required

Palladium chloride [$PdCl_2$, Reagent Plus 99%, Sigma Aldrich] and chloroplatinic acid hexa-hydrate [$H_2PtCl_6.6H_2O$, ACS reagent] were used as active metal precursor and aluminium nitrate nona-hydrate [$Al(NO_3)_3.9H_2O$, Merck] was used as alumina precursor. Ammonia solution [30 mol%, Merck] was employed as precipitating agent for the synthesis of aluminium oxide. Hydrazine hydrate [$N_2H_4.H_2O$, Merck] was used as reducing agent. Hydrochloric acid [HCl, 37% Merck] and ammonia solution were used for pH balance.

2.2.2 Preparation of support

Preparation scheme for the aluminium oxide by precipitation using ammonia is shown in Figure 2.1. The aluminium nitrate [$Al(NO_3)_3.9H_2O$] precursor was dissolved in required amount of deionised water. Then, 30% ammonia solution was added to it gradually to carry out the precipitation. The pH of the solution was maintained at 10.5 ± 0.2. The resulted aluminium hydroxide precipitate was aged under reflux at 75 °C for 6 h. Precipitated aluminium hydroxide was then filtered, washed and dried at 100 °C overnight in hot air oven. The dried aluminium hydroxide was calcined at 550 °C for 6 h to obtain aluminium oxide. The aluminium oxide was subsequently used as support for the preparation of catalysts.

2.2.3 Preparation of monometallic catalysts

a) Electroless deposition method

The monometallic supported Pd and Pt catalysts were prepared by electroless deposition method using powdered aluminium oxide as support and hydrazine as the reducing agent. The steps of the preparation procedure were modified with respect to conventional electroless plating process. In the modified method, instead of dipping the substrate in solutions containing all the reagents, metal precursor and reducing agent solutions were passed through the substrate sequentially in a cyclic form. This facilitated deposition of metal on the powdered substrate with a minimal loss and gave a better control over interaction between metal precursor and reducing agent over the support surface. This modified method was also beneficial in reducing bulk diffusion resistance. The catalysts

were prepared using hydrazine as the reducing agent. The stoichiometric equation for reduction of Pt or Pd using hydrazine is given as:

$$H_2PtCl_6 + N_2H_4 \rightarrow Pt^0 + N_2 + 6HCl \quad [2.1]$$

$$2PdCl_2 + N_2H_4 \rightarrow 2Pd^0 + N_2 + 4HCl \quad [2.2]$$

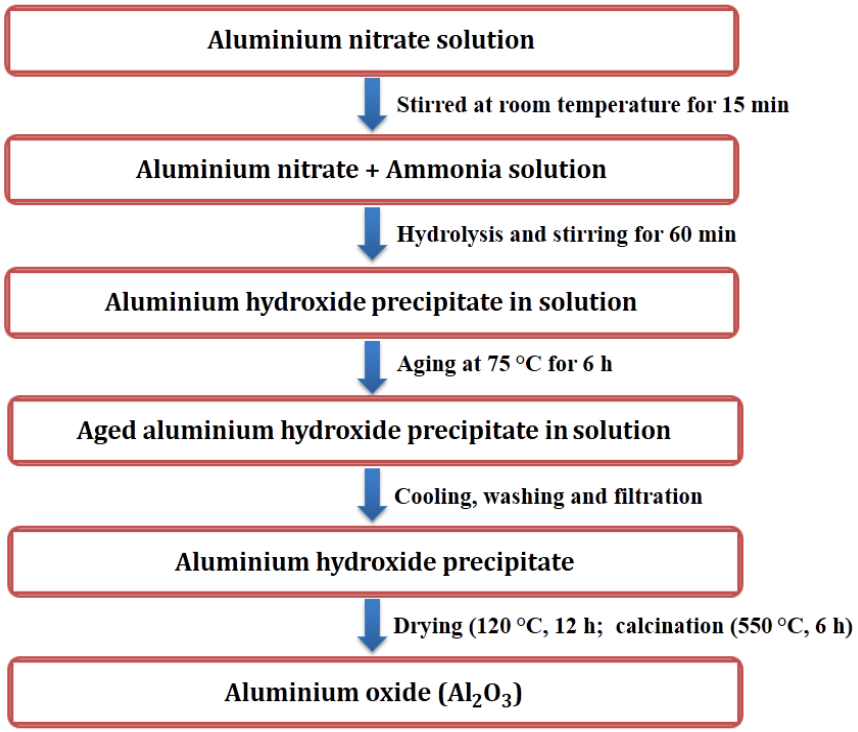

Figure 2.1. Steps involved in the preparation of alumina support.

Both the catalysts were synthesized targeting a final metal loading of 112.8 μmoles g^{-1} of catalyst corresponding to 1.2 wt% Pd and 2.1 wt% Pt loading. Palladium chloride solution was prepared by adding 40 mg of $PdCl_2$ in distilled water. Platinum precursor solution was prepared by dissolving 116.5 mg of H_2PtCl_6 in distilled water. Aqueous solution of hydrazine (reducing agent) was prepared by adding required volume of $N_2H_4.H_2O$ in distilled water. The molar ratio of reducing agent to metal precursor was maintained at 1:0.75 for $PdCl_2$ and 1:1.5 for H_2PtCl_6. At this molar ratio reducing agent was 50% excess to that of metal precursor.

In a typical experiment, 20 mL of hydrazine solution was passed through 2 g of aluminium oxide support using vacuum. Total time taken was 10 min. Then, 20 mL of mono-metal

precursor solution (Pd or Pt) was gradually poured through the filtered sample maintaining 10 min of interaction time. These two steps represented first cycle. In the second cycle, the filtrate of hydrazine solution (obtained after filtration of 1st cycle) was again passed through the support followed by filtrate of metal precursor solution maintaining similar interaction time of 10 min. In the third and fourth cycle, fresh and filtrate solutions were passed, respectively, to get sufficient deposition of metal (Pt or Pd) on aluminium oxide. Thereafter, the resulting catalyst was dried overnight at 110 °C for 12 h. Figure 2.2 shows the steps involved in the synthesis of catalysts by electroless deposition method.

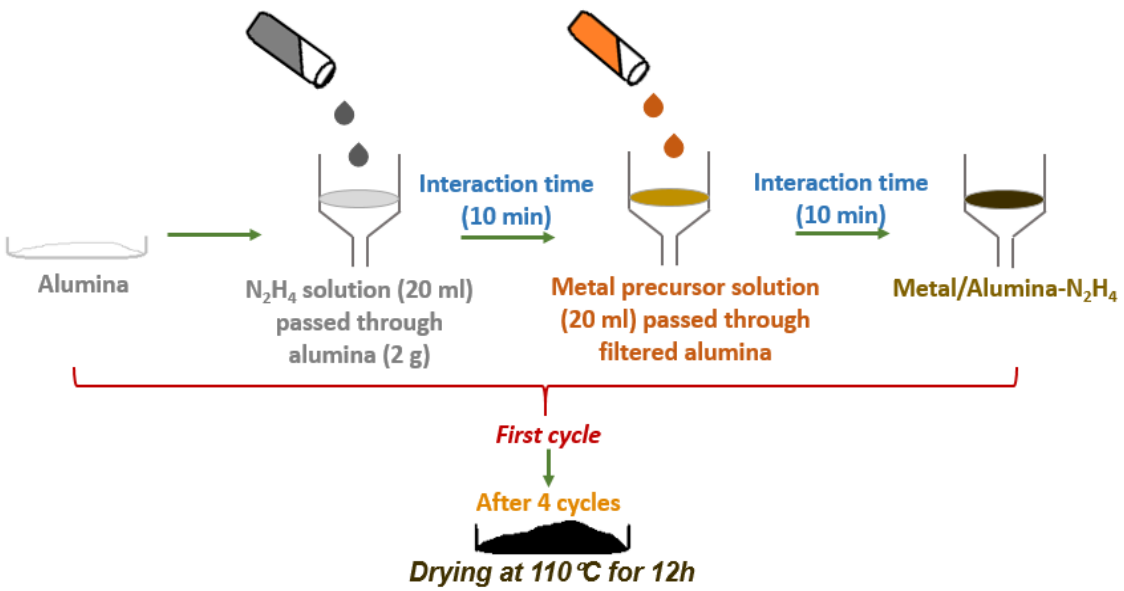

Figure 2.2. Schematic of steps for catalyst preparation using deposition method.

Both the monometallic supported Pt and Pd catalysts were prepared by keeping the total metal loading of 112.8 µmoles g^{-1} of catalyst. The metal loading on weight basis for Pt and Pd catalysts corresponded to 2.2 and 1.2 wt%, respectively. The Pt and Pd catalysts prepared by electroless deposition method are referred to as Pt/Al and Pd/Al, respectively, further in the chapter. Here "Al" represented Aluminium oxide.

The effect of various synthesis parameters involved in preparing catalyst by electroless deposition method were investigated. The effects were studied with Pt catalysts. The effects of metal precursor concentration, reducing agent concentration, type of reducing agent and sequence of reagent addition were studied on extent of deposition. For all the studies the number of deposition cycles was kept at 4. When one parameter was varied other parameters were kept similar.

The effect of concentration of metal precursor on the metal loading was investigated by varying the precursor concentration as 500, 1000, 2000 and 3000 ppm. For this study N_2H_4/Pt molar ratio was maintained at 1:1.5. To study the effect of reducing agent concentration, the samples were prepared by varying the N_2H_4 to Pt molar ratio as 1.5, 3 and 6, while precursor concentration was kept constant at 3000 ppm. The Pt based catalysts were further prepared by changing the sequence of addition of reducing agent and the precursor solution. The N_2H_4/Pt molar ratio was kept constant at 1:1.5 while the concentration of precursor solution was kept constant at 3000 ppm for these studies. Other than hydrazine, formaldehyde was also used as a reducing agent to study and compare the effects of different reducing agents.

b) Conventional impregnation method

The monometallic Pd and Pt catalysts were prepared by incipient impregnation method with a metal loading of 112.8 μmoles g^{-1} of catalyst, similar to that of catalyst prepared by electroless deposition. This corresponded to 1.2 and 2.1 wt% loading of Pd and Pt metals, respectively. Figure 2.3 shows a schematic depicting the steps involved in the catalyst synthesis by impregnation method.

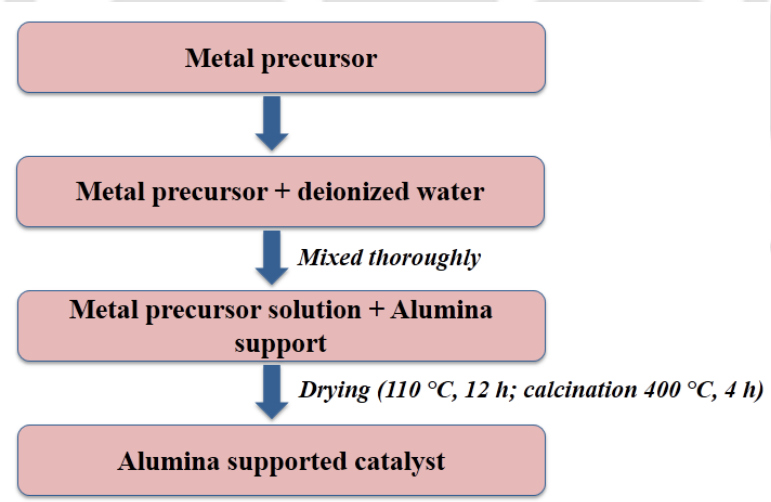

Figure 2.3. Steps for catalyst preparation by impregnation method.

In this method, required amount of Pd or Pt precursor was dissolved in 6 mL of water. This corresponded to volume slightly higher than the pore volume of 2 g support. The metal precursor solution was then added to the support material gradually and mixed thoroughly to make a uniform paste. The impregnated catalyst was then left at room temperature in air

for 2 h and dried overnight in an oven at 110 °C. The dried sample was then calcined in a muffle furnace at 400 °C for 4 h to obtain the final catalyst. These catalysts are further referred to as Pd/Al_WI and Pt/Al_WI in the text.

2.2.4 Catalyst characterization

The characterization of support as well as all the prepared catalysts was carried out using various techniques such as Energy dispersive X-ray spectroscopy (EDX), Brunauer-Emmett-Teller (BET) surface area and pore analysis, X-ray photon spectroscopy (XPS), Temperature Programmed Reduction (TPR), Transmission Electron Microscopy (TEM), X-Ray diffraction analysis (XRD), Fourier Transform Infrared Spectroscopy (FTIR) and Temperature Programmed Desorption (TPD) to determine the physicochemical properties and determine their role in butane dehydrogenation reactions.

Atomic Absorption Spectroscopy (AAS)

The metal loading of all the catalysts prepared by electroless deposition was determined initially by Atomic absorption spectroscopy (AAS). The AAS was used for measurement of concentration of respective metals in filtrate solutions after deposition to determine the metal loadings. The actual loading of metal was calculated based on the concentration determined by AAS as follows:

$$\text{Total metal loading (wt\%)} = \frac{\text{Metal deposited on support (mg)}}{\text{Amount of support (mg)}} \times 100 \qquad [2.3]$$

where,

Metal deposited (mg) = Initial amount of metal in precursor solution (mg) – Final amount of metal in filtrate solution (mg) [2.4]

Another parameter used to determine the efficiency of the process is ‘Metal Loss’, defined as the fraction of initial metal that was not deposited on the support. Loss percentage was calculated as the ratio of metal retained in the solution to the initial amount of metal used for preparation of catalysts.

$$\text{Metal loss (\%)} = \frac{\text{Final amount of metal in filtrate after deposition}}{\text{Initial amount of metal in solution before deposition}} \times 100 \qquad [2.5]$$

Energy dispersive X-ray spectroscopy (EDX)

The metal loadings on the prepared catalysts were further confirmed by energy dispersive X-ray spectroscopy (EDX) analysis using a EDX accessory attached to ZEISS FESEM (Model: SIGMA).

Surface area and pore analysis

The BET surface areas of the support and catalysts were obtained with nitrogen adsorption–desorption measurements at liquid nitrogen temperature using Quanta chrome (Model: Autosorb iQ) surface area analyser. The samples were degassed in vaccum at 200 °C for 6 h, prior to the experiment. The cumulative pore volume and pore size were calculated from the desorption branches of the isotherms employing the Barrett–Joyner–Halenda (BJH) method.

X-ray photon spectroscopy (XPS)

In order to obtain the composition of catalysts and chemical bonding states of the elements present, XPS (PHI 5000 Versa Probe II, FEI Inc.) technique using monochromatic A1 Kα (1486.6 eV) at 150 W was used. Survey scan of catalysts (around 100 mg) was conducted over a range of 1200 eV with a step size of 1 eV, 100 ms per step and 150 eV pass energy. Furthermore, a high resolution scan for detected elements (Pd and Pt) was obtained at a step size of 0.05 eV in order to ascertain chemical states of the elements present in the catalysts. All XPS peaks were fitted by the Gaussian–Lorentzian method, after background subtraction using the Shirley method. The charging effects were corrected by C 1s peak as a reference for all samples at binding energy of 284.9 eV.

Temperature Programmed Reduction (TPR)

The TPR experiments were carried out using a temperature program analyser (Micromeritics Chemisorb 2720), consisting of a gas mixing unit allowing both continuous and pulsed reactant dosing, U-shaped quartz tube with a thermocouple and a thermal conductivity detector (TCD), to study the reducibility of the metal catalysts. For TPR studies, 100 mg of sample was placed between quartz wool in a U-type quartz reactor. The sample was thermally treated under an Ar stream at 150 °C for 2 h to remove physically adsorbed water and other impurities. The samples were then cooled down to the room

temperature under Ar gas. After the pre-treatment, the catalysts were heated at 10 °C min^{-1} from room temperature up to 800 °C in 10% H_2/Ar stream with a flow rate of 30 mL min^{-1}.

Transmission Electron Microscopy (TEM)

The TEM images of the samples were recorded using JEM 2100 (Make: JEOL) at 200 kV. The sample preparation was done by first dispersing the sample in a solvent using ultra-sonication followed by deposition on a copper grid. The analysis of all the TEM images obtained was done using ImageJ.

X-Ray diffraction analysis (XRD)

The XRD patterns of the prepared catalysts were recorded on a diffractometer (Bruker D8 Advance) with Ni-filtered Cu Kα (λ= 0.15418 nm) as a radiation source. The operating voltage was 40 kV and the current was 5 mA. The scanning was done in the range of 5-80^o with a speed of 0.05^o s^{-1} in a continuous mode.

Fourier Transform Infrared Spectroscopy (FTIR)

The acidic properties of the prepared catalysts were evaluated by FTIR spectroscopy of adsorbed pyridine. Pyridine was adsorbed on the catalyst samples by placing each of them in two different round bottom flask connected to each other through necks. The pyridine solution was heated such that the pyridine vapours were carried by the nitrogen flowing through the flasks at a rate of 20 mL min^{-1} and adsorbed on the catalyst samples placed in a separate flask. The pyridine adsorbed samples were then analysed using a Perkin-Elmer 2000 FTIR spectrometer. Infrared spectra were acquired at 1 cm^{-1} resolution and averaged over 50 scans. The spectra of samples were recorded from 400 to 4000 cm^{-1}.

Temperature Programmed Desorption (TPD)

The acidic properties of the catalysts were also studied by temperature-programmed desorption of ammonia. NH_3-TPD experiments were conducted in a Micromeritics Chemisorb 2720 apparatus. Around 50 mg of sample was placed in the quartz glass tube. The sample was pre-treated in a flow of He maintaining a flow rate of 30 mL min^{-1} at 250 °C for 1 h. Then the sample was exposed to pulses of 10% NH_3/He mixture at room temperature until saturation. The gas phase NH_3 was removed by He purging for 1 h. The sample was then heated to 700 °C at a heating rate of 10 °C min^{-1} in a flow of He (30 mL

min^{-1}) to induce desorption of NH_3 which was monitored by a TCD detector. The quantification of the number of acidic sites was based on the calibration curves obtained by injecting different amounts of 10% NH_3/He mixture and the assumption that only one molecule could adsorb on one active centre. Blank tests without prior adsorption of any probe molecule were also conducted which did not show any signals over the entire temperature range.

2.2.5 Dehydrogenation tests

The n-butane dehydrogenation activity tests were conducted in a fixed-bed continuous downflow reactor in the temperature range of 100 – 600 °C at atmospheric pressure. The schematic of experimental setup used for conducting dehydrogenation study is shown in Appendix B. A thermocouple was placed in close contact with the catalyst bed to measure the reaction temperature. The catalyst (0.25 g) was mixed with 1 g of quartz powder and placed in the centre of the reactor. The feed gas mixture containing n-butane, H_2 and N_2 gases was introduced to the reactor in the volumetric ratio of 1:3:6. The feed gas mixture was allowed to flow through the catalyst bed maintaining a constant flow rate of 100 mL min^{-1}. At these conditions, no mass transfer effects were observed (Appendix A). Further details of experimental procedure are included in Appendix B.

The effluent gas mixture containing reactants as well as products were analysed using an on-line Gas chromatograph (Nucon 5765), which was equipped with a sebaconitrile column coupled to a flame ionization detector (FID). Nitrogen was used as the carrier gas. The oven temperature was maintained at 40 °C while the injector and detector temperature were kept at 160 °C and 180 °C. The products were identified by comparison with standard calibration mixtures. The performance of the catalysts was evaluated in terms of conversion, TOF, selectivity and yield as follows:

$$\text{Butane conversion (\%)} = \frac{\text{Moles of butane}_{in} - \text{Moles of butane}_{out}}{\text{Moles of butane}_{in}} \times 100 \qquad [2.6]$$

$$\text{Selectivity of product X (\%)} = \frac{\text{Moles of product X formed}}{\text{Total moles of products formed}} \times 100 \qquad [2.7]$$

$$\text{Yield of X (\%)} = \frac{\text{Moles of product X formed}}{\text{Moles of butane supplied}} \times 100 = \text{Conversion} \times \text{Selectivity} \qquad [2.8]$$

$$TOF = \frac{\text{Moles of butane converted}}{\text{Moles of metal x seconds}} \quad [2.9]$$

The butane conversion at 550 °C was considered. The total metal loading for all the catalysts was almost similar and was used for calculating the TOF for comparison.

The deactivation was calculated as :

$$\text{Percentage deactivation, } D(\%) = \frac{\text{Conversion}_{\text{initial}} - \text{Conversion}_{\text{final (t=10h)}}}{\text{Conversion}_{\text{initial}}} \times 100 \quad [2.10]$$

2.3 Results and discussion

2.3.1 Analysis of support

The nitrogen adsorption-desorption isotherms and pore size distribution of aluminium oxide are shown in Figure 2.4a and b. The nitrogen adsorption-desorption isotherm of the aluminium oxide support was of Type IV and H2 type hysteresis loop that indicated the mesoporous nature with interconnected pore network. The pore size distribution of the support was broad (2-18 nm) with average pore size of 7 nm. The BET surface area of support was 184 m^2 g^{-1} with total pore volume of 0.34 cc g^{-1}. Figure 2.4c shows the XRD profile of aluminium oxide support. For the support, peaks due to γ-Al_2O_3 were obtained at 2θ values of 37.6° (311), 45.8° (400) and 66.8° (440) [5].

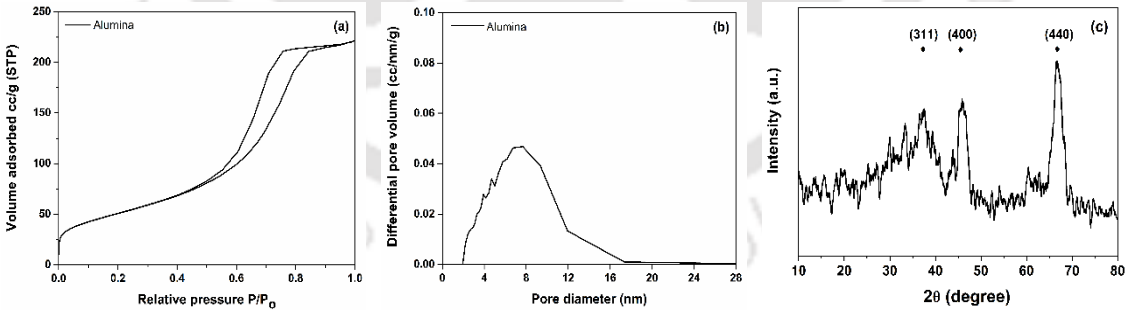

Figure 2.4. (a) Nitrogen adsorption-desorption isotherm, (b) pore size distribution and (c) XRD profile of alumina support.

2.3.2 Effect of synthesis parameters

In this section, results of the effects of precursor concentration, reducing agent concentration, reducing type and sequence of metal on metal deposition have been discussed.

2.3.2.1 Effect of precursor concentration

The platinum loadings obtained for catalysts prepared in presence of different precursor concentrations is shown in Table 2.1. The Pt loading on the catalysts increased from 0.37 to 2.12 wt% with the increase in the initial concentration of the metal precursor solution from 500 to 3000 ppm. This increase might have resulted from the increased contact of platinum ions with the support as concentration of metal precursor was increased. At lower concentrations of 500 and 1000 ppm, no metal loss was observed, while at higher concentrations metal loss was obtained after four cycles. However, the loss percentage at higher concentration was minimal to around 4% only. The loss at higher precursor concentration can be attributed to several factors including (i) partial desorption of the deposited Pt during subsequent steps when reducing agent solution is passed through the sample (ii) less availability of free surface on the support as loading increased (iii) repulsive interaction between the approaching and deposited metal atoms on surface.

Table 2.1. Platinum loading obtained for catalysts prepared using different synthesis parameters.

Catalysts	Pt used (mg)	Pt deposited (mg)	Actual Loading (wt%)	Pt Loss (%)	EDX Loading (wt%)	Metal dispersion (%)
Effect of precursor concentration						
Pt/Al-500	7.54	7.54	0.37	0	--	40.4
Pt/Al-1000	15.08	15.08	0.74	0	--	--
Pt/Al-2000	30.16	28.97	1.42	3.92	1.7	--
Pt/Al-3000*	45.24	43.49	2.12	3.86	2.6	33.2
Effect of reducing agent concentration						
N_2H_4/Pt-1.5*	45.24	43.49	2.12	3.9	2.6	33.2
N_2H_4/Pt-3	45.24	42.12	2.06	6.9	--	--
N_2H_4/Pt-6	45.24	42.86	2.10	5.3	1.9	36.5
Effect of sequence of reagent addition						
N_2H_4/Pt[a]*	45.24	43.49	2.12	3.9	2.6	33.2
Pt/N_2H_4[b]	45.24	42.77	2.09	5.46	1.9	26.9
Effect of different reducing agents						
N_2H_4/Pt*	45.24	43.49	2.12	3.9	2.6	33.2
HCHO/Pt	45.24	41.38	2.02	8.5	2.0	16.9

a: hydrazine added prior to metal precursor; b: metal precursor added prior to hydrazine;

** marked samples are basically the same sample but with different nomenclature to illustrate the effect of parameters*

As shown in Table 2.1, the metal loading determined for the catalyst prepared with 3000 ppm concentration of hexachloroplatinic acid was 2.6 wt%. This Pt loading obtained by EDX analysis was comparable to that calculated by AAS analysis (2.12 wt%).

The XRD profiles for the Pt catalysts prepared using different precursor concentration are shown in Figure 2.5a. The peaks observed at 37.6°, 45.8°, 60.9° and 66.8° may be attributed to the γ-aluminium oxide. The peaks corresponding to the presence of alumina were observed for all the samples without any change in the intensity. The peaks corresponding to different Pt phases are expected at 39.7°, 47° and 68° that corresponds to Pt (111), Pt (200) and Pt (220) [6]. These peaks were present at the overlapping positions to alumina peaks. Since no variation in peak intensity was observed in any of the catalyst samples compared to that of support alumina, it can be assumed that the deposited Pt metal was in a well dispersed state over the support in metal loading range from 0.37 to 2.1 wt%.

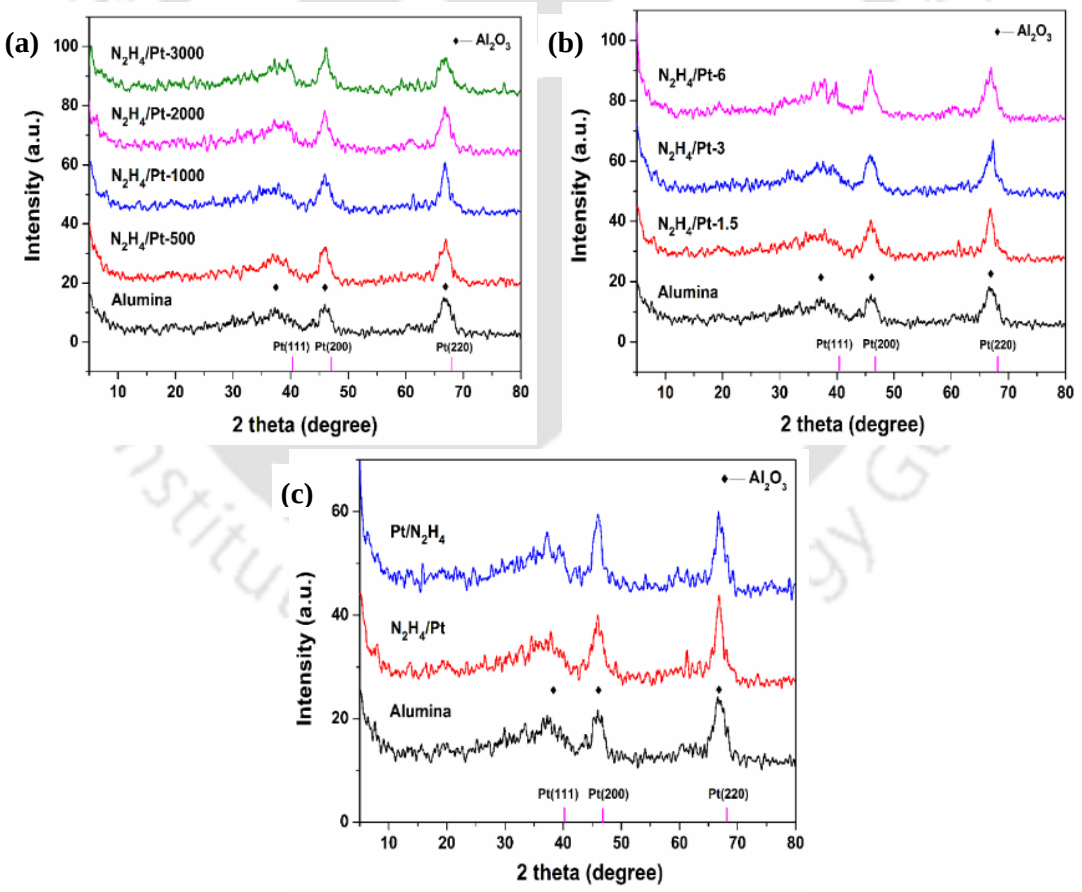

Figure 2.5. XRD profiles for Pt catalysts (a) Effect of metal precursor concentration, (b) Effect of reducing agent concentration and (c) Effect of sequence of reagent addition.

2.3.2.2 Effect of reducing agent concentration

The Pt loadings and percentage of metal loss obtained after deposition using different hydrazine concentrations are tabulated in Table 2.1. It can be observed that increasing the concentration of hydrazine from 1.5 to 6 stoichiometric ratio, which corresponded to 50 to 200% excess, increased the metal loss to small extent. Accordingly, metal loading decreased slightly. Two inferences that may be drawn from the results: i) 50% excess reducing agent was sufficient, ii) presence of hydrazine molecules in the solution had no significant hindering effect on deposition of metal ions on the support surface even when highly excess amount of hydrazine was used.

The metal loading of the N_2H_4/Pt-6 catalyst, prepared using hydrazine in the highest molar ratio of 1:6, was 1.9 wt% as obtained from EDX analysis (Table 2.1). This was comparable to that calculated from AAS (2.01 wt%). Presence of N_2 was not detected in any of the samples. Hence, even if any hydrazine was entrapped during deposition, it was removed during drying at ~110 °C as boiling point of hydrazine is 114 °C. The XRD profiles of the catalysts prepared in presence of different concentration of hydrazine were unaffected with the increase in hydrazine concentration as shown in the Figure 2.5b. No change in the peak intensities for the support and catalyst samples was observed and thereby suggested that the metal was in dispersed state.

2.3.2.3 Effect of sequence of reagent addition

The metal loading achieved by changing the sequence of addition of reducing agent and the metal precursor solution for the prepared catalysts is shown in the Table 2.1. The results showed that the metal loading was not affected too much by changing the sequence of addition of reagents. There was only a slight decrease in loading when metal precursor was added prior to the reducing agent in each cycle. It may be because when Pt precursor was added prior to hydrazine solution, hydrazine was the limiting reagent and reduction of platinum ion might have been hindered. On the contrary, when hydrazine was added prior to platinum solution, hydrazine was present in excess within the pores with respect to Pt ions. Consequently, an easy reduction and/or deposition of Pt^{2+} and/or Pt^0 was facilitated. Hence, introducing the reducing agent prior to the metal precursor to the porous substrate was favourable. The XRD profiles shown in Figure 2.5c confirmed that the deposited metal

was in well dispersed state on support surface even after changing the sequence of reagent addition, as no change in the intensity of the peaks was detected for both the catalysts.

2.3.2.4 Comparison of hydrazine and formaldehyde as reducing agents

In addition to hydrazine, the efficiency of formaldehyde as reducing agent was also studied. The molar ratio of formaldehyde to metal precursor solution was maintained at 50% excess, same as that used in case of hydrazine. All other conditions were also same as that used for hydrazine. The comparative results are shown in Table 2.1. Higher Pt loading was obtained on using hydrazine as the reducing agent in comparison to formaldehyde suggesting greater metal loss for latter. The hydrazine was thus better and more effective reducing agent than formaldehyde for platinum based catalysts. Table 2.1 shows that Pt loading obtained by EDX analysis was (2 wt%) comparable to that obtained by AAS analysis (2.02 wt%).

Figure 2.6 shows the TEM images of platinum catalysts prepared with varying synthesis parameters. It was observed that the metal particles were well dispersed in all the catalyst samples. The average particle size was lowest at 2.8 nm, when the precursor concentration was 500 ppm. It increased to 3.4 nm on increasing the precursor concentration to 3000 ppm. The lower cluster size of 3.1 nm was obtained when the N_2H_4 to Pt ratio was kept 6 compared to 3.4 nm when ratio was 1.5. The average metal cluster size was higher (4.2 nm) on depositing the Pt prior to hydrazine. Further, the Pt reduction by HCHO led to the highest average metal cluster size of 6.7 nm in comparison to reduction by hydrazine (3.4 nm) under similar conditions. Table 2.1 illustrates the corresponding metal dispersion for respective catalysts. The dispersion was calculated using the equation D=1.13/d, where d is the average metal particle size in nm as determined from TEM analysis [7]. Lower the metal size, higher was the dispersion of metal.

The above studies showed that all the synthesis parameters had a significant impact not only on the metal loading but also on metal cluster size. The metal loading increased with increase in metal precursor concentration with a slight metal loss at the highest precursor concentration. The 50% excess reducing agent was sufficient to facilitate reduction as well as considerable metal deposition. It was also observed that it was advantageous to introduce reducing agent prior to the metal solution to alumina support. The hydrazine was observed to be more effective than formaldehyde as a reducing agent. Effect of these parameters was also studied for alumina supported Pd catalysts and reported elsewhere [8]. The results

obtained for Pd/Al catalyst were almost similar. Pd metal loading increased linearly with concentration of Pd precursor solution. Loading increased with concentration of reducing agent up to N_2H_4/Pd molar ratio of 6, but decreased thereafter. The sequence of reagent addition affected the metal loading and it was favourable to pass the reducing agent prior to metal precursor. For Pd/Al catalyst, the study on effect of cycles of deposition showed that the percentage metal deposition was maximum after the first four cycles. The loading remained unaffected on increasing the deposition to six cycles and reduced on further increasing it to eight cycles.

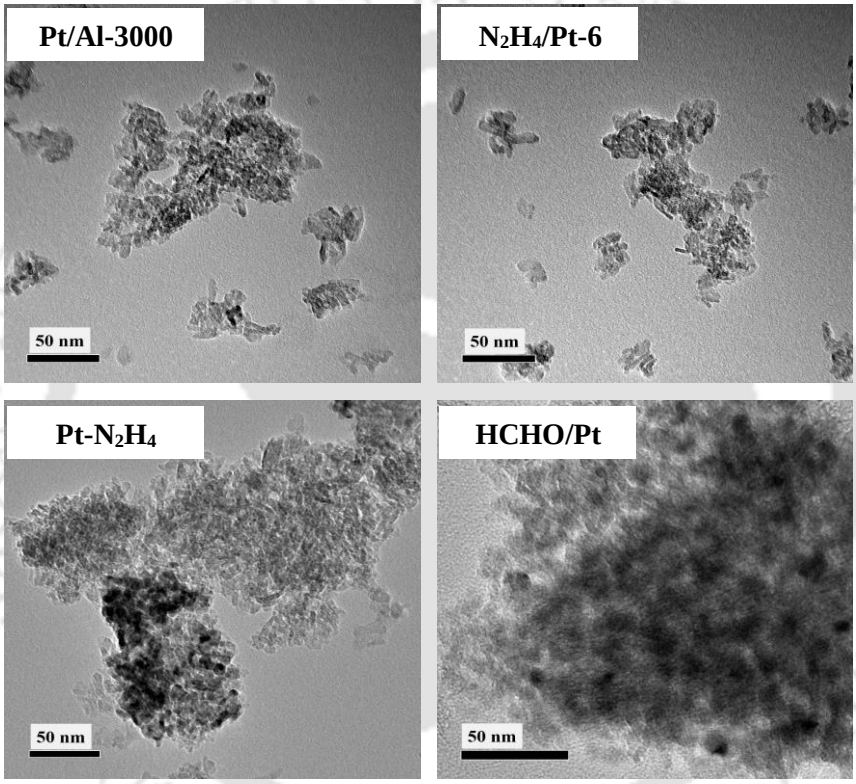

Figure 2.6. TEM images of Pt catalysts prepared by varying the synthesis parameters.

Based on the results discussed above, the Pt/Al was prepared at precursor concentration of 3000 ppm and Pd/Al at 1000 ppm corresponding to 112 μmoles of metal loading per gram of catalyst. The molar ratio of N_2H_4 to metal precursor was kept 1.5 and 0.75 for Pt/Al and Pd/Al respectively, which corresponded to 50% excess of reducing agent to metal precursor. The passage of reducing agent was done prior to Pt/Pd precursor in deposition cycles.

2.3.3 Comparison of catalysts synthesized by deposition and impregnation

The physicochemical properties of the monometallic catalysts prepared by electroless deposition and their performance for butane dehydrogenation reaction were determined and compared with that of prepared by conventional impregnation method. The comparative study was done to understand the effect of the modified preparation method on catalyst properties and their performance in reactions. The detailed analysis is presented in this section.

2.3.3.1 Effect on physicochemical properties

Table 2.2 compares the metal loading of monometallic Pt and Pd catalysts prepared by deposition and impregnation methods. For deposited catalysts, the loading of Pt/Al and Pd/Al were 2.08 and 1.13 wt%, respectively, by AAS. The EDX analysis also showed similar loading. For impregnated catalysts, loading by EDX were obtained as 2.5 and 1.4 wt%, respectively, for Pt/Al and Pd/Al. The slightly lower loading for deposited catalysts was due to slight loss of metal during deposition as discussed earlier.

Table 2.2. Metal loading obtained for monometallic catalysts prepared by different methods.

Catalysts	**Pt loading AAS** (wt%)	**Pd loading AAS** (wt%)	**Pt loading EDX** (wt%)	**Pd loading EDX** (wt%)
Pt/Al	2.08 (107)	--	2.1	--
Pd/Al	--	1.13 (106)	--	1.1
Pt/Al_WI	2.2 (112)	--	2.5	--
Pd/Al_WI	--	1.2 (112)	--	1.4

**Values in parenthesis represent the metal loading in μmoles g^{-1}*

Figure 2.7 shows the EDX mapping of Pt and Pd catalysts synthesized by electroless deposition and impregnation method. As shown by the images, the metal distribution was more uniform for both the catalysts prepared by electroless deposition method compared to that prepared by impregnation. In deposition method, the metal precursor was in dispersed state in solution and directly deposited on support in reduced state in presence of hydrazine. This might have resulted in less possibility of agglomeration of metals ions during deposition. However, in case of impregnated catalysts, impregnation of metal precursor was done in limited solvent condition followed by oxidation at higher

temperature. Both the steps might have resulted in more clustering of metal atoms on the support during preparation.

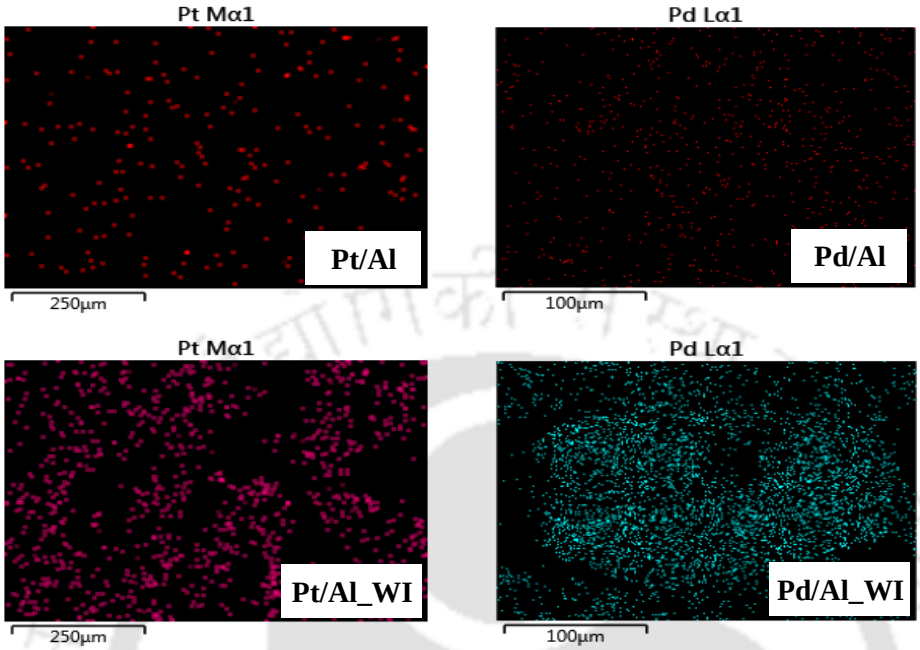

Figure 2.7. EDX mapping of monometallic catalysts prepared by different methods.

The core level XPS spectra of Pt (4f) and Pd (3d) region for monometallic Pt and Pd catalysts prepared by deposition and impregnation are shown in Figure 2.8. Table 2.3 illustrates the binding energies, oxidation states and the relative contents for both Pt and Pd metals in respective catalysts. For Pt/Al catalyst, the two peaks were obtained at 70.6 and 72.7 eV that corresponded to presence of metallic Pt^0 and oxidized Pt^{2+} species, respectively [9]. The Pd/Al catalyst showed two peaks at 335.1 and 336.3 eV in Pd $3d_{5/2}$ region corresponding to the presence of Pd^0 and Pd^{2+} species, respectively [10]. The concentration ratio of Pt^0/Pt^{2+} and Pd^0/Pd^{2+} in Pt/Al and Pd/Al was 70/30 and 64/36, respectively. The corresponding impregnated catalysts exhibited peaks at approximately similar position with a slight variation of 0.1 eV. However, the content of metallic Pt and Pd was significantly reduced in impregnated catalysts. The concentration ratio of Pt^0/Pt^{2+} and Pd^0/Pd^{2+} was 23/77 and 32/68 with dominance of oxidised state in impregnated catalysts. The dominant presence of oxidized state might have resulted due to final calcination step. Therefore, it can be concluded that electroless deposition facilitated reduction of the metal significantly as also evidenced by TPR analysis.

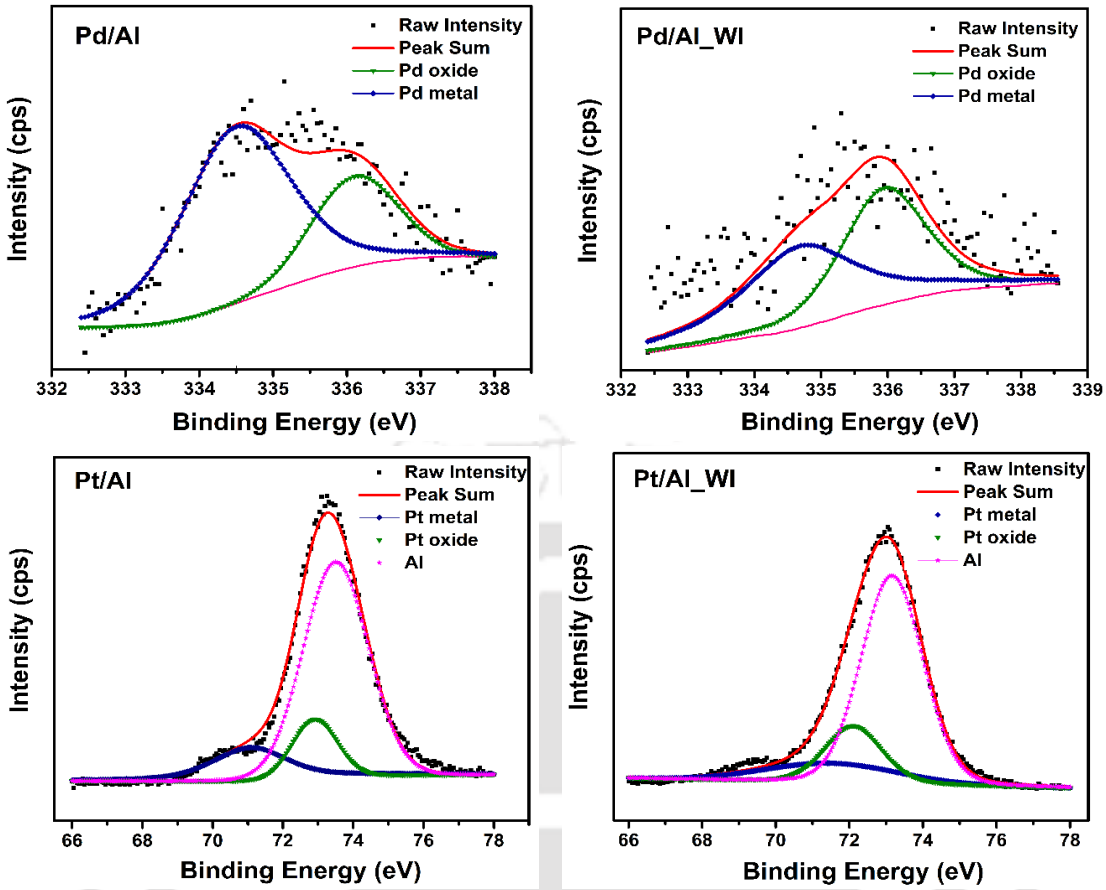

Figure 2.8. XPS spectra of Pd 3d region in Pd/Al and Pd/Al_WI; Pt 4f region in Pt/Al and Pt/Al_WI.

Table 2.3. Binding energy (B.E.) of Pd ($3d_{5/2}$) and Pt ($4f_{7/2}$), oxidation states and their relative contents in monometallic catalysts prepared by different methods.

Catalysts	Pd $3d_{5/2}$ B.E. (eV)	Pt $4f_{7/2}$ B.E. (eV)	Oxidation state	Relative content of respective metal (%)
Pt/Al	-	70.6	Pt^0	64
	-	72.7	Pt^{2+}	36
Pd/Al	335.1	-	Pd^0	70
	336.3	-	Pd^{2+}	30
Pt/Al_WI		70.7	Pt^0	23
		72.8	Pt^{2+}	77
Pd/Al_WI	335.1	-	Pd^0	32
	336.2	-	Pd^{2+}	68

The TPR profiles of the alumina support and the catalysts are presented in Figure 2.9. The alumina did not exhibit any significant reduction up to 550 ^oC. Beyond this temperature a very broad peak of very low intensity was observed. For all the catalysts, the reduction peaks were observed below 550 ^oC and hence, may be assigned to reduction of metal

oxides. For Pd, the reduction to metallic state occurs in single step from $Pd^{2+} \rightarrow Pd^{0}$ state, while for Pt, the reduction may occur in multiple steps: $Pt^{4+} \rightarrow Pt^{2+} \rightarrow Pt^{0}$ [11]. The presence of reduction peaks in the deposited monometallic catalysts may be explained as follows. Though the deposited catalyst were prepared in reducing environment in presence of hydrazine, the exposure to atmospheric conditions over time might had resulted in presence of fraction of both metals in oxidized state. The monometallic catalyst, Pd/Al exhibited three peaks centered at 90 °C, 160 °C and 340 °C followed by broad shoulder at 400-500 °C. The small reduction peaks appearing at lower temperatures of 90 and 160 °C corresponded to the reduction of the easily reducible palladium oxide crystallites having weaker interaction with the support [12]. The major and intense peak appearing at 340 °C can be assigned to the reduction of relatively small and stable oxide species that are in a stronger interaction with the support [13]. It is reported that higher the reduction temperature, stronger is the interaction between metal clusters and support [14]. The higher metal-support interaction stabilizes the nano clusters deposited on the support and inhibit them from re-grouping. The peaks were observed for Pt/Al at 196 and 345 °C. The higher reduction temperature of Pt oxide species suggested stronger interaction with the support. Pd/Al had a fraction of the Pd oxide nano clusters that were more strongly attached to support surface as observed by 400-500 °C shoulder.

When the corresponding Pt and Pd catalysts, having similar metal loadings, were prepared by impregnation method, the low-temperature reduction peaks in the impregnated catalysts shifted to a further lower temperature with respect to the corresponding deposited catalysts. The peak appeared at 185 °C for Pt/Al_WI catalyst. For Pd/Al_WI, a negative peak at 60 °C was observed that may be attributed to release of hydrogen due to decomposition of β-phase Pd hydride [15]. It is known that Pd can absorb hydrogen at room temperature to form palladium hydride [16]. The higher temperature reduction peak was observed in the temperature range of 300-500 °C for impregnated Pd/Al catalyst. The peak was broader for impregnated catalyst compared to that observed for deposited Pd catalyst. This suggested that impregnated catalyst exhibited wide particle size distribution as also evidenced by respective TEM histograms. Similarly, the reduction peak centered at 370 °C was broader for Pt/Al_WI catalyst in comparison to deposited Pt catalyst.

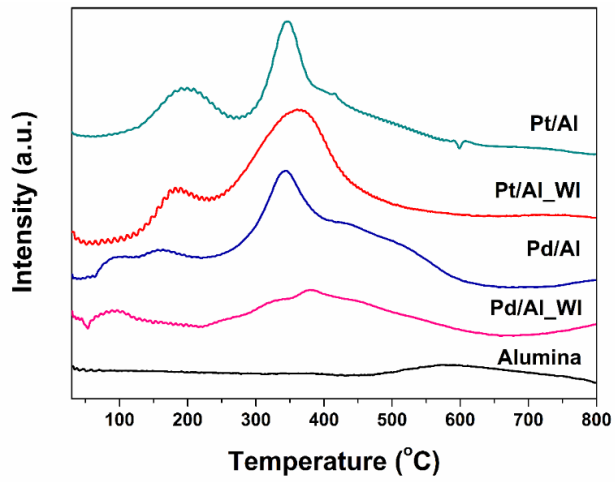

Figure 2.9. TPR profile of monometallic catalysts prepared by different methods.

The TEM images of the monometallic catalysts and their corresponding metal cluster size distributions are shown in Figure 2.10. The figure shows relatively homogeneous distributions of metal particles for catalysts prepared by deposition. The results agreed with that of the EDX mapping. The average metal cluster size for Pt/Al and Pd/Al catalysts, were 3.4 and 4.6 nm, respectively. The impregnated Pt and Pd catalysts exhibited a higher average particle sizes of 5.8 nm and 11.9 nm, respectively. Thus, the metal dispersion obtained for Pt/Al, Pd/Al, Pt/Al_WI and Pd/Al_WI catalysts was 33.2, 24.6, 19.5 and 9.5%, respectively. The lower average cluster size observed for deposited catalysts may be assigned to the fact that the metals were more in dispersed state during deposition. The in-situ reduction and deposition of metals in reduced state might have contributed in deposition of nano clusters. The strong interaction with the support might have further stabilized them.

For both preparation methods, the average cluster size for Pt was lower than that observed for Pd catalyst. Since the reduction potential of Pt is higher, Pt is expected to be reduced and deposited on the surface at a faster rate compared to that of Pd. This might have generated higher number of nucleation sites on surface in case of Pt deposition. Consequently, slightly lower growth of metal clusters was observed during deposition of Pt compared to that for Pd deposition.

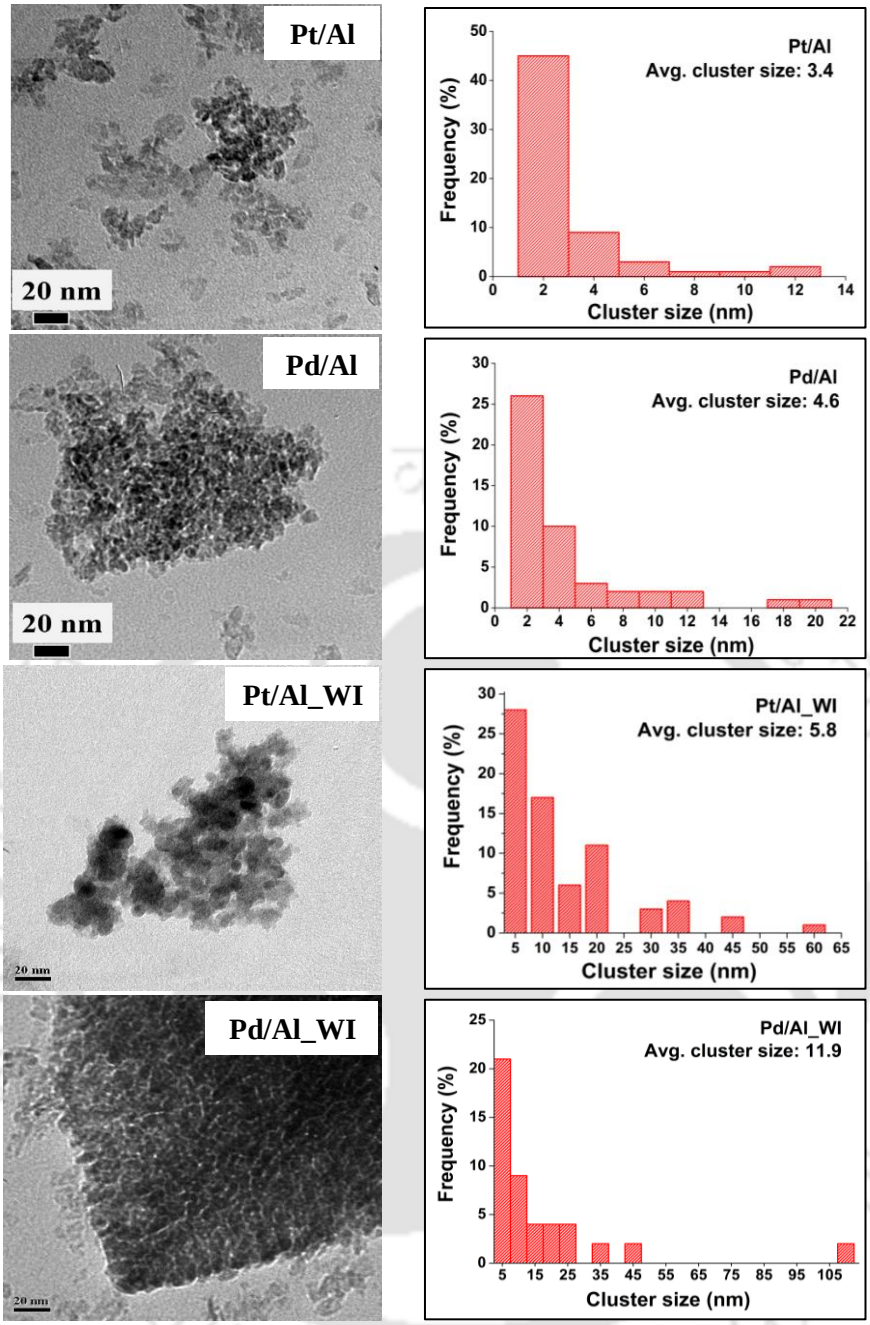

Figure 2.10. TEM images and metal size distribution of monometallic catalysts prepared by different methods.

Figure 2.11 shows the XRD profiles for the catalysts. Al_2O_3, used as support, exhibited peaks at 2θ values of 37.6°, 45.8° and 66.8° that corresponded to (311), (400) and (440) phases of γ-Al_2O_3 [5]. The peaks corresponding to Pd were expected at 40.15°, 46.15°, 68.19°, and the peaks for Pt at 39.7°, 47° and 68° [6,17]. Thus, the characteristics peaks corresponding to both metals were close to the peak positions of γ-Al_2O_3. For all the catalysts no significant variation in intensity or position of these peaks were observed

compared to that of the support. Hence, it can be suggested that metals were largely in dispersed state over the support for all the catalysts.

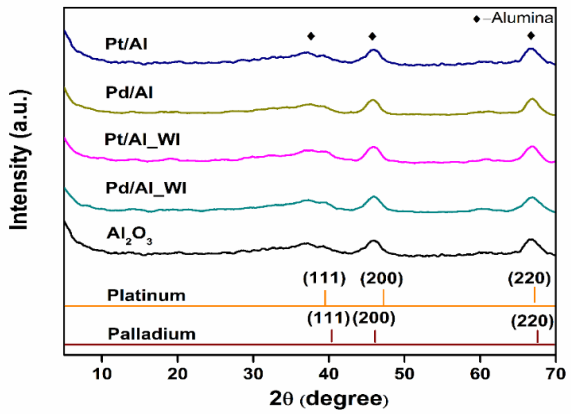

Figure 2.11. XRD profiles for monometallic catalysts prepared by different methods.

The presence of larger crystallites on support surface, if any, were lower in concentration and undetectable by XRD. The TEM analysis also showed that for deposited catalysts most of the metal clusters were below 4 nm, the detectable limit of XRD. For impregnated catalysts, though the fraction of larger clusters was higher than that of deposited catalysts, but still the total amount was lower than that can be detected by XRD [18].

2.3.3.2 Dehydrogenation study

Figure 2.12a illustrates the n-butane conversion obtained over all the monometallic catalysts in the temperature range of 100-600 °C. The time to achieve the steady state was around 8-10 min and total data collection time was approximately 150 min for procuring one data set of each catalyst. The conversion of n-butane steadily increased with an increase in the reaction temperature for all the catalysts. None of the catalyst showed conversion at 100 °C. The conversion picked up for the Pt/Al catalyst from 6.5% to 11.5% on raising the temperature from 200 to 450 °C. In the same temperature range for Pd/Al the conversion increased from 2.5 to 9.3%. Thus, Pt/Al catalyst exhibited higher activity in comparison to Pd/Al catalyst up to temperature of 500 °C. As the temperature increased, difference in activity diminished. At 550 °C, both the monometallic catalysts showed similar activity. Thereafter, the activity of Pt/Al started to decrease but that of Pd/Al continued to increase. The conversion was reduced from 18.4 at 550 °C to 16.3% at 600 °C for Pt/Al catalyst. In case of Pd/Al, the conversion of 17.9% at 550 °C increased to 21.1% at 600 °C. The results

showed that the Pd/Al catalyst was active at higher temperatures beyond 450 °C. This suggested that the energy barrier for dehydrogenation was higher on Pd sites compared to that on Pt sites. The higher energy barrier for Pd sites might have resulted from the lower interaction tendency of Pd towards hydrocarbons [19].

The impregnated Pd/Al_WI catalyst did not exhibit any conversion up to 300 °C however, the conversion increased significantly from 9.4% at 400 °C to 13.5% at 550 °C. On the contrary, Pt/Al showed 1-3% conversion at low temperature of 200-300 °C that increased sharply to 8.3% at 400 °C. Thereafter conversion steadily increased to 14.4% for Pt/Al_WI catalyst at 550 °C that decreased to 10% on raising the temperature to 600 °C. Likewise, the fall in conversion values from 14 to 11.9% at 600 °C was also observed for Pd/Al_WI catalyst. The overall conversion trend obtained at 550 °C was Pt/Al (18.4%) > Pd/Al (17.9%) > Pt/Al_WI (14.4%) > Pd/Al_WI (13.6%). The corresponding TOF obtained for all the catalysts followed the similar trend as: Pt/Al (0.44 s^{-1}) > Pd/Al (0.43 s^{-1}) > Pt/Al_WI (0.37 s^{-1}) > Pd/Al_WI (0.35 s^{-1}) at the reaction temperature of 550 °C.

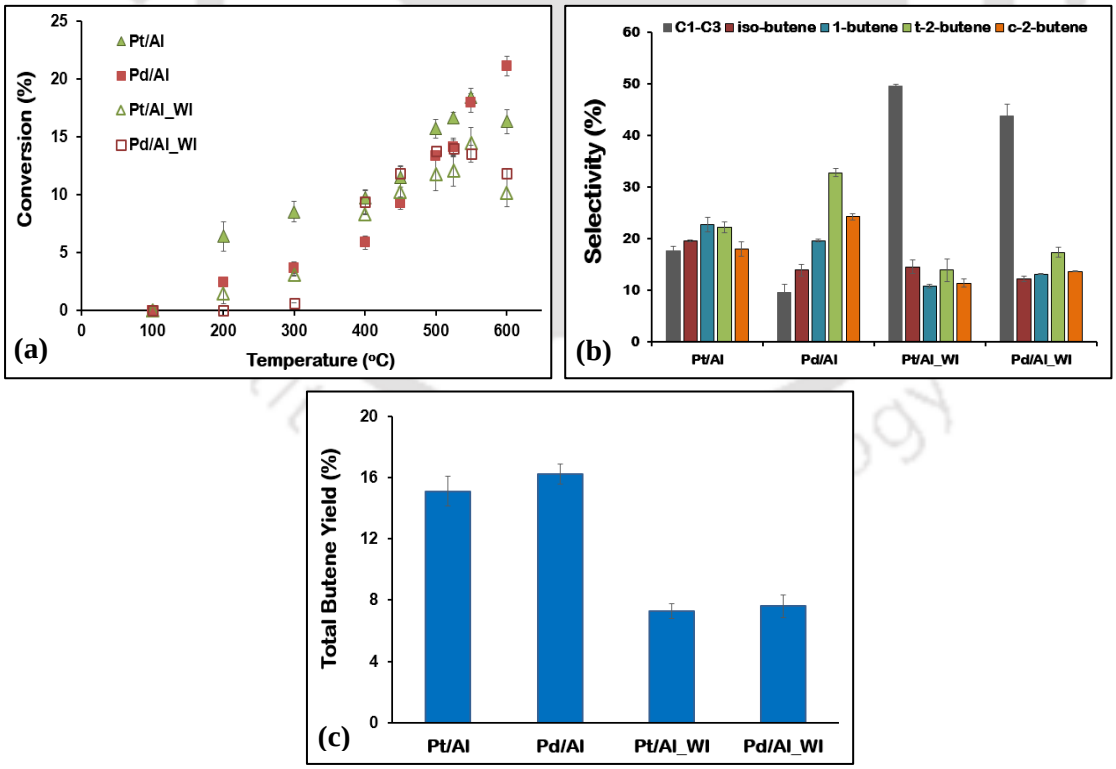

Figure 2.12. (a) Butane conversion profiles, (b) product distribution at 550 °C and (c) total butene yield at 550 °C obtained over monometallic catalysts prepared by different methods. Reaction conditions: Temperature = 100 - 600 °C, pressure = 1 atm, flow rate = 100 mL min^{-1} (C_4H_{10}:H_2:N_2 = 1:3:6), catalyst mass (W) = 0.25 g.

The TOF for other reported monometallic catalysts was observed to be in the range of 0.1 – 0.5 s^{-1}. Deng et al. (2018) reported the TOF value of 0.1 s^{-1} per total Pt at the start of catalytic run over monometallic Pt/SiO_2 catalyst for butane dehydrogenation. Further, Miguel et al. (2018) studied butane dehydrogenation over Pt/E-Mg-CN2 catalyst that gave a TOF value of 0.54 s^{-1}. In another work, Miguel et al. (2019) obtained a TOF value of 0.38 s^{-1} for dehydrogenation of butane over Sp-Zn-C supported monometallic Pt catalyst.

The overall selectivity towards the different products obtained over monometallic catalysts during n-butane dehydrogenation at 550 °C is summarized in Table 2.4. The lower hydrocarbons (C_1-C_3) were produced in addition to desired product of butenes. The C_1–C_3 compounds included methane, ethane, ethylene, propane, and propylene (Appendix G). For the deposited catalysts, Pd/Al exhibited higher selectivity towards overall butene formation (>90%) compared to Pt/Al (82%). The Pt/Al thus had a greater affinity towards the formation of C_1-C_3 products (18%) in comparison to that shown by Pd/Al catalyst (~9%). In comparison to deposited catalysts, impregnated catalysts exhibited considerably lower butene selectivity due to high selectivity towards cracked product formation. The impregnated Pt/Al_WI catalyst exhibited almost 50% selectivity towards C_1-C_3 products which was closely followed by Pd/Al_WI catalyst with 43.7% selectivity.

Table 2.4. Catalytic performance of monometallic catalysts for n-butane dehydrogenation [reaction temp. = 550 °C, gas ratio (n-butane:hydrogen:nitrogen) = 1:3:6].

Catalysts	Conversion (%)	TOF (s^{-1})	Selectivity (%)					
			Iso-butene	1-butene	T-2-butene	C-2-butene	Total Butene	C_1-C_3
Pt/Al	18.4	0.44	19.6	22.7	22.1	17.9	82.3	17.7
Pd/Al	17.9	0.43	13.9	19.6	32.8	24.2	90.5	9.5
Pt/Al_WI	14.4	0.37	14.5	10.7	13.9	11.4	50.5	49.5
Pd/Al_WI	13.5	0.35	12.2	13.2	17.3	13.6	56.3	43.7

For all the catalysts, all the isomers, iso-butene as well as cis and trans 2-butenes, were obtained. Figure 2.12b shows the selectivity of the butene isomers over all the catalysts at 550 °C. The Pt/Al showed higher selectivity for 1-butene, while Pd/Al showed higher selectivity for 2-butenes. Pt/Al catalyst showed 22.7% and 19.6% selectivity for 1-butene and isobutene respectively and the corresponding values were 19.6 and 13.9 % for Pd/Al. The Pd/Al catalyst exhibited 57% selectivity for 2 butenes (33% trans-2-butene and 24% cis-2-butenes) compared to 40% shown by Pt/Al catalyst (22% trans-2-butene and 18% cis-

2-butenes). A drastically reduced selectivity towards 2-butenes, 24% and 30% respectively, were obtained over Pt/Al_WI and Pd/Al_WI catalysts. Also, the 1-butene selectivity dropped to mere 10.7 and 13.2% for impregnated Pt and Pd catalysts, respectively.

The total butene yield was calculated for all the catalysts as product of conversion and selectivity (Eq. 2.8) and shown in Figure 2.12c. The deposited Pt and Pd catalysts exhibited higher butene yields of 15.1 and 16.2%, respectively, in comparison to corresponding impregnated Pt (7.3%) and Pd (7.6%) catalysts.

The Table 2.5 shows the initial conversion and final conversion of butane after 10 h of process time at 550 °C, over Pt and Pd catalysts. The deactivation parameter of the catalyst was calculated from initial and final conversion values of the catalyst (Eq. 2.9). The initial conversion corresponded to the point when temperature reached and stabilized at 550 °C. Thereafter, conversion of butane was determined for every one hour. All the monometallic catalysts suffered deactivation and lost their activity significantly by the end of 10 h, irrespective of the preparation method used. However, deposited catalysts were slightly more stable compared to impregnated monometallic catalysts. The corresponding percent deactivation calculated was as follows: Pd/Al (74%) > Pt/Al (75%) > Pd/Al_WI (79.5%) > Pt/Al_WI (81%). From the trend obtained, it can also be observed that the deactivation was slightly higher for Pt based catalysts compared to Pd catalysts for same preparation method.

Table 2.5. Deactivation data obtained for monometallic catalysts prepared by different methods.

Catalysts	Initial Conversion (%)	Final Conversion (%)	Deactivation (D%)
Pt/Al	19.7	4.9	75
Pd/Al	20.3	5.1	74
Pt/Al_WI	14.9	2.8	81
Pd/Al_WI	14.7	3.0	79.5

Hence, it can be concluded that catalysts prepared by deposition method were more active but inhibited the cracked product formation, thereby increasing the selectivity towards butene. As revealed by EDX mapping and TEM analysis, the low average particle size and hence enhanced metal dispersion in deposited catalysts might have resulted in their higher activity. The deposition method also facilitated reduction of metals on the support surface

and stronger metal-support interaction as evidenced by TPR and XPS analysis. These might have also contributed to its enhanced activity as well as stability during reaction.

Dehydrogenation was observed to be favoured by lower cluster size, while the higher cracking tendency in impregnated catalysts could be related with higher cluster size of the deposited metals. For a constant metal loading, when active metal was highly dispersed in a catalyst with lower metal cluster size, the availability of exposed support surface containing the stronger acid sites was comparatively less. Thus, the probability of formation of cracked products was reduced for catalysts with higher metal dispersion. Further, when the cluster size was larger, then the probability of interaction of primary products with additional neighbouring metal sites might have increased and contributed to occurrence of secondary reactions which led to formation of coke precursor compounds along with C_1-C_3 hydrocarbons, thereby reducing the butene selectivity [20]. The deactivation pattern obtained was closely related to the amount of coke formed during reaction. The coke deposition was in the range of 0.8 – 1.2 wt% for deposited catalysts, while it was significantly higher in the range of 2.5 – 4 wt% for impregnated catalysts. Thus, the coke deposition was slightly inhibited on the deposited catalysts with enhanced metal dispersion which led to higher activity and slightly improved stability in comparison to the impregnated catalysts.

2.4 Summary

This study showed that the preparation parameters of modified deposition method, such as metal precursor concentration, reducing agent concentration, reducing agent type etc., had significant effect not only on the metal loading but also on metal cluster size and hence on metal dispersion. The Pt loading on the catalysts increased from 0.37 to 2.12 wt% and average metal cluster size increased from 2.8 to 3.4 nm with the increase in metal precursor concentration from 500 to 3000 ppm. The use of 50% excess reducing agent was observed to be sufficient to facilitate reduction as well as considerable metal deposition. It was also observed that it was advantageous to introduce reducing agent prior to the metal solution to alumina support. The average metal cluster size was higher on depositing the Pt prior to hydrazine. The use of hydrazine as reducing agent gave higher metal deposition but lower metal cluster size compared to when formaldehyde was used as the reducing agent.

The average metal cluster size for Pt was lower than that of Pd irrespective of preparation method. The average metal cluster size for deposited catalysts was lower than corresponding catalysts prepared by impregnation. At lower temperature range Pt/Al showed higher activity while Pd/Al was more active at temperature above 550 ^{o}C. The overall conversion trend obtained at 550 °C was Pt/Al (18.4%) > Pd/Al (17.9%) > Pt/Al_WI (14.4%) > Pd/Al_WI (13.6%). The higher activity of Pt/Al catalyst may be explained by its higher metal dispersion. The Pd/Al exhibited higher selectivity towards overall butene formation (>90%) compared to Pt/Al (82%). The preferential formation of cracked products might have caused deactivation of Pt/Al at higher temperature. In comparison to deposited catalysts, impregnated catalysts exhibited higher selectivity (40-50 %) towards cracked product formation leading to their faster deactivation. The corresponding percent deactivation calculated was as follows: Pd/Al (74%) < Pt/Al (75%) < Pd/Al_WI (79.5%) < Pt/Al_WI (81%).

References

[1] K.D. Beard, M.T. Schaal, J.W. Van Zee, J.R. Monnier, Preparation of highly dispersed PEM fuel cell catalysts using electroless deposition methods, Appl. Catal. B Environ. 72 (2007) 262–271.

[2] K.D. Beard, J.W. Van Zee, J.R. Monnier, Preparation of carbon-supported Pt-Pd electrocatalysts with improved physical properties using electroless deposition methods, Appl. Catal. B Environ. 88 (2009) 185–193.

[3] M.T. Schaal, A.Y. Metcalf, J.H. Montoya, J.P. Wilkinson, C.C. Stork, C.T. Williams, J.R. Monnier, Hydrogenation of 3,4-epoxy-1-butene over Cu-Pd/SiO_2 catalysts prepared by electroless deposition, Catal. Today. 123 (2007) 142–150.

[4] M.T. Schaal, A.C. Pickerell, C.T. Williams, J.R. Monnier, Characterization and evaluation of Ag-Pt/SiO_2 catalysts prepared by electroless deposition, J. Catal. 254 (2008) 131–143.

[5] N. Salahudeen, A.S. Ahmed, A.H. Al-Muhtaseb, M. Dauda, S.M. Waziri, B.Y. Jibril, Synthesis of gamma alumina from Kankara kaolin using a novel technique, Appl. Clay Sci. 105–106 (2015) 170–177.

[6] Y. Feng, B. Huang, C. Yang, Q. Shao, X. Huang, Platinum porous nanosheets with high surface distortion and Pt utilization for enhanced oxygen reduction catalysis, Adv. Funct. Mater. 29 (2019) 1–10.

[7] S.R. de Miguel, I.M.J. Vilella, P. Zgolicz, S.A. Bocanegra, Bimetallic catalysts supported on novel spherical $MgAl_2O_4$-coated supports for dehydrogenation processes, Appl. Catal. A Gen. 567 (2018) 36–44.

[8] M Tech Thesis, Anand Vibhore, 2016, Department of Chemical Engineering, IIT Guwahati, India.

[9] S. Bhogeswararao, D. Srinivas, Catalytic conversion of furfural to industrial chemicals over supported Pt and Pd catalysts, J. Catal. 327 (2015) 65–77.

[10] A.K. Khudorozhkov, I.A. Chetyrin, A. V. Bukhtiyarov, I.P. Prosvirin, V.I. Bukhtiyarov, Propane Oxidation Over Pd/Al_2O_3: Kinetic and In Situ XPS Study, Top. Catal. 60 (2017) 190–197.

[11] J. Salmones, J.A. Wang, J.A. Galicia, G.Aguilar-Rios, H_2 reduction behaviors and catalytic performance of bimetallic tin-modified platinum catalyst for propane dehydrogenation, J. Mol. Catal. A-Chem. 184 (2002) 203–213.

[12] M. Radlik, A. Małolepszy, K. Matus, A. Śrębowata, W. Juszczyk, P. Dłużewski, Z. Karpiński, Alkane isomerization on highly reduced Pd/Al_2O_3 catalysts. The crucial role of Pd-Al species, Catal. Commun. 123 (2019) 17–22.

[13] S.K. Matam, E.H. Otal, M.H. Aguirre, A. Winkler, A. Ulrich, D. Rentsch, A. Weidenkaff, D. Ferri,

Thermal and chemical aging of model three-way catalyst Pd/Al_2O_3 and its impact on the conversion of CNG vehicle exhaust, Catal. Today. 184 (2012) 237–244.

[14] E. Merlen, P. Beccat, J.C. Bertolini, P. Delichère, N. Zanier, B. Didillon, Characterization of bimetallic $Pt\text{-}Sn/Al_2O_3$ catalysts: Relationship between particle size and structure, J. Catal. 159 (1996) 178–188.

[15] C. Amorim, M.A. Keane, Palladium supported on structured and nonstructured carbon: A consideration of Pd particle size and the nature of reactive hydrogen, J. Colloid Interface Sci. 322 (2008) 196-208.

[16] F. Pinna, F. Menegazzo, M. Signoretto, P. Canton, G. Fagherazzi, N. Pernicone, Consecutive hydrogenation of benzaldehyde over Pd catalysts: Influence of supports and sulfur poisoning, Appl. Catal. A Gen. 219 (2001) 195-200.

[17] L. Chen, J. Yan, Z. Tong, S. Yu, J. Tang, B. Ou, L. Yue, L. Tian, Nanofiber-like mesoporous alumina supported palladium nanoparticles as highly active catalyst for base-free oxidation of benzyl alcohol, Microporous Mesoporous Mater. 266 (2018) 126–131.

[18] J. Chen, Y. Wu, W. Hu, P. Qu, X. Liu, R. Yuan, L. Zhong, Y. Chen, Insights into the role of Pt on Pd catalyst stabilized by magnesia-alumina spinel on gama-alumina for lean methane combustion: Enhancement of hydrothermal stability, Mol. Catal. 496 (2020) 111185.

[19] M. Skotak, Z. Karpiński, C_6-alkane conversion over γ-alumina supported palladium and platinum catalysts, Chem. Eng. J. 90 (2002) 89–96.

[20] S.D. Jackson, S. Rugmini, Dehydrogenation of n-butane over vanadia catalysts supported on θ-alumina, J. Catal. 251 (2007) 59–68.

Chapter 3

SUPPORTED MONOMETALLIC CATALYSTS: EFFECT OF SURFACTANTS

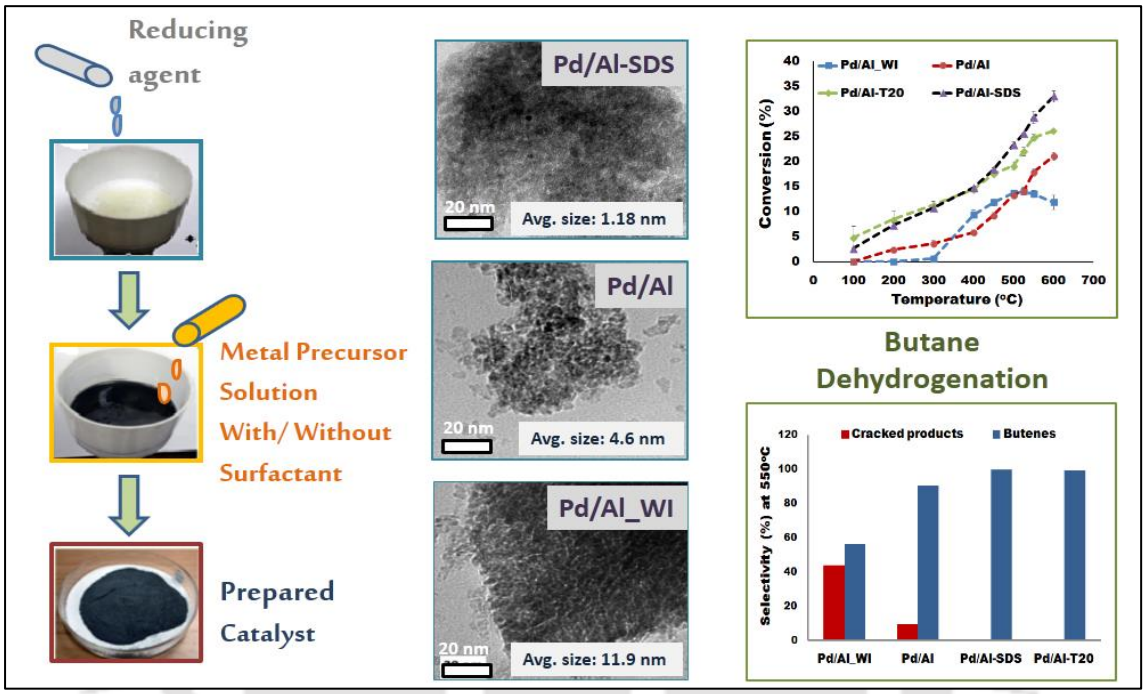

In this chapter, alumina supported palladium catalysts were prepared by modified electroless deposition in presence of surfactants and their performance was significantly improved compared to that prepared in absence of surfactants. Depending on the type of surfactant, loading and morphology of deposited palladium varied. Both anionic (Sodium dodecyl sulphate) and non-ionic (Tween 20) surfactants were observed to be most effective in dispersing the metals support surface. The conversion of butane and selectivity to butene was observed to be function of size of deposited Pd cluster.

Keywords

Surfactant assisted deposition; Palladium; Enhanced dispersion; Butane dehydrogenation

Chapter 3

3.1 Introduction

Electroless deposition as observed in Chapter 2 was very effective in preparation of well dispersed metal clusters on support surface compared to that of catalysts prepared by conventional impregnation process. The high metal dispersion for deposited catalysts resulted in comparatively higher catalytic activity to that of impregnated Pd catalysts. In this chapter, the effect of addition of surfactant as dispersing agent in metal precursor solution was investigated. The palladium was investigated as the base catalytic agent for n-butane dehydrogenation, as its precursor cost is lower than that of Pt. The surfactants were used to control the crystal growth of Pd clusters on support surface.

Surfactants are widely used in synthesis of structured metal nanoparticles by bulk reduction [1,2]. Shape directing and size limiting properties of different classes of surfactants during metal nanoparticle synthesis have been explored in multiple works [3,4]. Details have been discussed in Chapter 1. Coupling these properties of surfactants with an efficient metal particle deposition method can yield a highly dispersed catalyst.

In this study, the effects of different classes of surfactants on properties of deposited metal clusters on support surface have been investigated. The effect of anionic, cationic and non-ionic surfactants was studied using sodium dodecyl sulphate (SDS), cetyltrimethylammonium bromide (CTAB) and polyoxyethylene (20) sorbitan monolaurate (Tween 20), respectively. SDS consists of a 12-carbon tail attached to a sulphate group and the interaction of Pd cations with anionic head groups of SDS is likely to be highest as they both possess opposite charges. CTAB consists of a 16 carbon tail attached to a quaternary ammonium group which ionises by releasing a bromide counter ion in aqueous solution, resulting in a quaternary ammonium cation head group. However, in case of non-ionic surfactant Tween 20, palladium ions may interact with the surfactant monomer at multiple sites (carbonyl, ether and hydroxyl groups) unlike in case of SDS and CTAB (Figure A3, Appendix C). Details of the properties of used surfactant are given in Appendix C.

3.2 Experimental

3.2.1 Preparation of surfactant modified catalysts

Alumina was prepared from aluminium nitrate by precipitation as discussed in section 2.2.2 of Chapter 2. The Pd/Al_2O_3 catalysts were prepared with a target loading of 1.2 wt% by electroless deposition method using hydrazine as a reducing agent as discussed earlier in section 2.2.3 of Chapter 2. The surfactant modified Pd catalysts were also prepared by deposition method. The required amount of surfactant was directly added to 40 mL of metal precursor solution and stirred for 10 min. The mixture solution was used for subsequent deposition. The surfactant amount corresponded to CMC of respective surfactant as it gave highest metal dispersion as reported in earlier work done in our laboratory [5].

The effect of anionic, cationic and non-ionic surfactants was studied using Sodium dodecyl sulfate (SDS, Merck), Cetyl trimethylammonium bromide (CTAB, SRL) and Polyoxyethylene 20 sorbitan monolaurate (Tween 20, Merck), respectively. The deposited catalysts modified by SDS, Tween 20 and CTAB surfactant are referred to as $Pd/Al\text{-}S_1$, $Pd/Al\text{-}T_1$ and $Pd/Al\text{-}C_1$, respectively. The other steps were same as described for preparation of Pd/Al catalyst. To compare the performance of the catalysts prepared by deposition method in absence and presence of surfactant, a reference catalyst was prepared by conventional impregnation method with 1.2 wt% Pd metal loading as described in Chapter 2, section 2.2.3. The target loading of the impregnated catalyst was kept same to that prepared by deposition method. The catalyst prepared by conventional impregnation technique is referred as Pd/Al_WI in the text.

3.2.2 Catalyst characterization

The physicochemical properties of the prepared catalysts were determined using EDX analysis, BET surface area, Temperature Programmed Reduction (TPR), Transmission Electron Microscopy (TEM), X-ray Diffraction (XRD), FTIR spectroscopy, Temperature-programmed desorption (TPD) of ammonia. The details of the characterization methods are already discussed in section 2.2.4 in Chapter 2.

3.2.3 Dehydrogenation tests

The dehydrogenation of butane was performed in a fixed-bed down-flow using 0.25 g of catalyst. The temperature range was varied as 100 – 600 °C. The feed gas consisted of butane, hydrogen and nitrogen in a volumetric ratio of 1:3:6 introduced at a total flow rate of 100 mL min^{-1}. The experimental details are included in section 2.2.5 in Chapter 2.

3.3 Results and discussion

3.3.1 Effect on physicochemical properties

Table 3.1 shows the actual Pd loading of the catalysts prepared in absence and presence of different surfactants. The palladium loading was determined by EDX analysis and ranged between 0.9 - 1.1 wt% for the catalysts prepared in presence of surfactants.

Table 3.1. Physical properties of catalysts prepared with and without surfactants.

Catalysts	Pd loading[a] (wt%)	BET surface (m^2 g^{-1})	Pore volume (cc g^{-1})	Average pore (nm)
Pd/Al_WI	1.6	162	0.364	7.33
Pd/Al	1.3	173	0.315	6.00
Pd/Al-S_1	1.1	179	0.293	5.80
Pd/Al-T_1	1.1	175	0.276	5.57
Pd/Al-C_1	0.9	165	0.354	6.26

[a]*Pd loading was determined by EDX analysis*

The EDX spectra and EDX mapping of the catalysts synthesized by impregnation and surfactant assisted deposition method are included in Appendix D and E, respectively. On comparison of the images for Pd/Al-S_1 and Pd/Al_WI samples, higher agglomeration of metals can be observed for the latter. For Pd/Al-S_1, Pd metal was more uniformly distributed suggesting better dispersion of the metal over the surface. For samples prepared by surfactant assisted deposition, smaller metal ion clusters were deposited on the surface of the support due to interaction of the metal ions with the surfactant in the solution. This resulted in stronger interactions between support and the deposited metal, further stabilizing the nano metal clusters and increasing the final metal dispersion.

The nitrogen adsorption-desorption isotherms and pore size distributions of the support and the catalysts are compared in Figure 3.1. The N_2 adsorption-desorption isotherm of the

catalysts was similar to that of alumina irrespective of preparation method but with reduction in total volume of nitrogen adsorbed. Accordingly, surface area of all the catalysts was lower than that of the support. Pd/Al-S_1 catalyst exhibited the highest surface area of 179 m^2g^{-1} among all the catalysts followed by Pd/Al-T_1 (175 $m^2\ g^{-1}$) and Pd/Al (173 $m^2\ g^{-1}$). The other surfactant based catalyst Pd/Al-C_1 however exhibited a slightly lower surface area of 165 $m^2\ g^{-1}$. The catalyst prepared by impregnation method also had a lower surface area of 162 $m^2\ g^{-1}$. Table 3.1 summarizes the physical properties of the prepared catalysts.

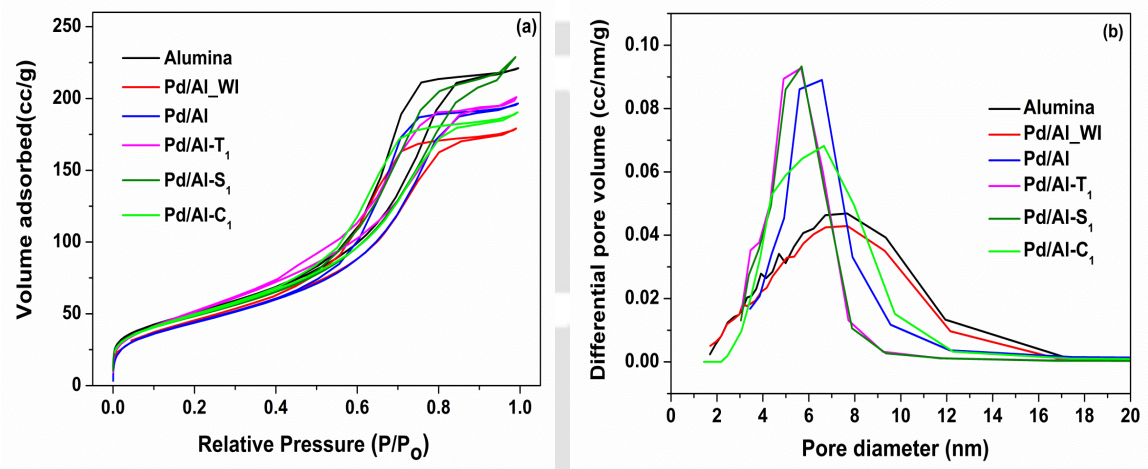

Figure 3.1. (a) Nitrogen adsorption-desorption isotherms and (b) BJH pore size distribution of Al_2O_3 support and catalysts prepared with and without surfactants.

For the support, the pore size was in the range of 2–17 nm. The catalysts showed a shift in pore size distribution with decrease in average pore size compared to that of Al_2O_3 support (7.7 nm). The Pd/Al and Pd/ Al-C_1 catalysts showed an average pore size of 6 and 6.3 nm, while average pore size of Pd/Al-T_1 and Pd/Al-S_1 was further lowered to 5.6 and 5.8 nm, respectively. No micropores were observed in any of the samples. The pore volume obtained for all the catalysts prepared by deposition method ranged between 0.28 and 0.35 cc g^{-1}. The impregnated Pd/Al_WI catalyst exhibited a broader pore size distribution and average pore diameter of 7.3 nm approximately similar to that of alumina support.

Figure 3.2 shows the TEM images of all the catalyst samples. All the images showed dispersed metals on the support. Darker part represented the metal clusters. As can be observed from the images, the metal distribution on the surface varied with the catalysts preparation method.

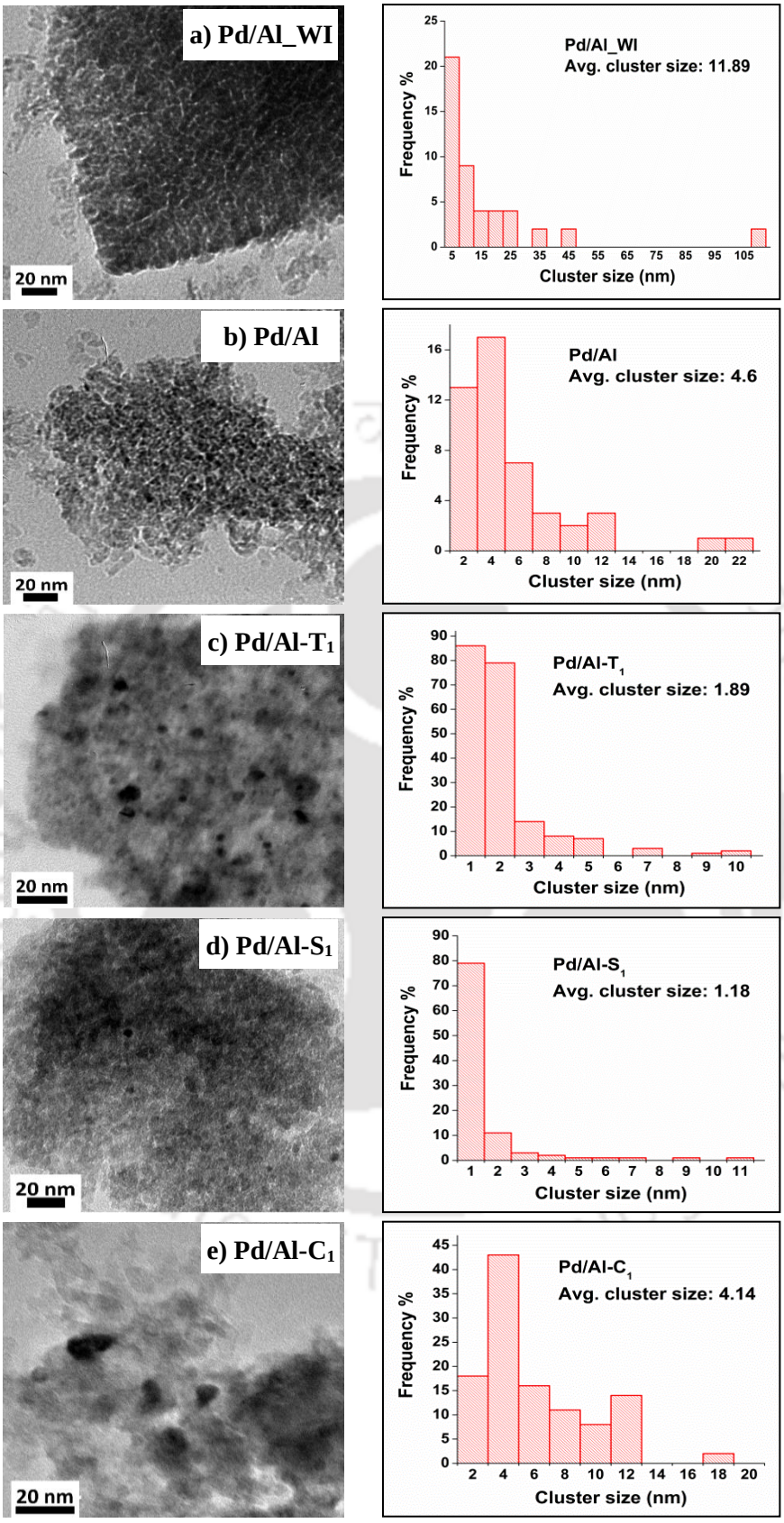

Figure 3.2. TEM images and metal size distribution of catalysts prepared by (a) impregnation; (b) electroless deposition in absence of surfactant and (c, d & e) presence of surfactant.

The corresponding size distribution of palladium metal clusters on catalyst surface was determined from TEM images using Image J software. The respective size distribution has been also included in Figure 3.2. The Pd/Al_WI catalyst prepared by impregnation showed the densest distribution of metals and accordingly had the highest average metal cluster size of 11.89 nm. All the catalysts prepared by electroless deposition method gave lower cluster size in comparison to impregnated catalyst. The use of surfactant was observed to further lower the average size of metal clusters. Catalyst Pd/Al, prepared by deposition gave an average cluster size of 4.6 nm while catalysts Pd/Al-T_1 and Pd/Al-S_1 prepared in presence of surfactant had an average cluster size of 1.89 and 1.18 nm, respectively. The catalyst prepared with CTAB surfactant exhibited an average cluster size of 4.14 nm. The corresponding dispersion of metals for the catalysts calculated from average cluster size are in the order of Pd/Al-S_1 (95.8%) > Pd/Al-T_1 (59.8%) > Pd/Al-C_1 (27.3%) > Pd/Al (24.6%) > Pd/Al_WI (9.5%).

These results agreed with the previous cluster size study in solution where SDS was observed to be the most efficient in dispersing Pd agglomerates in solution followed by Tween 20 [5]. This suggested that better dispersion in solution facilitated higher dispersion of deposited metal on the support. It was also observed in previous study that the CTAB surfactant failed to show any significant dispersion effect on agglomerates of metal ions in the solution [5]. Accordingly, minimal dispersion effect was observed on deposition of metal on support surface in presence of CTAB. The Pd/Al-C_1 showed an average metal cluster size close to that of Pd/Al catalyst. The significantly lower size of metal cluster for deposited catalyst compared to that of impregnated catalyst can be attributed to the preparation method which promoted metal dispersion as explained above.

Reduction in metal cluster size for catalysts prepared by surfactant assisted deposition method may be attributed to lowering of cluster size in metal precursor solution which facilitated deposition of lower metal entity on the surface. In addition, lowering of surface tension in presence of surfactant may have contributed to deposition of highly dispersed metal on the support. The lowering of surface tension with addition of surfactant facilitated lowering of metal cluster size on surface by either or combination of following phenomena: (1) increased substrate wettability (2) adsorption and growth inhibition of grains by surfactant monomers (3) restriction of electrochemical Ostwald ripening of deposited nanoparticles [6,7]. In case of a highly porous substrate like γ-alumina, efficiency of

deposition inside nano pores depends upon the wettability of substrate. Surface or interface tension of a liquid is inversely proportional to the concentration of surfactant in concentration ranges below critical micelle concentration (CMC) and stays constant beyond the CMC [8]. Hence, for the prepared catalysts the surface tension was close to the minimum, favouring rapid spreading of the precursor solution on the support. This ensured better and faster contact of metal with the substrate and further reduced the probability of agglomeration of particles on support surface. The lowering of surface tension also restricted electrochemical Ostwald ripening of deposited nanoparticles. Lower surface tension increased the stability of smaller nanoparticles [9].

The XRD patterns for the catalysts prepared using different surfactants are shown in Figure 3.3a. For none of the catalysts any variation in the peak intensity compared to γ-Al_2O_3 peaks was observed, neither any peaks due to Pd metal were detected in any of the profiles. This suggested that the deposited Pd metal was in a well dispersed state over the support and had not formed any detectable crystals as also observed and discussed in Chapter 2.

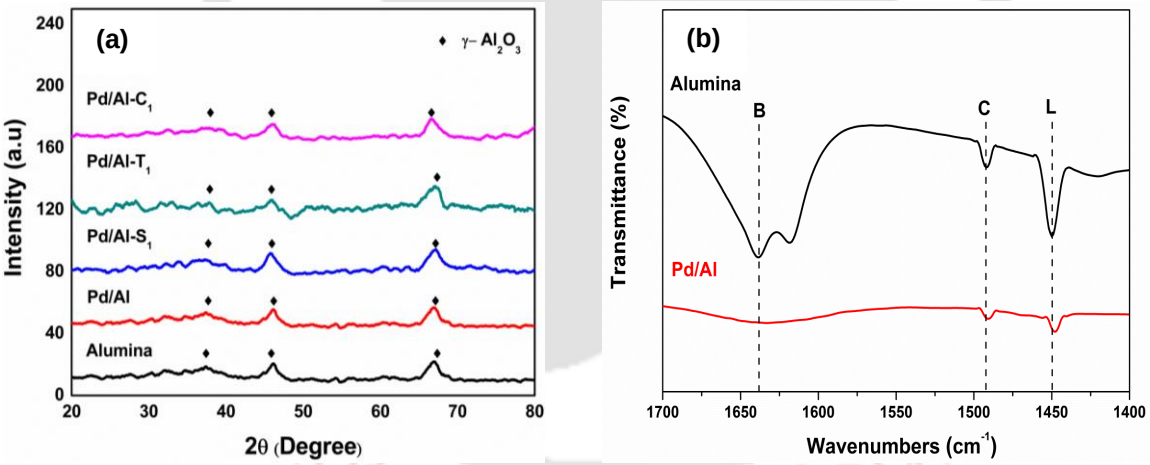

Figure 3.3. (a) XRD spectra of catalysts prepared in presence of different surfactants during electroless deposition; (b) FTIR spectra of alumina and Pd/Al catalyst after pyridine adsorption (L: Py bonded to Lewis acid sites; C: Coordinative bound pyridine; B: Py bonded to Brønsted acid sites).

The FT-IR spectra of support and Pd/Al catalyst after pyridine adsorption on acidic sites are shown in Figure 3.3b. Alumina exhibited high intensity peaks at 1450 and 1620 cm^{-1} that may be ascribed to pyridine coordinated to Lewis acid sites [10]. The peak appearing at 1637 cm^{-1} may be attributed to pyridine bound to Brønsted acid sites [11]. It can be observed that the intensity of both the peaks attributed to Lewis and Brønsted acid sites

decreased after the addition of metal. The decrease in the acidic sites may be attributed to the coverage or blocking of acidic sites due to deposition of metal on the alumina surface.

3.3.2 Dehydrogenation study

Figure 3.4a compares the conversion of n-butane over all the catalysts in the temperature range of 100 – 600 °C. The performance of conventionally impregnated catalyst Pd/Al_WI was also determined. The catalyst prepared by deposition method, Pd/Al exhibited conversion at temperature as low as 200 °C. Thereafter, conversion increased steadily with temperature and highest conversion was obtained as 21.1 % at 600 °C, the highest temperature studied. The corresponding turnover frequency was 0.51 s^{-1} that was calculated from total moles of reactant converted per mole of total metal per unit time.

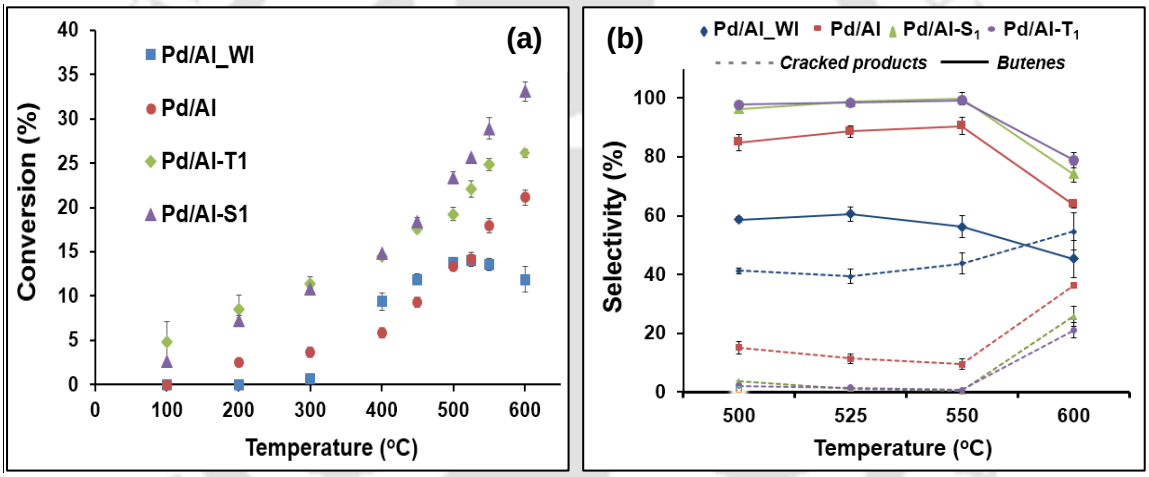

Figure 3.4. (a) Butane conversion (b) product selectivity at different temperatures for all catalysts.

When the catalysts were prepared in presence of surfactants, as in Pd/Al-S_1 and Pd/Al-T_1, both the catalysts showed higher activity compared to that of Pd/Al in entire temperature range studied. Conversion of 2-4% was observed even at 100 °C for catalysts prepared in presence of surfactant. The conversion for both the catalysts increased further with temperature maintaining the higher conversion compared to that of Pd/Al catalyst. The highest conversion of 33.1 % was observed for Pd/Al-S_1 followed by 26.2% for Pd/Al-T_1 at 600 °C. Thus, the anionic surfactant modified catalyst was more active compared to the catalyst prepared in presence of non-ionic surfactant. The effect was more prominent at higher temperature beyond 500 °C. In comparison, the

conventionally prepared Pd/Al_WI catalyst showed significant activity only after 300 °C. The activity picked up thereafter giving highest conversion of 14% at 525 °C. The conversion dropped to 12% on further increasing the temperature to 600 °C.

The results showed that in terms of conversion the catalyst prepared by electroless deposition showed better results compared to that by conventional impregnated catalyst. When surfactant was used during preparation of catalysts during electroless deposition the conversion was further improved drastically. Table 3.2 summarizes the catalytic activity of the catalysts in terms of conversion and turnover frequency at 550 °C. The activity in terms of the TOF values of the catalysts at 550 °C are in the order of Pd/Al-S_1 (0.79 s^{-1}) > Pd/Al-T_1 (0.64 s^{-1}) > Pd/Al (0.46 s^{-1}) > Pd/Al_WI (0.31 s^{-1}).

Table 3.2. Conversion and product selectivity for n-butane dehydrogenation over all catalysts [Reaction temperature: 550 °C, Feed ratio (n-butane:hydrogen:nitrogen) = 1:3:6].

Catalysts	Conversion (%)	TOF (s^{-1})	Selectivity (%)	
			C_1-C_3	Butenes
Pd/Al_WI	13.5	0.31	43.7	56.3
Pd/Al	17.9	0.46	9.5	90.5
Pd/Al-S_1	28.9	0.79	0.4	99.6
Pd/Al-T_1	24.8	0.64	0.7	99.3

The considerable enhancement in conversion achieved by catalysts synthesized employing anionic and non-ionic surfactants can be attributed to their enhanced metal dispersion as observed from their lower average size of metal cluster compared to that observed for Pd/Al catalyst, prepared without using surfactant. The plot of conversion as function of the size of the deposited metal clusters for different catalysts (Figure 3.5a) showed that conversion increased with decreasing metal cluster size. The Pd/Al-S_1 catalysts prepared in presence of anionic surfactant, having lowest metal cluster size of 1.18 nm, showed the highest activity followed by that of Pd/Al-T_1, which was prepared in presence of non-ionic surfactant with second lowest metal cluster size of 1.89 nm. The conventionally prepared catalyst Pd/Al_WI, with highest metal cluster size (11.9 nm), exhibited least activity. Similar results have been reported correlating the enhancement in conversion with better metal dispersion and decreasing particle size [12,13].

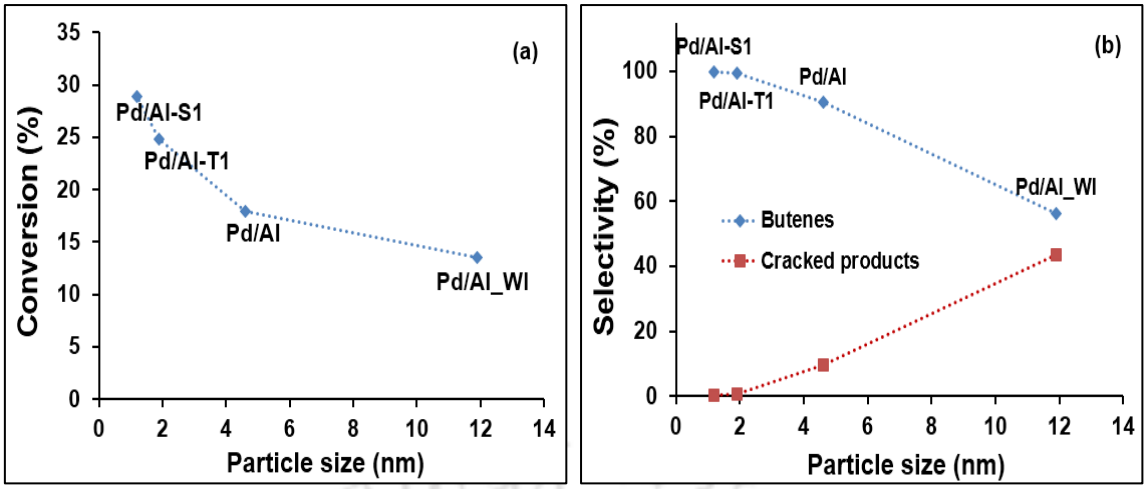

Figure 3.5. (a) Butane conversion and (b) product selectivity as a function of Pd particle size at 550 °C.

C_1-C_3 hydrocarbons and butenes were the main products obtained during the dehydrogenation reactions. The C_1-C_3 products included methane, ethane, ethylene, propane and propylene (Appendix G). These were reported to be produced by C-C bond cleavage [14]. Figure 3.4b shows the overall selectivity of the catalysts towards C_1-C_3 products and butenes in the temperature range of 500 – 600 °C. The Pd/Al catalyst showed high butene selectivity of ~90%. For catalysts synthesized using surfactant, the butene selectivity was further improved; Pd/Al-S_1 and Pd/Al-T_1 exhibited over 99% selectivity towards butenes with negligible formation of cracked products in the temperature range of 525-550 °C. In the same temperature range, the impregnated catalyst showed the lowest selectivity for butenes (56%) and the highest selectivity for C_1-C_3 products (44%). In the temperature range of 500 °C to 550 °C, there was only slight change in selectivity profiles for all the catalysts. However, at higher temperature of 600 °C selectivity of C_1-C_3 products increased significantly for all the catalysts with drop in selectivity of butenes. Higher temperatures have been reported to promote C-C cleavage and formation of corresponding C_1-C_3 products [15].

Comparing the selectivity of the catalysts, the cluster size of metal on the support also seemed to have played an important role on determining the selectivity patterns of products. The Figure 3.5b correlates the product selectivity of the catalysts at 550 °C with the metal cluster sizes on the support of different catalysts. Catalysts with higher cluster size of metal on support were observed to favour cracking whereas those with lower cluster sizes favoured dehydrogenation. At similar metal loading, for highly dispersed catalyst with

lower metal cluster size, there was less availability of exposed support surface containing the stronger acid sites that are reported to favour cracking [14]. Thereby, the probability of formation of C_1-C_3 products was reduced for catalysts with higher metal dispersion.

In addition, the larger metal cluster size might also have directly facilitated the secondary reactions leading to formation of coke precursors along with C_1-C_3 hydrocarbons, thereby again reducing the butene selectivity [16]. When the cluster size was larger, then the probability of interaction of primary products with additional neighbouring metal sites might have increased and contributed to occurrence of secondary reactions which led to formation of coke precursor compounds. At the same time, primary as well as secondary products forming at different stages may migrate to the exposed support surface, higher for larger metal cluster, and may undergo further condensation and polymerization reactions leading to coke deposition [16]. The secondary reactions leading to coke formation are promoted by stronger acidic sites of the supports in comparison to active metal sites [17].

Figure 3.6a illustrates the yield of different products obtained at 550 °C. The percentage yield obtained for the targeted products i.e. butenes was much higher for the catalysts prepared in presence of surfactant due to higher conversion and more than 99% selectivity (Table 3.2). Pd/Al-S_1 and Pd/Al-T_1 showed the maximum yield of 23% and 22%, respectively, at 550 °C. The Pd/Al catalyst prepared without presence of surfactant exhibited a lower yield of 16%. However, all the catalysts prepared by electroless deposition showed better yield in comparison to catalyst prepared by conventional impregnation method (7%). Lowest conversion and butene selectivity resulted in lowest yield of butenes for the impregnated catalyst.

The major problem associated with all the processes involving reactions of hydrocarbon is deactivation of catalyst. The deactivation mainly results from the deposition of coke or condensed products on the surface of the catalyst covering its active sites. The stability of the catalyst is measured in terms of conversion as a function of time on stream. For this study, the conversion was determined as function of time at 550 °C for 10 h as shown in Figure 3.6b. The deactivation parameter of the catalyst was calculated from initial and final conversion values of the catalyst as given by the Eq. 2.9 given in experimental section 2.2.5 of Chapter 2. The initial conversion corresponded to the point when temperature reached and stabilized at 550 °C, which took approximately 50 min from start of heating of the

catalysts. Thereafter, every one hour the products were analysed to calculate the conversion.

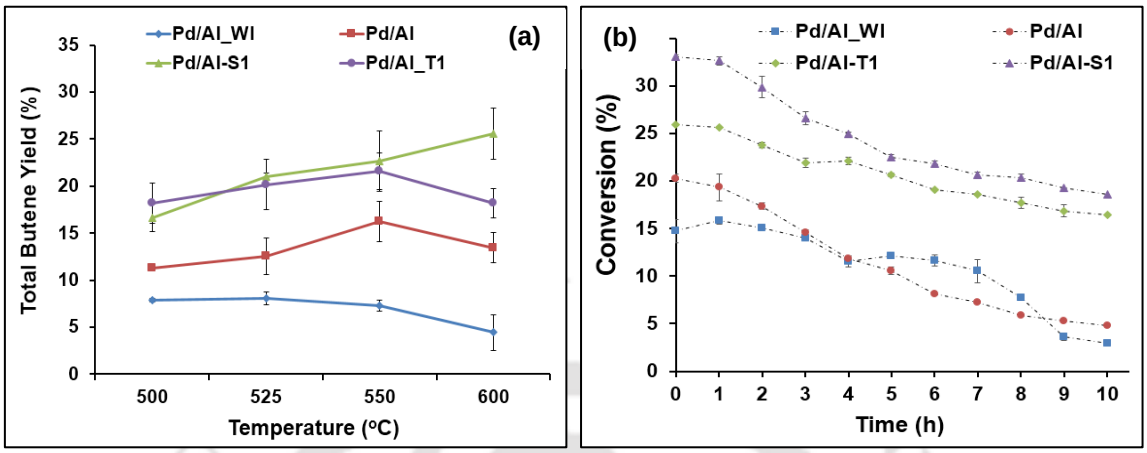

Figure 3.6. (a) Butene yield obtained at different temperatures and (b) Stability tests of different catalysts at 550 °C during butane dehydrogenation reaction.

The catalysts prepared in presence of surfactant exhibited greater stability in comparison to Pd/Al catalyst prepared in absence of surfactant. The Pd/Al-S_1 catalyst showed the higher activity compared to Pd/Al-T_1 over the entire range of time on stream. However, with respect to the initial activity, the drop in conversion was more for Pd/Al-S_1 catalyst compared to that for Pd/Al-T_1 catalyst. The Pd/Al-S_1 initially showed 33.1% conversion that reduced to 18.6% after 10 h whereas, Pd/Al-T_1 catalyst showed lower initial conversion value of 26% which dropped to 16.5% after 10 h of operation. This corresponded to 43.7 and 36% deactivation for Pd/Al-S_1 and Pd/Al-T_1 catalysts, respectively. The Pd/Al catalyst showed an initial conversion of 20% that reduced to 5% at the end of 10 h of operation. The Pd/Al_WI catalyst, prepared by impregnation method, lost its activity drastically from 15 to 3% conversion over same time period of 10 h. This corresponded to 80% overall deactivation for impregnated catalyst compared to 75% for Pd/Al catalyst prepared by deposition. Hence, the stability of the catalysts was improved when prepared by electroless deposition and was further enhanced by presence of surfactant during the process. The order of deactivation of the catalysts during butane conversion for 10 h reaction is: Pd/Al-T_1 (36%) > Pd/Al-S_1 (43.7%)> Pd/Al (75%) > Pd/Al_WI (80%).

As it has been discussed earlier, the cracking, polymerization and condensation reactions were responsible for formation and deposition of coke and condensed products leading to deactivation of the dehydrogenation catalysts [18]. The deactivation trend of the catalysts

agreed well with their product selectivity pattern as shown in the Figure 3.4b. The catalysts prepared in presence of surfactants, Pd/Al-T_1 and Pd/Al-S_1, which had the highest dispersion of the catalysts (thus lowest metal cluster size), exhibited the lowest selectivity towards C_1-C_3 hydrocarbons and highest stability or least deactivation. In contrast, impregnated catalyst, which had largest metal cluster size, showed the highest yield of cracked products and least stability.

The higher activity of anionic surfactant modified catalyst, Pd/Al-S_1, compared to the catalyst prepared in presence of non-ionic surfactant, Pd/Al-T_1, at higher temperature beyond 500 °C may be explained on basis of their metal cluster size and selectivity pattern. From Table 3.2, it can be observed that the selectivity of Pd/Al-T_1 was slightly higher for cracked products compared to that of Pd/Al-S_1. This can be explained based on the size effect of the metal cluster. The slightly higher cluster size for Pd/Al-T_1 catalyst compared to that of Pd/Al-S_1, as observed from TEM analysis, might have resulted in less coverage of surface acid sites for former, resulting in more cracked products as can be observed from Figure 3.4b. Since the highly endothermic cracking reactions are favoured more at higher temperatures, the effect of deactivation by cracking was observed mainly at higher temperatures resulting in lower activity for Pd/Al-T_1 compared to that of Pd/Al-S_1 catalyst. However, the difference in cluster size or selectivity was small hence the deactivation by cracking reactions was also small resulting in only slightly higher activity for Pd/Al-S_1 compared to that of Pd/Al-T_1 at higher temperature.

3.4 Summary

An efficient method of catalyst preparation was established involving modified electroless deposition of metal in presence of surfactant that increased metal dispersion on the porous support significantly. The presence of anionic (SDS) and non-ionic (Tween 20) surfactants during deposition resulted in the most effective reduction of size of metal clusters deposited on support surface. Average metal cluster size obtained for catalysts prepared by impregnation, deposition and surfactant assisted deposition method were 11.89, 4.6 and 1.18 nm, respectively. The catalysts prepared in presence of surfactant by deposition exhibited the highest catalytic activity. Pd/Al-S_1 catalyst with the highest metal dispersion showed the best catalytic performance with a conversion of 33% at 600 °C and 99.7% selectivity towards butenes at 550 °C, followed by Pd/Al-T_1 with 25% conversion and over

99% butene selectivity. The conversion and butene selectivity were observed to be function of deposited Pd cluster size. The conversion increased with the decreasing particle size. The SDS surfactant assisted prepared catalyst having the lowest metal size (1.18 nm) showed the highest activity while conventionally prepared catalyst with the highest metal particle size (11.89 nm) exhibited least activity. Catalysts with higher cluster sizes of Pd on support were observed to favour cracking whereas those with lower metal cluster sizes favoured butene formation. Thus, it can be concluded that surfactant assisted deposition method of catalyst preparation improved the performance of the catalysts.

References

[1] N.R. Jana, L. Gearheart,, C.J. Murphy, Seed-mediated growth approach for shape-controlled synthesis of spheroidal and rod-like gold nanoparticles using a surfactant template, Adv. Mater. 13 (2001) 1389–1393.

[2] K. Zielińska, A. Stankiewicz, I. Szczygieł, Electroless deposition of Ni-P-nano-ZrO_2 composite coatings in the presence of various types of surfactants, J. Colloid Interface Sci. 377 (2012) 362–367.

[3] C.J. Johnson, E. Dujardin, S.A. Davis, C.J. Murphy, S. Mann, Growth and form of gold nanorods prepared by seed-mediated, surfactant-directed synthesis, J. Mater. Chem. 12 (2002) 1765–1770.

[4] Z. Shervani, Y. Ikushima, M. Sato, H. Kawanami, Y. Hakuta, T. Yokoyama, T. Nagase, H. Kuneida, K. Aramaki, Morphology and size-controlled synthesis of silver nanoparticles in aqueous surfactant polymer solutions, Colloid Polym. Sci. 286 (2008) 403–410.

[5] M. Tech Thesis, Syam U.A., 2016, Department of Chemical Engineering, IIT Guwahati.

[6] V.M. Starov, Surfactant solutions and porous substrates: spreading and imbibition, Adv. Colloid Interface Sci. 111 (2004) 3–27.

[7] Z. Zhang, Z. Wang, S. He, C. Wang, M. Jin, Y. Yin, Redox reaction induced Ostwald ripening for size- and shape-focusing of palladium nanocrystals, Chem. Sci. 6 (2015) 5197–5203.

[8] M. Rosen, Relationship of structure properties in surfactants: II. Efficiency in surfaces or interfacial tension reduction, J. Am. Oil Chem. Soc. 51 (1974) 461–465.

[9] W.J. Plieth, Electrochemical properties of small clusters of metal atoms and their role in surface enhanced Raman scattering, J. Phys. Chem. 86 (1982) 3166–3170.

[10] O. Machynskyy, E. Kemnitz, Z. Karpiński, Aluminum fluoride-supported platinum and palladium as highly efficient catalysts of n-pentane hydroisomerization, ChemCatChem. 6 (2014) 592–602.

[11] M. Tamura, K.I. Shimizu, A. Satsuma, Comprehensive IR study on acid/base properties of metal oxides, Appl. Catal. A Gen. 433–434 (2012) 135–145.

[12] Z. Nawaz, F. Baksh, J. Zhu, F. Wei, Dehydrogenation of C_3-C_4 paraffin's to corresponding olefins over slit-SAPO-34 supported Pt-Sn-based novel catalyst, J. Ind. Eng. Chem. 19 (2013) 540–546.

[13] H. Seo, J.K. Lee, U.G. Hong, G. Park, Y. Yoo, J. Lee, H. Chang, I.K. Song, Direct dehydrogenation of n-butane over Pt/Sn/M/γ-Al_2O_3 catalysts: Effect of third metal (M) addition, Catal. Commun. 47 (2014) 22–27.

[14] B.M. Nagaraja, C.H. Shin, K.D. Jung, Selective and stable bimetallic PtSn/θ-Al_2O_3 catalyst for dehydrogenation of n-butane to n-butenes, Appl. Catal. A Gen. 467 (2013) 211–223.

[15] L. Rodríguez, D. Romero, D. Rodríguez, J. Sánchez, F. Domínguez, G. Arteaga, Dehydrogenation of n-butane over Pd-Ga/Al_2O_3 catalysts, Appl. Catal. A Gen. 373 (2010) 66–70.

[16] B.M. Nagaraja, H. Jung, D.R. Yang, K.D. Jung, Effect of potassium addition on bimetallic PtSn supported θ-Al_2O_3 catalyst for n-butane dehydrogenation to olefins, Catal. Today. 232 (2014) 40–52.

[17] B.Gu, S. He, X. Rong, Y. Shi, C. Sun, Dehydrogenation of i-butane over Tunable Mesoporous Alumina Supported Pt–Sn Catalys, Catal Letters. 146 (2016) 1415–1422.

[18] S.D. Jackson, S. Rugmini, Dehydrogenation of n-butane over vanadia catalysts supported on θ-alumina, J. Catal. 251 (2007) 59–68.

Chapter 4

SUPPORTED Pd CATALYSTS: EFFECT OF PROMOTERS

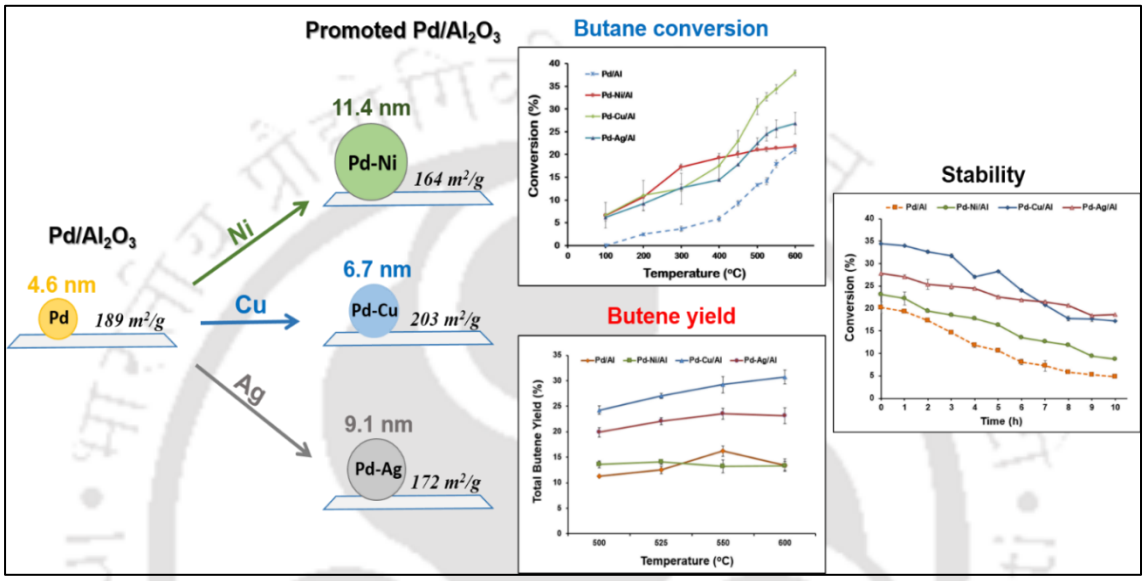

This chapter discusses the synthesis of Ni, Cu and Ag promoted palladium catalysts which were tested for butane dehydrogenation reactions. The catalysts were prepared by modified electroless co-deposition of metals on alumina support. The co-deposition of 10 mol% promoters along with palladium effectively increased the catalytic activity and butene yield. The extent of enhancement depended on type of the promoter metal. The effect of Cu content on Pd catalysts was also investigated by varying the copper loading as 5, 10 and 20 mol%.

Keywords

Supported palladium; Ni/Cu/Ag Promoter; Butane dehydrogenation

Chapter 4

4.1 Introduction

In previous chapters, monometallic Pd based catalysts showed better butene selectivity and stability during butane dehydrogenation. To further increase the efficiency of Pd catalysts, the effect of addition of promoters was investigated. It has been reported that on addition of promoter, the resultant alloy or inter-metallic species exhibited superior catalytic activity in comparison to the monometallic catalysts [1]. The promoters suppress metal sintering and inhibit side reactions such as coking or hydrogenolysis [2]. The effects of promoters such as Sn (most widely used), Zn, K, Pb or In have been investigated but mainly with Pt based catalysts [3-6]. Limited studies have been also reported on Ni, Cu, or Ag as promoters in dehydrogenation process [2,7-9]. Copper was reported to have a geometric effect on Pt thus leading to high selectivity during dehydrogenation. Ma et al. [2] reported that the incorporation of Cu to Pt increased the propene selectivity from 61 to 96% at 20% propane conversion. Lee et al. [7] demonstrated that the Cu addition to Pt catalyst led to significant improvement in selectivity from 40 to 73% thereby, enhancing the propene yield. Simultaneously, the catalyst deactivation was also decreased as copper addition reduced the acid sites. Kurokawa et al. [9] reported that the presence of Ag as a promoter in the Pt/Al_2O_3 catalyst increased the conversion from 28 to 50% with enhancement in product selectivity to 78% during butane dehydrogenation. The details of studies reporting employment of Ni, Cu or Ag as promoter or secondary metal for Pt/Pd catalysts in dehydrogenation processes are summarized in Table 4.1.

Pd based catalysts have been employed for propane dehydrogenation, where addition of Sn improved the initial selectivity to 61% as well as catalytic stability in comparison to monometallic Pd (15%) [10]. Rodriguez et al. [11] studied butane dehydrogenation over Pd and Pd-Ga catalysts. The addition of Ga promoter in high amounts was found to enhance dehydrogenation activity and selectivity (>98%) compared to that of Pd catalyst alone (75%). The promoters thus played an important role in increasing butene selectivity and suppressing coke formation by exhibiting electronic and geometric effects on the metal active sites. In this chapter, the supported Pd catalyst was modified using a promoter. The Cu, Ni or Ag were selected as promoters to be added in 10 mol%. The promoter metals were selected based on their importance in promoting dehydrogenation reactions [2,9,12]. The catalysts were prepared by deposition method for better metal dispersion as observed in earlier chapters.

Table 4.1. Reported studies on catalytic performance for dehydrogenation reactions over Ni, Cu or Ag promoted Pt/Pd catalysts.

S. No.	Catalyst samples and composition	Feed	Feed composition and Flow rate (mL min^{-1})	Reaction Temp (°C)	Conversion (%)	Selectivity (%)	Yield[a] (%)	Reference
1	PtCu/silica *Cu (1.6), Pt (0.7)*	Propane	$N_2/H_2/C_3H_8$ 100	550	20	96	19.2	[2]
2	PtCu/γ-Al_2O_3 *Cu (5), Pt (1.5)*	Propane	$N_2/H_2/C_3H_8$ 100	600	42	73	30.6	[7]
3	Pt-Cu/BN sheet *Cu (1), Pt (0.01)*	Propane	$N_2/H_2/C_3H_8$ 20	520	15	99	14.9[a]	[8]
4	PtAg/Al_2O_3 *Ag (4) Pt (1.1)*	Butane	$He/H_2/C_4H_{10}$ 99	550	38	82	31.1[a]	[9]
5	PdSn/Al_2O_3 *Sn (0.08), Pt (0.34)*	Propane	H_2/C_3H_8 85	500	10.5	61.3	6.43[a]	[10]
6	**Pd-Cu_{20}/Al** ***Cu (0.3), Pd (1.2)***	**Butane**	**$N_2/H_2/C_4H_{10}$** **100**	**550**	**37.1**	**86.5**	**32.1**	**[Present study]**

[a]*Yield determined as a product of conversion and selectivity*

4.2 Experimental

4.2.1 Catalyst preparation

The supported palladium catalyst was prepared with a target metal loading of 1.2 wt% Pd corresponding to 112.8 µmoles of metal per gram of catalyst. The Pd catalyst was synthesized using a modified electroless deposition method as described in section 2.2.3 of Chapter 2.

a) Promoted catalysts

The alumina support and the promoted catalysts were prepared by steps similar to that described in Chapter 2. The total metal loading for promoted catalysts was kept same as that in Pd/Al catalyst. The Pd loading was kept 90 mol% with 10 mol% promoter loading. In this case, separate aqueous solutions of metal precursors were prepared. Required amounts of palladium metal precursor ($PdCl_2$, 99% Sigma-Aldrich) was dissolved in 20 mL water. The precursor of promoters such as nickel nitrate ($Ni(NO_3)_2$, Merck), copper nitrate trihydrate ($Cu(NO_3)_2.3H_2O$, Merck) or silver nitrate ($AgNO_3$, ACS reagent 99%, Sigma Aldrich) were dissolved in 20 mL water each. Initially, 20 mL of respective promoter solution was mixed with 20 mL of Pd precursor solution. The resulting 40 mL mixture solution containing of Pd and promoter metal precursors was used for co-deposition on alumina in four cycles along with 40 mL hydrazine in cyclic patterns. The steps for Cu promoted catalyst preparation are shown in Figure 4.1. Similar procedure was adapted for preparation of Ni and Ag promoted Pd catalysts.

The promoted catalysts are referred as Pd-Ni/Al, Pd-Cu/Al and Pd-Ag/Al in this chapter. Except for Pd-Ni/Al, for all other catalysts the entire deposition was carried out at room temperature. For Pd-Ni/Al catalyst, involving deposition of Ni, the process was carried out at a higher temperature of 80 °C to facilitate Ni reduction. In order to determine the effective reduction temperature for Ni, the temperature was raised at an interval of 5 °C starting from room temperature. The characteristic colour change from pale green to grey pertaining to metal reduction was obtained at 80 °C [13]. Hence, the electrodeposition for Pd-Ni/Al catalyst was carried out at 80 °C. Most of the studies using hydrazine as reducing agent for reduction of Ni have reported the reduction temperature in the range of 60-80 °C [14,15].

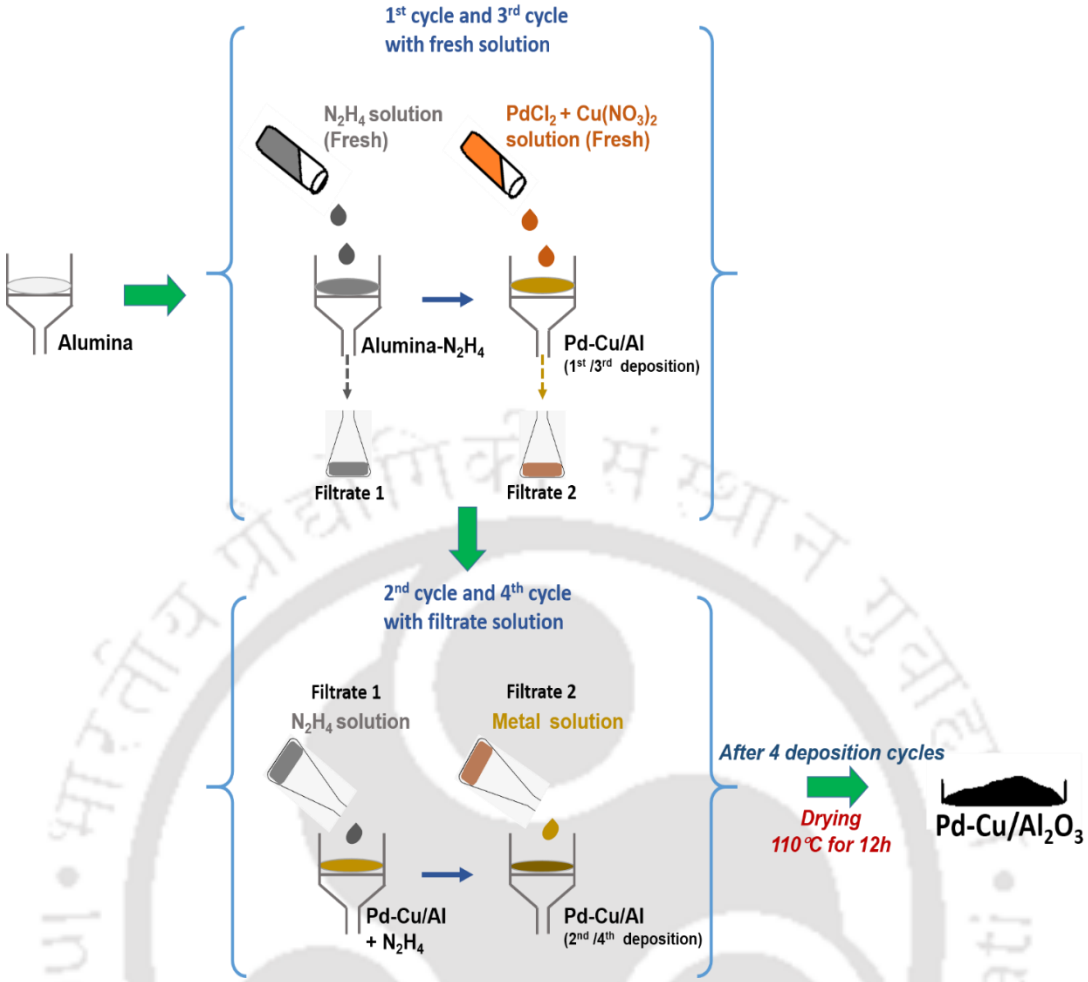

Figure 4.1. Schematic for steps involved in preparation of promoted catalyst by modified electroless deposition method.

In addition, the effect of promoter content on catalytic performance was evaluated by varying the copper content in Pd-Cu/Al catalyst. Catalysts with 5 and 20 mol% copper content were prepared in addition to 10 mol%. The corresponding catalysts were represented as Pd-Cu_5/Al, Pd-Cu_{10}/Al and Pd-Cu_{20}/Al corresponding to amount of copper. The Pd-Cu/Al and Pd-Cu_{10}/Al mentioned in the text are essentially the same catalyst, containing 10 mol% copper, represented by two different nomenclatures in two sections for better clarity.

b) Reference catalysts

The monometallic catalysts of promoting metals, Ni, Cu or Ag, were also prepared using modified deposition method for reference purpose. The preparation steps were similar to that used for preparations of Pd/Al catalysts. The targeted metal loading for reference

catalysts in terms of moles was same as that of monometallic Pd/Al catalyst. The reference catalysts are further referred as Ni/Al, Cu/Al and Ag/Al. For nickel, the deposition was carried out at 80 °C, as mentioned earlier.

4.2.2 Catalyst characterization

The promoted catalysts were characterized using techniques such as EDX, BET surface area, XPS, TPR, XRD, TEM and FTIR spectroscopy using pyridine as probe molecule. The details of characterization methods employed are included in section 2.2.4 in Chapter 2.

4.2.3 Dehydrogenation tests

The n-butane dehydrogenation was carried out in a fixed-bed down flow reactor in the temperature range of 100 – 600 °C using 0.25 g catalyst. The feed gas mixture, containing n-butane, H_2 and N_2 gases in the ratio of 1:3:6, was introduced to the reactor with a total flow rate of 100 mL min^{-1}. The details are included in section 2.2.5 in Chapter 2.

4.3 Results and discussion

4.3.1 Effect of different promoters

The composition for the promoted catalysts as obtained by EDX is shown in Table 4.2. The palladium loading for Pd/Al was 2.76 at% (1.1 wt%). For promoted catalysts, palladium loadings were in the range 2.3 – 2.6 at% (~ 1 – 1.1 wt%) and the promoter metal loading was in range of 0.2 – 0.25 at% (0.1 to 0.3 wt%). The corresponding wt% differed in the range due to their different atomic weights. Thus, total metal loadings in promoted catalysts varied in the range of 2.5 – 2.9 at% close to metal loading for monometallic Pd/Al catalyst. The corresponding EDX spectra obtained for all the promoted catalysts are included in Appendix D. The composition analysis showed that for the catalysts, co-deposition of the Pd metal did not seem to have been affected by the presence of precursor of promoter metal in the solution and vice versa.

The elemental composition of the reference catalysts was determined by EDX analysis. Ni/Al, Cu/Al and Ag/Al exhibited loading of 1.9, 2.4 and 2.2 at% that corresponded to 0.6, 0.7 and 1.1 wt% loading, respectively. As stated earlier, for the reference catalysts the targeted metal loading in terms of moles was same as that of monometallic Pd/Al catalyst.

The metal loading for reference catalysts was slightly lower than that of Pd/Al having 2.8 at% loading. The lower loadings can be explained based on lower reduction potentials of promoter metals compared to that of palladium. Lower reduction potential of the promoter metals might have caused hindrance in their deposition on the support surface in a reduced state. The order of their reduction potential values is Ni (- 0.26) < Cu (0.34) < Ag (0.80) < Pd (0.91). For Ni, the lowest reduction potential might had caused difficulty in its reduction and deposition and higher temperature was required for the same [16]. The difficulty in reduction of Ni precursor by hydrazine might have also resulted from its tendency to form complex with hydrazine at a faster rate than reduction [13]. The higher temperature may had facilitated both breaking of complexes and reduction reaction. This difficulty in reduction of nickel ion precursors might had resulted in lowest metal loading for Ni/Al among the reference catalysts.

Table 4.2. Metal loadings obtained over promoted Pd catalysts.

Catalysts	**Loading** (at%) (EDX)	
	Palladium	Promoter
Alumina	--	--
Pd/Al	2.76 (1.1)*	--
Pd-Ni/Al	2.50 (1.0)	0.25 (0.3)
Pd-Cu/Al	2.62 (1.0)	0.27 (0.1)
Pd-Ag/Al	2.30 (1.1)	0.24 (0.4)

** Values in parenthesis corresponds to metal loading in wt%*

The nitrogen adsorption-desorption isotherms and pore size distributions of the support and catalysts are compared in Figure 4.2a and b, respectively. All the catalysts exhibited type IV isotherm with H2 type hysteresis loop, similar to that observed for the support alumina [17]. As can be observed from the figure, the nitrogen adsorption decreased on addition of metals. The extent of decrease depended on type of promoter metal. It was lowest for Pd-Ni/Al catalyst. Accordingly, the surface area and pore volume were also lowest for this catalyst, 164 m^2 g^{-1} and 0.273 cc g^{-1} (Table 4.3), respectively.

The sintering tendency of nickel metal might had caused the highest extent of blockage of the pores resulting in lowest surface area and pore volume for Pd-Ni/Al. The Pd-Cu/Al catalyst on the other hand, exhibited highest surface area of 203 m^2 g^{-1} among all the catalysts. The lower atomic size of Cu compared to that of Pd and Ag might have resulted

in lesser blockage of pores. This was also reflected in highest pore volume for the Pd-Cu/Al catalyst, 0.314 cc g^{-1}.

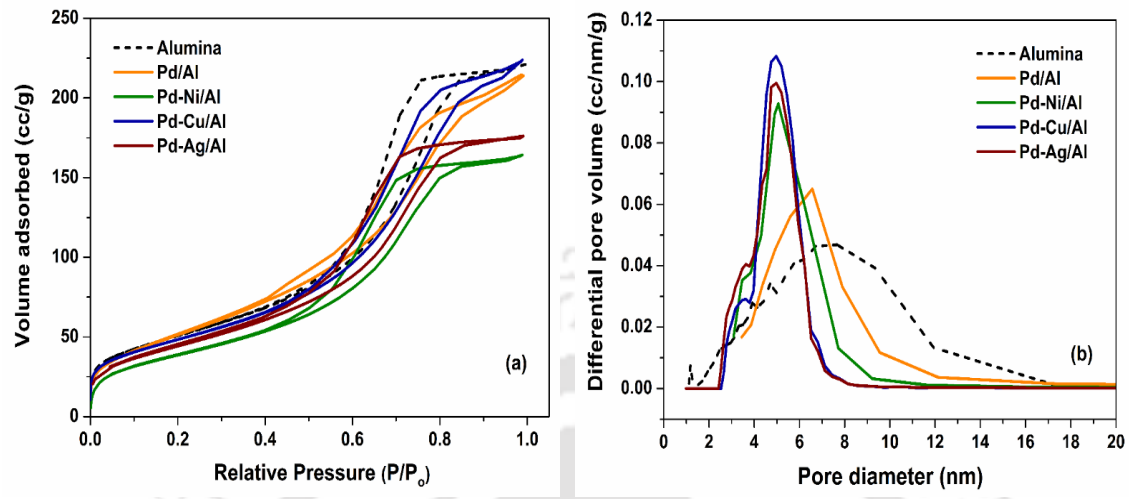

Figure 4.2. Physical properties of support and catalysts (a) nitrogen adsorption-desorption isotherms and (b) pore size distribution.

This trend agreed well with the surface area and pore volume values obtained for the reference catalysts (Table 4.3). The reference sample of Cu/Al showed the highest surface area of 181 $m^2 g^{-1}$ followed by Ag/Al (178 $m^2 g^{-1}$). The lowest surface area of 124 $m^2 g^{-1}$ was observed for Ni/Al catalyst in spite of lowest metal loading among the reference catalysts. This result agreed with the higher sintering tendency of Ni metal which might had further increased in Ni/Al in absence of any other co-metal such as Pd. The higher sintering tendency of Ni was also confirmed by larger size of metal clusters observed in TEM images for both Ni/Al and Pd-Ni/Al catalysts as discussed later.

The doping of metals resulted in a narrowing of pore size distribution and average pore size for all the catalysts compared to that of support (Figure 4.2b). The Pd/Al catalyst exhibited a pore size distribution in the range of 3 – 12 nm with an average pore diameter of 6.4 nm. Addition of promoter metal further narrowed the pore size distribution. The Pd-Cu/Al and Pd-Ag/Al showed pores in the range of 3 – 7 nm while Pd-Ni/Al showed a little broader pore range of 3 – 9 nm. The average pore size was ~ 5 nm for all the promoted catalysts. The reference catalysts Cu/Al and Ag/Al showed similar pore size distribution in the range 5 – 6 nm (Figure 4.3). The Ni/Al showed slightly wider pore size distribution (3 – 8 nm). No micropores were observed in any of the samples. The pore volumes for the promoted as well as reference catalysts ranged between 0.23 to 0.33 cc g^{-1}.

Table 4.3. Physical properties of promoted Pd and reference catalysts.

Catalysts	BET surface area (m^2 g^{-1})	Pore volume (cc g^{-1})	Average pore diameter (nm)
Alumina	214	0.391	7.7
Pd/Al	189	0.295	6.4
Pd-Cu/Al	203	0.314	5.1
Pd-Ag/Al	172	0.288	5.1
Pd-Ni/Al	164	0.273	5.2
Cu/Al	181	0.282	6.0
Ag/Al	178	0.290	5.8
Ni/Al	124	0.231	5.2

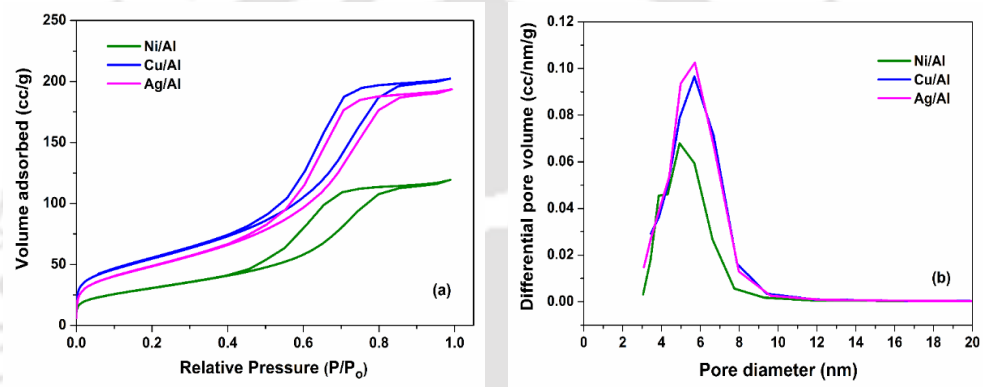

Figure 4.3. (a) Nitrogen adsorption-desorption isotherms and (b) pore size distribution of reference monometallic catalysts.

Figure 4.4 depicts the XPS spectra in the Pd_{3d} region in the catalysts. For Pd/Al, the major peak at 334.6 may be attributed to the palladium existing in metallic state (Pd^0) while the minor peak at 336.2 eV corresponded to oxidized form Pd^{2+} [18]. On addition of promoter metals, the binding energy (B.E.) of these peaks showed a positive shift in all the promoted catalysts. The corresponding peak positions of all the catalysts are summarized in Table 4.4. The significant positive shift in binding energy of Pd may be attributed to the strong interaction between palladium and the promoter metal leading to alloy formation. Similar interactions and shifts of B.E. have been reported in literature [19,20]. The relative content of Pd^0/Pd^{2+} as summarized in Table 4.4 suggested that the palladium existed mostly in the metallic state in all the catalysts. For promoted catalysts, about 70% palladium was in metallic states. The presence of oxidized palladium might have resulted from incomplete reduction during catalyst preparation in presence of hydrazine or/and to the atmospheric oxidation of the metal.

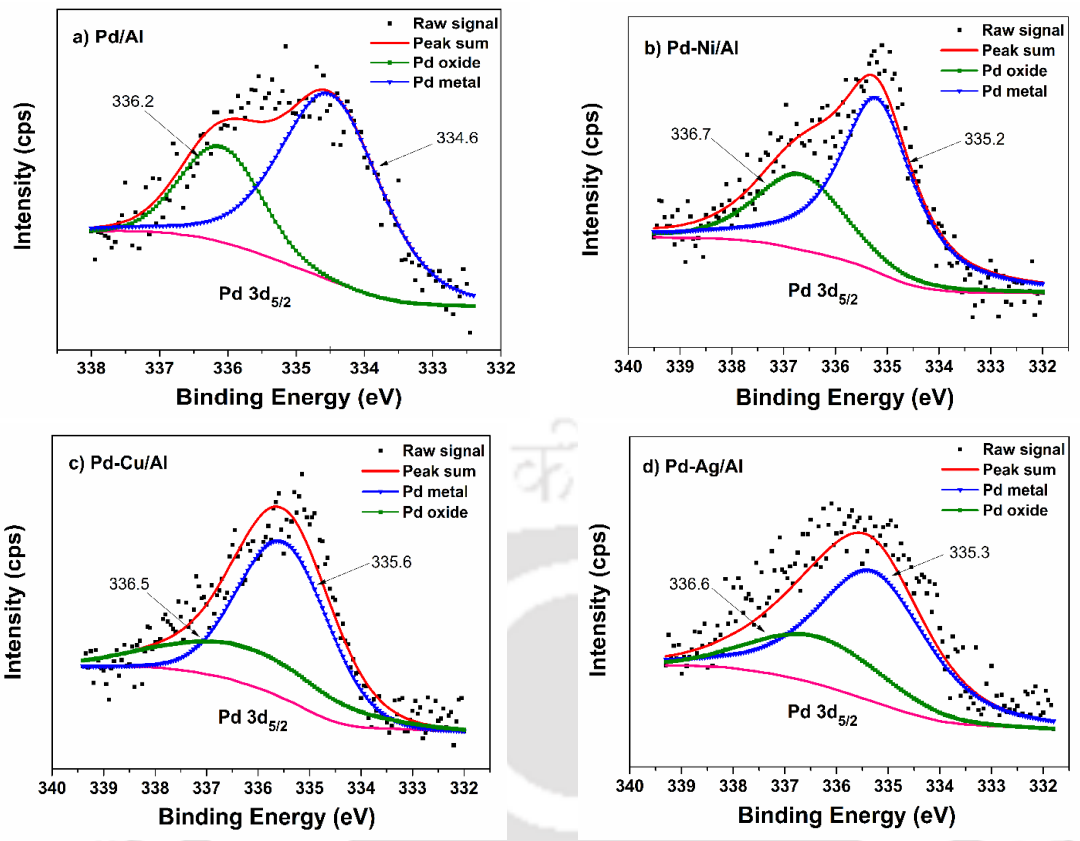

Figure 4.4. XPS spectra of Pd 3d region for (a) Pd/Al, (b) Pd-Ni/Al, (c) Pd-Cu/Al and (d) Pd-Ag/Al catalysts.

Table 4.4. XPS analysis for the promoted catalysts.

Catalysts	**Binding Energy** (eV) **Pd $3d_{5/2}$**	**Oxidation state**	**Relative content of respective metal** (%)
Pd/Al	334.6	Pd^0	62
	336.2	Pd^{2+}	38
Pd-Ni/Al	335.2	Pd^0	69
	336.7	Pd^{2+}	31
Pd-Cu/Al	335.6	Pd^0	70
	336.5	Pd^{2+}	30
Pd-Ag/Al	335.3	Pd^0	73
	336.6	Pd^{2+}	27

XPS analysis also confirmed the presence of promoter metals on catalyst surface. Peaks due to Ni 2p, Cu 2p and Ag 3d were observed in high resolution spectra for Pd-Ni/Al, Pd-Cu/Al and Pd-Ag/Al catalysts, respectively (Figure 4.5). The peaks appearing at binding energy values of 852.1 eV, 932.1 eV and 367.8 eV may be attributed to the presence of metallic Ni, Cu and Ag species respectively, over the catalyst surface.

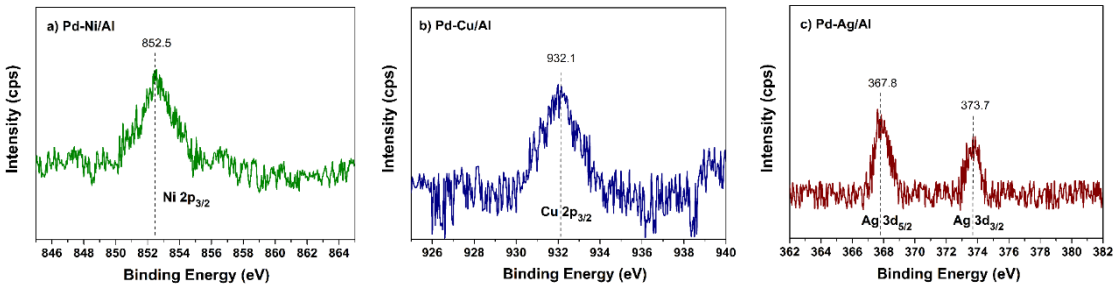

Figure 4.5. XPS spectra of (a) Ni 2p region of Pd-Ni/Al, (b) Cu 2p region of Pd-Cu/Al and (c) Ag 3d region of Pd-Ag/Al catalyst.

Figure 4.6 illustrates the temperature programmed reduction (TPR) profiles of the catalysts. The presence of reduction peaks in the profiles confirmed that a fraction of metals was in oxide form in all the catalysts. This was also observed in XPS spectra. Multiple reduction peaks of broad nature were observed in the TPR profiles of all the samples. The maxima of these peaks are tabulated in supplementary Table 4.5.

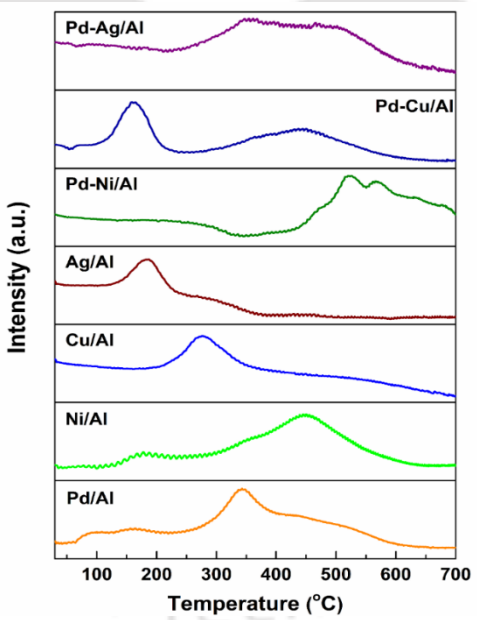

Figure 4.6. TPR profiles of promoted and monometallic reference catalysts.

The monometallic catalyst, Pd/Al exhibited three main reduction peaks centred at 90, 153 and 340 °C. Among the reference catalysts, Ni/Al showed peaks at 175 and 460 °C, tentatively assigned to the reduction of Ni^{2+} species in weak and strong interaction, respectively, with alumina support [21]. The Cu/Al and Ag/Al showed major broad peaks

with maxima at 285 and 190 °C, respectively, corresponding to the reduction of oxides to metallic form [22-24]. Thus, silver oxide clusters showed most ease of reduction.

Table 4.5. Reduction peak maxima obtained in TPR profiles of promoted and reference catalysts.

Catalysts	Reduction peak position (°C)
Pd/Al	90, 153, 340
Ni/Al	175, 460
Cu/Al	285
Ag/Al	190
Pd-Ni/Al	520, 560
Pd-Cu/Al	165, 450
Pd-Ag/Al	350-520

When the promoter metals were added to Pd/Al, the main peak of Pd shifted to higher or lower temperature depending on type of promoter metal. For Pd-Ni/Al, the reduction peak was shifted to higher temperature at 520 and 560 °C, with respect to both Pd/Al and Ni/Al. This shift in reduction peak suggested stronger interaction between the two metals in promoted catalyst tending towards alloy formation [25]. Further, the shift of the reduction peaks to higher temperature suggested stronger interactions of these alloyed metal clusters with the support. The TPR profile of Pd-Cu/Al catalyst also showed two distinct peaks at 165 and 450 °C, reducing at temperatures different from that of corresponding metal clusters on monometallic samples. This agreed with strong interaction between Pd and Cu metals as observed in XPS analysis. The higher reduction temperature suggested alloyed Pd-Cu to be in stronger interaction with the support. The TPR profiles of Pd-Ag/Al showed very broad peak of reduction in the temperature ranging of 350 to 520 °C. The disappearance of the reduction peak for AgO, which was observed in Ag/Al sample, suggested engagement of most the silver in strong interaction with Pd. The resultant alloyed metal cluster was less reducible and strongly bounded to the support as observed from its higher reduction temperature.

Above analysis confirmed that all the promoted metals had strong interaction with palladium leading to alloy formation. The type and extent of interaction depended on the type of promoter metal. The Cu was observed to form most easily reducible alloy with Pd followed by Ag and Ni. The results showed that the co-deposition of Pd and promoter

metals on the support facilitated not only the strong interaction between Pd and promoter metal but also the interaction of the alloying metal clusters with the support. The stronger interaction of alloyed metal clusters with the support might have inhibited sintering tendency of metal clusters in promoted catalysts.

The TEM images of the promoted Pd catalysts are displayed in Figure 4.7. The average metal cluster size for Pd/Al catalyst was 4.6 nm. On addition of the promoters to palladium catalyst, the average metal cluster size increased. The average metal cluster size was highest for Pd-Ni/Al catalyst with 11.4 nm followed by 9.1 nm for Pd-Ag/Al and 6.7 nm for Pd-Cu/Al catalyst. The Ni promoted catalyst exhibited much broader particle size distribution. The corresponding dispersion (D%) of metals was calculated using the equation: D=1.13/d, where d is the average metal particle size in nm as determined from TEM analysis [26]. The dispersion values obtained for Pd/Al, Pd-Ni/Al, Pd-Cu/Al and Pd-Ag/Al were 24.5, 9.9, 16.9 and 12.4%, respectively.

Among the reference catalysts, the highest average cluster size of 18.4 nm was observed for Ni/Al catalyst followed by Ag/Al (13.2 nm) and least for Cu/Al (7.9 nm) (Figure 4.8). The corresponding dispersion values were calculated as 6.1, 8.6 and 14.3%, respectively, for Ni/Al, Ag/Al and Cu/Al. Thus, all the promoter metals had higher sintering tendency compared to that of the palladium. This higher sintering tendency of the promoter metals might had resulted in higher average metal cluster sizes for all promoted catalysts compared to that of monometallic Pd/Al catalyst. The addition of copper, with lowest sintering tendency as observed for the reference Cu/Al, resulted in lowest metal cluster size among promoted catalysts.

On the other hand, the highest tendency of the nickel particles to agglomerate as observed for the reference Ni/Al catalyst might have contributed to highest crystallite size for Pd-Ni/Al catalyst. The increase of average size of metal clusters on addition of 10 mol% promoter metal to palladium in all the promoted catalysts might have resulted from significant interaction between the two metals as shown by TPR analysis. The strong metal-metal interaction tends to formation of alloys between palladium and promoter metals. For the Cu promoted catalyst, the smallest metal cluster size confirmed not only the strongest interaction of the copper with primary metal Pd but also with that of the support. These strong interactions resulted in highest and stable dispersion of the Pd-Cu alloyed metals on the support.

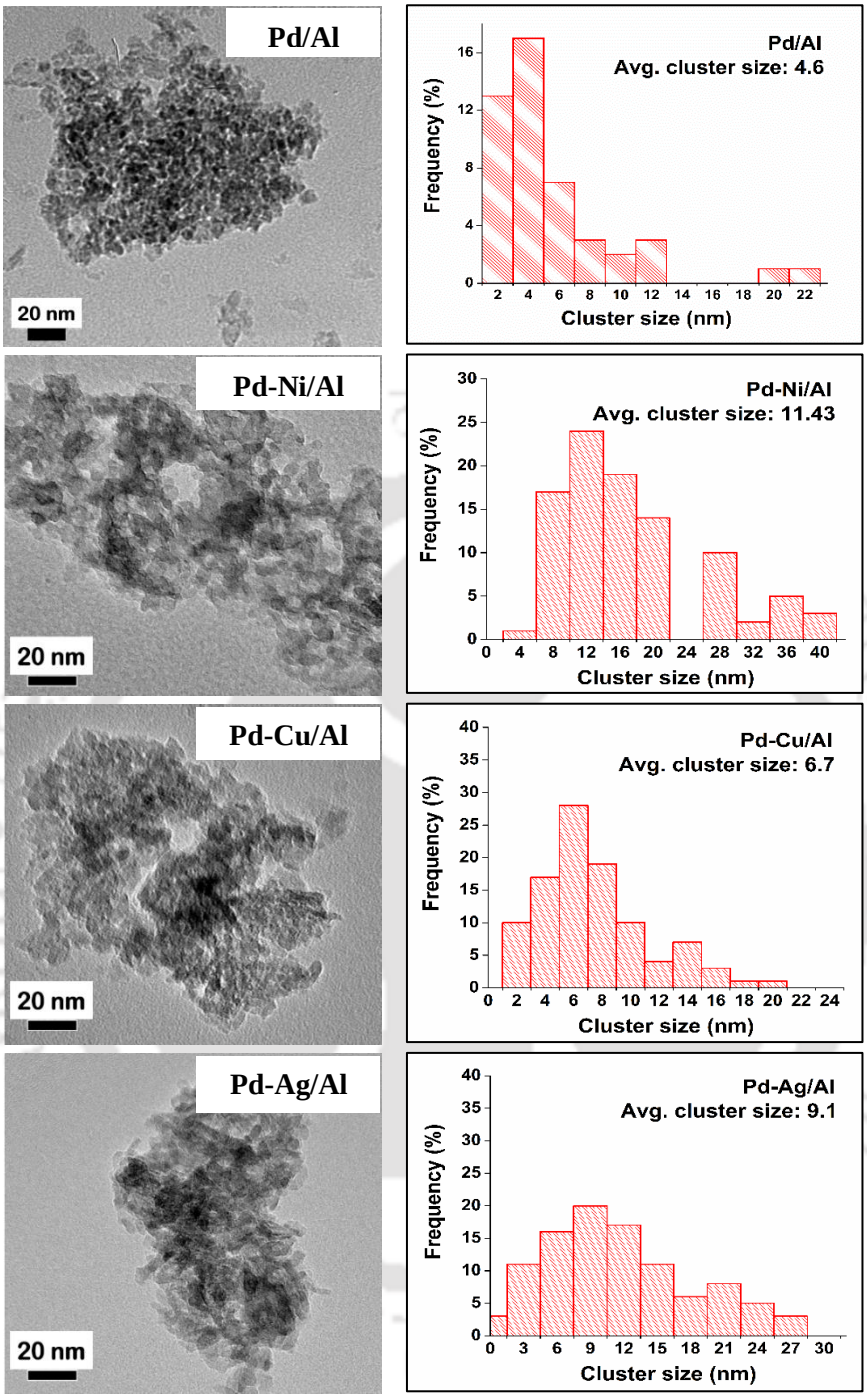

Figure 4.7. TEM images and particle size distribution of Pd/Al and promoted Pd catalysts.

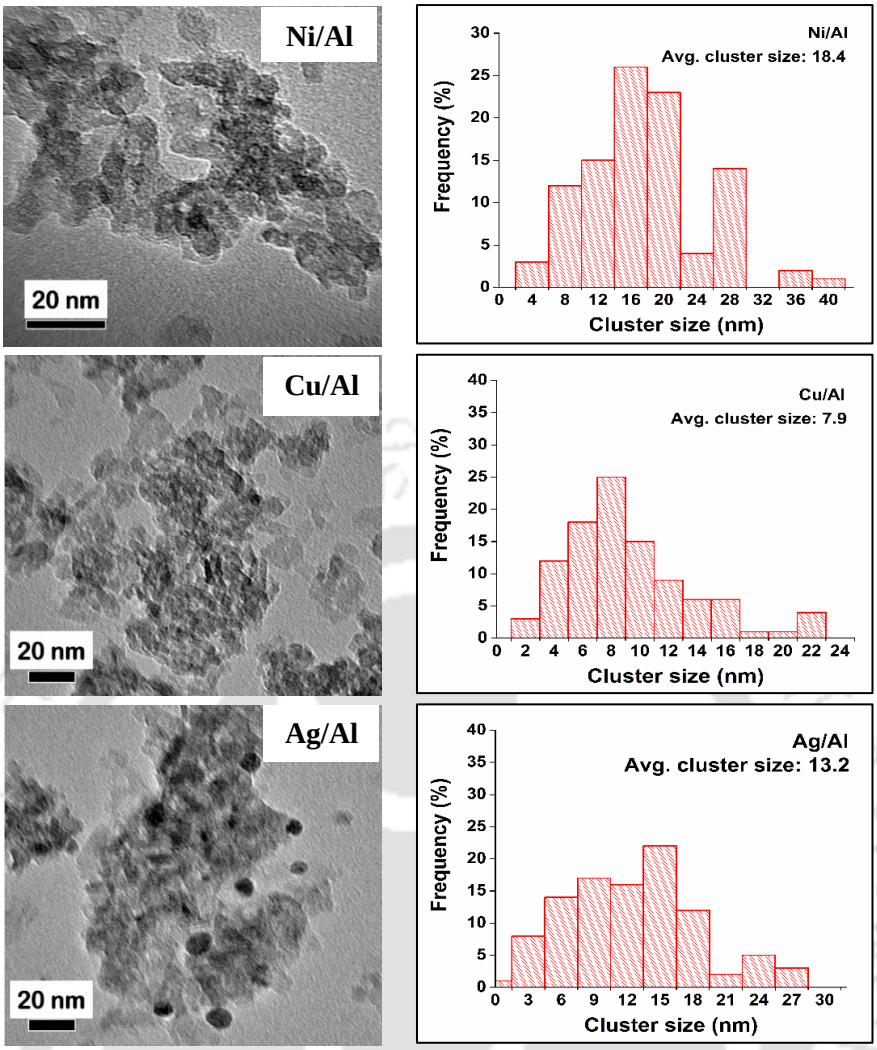

Figure 4.8. TEM images and particle size distribution of reference monometallic catalysts.

The XRD spectra of the support showed peaks due to γ-alumina at 2θ = 37.6° (311), 45.8° (400) and 66.8° (440). The XRD profiles of all the catalysts are included in Figure 4.9. All the promoted catalyst showed peaks at similar positions. None of the promoted catalysts showed any peaks that can be exclusively assigned to the deposited metals. The reference catalysts also did not show any peaks due to metals on support except that for Ag/Al, which exhibited very small peaks at 38° and 77.8° corresponding to Ag phases (111) and (220), respectively.

Figure 4.10a shows the FTIR spectra for support and catalysts adsorbed with pyridine as probe molecule to determine the acid sites present on the sample surface. The alumina support exhibited strong Lewis and Brønsted acidity corresponding to peaks observed for adsorbed pyridine at 1450 and 1637 cm^{-1} respectively [27]. The co-ordinatively

unsaturated aluminium ions act as Lewis sites, while surface hydroxyls groups act as Brønsted sites on alumina surface [28,29].

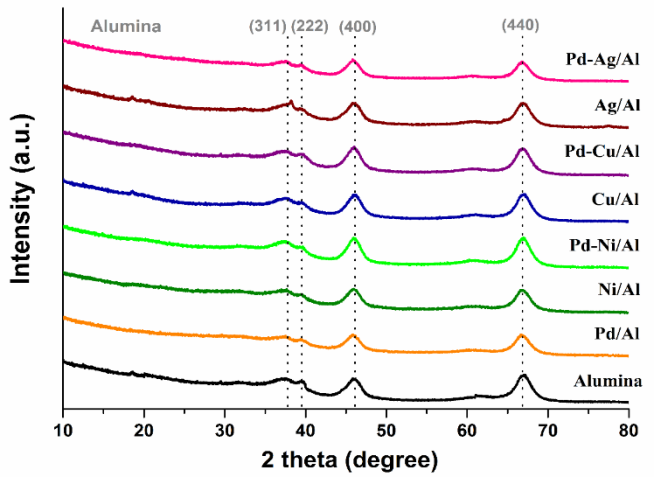

Figure 4.9. XRD spectra of alumina support, promoted Pd catalysts and reference monometallic catalysts.

The high intensity of the peaks suggested high acidity of the alumina support [30]. Again, concentration of Brønsted acidity was higher than Lewis acidity as the peak intensity was much higher for the former. The Brønsted acidity might had resulted from the hydroxyl groups due to adsorbed moisture on alumina surface caused by an exposure to the environment.

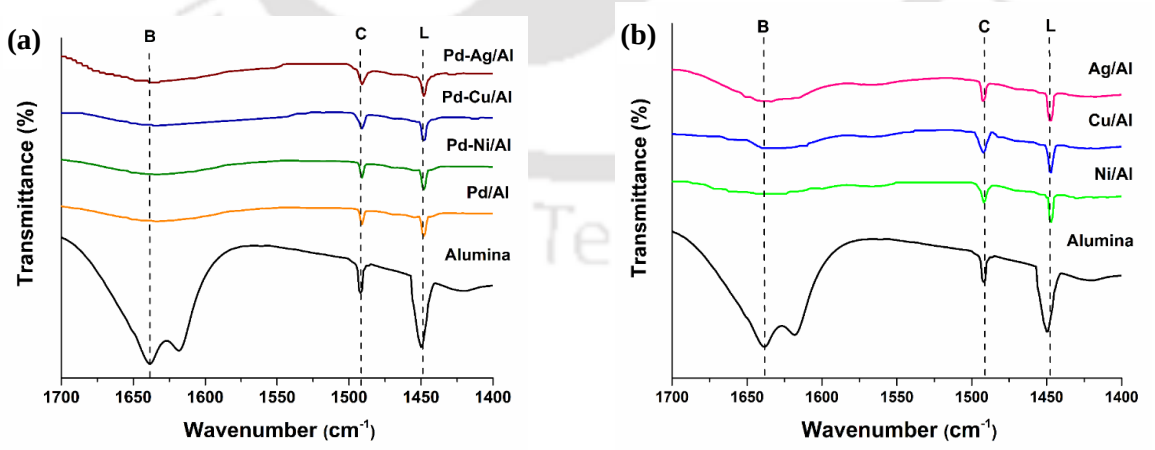

Figure 4.10. FTIR spectra of pyridine chemisorbed on (a) support and promoted Pd catalysts and (b) reference catalysts (L: Pyridine bonded to Lewis acid sites; C: Coordinative bound pyridine; B: Pyridine bonded to Brønsted acid sites).

The intensity of peaks decreased significantly after the addition of metals to the support. The decrease in acidity may be attributed to the partial coverage or blocking of support acidic sites by deposition of metals on the alumina surface [7]. The Brønsted sites were almost negligible in Pd/Al catalyst. Further addition of promoter metals did not have significant effect on distribution of acidic sites of Pd/Al catalyst. The reference samples also exhibited only Lewis acidity, but it was higher than that of Pd/Al or promoter catalysts as can be observed from the relative intensity of the peaks of Figure 4.10a and b. The higher acidity of the reference catalysts can be explained based on their lower metal dispersion, as discussed earlier, exposing more support acidic sites. The peak for co-ordinatively bounded pyridine were observed in all the samples at 1490 cm^{-1}.

4.3.2 Dehydrogenation study

Figure 4.11a compares the conversion of n-butane in the temperature range of 100-600 °C over promoted and Pd/Al catalysts. The conversion increased with increase in the reaction temperature. The monometallic palladium catalyst did not show any significant butane conversion up to 400 °C. Thereafter, the conversion increased sharply and was 21.3% at 600 °C. The addition of Ni, Cu or Ag to the primary Pd/Al catalyst improved its catalytic performance. The promoted catalysts exhibited much higher conversion in comparison to Pd/Al catalyst in the entire range of reaction temperatures studied. All the promoted catalysts showed initial conversion of about 6% below 200 °C. The activity of Ni promoted catalyst, Pd-Ni/Al, increased significantly to 19% at 400 °C but thereafter, the increase was slow. It was only 21.4 and 21.8% at 550 and 600 °C, respectively. In contrast, Pd-Cu/Al showed significant increase in activity after 400 °C followed by that of Pd-Ag/Al. The Pd-Cu/Al exhibited butane conversion of 34% at 550 °C that increased to 38% at 600 °C. The Pd-Ag/Al exhibited conversions of 25.6 and 26.9% at 550 and 600 °C, respectively.

Hence, for all the samples, the increase in conversion was less prominent as temperature was raised from 550 to 600 °C. The increase in activity was least for nickel promoted sample and highest for copper promoted catalyst. The decrease in activity at higher temperature may be attributed to slight coke deposition and metal sintering (as observed from analysis of spent catalysts discussed in later section) as the temperature was raised. The trend obtained for conversion at 550 °C was: Pd-Cu/Al (34.4%) > Pd-Ag/Al (25.6%) > Pd-Ni/Al (21.4%) > Pd/Al (17.9%). The corresponding turn over frequency (TOF) at 550

°C for the catalysts also followed the same order (Table 4.6); Pd-Cu/Al (0.84 s^{-1}) > Pd-Ag/Al (0.63 s^{-1}) > Pd-Ni/Al (0.53 s^{-1}) > Pd/Al (0.44 s^{-1}). The TOF was calculated as moles of butane reacting per mole of metal present in catalyst per unit time.

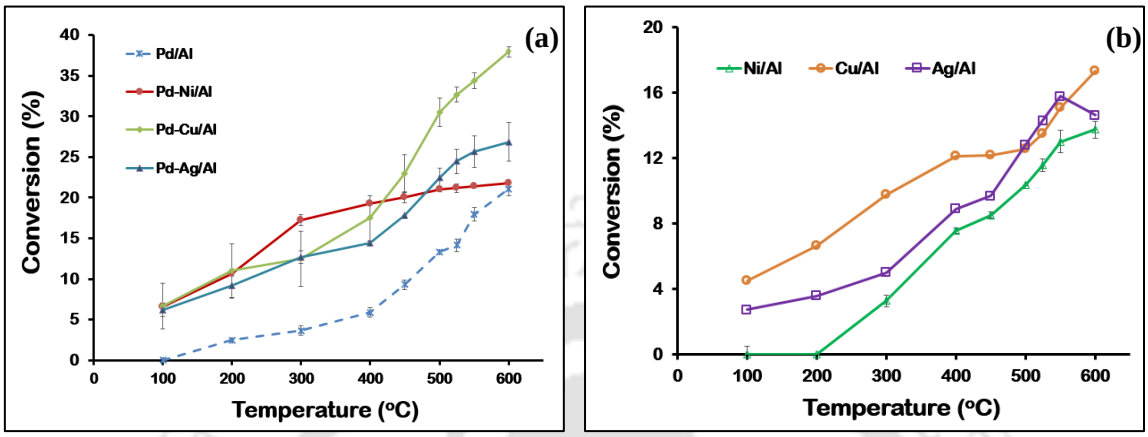

Figure 4.11. Catalytic activity obtained at different temperatures over (a) Pd/Al and promoted Pd catalysts; (b) Ni/Al, Cu/Al and Ag/Al reference catalysts.

The reference catalysts showed activity in low temperature zone. At 300 °C, the activity order for reference catalysts was Cu/Al > Ag/Al > Ni/Al (Figure 4.11b). The activity order may be explained by their respective metal dispersion and surface area. As determined earlier, the Cu/Al showed highest metal dispersion (7.9 nm) followed by Ag/Al (9.1 nm) and Ni/Al (11.4 nm). At higher temperature of 600 °C, the same order of activity was observed for the reference catalysts; Cu/Al showed highest activity of 17.3% followed by Ag/Al (14.6%) and Ni/Al (13.7%). The activity of the reference catalysts thereby was lower than that of Pd/Al catalyst (21.3%) at higher temperature.

The results showed that at lower temperature, the monometallic Pd/Al catalyst showed negligible activity while, all the reference catalysts showed considerable conversions but their activity at higher temperatures was lower than that of Pd/Al. The promoted catalysts showed significant activity over the entire range of temperature studied. The activity of the promoted catalysts at lower temperature may be attributed to presence of promoting metals. The significant activity at high temperatures might have resulted from higher activity of palladium at raised temperature. However, the activity shown by the promoted catalysts was always higher compared to that of both monometallic Pd/Al and the reference catalysts over the entire range of temperature studied. The higher activity of the promoted catalysts with respect to the monometallic catalysts was observed in spite of lower surface area and

metal dispersion of the former. This higher activity of the promoted catalysts suggested significant role of alloys formed between the base metal palladium and respective promoter metal. The alloy formation was established by TPR and XPS analysis. Among the promoted catalysts, the highest surface area, highest metal dispersion and stronger metal-metal interaction of Pd-Cu/Al might have acted as the contributory factors towards its highest conversion.

Table 4.6. Catalytic performance of promoted Pd catalysts for n-butane dehydrogenation at 550 °C [feed gas ratio (n-butane:hydrogen:nitrogen) = 1:3:6].

Catalysts	Conversion (%)	TOF (s^{-1})	Selectivity (%)					
			Iso-butene	1-butene	Cis-2-butene	Trans-2-butene	Total butene	C_1-C_3
Pd/Al	17.9	0.44	13.9	19.6	24.2	32.8	90.5	9.5
Pd-Ni/Al	21.4	0.53	13.5	16.4	14.2	17.4	61.5	38.5
Pd-Cu/Al	34.4	0.84	12.3	17.1	23.7	31.9	85	15
Pd-Ag/Al	25.6	0.63	15.6	22.4	22.5	31.4	91.9	8.1

The butane dehydrogenation products over Pd/Al catalyst may be grouped into C_1-C_3 hydrocarbons and butenes. The C_1-C_3 hydrocarbons resulted mainly from cracking of C-C bonds and consisted of methane, ethane, ethylene, propane and propylene (Appendix G). Among C_4 products, both 1 and 2-butenes were obtained (Table 4.6). All corresponding isomers such as iso-butene, 1-butene, cis and trans forms of 2 butenes were detected. Figure 4.12a shows the product selectivity pattern of the catalysts in the temperature range of 500-600 °C. For all the catalysts, overall selectivity of butene increased as the temperature increased from 500 to 550 °C and thereafter dropped at higher temperature of 600 °C. The Pd-Cu/Al had a butene selectivity of 85% at 550 °C, which dropped to 63.8% at 600 °C. The lowering of selectivity of butene at higher temperature suggested increasing tendency of the catalysts towards cracking reactions at higher temperature [11,31]. Since the activation energy of butane cracking is higher than that of butane dehydrogenation hence, the former is favoured at higher temperatures [32].

The effect of addition of promoter metals on selectivity pattern of Pd/Al depended on the type of promoter metals. The overall butene selectivity order at 550 °C was Pd-Ag/Al (91.9%) > Pd/Al (90.5%) > Pd-Cu/Al (85%) > Pd-Ni/Al (61.5%) while that at 600 °C was Pd-Ag/Al (86.2%) > Pd-Cu/Al (81%) > Pd/Al (63.8%) > Pd-Ni/Al (60.8%). Thus, Ag

promoted catalyst showed highest selectivity at both temperatures, while Ni promoted catalyst showed the lowest. On comparison of selectivity at two temperatures, it may be observed that the drop in selectivity of butene was highest for Pd/Al compared to the promoted catalysts. Though, for both Pd-Ag/Al and Pd-Cu/Al, the selectivity towards butene was reduced at higher temperature (600 °C), but still it was much higher compared to that of Pd/Al. The addition of both Ag and Cu as a promoter thus had a positive effect on butene selectivity. The more number of exposed support acidic sites in Ni promoted catalyst, due to higher sintering tendency of nickel, might have caused higher extent of cracking reactions. Consequently, low butene selectivity was observed over Ni promoted catalyst.

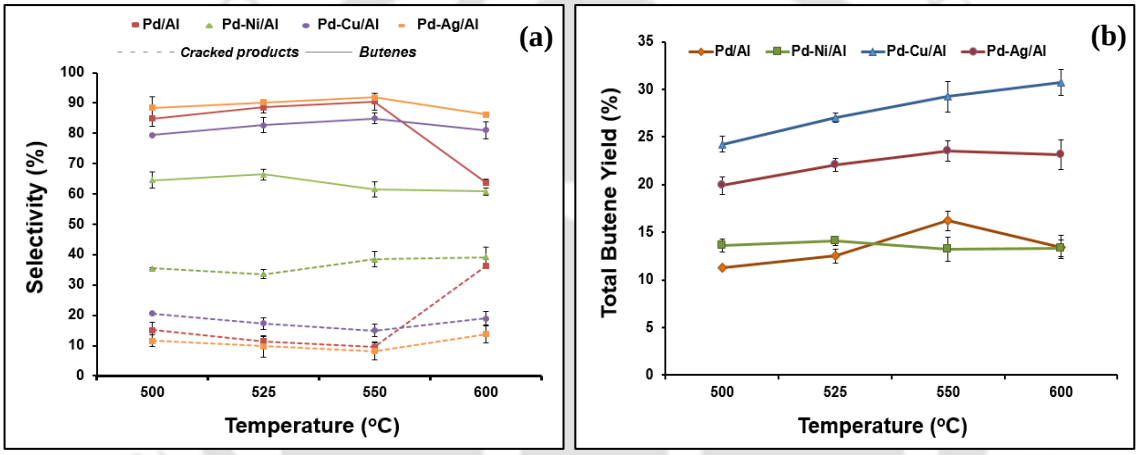

Figure 4.12. (a) Product selectivity trend and (b) Total butene yield obtained over Pd/Al and promoted Pd catalysts at different temperatures.

The selectivity trend shown by the promoted catalysts can also be understood from the selectivity pattern of the reference catalysts containing only the promoter metal supported on alumina. All the reference catalysts showed high selectivity for cracked products at 550 °C (Table 4.7). This high selectivity can be explained based on their higher acidity and lower dispersion compared to Pd/Al catalyst as observed from the FT-IR and TEM analysis, respectively.

Among the reference catalyst, Ag/Al gave the lowest selectivity (29.6%) towards cracked product formation, while Ni/Al showed highest selectivity (49.3%) towards cracking followed by Cu/Al (47.4%). The application of these metals as promoter resulted in same trend as Pd-Ni/Al gave highest selectivity for C_1-C_3 products and Pd-Ag/Al showed the least, as discussed earlier. However, the effect of alloying with palladium was dominant as

the promoted catalysts exhibited much higher selectivity towards butene in contrast to the respective reference catalysts. The comparison of selectivities of the different butenes over promoted catalysts with respect to that of Pd/Al at 550 °C (Table 4.6), showed that the addition of promoter metals did not have significant effect on the distribution of butene isomers. The 2-butene was the major product obtained for all the catalysts. The selectivity order was 2-butene > 1-butene > iso-butene. The highest selectivity was observed towards trans-2-butenes for all the catalysts. The Pd/Al catalyst showed highest selectivities of 33 and 24% towards trans-2-butene and cis-2-butene, respectively, with total selectivity of 57% towards 2-butene. This 2-butene distribution did not change much for Pd-Cu/Al (32 and 24%) and Pd-Ag/Al (31.3 and 22.4%). However, addition of nickel drastically decreased the selectivity for cis and trans-2-butene to 14.2% and 17.4%, respectively.

Table 4.7. Catalytic activity (conversion and selectivity) of reference catalysts for n-butane dehydrogenation at 550 °C [feed gas ratio (n-butane:hydrogen:nitrogen) = 1:3:6].

Catalysts	Conversion (%)	Selectivity (%)					
		Iso-butene	1-butene	Trans-2-butene	Cis-2-butene	Total butenes	C_1-C_3
Ni/Al	13.0	6.1	15.1	15.9	13.6	50.7	49.3
Cu/Al	15.1	7.7	8.6	22.2	14.1	52.6	47.4
Ag/Al	15.8	10	15.7	22.9	21.7	70.3	29.7

Figure 4.12b compares the total butene yield at 550 °C calculated from respective conversion and selectivity as mentioned in section 2.2.5, Chapter 2. The overall yield pattern of butene in the higher temperature range of 500-600 °C for promoted catalysts depended on the type of promoter metal. For Pd-Ni/Al, it remained more or less same as that of Pd/Al catalyst. The Pd-Cu/Al had the highest yield of butene over the entire temperature range followed by that of Pd-Ag/Al. The lower yield of total butene for nickel promoted catalyst resulted from its lower selectivity in spite of having higher conversion than that of Pd/Al. The higher percentage yield of butenes obtained for both the Cu and Ag promoted catalysts resulted from better conversion and high selectivity (>90%) exhibited by both the catalysts. The order of yield of butene obtained at 550 °C was Pd-Cu/Al (29%) > Pd-Ag/Al (23%) > Pd/Al (16%) > Pd-Ni/Al (13%).

The stability of the promoted catalysts was studied for butane dehydrogenation reactions for a process time of 10 h at 550 °C. The stability of the catalysts was measured in terms

of deactivation parameter as per Eq. 2.9 given in Chapter 2. Figure 4.13 compares the conversion of butane as function of reaction time for 10 h over all the catalysts. The initial conversion of 20.5% for Pd/Al catalyst was reduced to 5% after 10 h of time on stream study. This corresponded to 76% deactivation of Pd/Al catalyst. The addition of promoters to the Pd catalyst improved the stability of the catalysts, the extent of which depended on the type of metal. Initially the Pd-Cu/Al showed highest activity (34%) but thereafter, its activity steadily decreased with time. The Ag promoted catalyst showed second highest conversion (27%) at initial condition. It also decreased with time. But, the rate of decrease of conversion was slower for Pd-Ag/Al than that of Pd-Cu/Al catalyst, as may be observed from the respective profiles.

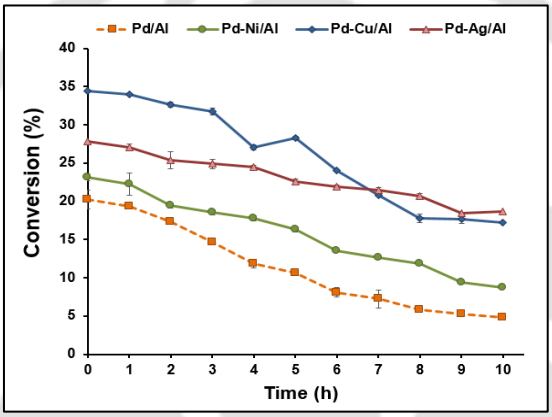

Figure 4.13. Conversion over promoted Pd catalysts at 550 °C for 10 h process time.

After 7 h of process time, the conversion over Pd-Cu /Al decreased further to a lower value than that of Pd-Ag/Al. Thereafter, Pd-Cu /Al showed slightly lower activity than that of Pd-Ag/Al catalyst. The total drop in conversion for Pd-Cu/Al was from 34 to 17% over 10 h, corresponding to 50% deactivation. In same time, the Pd-Ag/Al showed only 30% deactivation as conversion gradually decreased to 18.7% after 10 h. The stability profile of the Ag and Cu promoted catalysts with time may be explained based on their selectivity pattern. The higher deactivation tendency for Pd-Cu/Al might be explained based on its higher tendency towards C-C bond cleavage in comparison to Pd-Ag/Al. Higher formation of cracked product over Cu based catalyst contributed towards its faster deactivation rate. On the contrary, Ag more effectively suppressed the cracked product formation leading to less deactivation and more steady conversion as observed. The sintering of the metal clusters might also have contributed to gradual deactivation of the promoted catalysts over 10 h process time.

The higher stability of the Ag and Cu promoted catalysts may be explained by their selectivity pattern. Ag based catalysts suppressed the formation of cracked products to a greater extent accounting for better stability. The higher activity of alloyed Pd-Ag and Pd-Cu might also have contributed to sustain their higher butane conversion over 10 h process time. Over the entire range of 10 h study, Pd-Ni/Al showed lower conversion than other two promoted catalysts but higher than that of Pd/Al. The Pd-Ni/Al catalyst suffered the maximum deactivation among the promoted catalysts, about 61% over the same period and was least effective in terms of improving the stability of primary Pd/Al catalyst.

As discussed earlier, the sintering tendency of the nickel resulted in lowest dispersion of alloyed metal exposing more acidic sites on support. This contributed to the higher cracking reactions, ultimately leading to coke deposition and blockage of active metal sites. The larger metal cluster of this catalyst may also have promoted more secondary and poly-condensation reactions leading to more coke formation and faster deactivation. However, activity of Pd-Ni/Al was still higher than that of Pd/Al for entire 10 h of process time studied. This was in spite of the fact that Ni promoted catalyst exhibited higher selectivity towards the cracked products compared to Pd/Al catalyst. The higher activity of the Pd-Ni alloy might be the reason for its better performance during longer process time. The results suggested that the alloys formed between palladium and promoter metals contributed significantly to the improved stability of metal cluster and retaining of the activity.

4.3.3 Analysis of spent catalysts

The spent promoted catalysts were analysed by various characterization methods such as BET, TEM and Raman spectroscopy and the results are compared with the corresponding fresh catalysts to understand the variation in physicochemical properties of the catalysts after undergoing reaction. Table 4.8 compares the physical properties of the spent catalysts. The surface area values obtained for Pd/Al_spent, Pd-Ni/Al_spent, Pd-Cu/Al_spent and Pd-Ag/Al_spent were 181, 132, 186 and 166 m^2 g^{-1}, respectively (Table 4.8). The values obtained for corresponding fresh catalysts were 189, 164, 203, 172 m^2 g^{-1}, respectively (Table 4.3). The associated decrease in surface area of the spent catalysts compared to respective fresh catalysts was highest for Pd-Ni/Al_spent (19.5%) followed by that of Pd-Cu/Al_spent (8.3%). The decrease in surface area was least for Pd-Ag/Al_spent (3.5%) among all the catalysts.

Table 4.8. Physical properties of spent Pd and spent promoted Pd catalysts.

Catalysts	BET surface area (m^2 g^{-1})	Pore volume (cc g^{-1})	Average pore diameter (nm)
Pd/Al_spent	181 (4.2)	0.288 (2.4)	6.2
Pd-Ni/Al_spent	132 (19.5)	0.260 (4.8)	4.9
Pd-Cu/Al_spent	186 (8.3)	0.308 (1.9)	5.0
Pd-Ag/Al_spent	166 (3.5)	0.281 (2.4)	5.1

Values in parenthesis illustrate the percent decrease in surface area and pore volume with respect to corresponding fresh catalysts

The average pore size and pore volume of spent catalysts also reduced marginally compared to fresh catalysts (Table 4.8). The slight decrease in surface area, pore volume and average pore size for all the spent catalysts may be attributed to morphological modification of catalyst during reaction. The decrease was comparatively higher for Pd-Ni/Al_spent catalyst. Except for Pd-Ni/Al_spent, the low percentage drop in surface area and pore volume of spent catalysts suggested that there was no significant coke deposition during reaction. However, higher drop of surface area and pore volume observed for spent Ni promoted catalyst in comparison to other promoted catalysts suggested higher modification of metal cluster. This higher modification may be attributed to higher sintering tendency of the Ni as discussed earlier. The percent decrease was lowest (3.5%) for Ag promoted catalyst followed by Pd/Al catalyst which was in agreement with the stability and selectivity trend of the catalysts discussed earlier.

TEM analysis was employed to investigate the structural modifications in the spent catalysts. The TEM images of spent catalysts are shown in Figure 4.14 along with corresponding particle size distribution (inset). The average metal cluster size after the dehydrogenation reaction was observed to increase for both monometallic Pd as well as promoted Pd catalysts. The average cluster sizes grew to 4.9, 14.3, 7.2 and 10.4 nm for spent catalyst from 4.6, 11.4, 6.7 and 9.1 nm for fresh Pd, Pd-Ni, Pd-Cu and Pd-Ag catalysts, respectively. The corresponding dispersion values also decreased to 23, 7.9, 15.7 and 10.9% for spent Pd, Pd-Ni, Pd-Cu and Pd-Ag catalysts, respectively. The increase in average metal cluster size and corresponding lowering in dispersion values for spent catalysts may be attributed to modification of metal cluster due to sintering of metal under reaction conditions. However, the change in dispersion was small (5 - 15%) for all the catalysts.

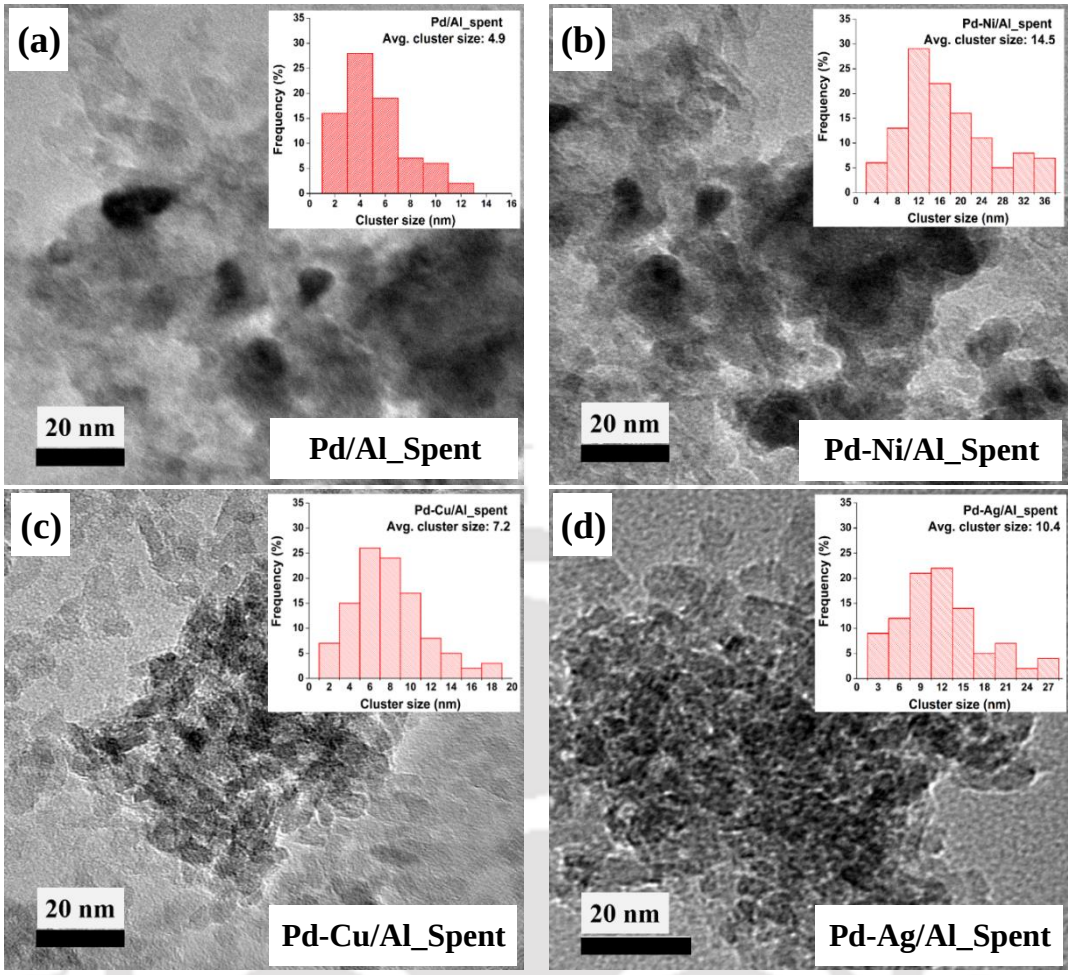

Figure 4.14. HRTEM images and particle size distribution of (a) Pd/Al_spent, (b) Pd-Ni/Al_spent, (c) Pd-Cu/Al_spent and (d) Pd-Ag/Al_spent catalysts.

The weight analysis of all the catalysts before and after reaction confirmed the coke deposition to be negligible. The change in wt% of the Pd/Al, Pd-Ni/Al, Pd-Cu/Al and Pd-Ag/Al catalysts post reaction was 0.83, 1.07, 0.75 and 0.48%, respectively. The low coke deposition may be attributed to the presence of hydrogen in the reaction feed which suppressed the formation of coke precursors.

4.3.4 Effect of promoter content

The Pd-Cu/Al catalyst gave the highest activity and butene yield. The content of copper was varied to comprehend the effect of copper loading. The composition of these catalysts obtained by EDX analysis are given in Table 4.9. The palladium loading was about 1 wt% in the catalysts, while loadings of copper were varied as 0.1, 0.2 and 0.3 wt% in Pd-Cu_5/Al, Pd-Cu_{10}/Al and Pd-Cu_{20}/Al, respectively. The total metal deposition for all the catalysts was close to the targeted loading.

Table 4.9. Composition and physical properties for promoted catalysts with varying Cu content.

Catalysts	Loading (at%)		BET surface area (m^2 g^{-1})	Pore volume (cc g^{-1})	Average pore diameter (nm)
	Palladium	Copper			
Pd-Cu_5/Al	2.7 (1)	0.20 (0.1)	192	0.293	6.0
Pd-Cu_{10}/Al*	2.6 (1)	0.27 (0.2)	203	0.314	5.1
Pd-Cu_{20}/Al	2.3 (0.9)	0.36 (0.3)	204	0.304	5.8

Values in parenthesis corresponds to metal loading in wt%
**Pd-Cu/Al catalyst and Pd-Cu_{10}/Al are same*

The N_2 adsorption–desorption isotherms of promoted catalysts with varying copper content are shown in Figure 4.15a. As discussed earlier, the catalysts showed type IV isotherms with prominent hysteresis loops corresponding to mesoporous structures. The hysteresis loops were of H2 type and attributed to interconnected complex pore network. The BET surface areas, average pore diameter and pore volumes are summarized in Table 4.9.

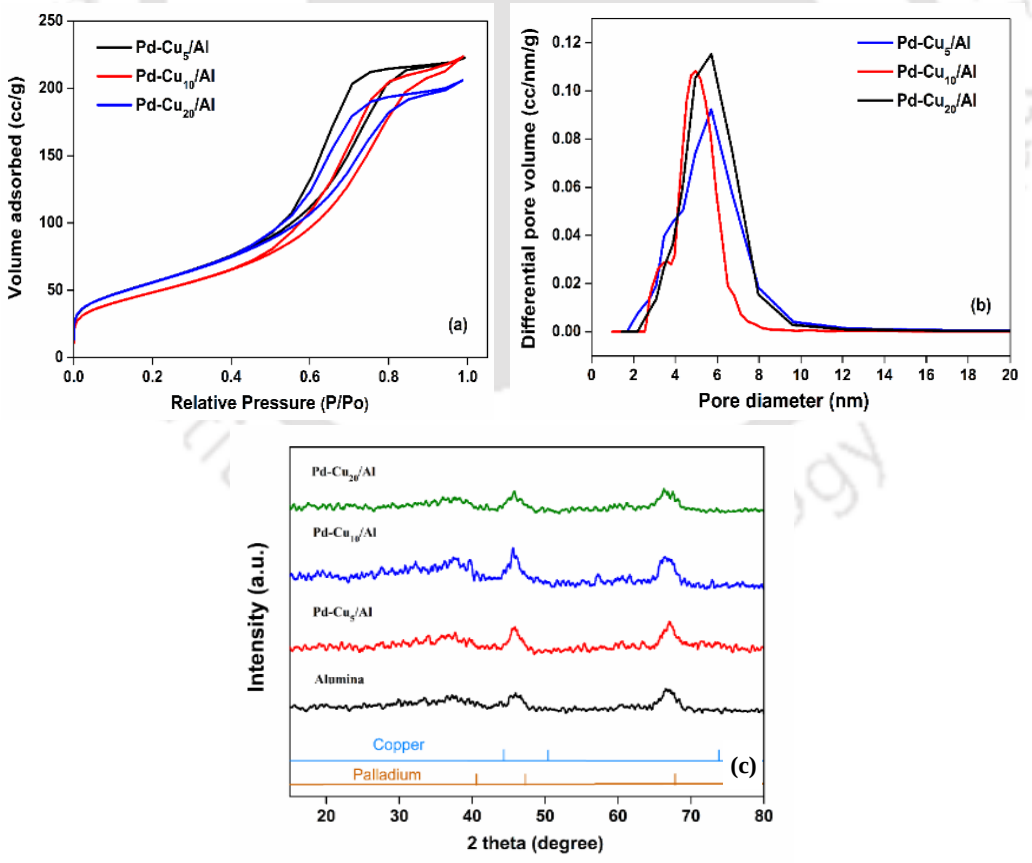

Figure 4.15. (a) Nitrogen adsorption-desorption isotherms; (b) pore size distribution and (c) XRD spectra of Cu promoted Pd catalysts with various copper loadings.

The variation in copper content in the studied range did not cause any significant difference in physical properties of the Cu promoted catalysts. The surface areas were in the range of 192-204 $m^2 g^{-1}$ while the pore volumes varied in the range of 0.293 to 0.314 cc g^{-1}. The pore size distribution of the catalysts is shown in Figure 4.15b. All the samples exhibited narrower pore size distribution in comparison to the support material. The average pore size of Cu promoted catalysts was in the range of 5 - 6 nm. The XRD patterns of the catalysts showed no peaks of metallic copper and palladium in any of the samples suggesting high dispersion of both the metals on the support. The XRD spectra are included in Figure 4.15c.

The TEM images of these catalysts are shown in Figure 4.16. The metal particles were observed to be evenly distributed and well dispersed on the support surface of the catalyst samples. The average cluster size for Pd-Cu_5/Al catalyst was 5.2 nm, which was slightly changed with respect to the Pd/Al catalyst (4.6 nm) indicating that copper addition in such a small amount did not have a significant effect on particle size. The average particle size increased to 6.7 nm on increasing the copper content in Pd-Cu_{10}/Al catalyst. The further enhancement in copper loading in Pd-Cu_{20}/Al catalyst slightly increased the cluster size to 7.1 nm in comparison to that observed for Pd-Cu_{10}/Al catalyst.

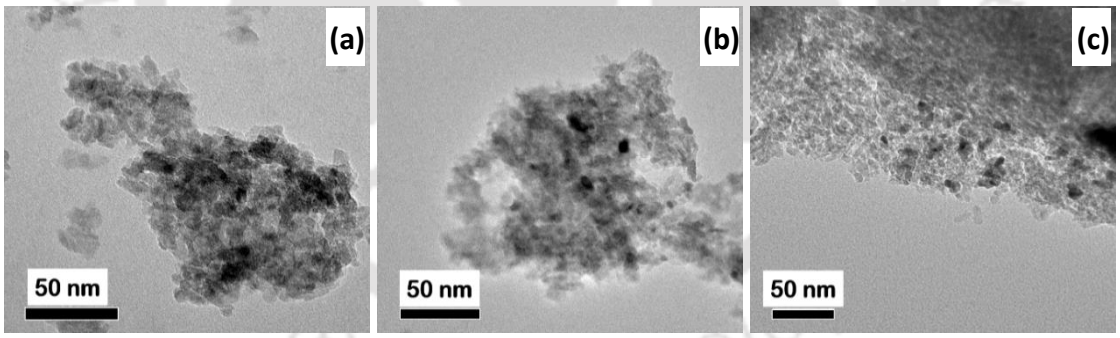

Figure 4.16. HRTEM images of Cu promoted palladium catalysts having various copper loadings (a) Pd-Cu_5/Al, (b) Pd-Cu_{10}/Al and (c) Pd-Cu_{20}/Al.

Figure 4.17a illustrates the conversion of n-butane for Cu promoted catalysts with various copper loadings in the temperature range of 100-600 °C. It is apparent from the figure that the conversion of n-butane increased with increase in the reaction temperature for all the catalysts. As it was discussed earlier, Cu promoted catalysts showed a better catalytic performance with a higher conversion in comparison to both monometallic Pd and Cu

catalysts. It can be observed that increase in copper content increased the conversion significantly.

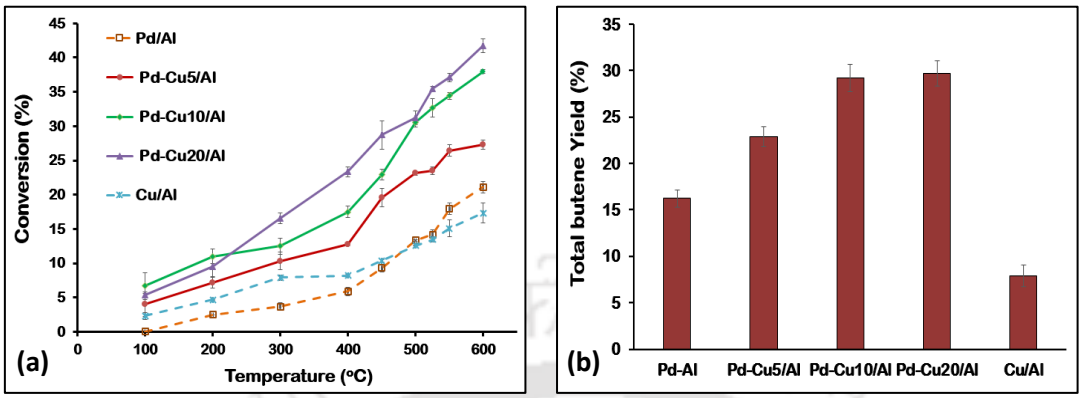

Figure 4.17. Catalytic performance of Cu promoted Pd catalysts (a) Butane conversion at different temperatures and (b) Total butene yield at 550 °C at various copper loadings.

The Pd-Cu_{20}/Al showed the highest catalytic activity with a conversion of 37% at 550 °C. The conversion further increased to 41% on increasing the temperature to 600 °C. At 550 °C, the highest TOF of 0.88 s^{-1} was exhibited by Pd-Cu_{20}/Al catalyst followed by Pd-Cu_{10}/Al catalyst (0.84 s^{-1}). These values were approximately twice to that observed for Pd/Al catalyst (0.44 s^{-1}). The conversion trend at 550 °C for different Cu promoted catalysts followed the order: Pd-Cu_{20}/Al (37.1%) > Pd-Cu_{10}/Al (34.4%) > Pd-Cu_5/Al (26.4%) > Pd/Al (17.9%) > Cu/Al (15.1%) (Table 4.10).

Table 4.10. Catalytic performance of promoted Pd catalysts with various Cu loading for n-butane dehydrogenation at 550 °C [feed gas ratio (n-butane:hydrogen:nitrogen) = 1:3:6].

Catalysts	Conversion (%)	TOF (s^{-1})	Selectivity (%)					
			Iso-butene	1-butene	Trans-2-butene	Cis-2-butene	Total butene	C_1-C_3
Pd/Al	17.9	0.44	13.9	19.6	32.8	24.2	90.5	9.5
Pd-Cu_5/Al	26.4	0.75	13.1	17.0	28.8	23.1	82	18
Pd-Cu_{10}/Al*	34.4	0.84	12.3	17.1	31.9	23.7	85	15
Pd-Cu_{20}/Al	37.1	0.88	17	19.3	27.8	21.3	86.5	13.5
Cu/Al	15.1	0.38	7.7	8.6	22.16	14.15	52.6	47.4

Total metal loading for Pd/Al and Cu/Al was kept constant at 225 µmoles
**Pd-Cu/Al catalyst and Pd-Cu_{10}/Al are same*

Addition of copper decreased the selectivity of total butene to some extent in Pd-Cu_5/Al (82%) compared to 90.5% for Pd/Al. But thereafter, there was marginal increase in selectivity with 85% for Pd-Cu_{10}/Al and ~ 87% for Pd-Cu_{20}/Al. The remaining products were C_1-C_3 hydrocarbons. No significant change in distribution of products was observed with variation of copper content (Table 4.10). Pd-Cu_{20}/Al catalyst showed the highest selectivity towards 1-butene (19%) followed by 17% selectivity towards formation of iso-butene. Figure 4.17b compares the total butene yield of different copper containing promoted catalysts with that of monometallic Pd/Al and Cu/Al at 550 °C. Pd/Al exhibited a butene yield of 16.2% while the butene yield was observed to be low (8%) for reference Cu/Al catalyst. However, the addition of Cu as promoter increased the butene yield. The butene yield increased with the increase in copper content. Pd-Cu_5/Al exhibited 22.9% butene yield that increased to 29.2% for Pd-Cu_{10}/Al catalyst. Thereafter, the increase for Pd-Cu_{20}/Al was only marginal. The highest yield of 32.1% was observed for Pd-Cu_{20}/Al. This yield value is better or at par with reported yield values at similar conditions (Table 4.1).

4.4 Summary

In this chapter, Ni, Cu and Ag promoted palladium catalysts were prepared by modified electroless co-deposition of metals on alumina support. The performance for butane dehydrogenation was determined in terms of activity, selectivity, yield and stability in temperature range of 100–600 °C under atmospheric pressure. The co-deposition of 10 mol% promoters along with palladium, very effectively increased activity and yield of butene. The extent of enhancement depended on type of the promoter metal. The copper promoted sample showed highest conversion of 34% at 550 °C that further increased to 38% on increasing the temperature to 600 °C. The Ag promoted catalyst possessed highest selectivity towards butenes (>90% at 550 °C). The order of yield of butene was Pd-Cu/Al (29%) > Pd-Ag/Al (23%) > Pd/Al (16%) > Pd-Ni/Al (13%) at 550 °C. Moreover, increase in copper content increased yield of butene and highest yield of 32% was observed for Pd-Cu_{20}/Al with 20 mol% copper. The palladium metal was in strong interaction with the promoter metals forming alloys. Higher activity of these alloys enhanced performance of the promoted catalysts. The stability of the catalysts was also enhanced by addition of

promoters. The deactivation order was Pd-Ag/Al (27%) < Pd-Cu/Al (34%) < Pd-Ni/Al (61%) < Pd/Al (76%).

References

[1] S. Furukawa, M. Endo, T. Komatsu, Bifunctional catalytic system effective for oxidative dehydrogenation of 1-butene and n -butane using Pd-based intermetallic compounds, ACS Catal. 4 (2014) 3533–3542.

[2] Z. Ma, Z. Wu, J.T. Miller, Effect of Cu content on the bimetallic Pt–Cu catalysts for propane dehydrogenation, Catal. Struct. React. 3 (2017) 43–53.

[3] B.M. Nagaraja, H. Jung, D.R. Yang, K.D. Jung, Effect of potassium addition on bimetallic PtSn supported θ-Al_2O_3 catalyst for n-butane dehydrogenation to olefins, Catal. Today. 232 (2014) 40–52.

[4] S.A. Bocanegra, A. Guerrero-Ruiz, S.R. de Miguel, O.A. Scelza, Performance of PtSn catalysts supported on MAl_2O_4 (M: Mg or Zn) in n-butane dehydrogenation: Characterization of the metallic phase, Appl. Catal. A Gen. 277 (2004) 11–22.

[5] S.A. Bocanegra, O.A. Scelza, S.R. De Miguel, Behavior of PtPb/$MgAl_2O_4$ catalysts with different Pb contents and trimetallic PtPbIn catalysts in n-butane dehydrogenation, Appl. Catal. A Gen. 468 (2013) 135–142.

[6] V. Shashikala, H. Jung, C.H. Shin, H.L. Koh, K.D. Jung, N-butane dehydrogenation on PtSn/carbon modified MgO catalysts, Catal. Letters. 143 (2013) 651–656.

[7] H. Lee, W. Il Kim, K.D. Jung, H.L. Koh, Effect of Cu promoter and alumina phases on Pt/Al_2O_3 for propane dehydrogenation, Korean J. Chem. Eng. 34 (2017) 1337–1345.

[8] L. Wang, Y. Wang, C.W. Zhang, J. Wen, X. Weng, L. Shi, A boron nitride nanosheet-supported Pt/Cu cluster as a high-efficiency catalyst for propane dehydrogenation, Catal. Sci. Technol. 10 (2020) 1248–1255.

[9] H. Kurokawa, H. Namoto, A. Horinouchi, M. Sato, M. Usui, H. Ogihara, H. Miura, Dehydrogenation of n-Butane to Butenes and 1,3-Butadiene over PtAg/Al_2O_3 Catalysts in the Presence of H_2, J. Mater. Sci. Chem. Eng. 06 (2018) 16–24.

[10] J. Valecillos, D. Rodnguez, J. Méndez, R. Solano, C. González, T. Acosta, J. Sánchez, G. Arteaga, Propane dehydrogenation over alumina-supported palladium and palladium-tin catalysts, Ciencia (Special Number on Adsorption and Catalysis) 14 (2006) 125–134.

[11] L. Rodríguez, D. Romero, D. Rodríguez, J. Sánchez, F. Domínguez, G. Arteaga, Dehydrogenation of n-butane over Pd-Ga/Al_2O_3 catalysts, Appl. Catal. A Gen. 373 (2010) 66–70.

[12] G. Wang, S. Zhang, X. Zhu, C. Li, H. Shan, Dehydrogenation versus hydrogenolysis in the reaction of light alkanes over Ni-based catalysts, J. Ind. Eng. Chem. 86 (2020) 1–12.

[13] Z.G. Wu, M. Munoz, O. Montero, The synthesis of nickel nanoparticles by hydrazine reduction, Adv. Powder Technol. 21 (2010) 165–168.

[14] J.W. Park, E.H. Chae, S.H. Kim, J.H. Lee, J.W. Kim, S.M. Yoon, J.Y. Choi, Preparation of fine Ni powders from nickel hydrazine complex, Mater. Chem. Phys. 97 (2006) 371–378.

[15] R. Wojcieszak, S. Monteverdi, J. Ghanbaja, M.M. Bettahar, Study of Ni-Ag/SiO_2 catalysts prepared by reduction in aqueous hydrazine, J. Colloid Interface Sci. 317 (2008) 166–174.

[16] Z. Li, C. Han, J. Shen, Reduction of Ni^{2+} by hydrazine in solution for preparation of nickel nano-particles, J. Mater. Sci. 41 (2006) 3473–3480.

[17] S. Sepehri, M. Rezaei, G. Garbarino, G. Busca, Facile synthesis of a mesoporous alumina and its application as a support of Ni-based autothermal reforming catalysts, Int. J. Hydrogen Energy. 41 (2016) 3456–3464.

[18] L.M. Neal, S.D. Jones, M.L. Everett, G.B. Hoflund, H.E. Hagelin-Weaver, Characterization of alumina-supported palladium oxide catalysts used in the oxidative coupling of 4-methylpyridine, J. Mol. Catal. A Chem. 325 (2010) 25–35.

[19] Y. Han, G. Gu, J. Sun, W. Wang, H. Wan, Z. Xu, S. Zheng, Selective hydrodechlorination of 1,2-dichloroethane to ethylene over Pd-Ag/Al_2O_3 catalysts prepared by surface reduction, Appl. Surf. Sci. 355 (2015) 183–190.

[20] T. Jiang, Q. Huai, T. Geng, W. Ying, T. Xiao, F. Cao, Catalytic performance of Pd-Ni bimetallic catalyst for glycerol hydrogenolysis, Biomass and Bioenergy. 78 (2015) 71–79.

[21] S. Velu, S.K. Gangwal, Synthesis of alumina supported nickel nanoparticle catalysts and evaluation of nickel metal dispersions by temperature programmed desorption, Solid State Ionics. 177 (2006)

803–811.

[22] B.T. Meshesha, N. Barrabés, J. Llorca, A. Dafinov, F. Medina, K. Föttinger, PdCu alloy nanoparticles on alumina as selective catalysts for trichloroethylene hydrodechlorination to ethylene, Appl. Catal. A Gen. 453 (2013) 130–141.

[23] K. Arve, L. Čapek, F. Klingstedt, K. Eränen, L.E. Lindfors, D.Y. Murzin, J. Dědeček, Z. Sobalik, B. Wichterlová, Preparation and characterisation of Ag/alumina catalysts for the removal of NO_x emissions under oxygen rich conditions, Top. Catal. 30–31 (2004) 91–96.

[24] R. Zhang, S. Kaliaguine, Lean reduction of NO by C_3H_6 over Ag/alumina derived from Al_2O_3, AlOOH and $Al(OH)_3$, Appl. Catal. B Environ. 78 (2008) 275–287.

[25] F. Gauthard, F. Epron, J. Barbier, Palladium and platinum-based catalysts in the catalytic reduction of nitrate in water: Effect of copper, silver, or gold addition, J. Catal. 220 (2003) 182–191.

[26] S.R. de Miguel, I.M.J. Vilella, P. Zgolicz, S.A. Bocanegra, Bimetallic catalysts supported on novel spherical $MgAl_2O_4$-coated supports for dehydrogenation processes, Appl. Catal. A Gen. 567 (2018) 36–44.

[27] O. Machynskyy, E. Kemnitz, Z. Karpiński, Aluminum fluoride-supported platinum and palladium as highly efficient catalysts of n-pentane hydroisomerization, ChemCatChem. 6 (2014) 592–602.

[28] R. Pearson, Measurement of Brønsted acd sites on aluminium oxide surfaces using deuterated pyridine and wide line nuclear magnetic resonance, J. Catal. 288 (1977) 279–288.

[29] A. V. Fionov, Lewis acid properties of alumina based catalysts: Study by paramagnetic complexes of probe molecules, Surf. Sci. 507–510 (2002) 74–81.

[30] J. Escobar, S. Núñez, A. Montesinos-Castellanos, J.A. De Los Reyes, Y. Rodríguez, O.A. González, Dibenzothiophene hydrodesulfurization over $PdPt/Al_2O_3$-TiO_2. Influence of Ti-addition on hydrogenating properties, Mater. Chem. Phys. 171 (2016) 185–194.

[31] Q. Zhu, G. Wang, H. Zhang, X. Zhu, C. Li, n-Butane dehydrogenation over $Ni\text{-}Sn/SiO_2$: Adsorption modes and reaction paths of n-butane and 1-butene, Appl. Catal. A Gen. 566 (2018) 113–120.

[32] A.N. Matveyeva, J. Wärnå, N.A. Pakhomov, D. Yu. Murzin, Kinetic modeling of isobutane dehydrogenation over Ga_2O_3/Al_2O_3 catalyst, Chem. Eng. J. 381 (2020) 122741.

भारतीय प्रौद्योगिकी संस्थान गुवाहाटी
Indian Institute of Technology Guwahati

Chapter 5

SUPPORTED BIMETALLIC CATALYSTS: EFFECT OF METAL COMPOSITION AND PREPARATION

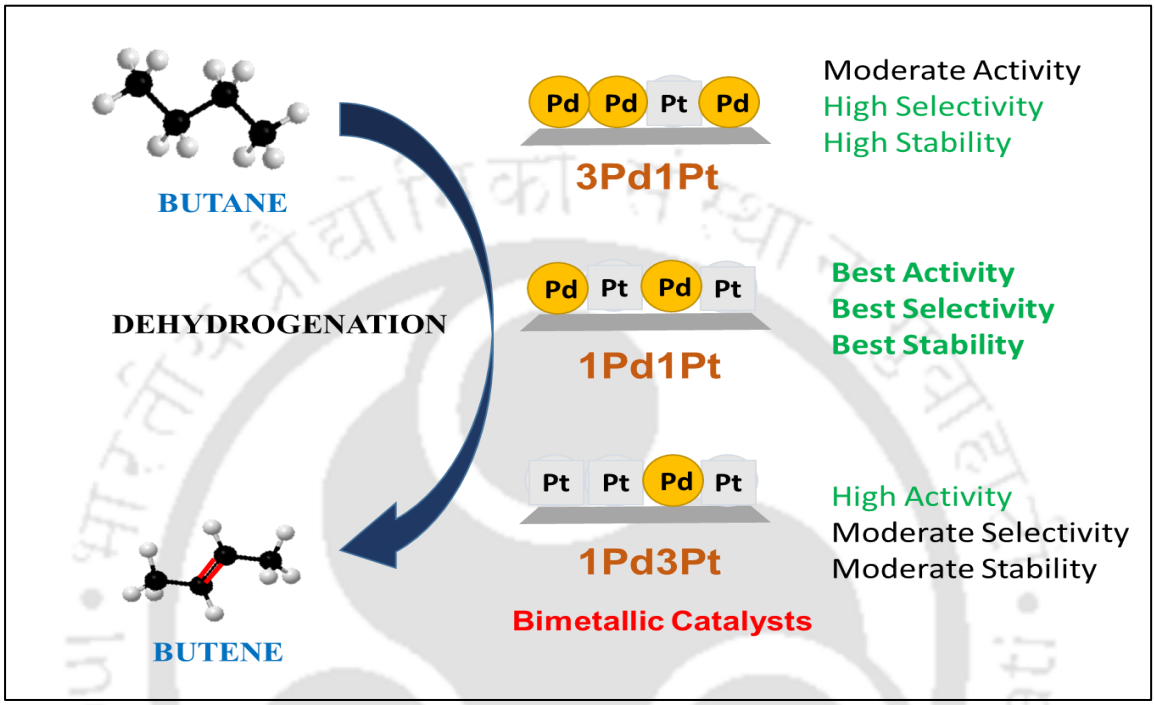

This chapter explored the performance of supported Pd and Pt based bimetallic catalysts prepared by modified electroless deposition method. Their physicochemical properties and performance for butane dehydrogenation reaction was evaluated and compared with that of catalysts prepared by impregnation methods. The effect of metal composition was studied by varying the Pd to Pt metal ratio in bimetallic catalysts as 3:1, 1:1 and 1:3. Catalysts with higher Pd content exhibited lower acidity and highest selectivity while, higher Pt content led to improved metal dispersion and higher activity. The equimolar Pd-Pt catalyst showed the highest butane conversion and butene yield.

Keywords

Bimetallic Pd-Pt catalyst; composition; catalyst preparation; modified electroless deposition; butane dehydrogenation

Chapter 5

5.1 Introduction

In chapter 2, it was observed that for butane dehydrogenation reaction, Pt was more active at lower reaction temperatures and got deactivated at higher temperatures. The Pd based catalysts though was less active at lower temperature, showed comparable or higher activity at higher temperature beyond 500 °C. In addition, Pd/Al was more selective towards butene and showed higher stability compared to Pt catalysts. Hence, the attainment of an enhanced efficiency can be targeted by an employment of both the metals in an optimal ratio. In literature also, the bimetallic catalysts are reported as more active than corresponding monometallic under optimum conditions [1-3]. However, the main challenge remains with achieving high activity along with minimizing deactivation over time. Thus, it is necessary to optimize the relative amount of the two metals, to obtain maximum effectiveness on catalytic performance.

Several studies have reported the effect of relative composition of two metals in bimetallic catalysts on reaction [4-6]. Most of the studies are reported for Pt-Sn systems [7,8-10]. Lee et al. studied butane dehydrogenation over Pt-Sn catalysts by varying amount of tin (0.5 to 1.5 wt%) [5]. The authors reported that small amount of tin (0.75 wt%) was effective in enhancing the butene yield to 33.2% in comparison to higher tin content. Nagaraja et al. reported the dehydrogenation of butane to butenes using PtSn catalysts with different metal loadings [6]. The Sn loading was varied between 0.5 to 2 wt%. For 1.5 wt% Pt loading, $Pt_{1.5}Sn_{1.5}$ gave best product yield. The catalytic activity data for these literatures is summarized in Table 5.1. The other metals that have been reported in combination with Pt for dehydrogenation processes include Na, In, Pb, Ge, etc. [11-14]. Wu et al. demonstrated that the performance of Pt/Mg(In)(Al)O catalysts for butane dehydrogenation was dependent on the In/Pt ratio [4]. The optimal ratio was reported to be between 0.33 and 0.88, yielding >95% butene selectivity.

For Pt-Pd bimetallic systems, limited studies have been reported by varying the composition of metals for various dehydrogenation and hydrogenation reactions [15-17]. Lei et al. (2012) synthesized Pt-Pd bimetallic catalysts by atomic layer deposition and employed them for oxidative dehydrogenation of propane. They reported that bimetallic catalysts exhibited better activity than the monometallic counterparts [17].

Table 5.1. Details of various studies reported for butane dehydrogenation over Pt and Pd based bimetallic catalysts including the present one.

S. No.	Catalysts	Metal loading (wt%)	Feed	Feed flow rate (mL min^{-1})	Reaction Temp (^oC)	Conversion (%)	Selectivity (%)	Yield (%)	Reference
1	Pt/Mg(In)(Al)O	Pt (0.9); In (0.17)	H_2/C_4H_{10}	80	530	13	96	12.5[a]	[4]
2	$PtSn/Al_2O_3$	Pt (0.5); Sn (0.75)	$N_2/H_2/C_4H_{10}$	30	550	37.5	89	33.4	[5]
3	$PtSn/Al_2O_3$	Pt (1.5); Sn (1.5)	$N_2/H_2/C_4H_{10}$	30	550	43.6	86.4	37.7	[6]
4	PtSn/SBA-15	Pt (3); Sn (1.5)	N_2/C_4H_{10}	100	550	29.5	-	35.5	[7]
5	Pt-Sn/SAPO-34	Pt (0.5); Sn (1)	H_2/C_4H_{10}	-	585	36.1	92.7	33.5[a]	[8]
6	PtSn/OMSO	Pt (0.5); Sn (0.5)	$N_2/H_2/C_4H_{10}$	36	575	37.3	95.8	35.7	[9]
7	PtSn/CMgO	Pt (1.1); Sn (0.3)	$N_2/H_2/C_4H_{10}$	30	550	30.6	95.2	29.1	[10]
8	$InPtSn/MgAl_2O_4$	Pt(0.3); In(0.28) Sn (0.37)	H_2/C_4H_{10}	18	530	30	96	29	[12]
9	$PtPb/MgAl_2O_4$	Pt (0.3); Pb (0.5)	H_2/C_4H_{10}	18	530	15	90	13.5	[13]
10	PdSn	Pd (0.3); Sn (0.08)	H_2/C_3H_8	85	500	12.5	61.3	7.6	[18]
11	PdGa	Pd (0.6); Ga (0.7)	H_2/C_4H_{10}	-	500	-	99	-	[19]
12	**$1Pd1Pt_{ED}$**	**Pt (1.1); Pd (0.6)**	**$N_2/H_2/C_4H_{10}$**	**100**	**550**	**49**	**86**	**42.2**	**[Present work]**

[a]*Yield determined as product of conversion and selectivity.*

However, the literatures on butane dehydrogenation over Pd based catalysts are still limited [18,19]. Valecillos et al. [18] reported that modification of Pd with Sn (0.03 wt%) led to increase in the product selectivity from 15% to 33%, that further improved to 62% on increasing the Sn content to 0.08 wt%. Similarly, Ga-Pd bimetallic catalyst (0.72 wt% Ga - 0.66 wt% Pd) also exhibited higher butene selectivity of 95% in comparison to monometallic Pd (~80%) [19].

Hence, there is a wide scope of exploring effectiveness of Pd-Pt bimetallic catalysts for butane dehydrogenation. In this study, the bimetallic Pd-Pt catalysts supported on an alumina support were prepared with varying composition of Pd and Pt metals using electroless deposition method. The amount of Pd and Pt loadings were varied in the molar ratio of 1:3, 1:1 and 3:1 to study its effect on catalytic performance for butane dehydrogenation. The performance of bimetallic catalysts was also compared with that of conventionally prepared impregnated catalysts for all loadings.

5.2 Experimental

5.2.1 Preparation of bimetallic catalysts

The catalysts were prepared by modified electroless deposition as well as impregnation method. The total metal loading was kept constant on molar basis in all the bimetallic catalysts. All the catalysts had a metal loading of 112.8 μmoles per gram of catalyst. The composition of Pd to Pt was varied in the molar ratio of 3:1, 1:1 and 1:3.

a) Electroless deposition method

The Pd and Pt precursor solutions were prepared by dissolving required amount of $PdCl_2$ and H_2PtCl_6, respectively, in 20 mL of de-ionised water. Then, 20 mL of each Pd and Pt precursor solution were mixed and stirred for 5 min. The resulting 40 mL solution contained both the metal precursors in the desired ratio. The aqueous solution of hydrazine (reducing agent) was prepared by adding required volume of $N_2H_4.H_2O$ in distilled water to facilitate reduction of metals over the support. In a typical experiment, hydrazine solution (20 mL) was passed through 2 g of alumina support and filtered after 10 min using vacuum. Then, 20 mL of co-deposited Pd-Pt metal precursor solution was gradually poured through the filtered sample maintaining 10 min of interaction time. The filtrates for both hydrazine and

metal precursor solutions were collected separately. These two steps represented the first cycle. In the second cycle, the collected filtrate of hydrazine from the first cycle was again passed through the same substrate followed by that of filtrate of Pd-Pt precursor solution. In this cycle, as well, contact time of 10 min was maintained. Similarly, in the third and fourth cycle, fresh and filtrate solutions were passed, respectively, leading to sufficient co-deposition of both Pd and Pt metals in a desired ratio over the alumina support. The resulting wet catalyst was then dried in an oven at 110 °C for 12 h. The deposited catalysts were referred to as $3Pd1Pt_{ED}$, $1Pd1Pt_{ED}$ and $1Pd3Pt_{ED}$ where the ratio of Pd to Pt was varied as 3:1, 1:1 and 1:3, respectively.

b) Impregnation method

In this method, required amount of both Pd and Pt precursors were dissolved simultaneously in 3 mL of water corresponding to a value slightly higher than the pore volume of the support material. The bimetal precursor solution was then added to the support slowly and mixed thoroughly to make a uniform paste. The impregnated catalyst was then left at room temperature in air for 2 h and dried overnight in an oven at 110 °C. The dried sample was then calcined in a muffle furnace at 400 °C for 4 h to obtain a final catalyst. The nomenclature for the impregnated bimetallic catalysts used as $3Pd1Pt_{WI}$, $1Pd1Pt_{WI}$ and $1Pd3Pt_{WI}$ corresponding to Pd to Pt ratio of 3:1, 1:1 and 1:3, respectively.

5.2.2 Catalyst characterization

The prepared catalysts were characterized using AAS, EDX, BET surface area, Reduction TPR, TEM, XRD, FTIR spectroscopy, TPD of ammonia. The details of the characterization methods are already included in section 2.2.4 in Chapter 2.

5.2.3 Dehydrogenation tests

The dehydrogenation of butane was performed in a fixed-bed down-flow reactor under atmospheric pressure in the temperature range of 100 – 600 °C. Butane in gas phase was fed into the reactor along with H_2 and N_2 gases (volumetric ratio-1:3:6) with a total flow rate of 100 mL min^{-1}. The experimental details are included in section 2.2.5 in Chapter 2.

5.3 Results and discussion

5.3.1 Effect on physicochemical properties

The Pd and Pt metal loadings in the bimetallic catalysts prepared by electroless deposition were determined by AAS analysis of initial solution and final solution after metal deposition. On molar basis, the obtained Pd and Pt loadings were almost in the same range as targeted. The Pd and Pt content varied in the range of 28-84 μmoles, that corresponded to 0.3-0.9 wt% loading for Pd and 0.55-1.65 wt% loading for Pt catalysts, in all the bimetallic catalysts as can be observed from Table 5.2. For impregnated catalysts, there was no metal loss involved. The composition of the catalysts was also determined by EDX and results were comparable to that obtained through AAS analysis for deposited bimetallic catalysts. The EDX mapping images of the bimetallic catalysts synthesized by deposition and impregnation methods are included in Appendix E. In $1Pd1Pt_{ED}$ catalyst prepared by deposition method, Pd and Pt metals were more uniformly distributed suggesting better dispersion of the metal over the surface. However, mapping images of corresponding impregnated catalysts showed less uniform dispersion and clusters of the deposited metals appeared.

Table 5.2. Metal loadings of bimetallic catalysts prepared by different methods with varied Pd-Pt compositions.

Catalysts	Ratio	Loading[a]		Loading[b]	
	Pd:Pt	Palladium	Platinum	Palladium	Platinum
		(μmoles)		(wt%)	
$3Pd1Pt_{ED}$	3:1	80.6	27	0.8 (75.2)	0.5 (25.6)
$1Pd1Pt_{ED}$	1:1	45.4	49.3	0.55 (51.7)	1.1 (56.4)
$1Pd3Pt_{ED}$	1:3	26.7	81.2	0.3 (28.2)	1.6 (82.0)
$3Pd1Pt_{WI}$	3:1	–	–	0.9 (84.6)	0.55 (28.2)
$1Pd1Pt_{WI}$	1:1	–	–	0.6 (56.4)	1.1 (56.4)
$1Pd3Pt_{WI}$	1:3	–	–	0.3 (28.2)	1.65 (84.6)

1. *Metal loading determined by a) AAS analysis and b) EDX analysis.*
2. *Total metal loading kept constant to 112.8 μmoles per g of catalyst in all the samples.*
3. *Values in parenthesis corresponds to mol%.*

The N_2 adsorption-desorption isotherms and pore size distributions for support as well as the bimetallic catalysts are shown in Figure 5.1a and b, respectively. All the catalysts exhibited isotherms with similar characteristics as that of the support. The BET surface area, pore volume and average pore size of the support and bimetallic catalysts with varying

metal compositions and prepared by different methods are summarized in Table 5.3. The surface area of all the catalysts decreased in comparison to the support, which can be ascribed to the deposition of metal species within the pores [21].

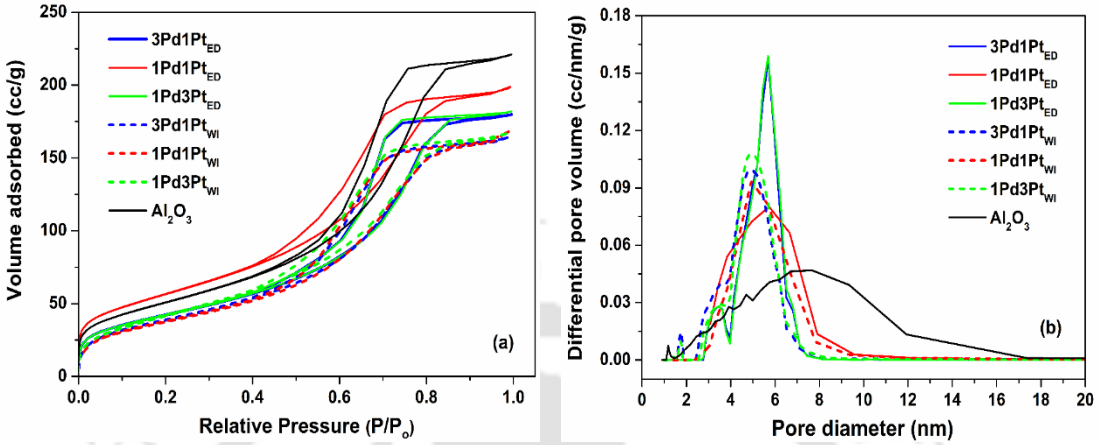

Figure 5.1. (a) Nitrogen adsorption-desorption isotherms and (b) BJH pore size distribution of alumina support and Pd-Pt bimetallic catalysts prepared by deposition and impregnation method.

The bimetallic catalysts prepared by deposition method showed only a slight decrease in surface area with respect to the support. The 1Pd3Pt$_{ED}$ catalyst exhibited the highest surface area of 183 $m^2 g^{-1}$ followed by 1Pd1Pt$_{ED}$ (181 $m^2 g^{-1}$) while it was 179 $m^2 g^{-1}$ for 3Pd1Pt$_{ED}$ catalyst. Thus, the variation in metal composition did not lead to any significant changes in surface area among the bimetallic samples. This agrees well with the fact that total metal loading was kept constant for all the catalysts. However, the surface area of the bimetallic catalysts prepared by impregnation method dropped significantly and was approximately in the range of 169-172 $m^2 g^{-1}$, lower in comparison to that observed for deposited catalysts.

The significant decrease in the BET surface areas of the impregnated bimetallic samples with respect to alumina support, suggested that the impregnation of the metals resulted in higher pore blockage. This was in spite of the fact that the total metal loadings for all the impregnated catalysts were kept same as that of the catalysts prepared by electroless deposition. Accordingly, the decrease in pore volume was also significant for impregnated catalysts as can be observed from Table 5.3. For alumina support, the total pore volume was 0.39 cc g^{-1} was lowered to 0.293-0.298 cc g^{-1} for impregnated bimetallic catalysts, while for deposited catalysts, it was in the range of 0.307-0.327 cc g^{-1}.

Table 5.3. Physical properties of support and bimetallic catalysts prepared by deposition and impregnation methods with different Pd-Pt compositions.

Catalysts	BET Surface area (m^2 g^{-1})	Pore volume (cc g^{-1})	Average pore diameter (nm)
Alumina	214	0.391	7.7
$3Pd1Pt_{ED}$	180	0.307	5.9
$1Pd1Pt_{ED}$	181	0.327	6.0
$1Pd3Pt_{ED}$	183	0.314	5.9
$3Pd1Pt_{WI}$	169	0.298	5.1
$1Pd1Pt_{WI}$	172	0.295	5.2
$1Pd3Pt_{WI}$	171	0.293	5.0

The average pore size of all the deposited catalysts also decreased with respect to that of support and was in the range of 5.9 - 6 nm. The variation in metal composition did not bring about any significant change in pore size distribution for the deposited catalysts. Same results were observed for impregnated catalysts, as they exhibited pore size in the range of 5-5.2 nm. Also, the pore size distribution was slightly broader for catalyst having equal Pd-Pt content than the other two impregnated catalysts. However, lower average pore size for impregnated catalysts compared to that of deposited catalysts agrees with the earlier observation of higher pore blockage for former. No micropores were observed in any of the catalysts (Figure 5.1b). The mesoporous character is expected to facilitate the easy transport of the reactants as well as products to the active sites [22]. From these results, it can be inferred that variation in preparation method affected the pore structure and surface area of the bimetallic catalysts but the variation of metal composition had negligible effect.

All the bimetallic catalysts were further studied using H_2-TPR analysis and Figure 5.2 shows the respective TPR profiles. All the catalysts exhibited multiple reduction peaks in wide temperature range. As also discussed in earlier chapters, the 100 – 150 °C peak results due to reduction of Pd or Pt oxide species less attached to the support, while peak at 300 – 400 °C results from reduction of oxide species strongly attached to the support. As depicted in Fig. 5, the 1Pd3PtED catalyst showed a low temperature reduction peak centered at 160 °C, due to reduction of agglomerated bulk platinum species on the surface. The second peak located at 350 °C with a small broad shoulder at 460 °C may be assigned to the reduction of platinum species in a stronger interaction with co-deposited metal and the support. When the catalyst with same composition was prepared by impregnation method, the reduction peaks shifted to a lower temperature (130 and 310 °C) indicating weaker

interaction of the deposited metals with support. The peaks corresponding to the presence of platinum were more dominant in $1Pd3Pt_{ED}$ and $1Pd3Pt_{WI}$ catalysts having higher Pt content.

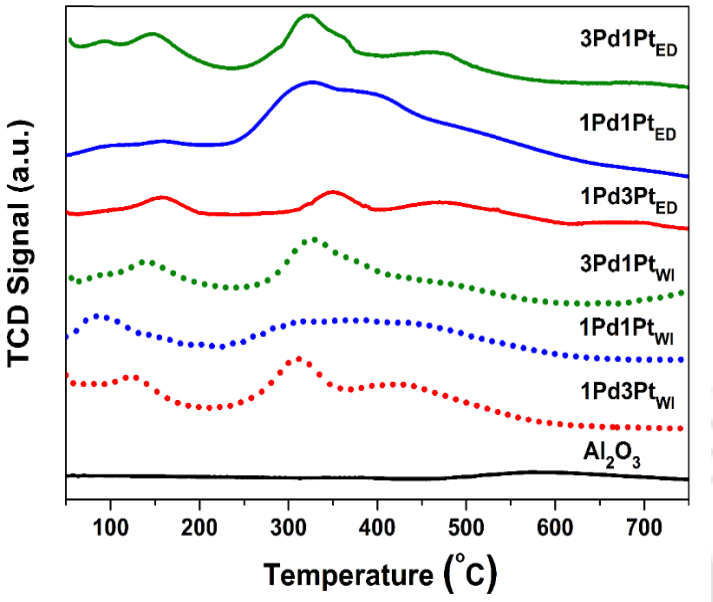

Figure 5.2. TPR profiles of bimetallic catalysts prepared by deposition and impregnation methods with different Pd-Pt compositions.

Similarly, the traits of Pd were dominant in $3Pd1Pt_{ED}$ catalyst, wherein, two low temperature reduction peaks were obtained at 90 and 145 °C that can be attributed to the reduction of weakly interacting PdO clusters. The $3Pd1Pt_{ED}$ catalyst also exhibited a high temperature peak at 340 °C along with a small shoulder at 460 °C that disappeared in corresponding impregnated $3Pd1Pt_{WI}$ catalyst. For the deposited $1Pd1Pt_{ED}$ catalyst, with equimolar content of Pd and Pt, the appearance of high intensity single broad peak in the higher temperature range of 260-460 °C suggested stronger metal – metal interaction as well as strengthening of the metal-support interaction. Non-appearance of any bulk peak at lower temperature confirmed stronger interaction between species in $1Pd1Pt_{ED}$ catalyst compared to other two metal composition catalysts. However, for impregnated $1Pd1Pt_{WI}$ catalyst a peak at lower temperature was observed at 85 °C. The intensity of the high temperature broad reduction peak at 260-450 °C was also lower in this impregnated catalyst compared to that of corresponding deposited catalyst$1Pd1Pt_{ED}$. These observations suggested relatively lower metal-support or metal-metal interaction for impregnated catalyst compared to that in deposited catalysts at same equimolar composition.

The TEM images of the deposited bimetallic catalysts are shown in Figure 5.3. Metals sites with higher atomic weight than that of support elements (aluminium and oxygen) represented the darker spots. Since Pt is heavier atom with molecular weight almost double (195.08) than that of Pd (106.4), the darkest spot may be identified with unalloyed Pt sites. As it can be observed from images that these darkest zones are highest in $1Pd3Pt_{ED}$ catalyst with highest Pt content and lowest in $3Pd1Pt_{ED}$ catalyst with lowest Pt content. In $1Pd1Pt_{ED}$ catalyst, where alloy formation is expected to be maximum, showed fewer dark spots.

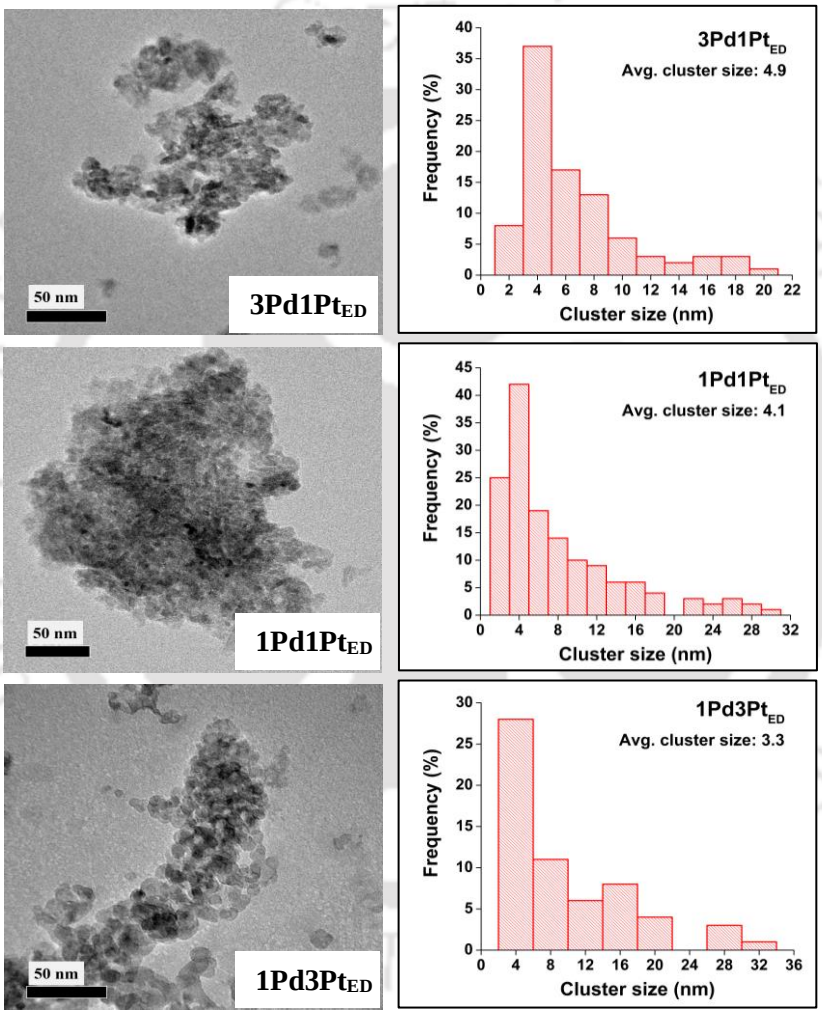

Figure 5.3. HRTEM images and corresponding particle size distributions of bimetallic catalysts prepared by deposition method with different Pd-Pt compositions.

The average size of the metal clusters calculated from TEM images ranged from 3 to 5 nm. The $1Pd3Pt_{ED}$ catalyst with higher Pt content exhibited smallest average cluster size of 3.3 nm, while $3Pd1Pt_{ED}$ had an average metal cluster size of 4.9 nm. For $1Pd1Pt_{ED}$ catalyst with equal Pd and Pt content, the average metal cluster size existed between the two

extreme values, at 4.1 nm. The metallic dispersion (D%) for the catalysts was calculated using the equation: D=1.13/d, where d is the mean particle size in nm as determined from TEM analysis. Particles are assumed to be spherical for this calculation. The highest metal dispersion of 34% was obtained for $1Pd3Pt_{ED}$ catalyst followed by 27.5 and 23% for $1Pd1Pt_{ED}$ and $3Pd1Pt_{ED}$, respectively. Since the reduction potential of platinum is higher than palladium, platinum ions tends to get reduced and deposited on the catalyst surface at a faster rate compared to that of co-existing palladium ions in solution. This simultaneous fast deposition of Pt metal ion clusters on bare support surface resulted in formation of more nucleation sites. Hence with higher Pt content, higher concentration of nucleation sites on support surface contributed to lower growth of metal clusters on surface. This explained the lowest cluster size observed for $1Pd3Pt_{ED}$ with highest Pt content. The reverse was observed for catalyst with lowest Pt content in $3Pd1Pt_{ED}$ with highest average particle size.

Figure 5.4 shows the TEM images of the corresponding impregnated catalysts with varied Pd-Pt composition. The TEM images revealed that the metal clusters were more densely populated in all impregnated catalysts and corresponding average size was in the range of 7-8.5 nm, which was much higher compared to that of deposited bimetallic catalysts. Accordingly, the corresponding dispersion values were much lower at 16, 14.7 and 13.8% for $1Pd3Pt_{WI}$, $3Pd1Pt_{WI}$ and $1Pd1Pt_{WI}$ catalysts, respectively compared to that of corresponding deposited catalysts. For $1Pd3Pt_{WI}$ catalyst, having higher Pt ratio, the lowest average size of 7.1 nm was obtained. This may be explained by the fact that Pt being in higher content in precursor solution, was naturally deposited first. On contrary, for the $3Pd1Pt_{WI}$ catalyst, Pd present in higher amount was deposited prior to Pt. Now, the precursor for Pt was chloroplatinic acid in which each Pt ion remains in coordination with 6 chloride ions [23]. In limited solvent condition of impregnation, movement of ions are restricted and, ligand effect of chloride ions may have contributed towards lowering the agglomerating tendency of Pt ion clusters. However, similar ligand effect by counter ions are not observed in case of palladium precursors. Hence, prior deposition of Pt due to its higher concentration provided more nucleation sites in $1Pd3Pt_{WI}$ catalyst than that in $3Pd1Pt_{WI}$ catalyst, where Pd was expected to be initially deposited as it was in higher concentration in precursor solution in this case. Consequently, higher average metal size of 7.7 nm was obtained for the latter. However, for $1Pd1Pt_{WI}$ catalyst with equal amount of both metals, limited solvent condition might have increased the interaction between co-

depositing metals and results in formation of larger metal clusters on the surface. The highest average metal cluster size of 8.2 nm was obtained for this catalyst. The higher metal cluster size for the impregnated catalysts might be the reason for their higher pore blockage and consequent lower surface area as well as average pore size observed during surface area and pore analysis.

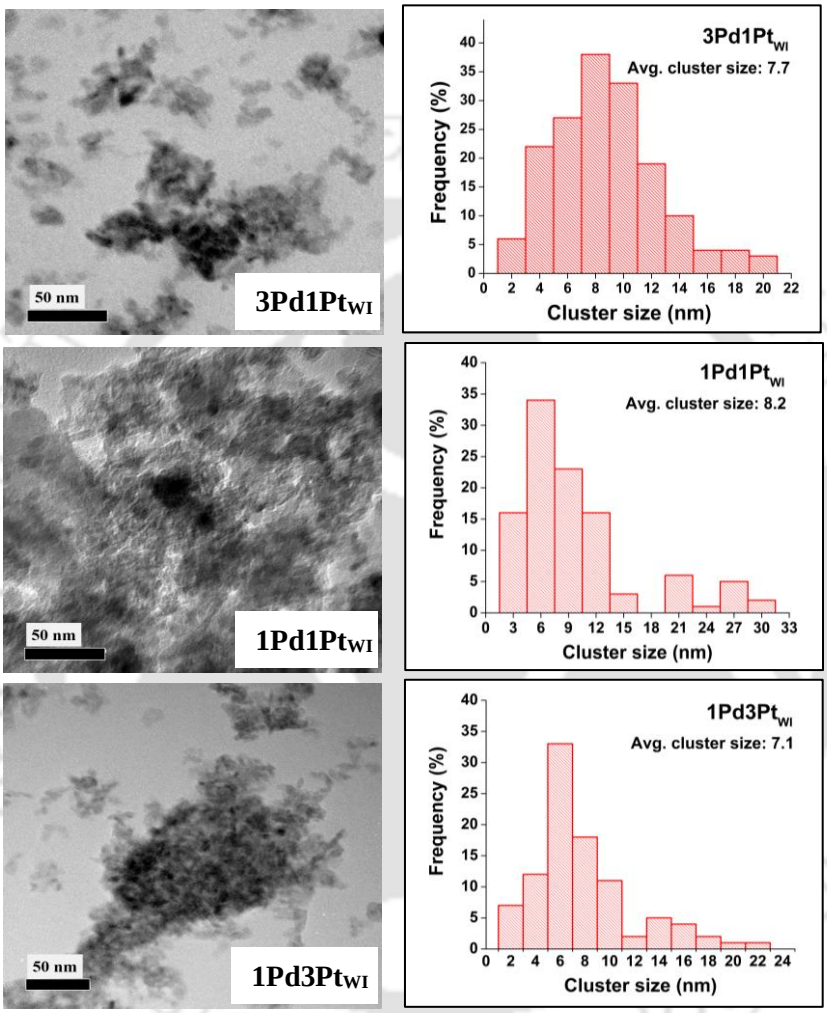

Figure 5.4. HRTEM images and corresponding particle size distributions of bimetallic catalysts prepared by impregnation method with different Pd-Pt compositions.

The structures of the deposited bimetallic catalysts were also analysed using SAED (Selected Area Electron Diffraction) patterns of metal clusters obtained during HRTEM analysis as shown in Figure 5.5. The SAED patterns of corresponding impregnated catalysts are also included in Figure 5.5. The ring identification was done through CrysT Box software. The diffraction pattern obtained for the catalysts provided information on the perpendicular distance between adjacent lattice planes (i.e. d-spacing) of Pt and Pd. The

ring patterns obtained from the SAED analysis of the deposited bimetallic catalyst showed the presence of Pd and Pt in accordance with the loading of each metal. The SAED pattern of the $1Pd3Pt_{ED}$ and $3Pd1Pt_{ED}$ catalysts showed four diffraction rings corresponding to the four planes of Pd-Pt particles, while $1Pd1Pt_{ED}$ catalyst showed six diffraction rings. The presence of Pd (111) and (222) planes and Pt (111) and Pt (022) planes corresponded to the FCC structure of Pd and Pt particles in deposited bimetallic Pd-Pt catalysts [24]. Further, the SAED images revealed the occurrence of more platinum phases in $1Pd3Pt_{ED}$ catalyst with higher Pt content. More palladium phases observed in $3Pd1Pt_{ED}$ is in accordance with higher Pd content in the sample compared to Pt.

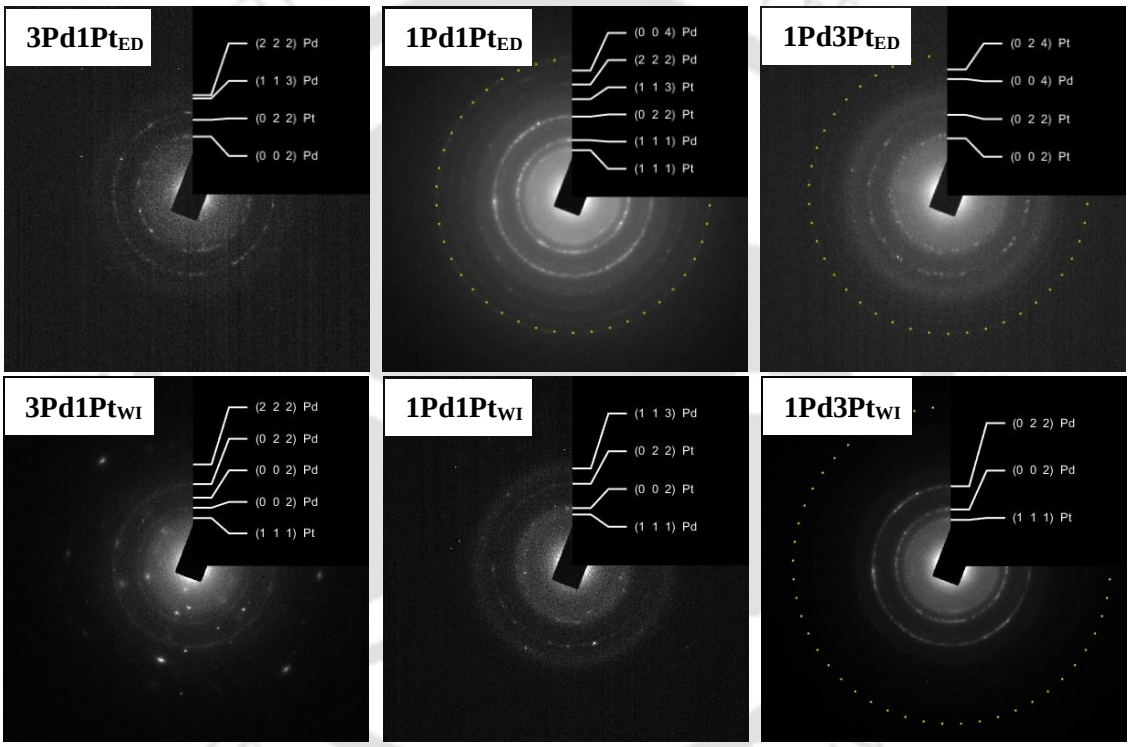

Figure 5.5. SAED patterns obtained over bimetallic catalysts prepared by deposition method (above) and impregnation method (below) with different Pd-Pt compositions.

In $1Pd1Pt_{ED}$ catalyst, uniform distribution and occurrence of Pd and Pt phases was observed. The images showed that the inner most rings were that of Pt and Pd, in $1Pd3Pt_{ED}$ and $3Pd1Pt_{ED}$ catalyst, respectively. This may be correlated with preferential deposition of Pt and Pd on support in respective catalyst surface due to their higher concentration in corresponding precursor solution as was also discussed earlier. Similarly, higher concentration of Pt and Pd also resulted in observation of their outer rings in $1Pd3Pt_{ED}$ and $3Pd1Pt_{ED}$ catalysts, respectively. Interestingly, in $1Pd1Pt_{ED}$ with equal content of both the

metals, faster deposition of Pt due to its higher reduction potential (1.18 V) than that of Pd (0.91 V) resulted in inner rings for Pt while more rings assigned to Pd were detected at outer periphery.

The XRD profiles for the support and catalysts are shown in Figure 5.6. It can be observed that for all the bimetallic catalysts no sharp peaks corresponding to Pd or Pt were observed. Neither any significant variation in peak intensity or peak position for γ-Al_2O_3 was detected in any of the bimetallic catalysts compared to that of the support. This confirmed that the metal crystallites were in dispersed state over the alumina support, as was also observed from TEM analysis. Absence of any prominent peak due to Pt or Pd metals suggested that the fraction of metal cluster size above 4 nm, the detection limit of XRD, were too low to be detected by XRD [25]. The TEM analysis also confirmed that the fraction of cluster above 4 nm was only 17% for the deposited catalysts.

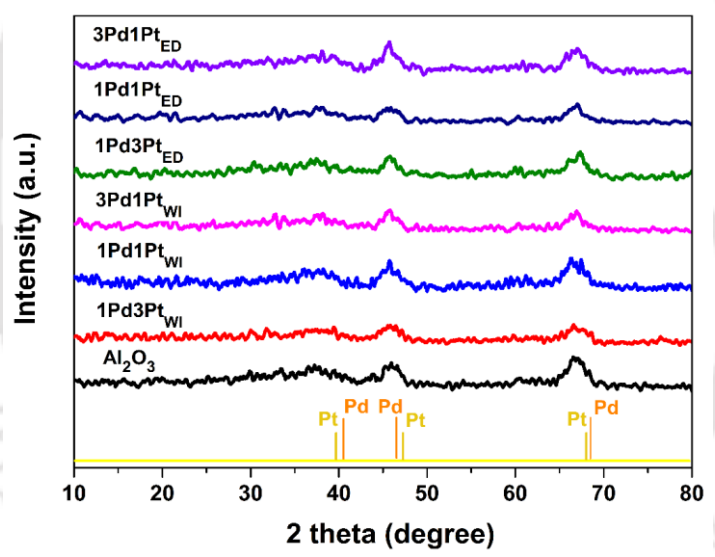

Figure 5.6. XRD spectra of alumina support and bimetallic catalysts with different Pd-Pt compositions prepared by different methods.

Figure 5.7a depicts the NH_3-TPD profiles obtained for the alumina support and the deposited bimetallic catalysts with varying Pd and Pt ratio. The corresponding total acidity in terms of ammonia uptake in mmol g^{-1} calculated from the respective desorption profiles is summarized in Table 5.4. Alumina showed the high surface acidity with highest ammonia uptake of 8.83 mmol g^{-1}. The broad desorption profiles showed a wide distribution of acid strength in the range of 100-600 °C with dominance of acid sites of medium strength, 250-350 °C. As can be observed from Table 5.4, the total acidity for the bimetallic catalysts

decreased with deposition of metals on support surface which may be explained by partial blockage of acid sites. However, the total acidity and acid strength distribution depended on the metal composition. It was observed that higher Pt content resulted in highest acidity among bimetallic catalysts and highest palladium content resulted in lowest total acidity. The $1Pd3Pt_{ED}$ catalyst with highest Pt content showed the highest acidity of 8.46 mmol NH_3 g^{-1} while, $3Pd1Pt_{ED}$ with highest Pd content showed lowest acidity of 5.66 mmol NH_3 g^{-1}. The $1Pd1Pt_{ED}$ with equimolar Pd-Pt content showed in-between acidity of 7.35 mmol NH_3 g^{-1}. The overall order of acidity in terms of total ammonia uptake was Alumina > $1Pd3Pt_{ED}$ > $1Pd1Pt_{ED}$ > $3Pd1Pt_{ED}$.

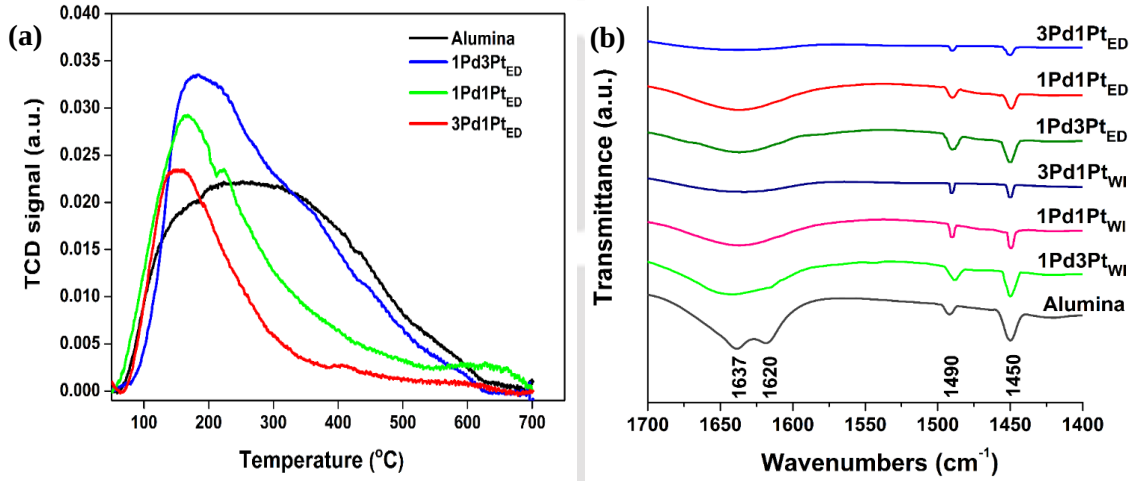

Figure 5.7. (a) NH_3-TPD profiles of alumina support and deposited bimetallic catalysts prepared with different Pd-Pt compositions and (b) Comparison of FTIR spectra of pyridine adsorbed on deposited and impregnated bimetallic catalysts prepared with different Pd-Pt compositions.

The comparison of profiles showed that for all the bimetallic catalysts desorption peaks were narrower in comparison to the support suggesting fraction of acid sites of lower strength increased in bimetallic compared to that in support. The peak maxima shifted to lower temperature from 198 °C for $1Pd3Pt_{ED}$ to 154 °C for $3Pd1Pt_{ED}$ with decreasing Pt and increasing Pd content. The area under the curve also decreased with increasing Pd content corresponding to lower total acidity as discussed above. The peaks also became narrower corresponding to disappearance of acidic sites of higher strength with increasing deposition of palladium. The results suggested more acidic nature for Pt metal compared to that of Pd metal.

Table 5.4. Acidity measurement of alumina support and deposited bimetallic catalysts prepared with different Pd-Pt compositions.

Catalysts	Total acidity mmol NH_3 g^{-1} (cat)
Alumina	8.83
$3Pd1Pt_{ED}$	5.66
$1Pd1Pt_{ED}$	7.35
$1Pd3Pt_{ED}$	8.46

Further, the surface acidity of the deposited and impregnated Pd-Pt bimetallic catalysts of varying Pd and Pt content was compared using FTIR with pyridine as a probe molecule (Figure 5.7b). All the catalyst samples exhibited peaks at 1450 and 1620 cm^{-1} which was attributed to the pyridine adsorption on Lewis acid sites. A peak at 1490 cm^{-1} common to the vibrational bands for Lewis as well as Brønsted acid sites was also observed for both support as well as all the catalyst samples. The other peak appearing at 1637 cm^{-1} was attributed to the adsorption of pyridine to Brønsted acid sites that might have resulted from the surface hydroxyl groups generated from exposure to environment. Among the deposited bimetallic catalysts, the catalyst with higher Pt content exhibited most intense peaks i.e. higher acidity followed by catalyst with equimolar Pt and Pd content. The peaks were less intense for $3Pd1Pt_{ED}$ catalyst suggesting low surface acidity. The difference in surface acidity of the catalysts could be explained on basis of metal-acid site interaction.

On interaction with Lewis sites, Pd and Pt metal tend to get partially oxidized. Since the oxidation potential of Pt is lower than that of Pd, interaction of Pt was lower with Lewis acid sites. Hence, more availability of free Lewis sites on catalyst with higher Pt content led to higher peak intensity of adsorbed pyridine compared to that observed for catalyst having higher Pd content. Further, metal crystallites themselves can also act as Lewis acid sites [26]. Because Pt has a higher reduction potential in comparison to Pd, it interacts strongly with electron lone pair of pyridine, thus giving higher peak intensity for $1Pd3Pt_{ED}$ catalyst in comparison to $3Pd1Pt_{ED}$. The $1Pd1Pt_{ED}$ showed an intermediate acidity. Furthermore, the very low intensity peaks for Brønsted acid sites in $3Pd1Pt_{ED}$ catalyst suggested that higher affinity of Pd for hydrogen neutralized all the Brønsted sites involving OH groups on the support surface.

Similar trend was also obtained for impregnated samples, where $1Pd3Pt_{WI}$ catalyst exhibited highest surface acidity followed by $1Pd1Pt_{WI}$ and $3Pd1Pt_{WI}$ catalysts. However,

the surface acidity of all the impregnated bimetallic catalysts, as observed from the FTIR spectra of adsorbed pyridine, was higher compared to that of corresponding deposited bimetallic catalysts. This was confirmed from higher intensity of the peaks for the impregnated catalysts. The higher acidity of impregnated catalysts may be attributed to their lower dispersion and larger cluster size of metals, thereby, exposing stronger acidic sites of the support surface.

5.3.2 Dehydrogenation study

Figure 5.8a illustrates the n-butane conversion in the temperature range of 100-600 °C obtained over bimetallic catalysts with varying Pd-Pt composition synthesized using deposition and impregnation methods. The conversion of n-butane steadily increased with increase in the reaction temperature for all the catalysts. The conversion trends suggested that the variation in both metal composition and preparation methods considerably affected the catalytic activity. Among the deposited catalysts, the $1Pd1Pt_{ED}$ catalyst exhibited highest conversion in the entire reaction temperature studied. In the lower temperature range, $1Pd1Pt_{ED}$ catalyst exhibited a considerable conversion of 8% even at 100 °C. The other two deposited catalysts, $3Pd1Pt_{ED}$ and $1Pd3Pt_{ED}$ exhibited lower conversion in the low temperature range. The conversion picked up sharply for all three deposited catalysts on increasing the temperature beyond 400 °C. At 400 °C, the $1Pd1Pt_{ED}$ catalyst with equal Pd-Pt content showed highest butane conversion of 31.3%, nearly double to that observed for other catalysts i.e. 14.5 and 17.3% for $3Pd1Pt_{ED}$ and $1Pd3Pt_{ED}$, respectively. The difference in activity decreased at the high reaction temperature range of 500-600 °C. At 500 °C, $1Pd3Pt_{ED}$ exhibited highest conversion (43.2%) closely followed by $1Pd1Pt_{ED}$ (42.8%) and $3Pd1Pt_{ED}$ (39.7%). On increasing the temperature further to 550 °C, both $1Pd3Pt_{ED}$ and $1Pd1Pt_{ED}$ catalysts showed similar activity exhibiting approximately 48% butane conversion. At the same reaction temperature, $3Pd1Pt_{ED}$ catalyst showed 44.3% conversion. However, the activity of $1Pd3Pt_{ED}$ catalyst dropped to 44.5% on further increase in temperature to 600 °C, while the conversion increased to 49.2 and 49.7% for $3Pd1Pt_{ED}$ and $1Pd1Pt_{ED}$ catalysts, respectively.

In the entire temperature range studied, bimetallic catalysts prepared by electroless deposition method exhibited superior activity than those prepared by impregnation method. At the initial temperature of 100 °C, none of the bimetallic catalysts synthesized by

impregnation method exhibited any conversion. Similarly, at 200 °C, $3Pd1Pt_{WI}$ and $1Pd1Pt_{WI}$ catalysts did not show conversion, however, the conversion of 5% was detected for $1Pd3Pt_{WI}$ catalyst. The conversion picked up gradually from 300 °C for all the impregnated catalysts, with $1Pd3Pt_{WI}$ catalyst showing the highest activity in the temperature range of 100-550 °C. The highest conversion of 35.4% was obtained over $1Pd3Pt_{WI}$ catalyst followed by that for $3Pd1Pt_{WI}$ (30.3%) and $1Pd1Pt_{WI}$ catalyst (29.1%) at 550 °C. However, with the further increase in temperature to 600 °C, conversion dropped to 27.3% for $1Pd3Pt_{WI}$ catalyst, while it increased to 33.4% for $3Pd1Pt_{WI}$ catalyst. The conversion remained similar at 29.9% for $1Pd1Pt_{WI}$ catalyst at 600 °C.

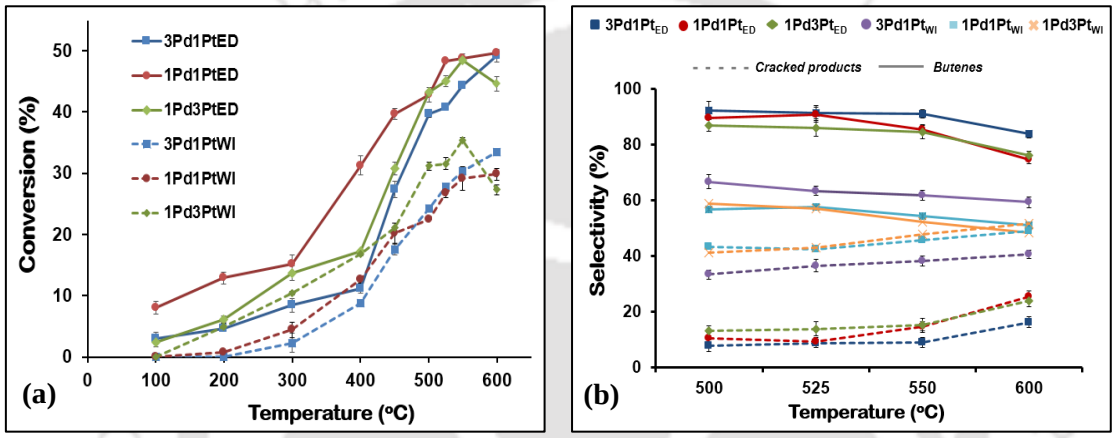

Figure 5.8. Catalytic performance of bimetallic Pd-Pt catalysts at different temperatures (a) butane conversion profiles and (b) product selectivity profiles.

The turnover frequencies (TOFs) of the catalysts were determined based on the total metal loading. Table 5.5 shows the TOF values at 550 °C, obtained for all the bimetallic catalysts. Deposited bimetallic catalysts exhibited higher TOFs than impregnated catalysts with $1Pd1Pt_{ED}$ showing highest TOF of 1.18 s^{-1} followed by $1Pd3Pt_{ED}$ catalyst (1.16 s^{-1}). The catalyst with higher Pd content exhibited slightly lower TOF of 1.09 s^{-1}. The TOFs were in the range of 0.7-0.9 s^{-1} for impregnated bimetallic catalysts at 550 °C. Both deposited and impregnated catalysts with high palladium content showed lower activity up to a temperature of 550 °C. The lower activity of these catalysts might be explained by the higher energy barrier for interaction of hydrocarbon with Pd compared to that with Pt [27]. Thereby, butane interacted less with Pd compared to that with Pt giving lower conversion. However, among deposited catalysts, significantly higher activity for $1Pd1Pt_{ED}$ catalyst compared to that of $1Pd3Pt_{ED}$ suggested presence of more active species on former. This

higher activity might had resulted from the alloying of Pd and Pt metal in $1Pd1Pt_{ED}$ catalyst as observed from the characterization analysis discussed above. The metal-metal interaction as well as metal support interaction was strongest for $1Pd1Pt_{ED}$ catalyst among all the compositions. At same composition of 1Pd1Pt alloying was higher when prepared by deposition compared to when prepared by impregnation. Thus lower alloying resulted in lower activity of $1Pd1Pt_{WI}$ catalyst.

Table 5.5. Catalytic activity of Pd-Pt bimetallic catalysts for n-butane dehydrogenation at 550 °C [Feed ratio (n-butane:hydrogen:nitrogen) = 1:3:6].

Catalyst	Conversion (%)	TOF (s^{-1})	Selectivity (%)					
			Iso-butene	1-butene	Trans-2-butene	Cis-2-butene	Total butene	C_1-C_3
$3Pd1Pt_{ED}$	44.3	1.09	15.8	24.7	28.4	22.2	91.1	8.9
$1Pd1Pt_{ED}$	48.8	1.18	19.4	20.3	24.3	21.5	85.5	14.5
$1Pd3Pt_{ED}$	48.5	1.16	17.4	22.5	25.7	19.1	84.7	15.3
$3Pd1Pt_{WI}$	30.3	0.72	12.4	16.3	19.4	13.7	61.8	38.2
$1Pd1Pt_{WI}$	29.1	0.71	9.0	10.6	19.9	14.8	54.3	45.7
$1Pd3Pt_{WI}$	35.4	0.87	15.3	12.8	13.7	10.3	52.1	47.9

At 600 °C, the conversion decreased for both the high Pt containing catalysts prepared by deposition and impregnation. At 600 °C, the sintering of Pt metal or deactivation by secondary reaction might have led to decrease in activity of high Pt containing catalysts. These observations have been later confirmed by analysis of spent catalysts. The overall higher activity of deposited catalysts over impregnated catalysts at all compositions may be explained by higher metal dispersion for former. The metal dispersion values were obtained in the range of 23-34% for deposited bimetallic catalysts compared to only 13.5-16% observed for impregnated catalysts at similar metal loadings. Thus, higher metallic dispersion for all the deposited bimetallic catalysts led to the availability of greater number of active metal sites, thereby increasing butane conversion. The pore analysis revealed that the addition of metal on support by deposition did not result in significant pore blockage. The decrease in surface area and pore volume for deposited catalysts was marginal at all compositions. This might have resulted from better dispersion of metal in deposited catalyst as discussed above. The less pore blockage in deposited catalysts might have offered lower hindrance to diffusion of reaction and products, thereby also facilitating conversion of butane.

Butane dehydrogenation resulted in formation of all the butene isomers including iso-butene, 1-butene and 2-butene along with C_1-C_3 hydrocarbons over all the catalysts. However relative amount varied with difference in composition and preparation method. Both saturated and unsaturated C_1–C_3 compounds were detected (Appendix G). Neither butadiene nor any higher hydrocarbons beyond butenes were detected in the product stream. The overall selectivity trends for products in the temperature range of 500-600 °C for all the catalysts are shown in Figure 5.8b. For all the deposited bimetallic catalysts, the selectivity towards C_1-C_3 compounds was observed to increase gradually with the increase in temperature up to 550 °C. A significant rise was noted on further increasing the temperature to 600 °C. The cracking reactions, having higher activation energy than that of dehydrogenations, are more favoured at higher temperature. Hence the observation of rise in C_1-C_3 compounds with increase in temperature. The results are in agreement with the reported works that observed enhanced generation of lower hydrocarbons by C-C cleavage at higher temperature, lowering selectivity of butene [19].

The selectivity pattern for the bimetallic catalysts was observed to depend on the metal composition. The bimetallic catalyst, $3Pd1Pt_{ED}$ showed highest selectivity of 91% towards butenes at 550 °C, followed by $1Pd1Pt_{ED}$ (85.5%). The $1Pd3Pt_{ED}$ catalyst having higher Pt content exhibited lowest butene selectivity of 84.7%. Accordingly, at 550 °C, the selectivity towards cracked product formation was lowest for $3Pd1Pt_{ED}$ catalyst (9%) followed by that of $1Pd1Pt_{ED}$ catalyst (14.5%), while it was highest for $1Pd3Pt_{ED}$, 15.3%. On further increasing the temperature to 600 °C, the butene selectivity decreased considerably for $1Pd1Pt_{ED}$ and $1Pd3Pt_{ED}$ catalysts to 74.5 and 76.2%, respectively. The decrease in butene selectivity was lower for $3Pd1Pt_{ED}$ catalyst with higher Pd ratio (84% at 600 °C). From the selectivity trends, it can be inferred that higher Pd content in catalysts favoured butene formation, while higher Pt ratio resulted in comparatively higher formation of C_1-C_3 hydrocarbons. This trend in selectivity can be explained by surface acidity of the catalyst surface. Higher surface acidity contributes towards cracking of hydrocarbons. It is reported that the cleavage of C-C bond is primarily catalysed by the strong acid sites which also restrain desorption of olefins precursors [28]. This leads to polymerization and formation of coke precursors. The $3Pd1Pt_{ED}$ catalyst exhibited least acidity, as observed from the NH_3-TPD analysis, and accordingly showed lowest selectivity towards cracked products and highest selectivity to butenes. While, the higher surface acidity in $1Pd3Pt_{ED}$ catalysts might have favoured formation of C_1-C_3 hydrocarbons.

Similar effect of metal composition on product selectivity was observed for impregnated bimetallic catalysts as well. The highest butene selectivity of 66.7% at 500 °C was observed for $3Pd1Pt_{WI}$ catalyst that dropped to 59.4% on increasing the temperature from 500 to 600 °C. The lowest butene selectivity was obtained over $1Pd3Pt_{WI}$ catalyst, wherein, butene selectivity decreased significantly from 58.7 to 48.3% on increasing the temperature to 600 °C. The bimetallic Pd-Pt catalysts prepared by impregnation thus exhibited much lower selectivity towards butenes in comparison to deposited catalysts for all compositions. The lower butene selectivity in impregnated catalysts was probably due to larger metal cluster size and higher surface acidity. The large clusters tend to interact with the formed primary products more easily, leading to secondary reactions such as oligomerization and polymerization. Thereby, the butene selectivity decreased. Further, higher surface acidity of impregnated catalysts led to enhanced cracking reaction as discussed earlier, ultimately leading to decreased selectivity towards butene formation.

The comparison of product distributions for all bimetallic catalysts at 550 °C is shown in Table 5.5. All the catalysts exhibited higher selectivity towards the formation of 2-butenes followed by 1-butene. Also, the catalyst with higher Pd content exhibited lower selectivity towards the formation of iso-butene in comparison to the other two catalysts having higher Pt content. The highest selectivity towards butene, (1-butene: 24 %, trans-2-butene: 28 % and cis-2-butene: 22 %) was obtained over $3Pd1Pt_{ED}$ catalyst.

Figure 5.9a illustrates the total butene yield obtained over different catalysts in the temperature range of 500-600 °C. The product yield was calculated by Eq. 2.8 (section 2.2.5 of Chapter 2). The butene yield over bimetallic catalysts varied with the composition of the metals as well as preparation method. The temperature at which the highest butene yields were achieved differed for different metal compositions. Among the catalysts prepared by deposition, the $1Pd1Pt_{ED}$ catalyst with equal Pd and Pt ratio showed the highest butene yield of 43.8% at 525 °C that thereafter decreased at higher temperatures; 41.7% at 550 and 37% at 600 °C. For $1Pd3Pt_{ED}$ and $3Pd1Pt_{ED}$ catalysts, the highest butene yields of 41% and 40.3% were obtained at 550 °C. On raising the temperature to 600 °C, the butene yield increased to 41.2% for $3Pd1Pt_{ED}$ catalyst with higher proportion of Pd, but decreased for the other two metal compositions. Moreover, higher butene yields were obtained over Pd-Pt bimetallic catalysts prepared by electroless deposition method in comparison to those prepared by impregnation method. The higher yield of all deposited catalysts may be

attributed to their higher butane conversion as well as butene selectivity. Among impregnated catalysts, the highest yield of 19.8% was obtained at 600 °C over $3Pd1Pt_{WI}$ catalyst. The overall yield order obtained at 550 °C was $1Pd1Pt_{ED}$ (41.7%) > $1Pd3Pt_{ED}$ (41%) > $3Pd1Pt_{ED}$ (40.3%) > $3Pd1Pt_{WI}$ (18.7%) > $1Pd3Pt_{WI}$ (18.4%) > $1Pd1Pt_{WI}$ (15.8%).

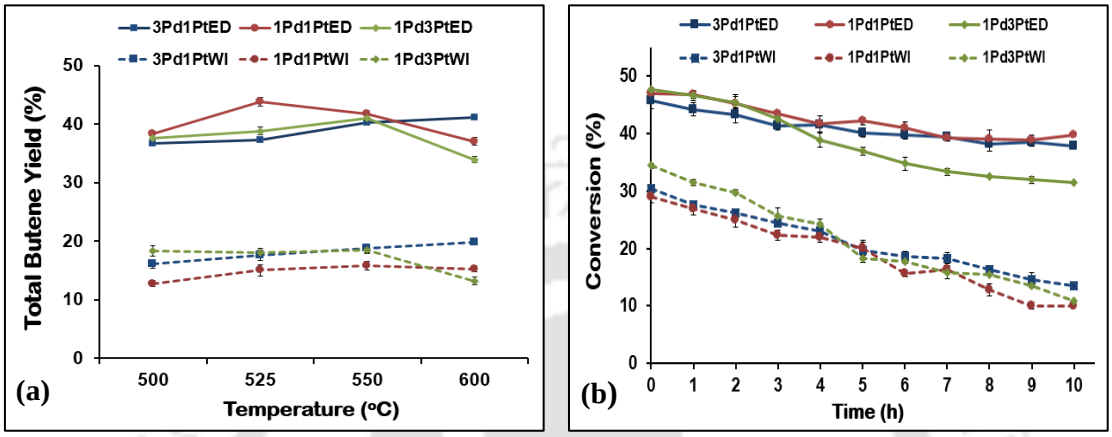

Figure 5.9. Catalytic performance of bimetallic catalysts prepared with different Pd-Pt compositions by deposition and impregnation methods (a) product yield and (b) deactivation profiles obtained at 550 °C.

Further, a deactivation study was carried out to investigate the effect of metal composition and preparation method on catalyst stability. Figure 5.9b shows the change in butane conversion at 550 °C with time on stream for 10 h. Among the deposited catalysts, $1Pd1Pt_{ED}$ catalyst showed greater stability in comparison to other two metal composition of catalysts. Further, it was observed that irrespective of the metal composition, the bimetallic catalysts synthesized by electroless deposition exhibited much greater stability than those prepared by impregnation. In addition, for both electroless deposition and impregnation method, the variation in metal composition had a similar effect on catalytic stability. The catalysts having higher proportion of Pd possessed higher stability in comparison to the catalysts having higher Pt proportion. The initial conversions obtained for $3Pd1Pt_{ED}$, $1Pd1Pt_{ED}$, $1Pd3Pt_{ED}$, $3Pd1Pt_{WI}$, $1Pd1Pt_{WI}$ and $1Pd3Pt_{WI}$ catalysts were 45.7, 47, 47.6, 30.4, 29 and 34.4% that decreased to 37.8, 39.7, 31.4, 13.4, 10 and 10.9%, respectively, after 10 h. Thus, percentage deactivation of the respective catalysts (Eq. 2.9, section 2.2.5, Chapter 2) after 10 h of time on stream study was as follows: $1Pd1Pt_{ED}$ (15%) < $3Pd1Pt_{ED}$ (17%) < $1Pd3Pt_{ED}$ (34%) < $3Pd1Pt_{WI}$ (56%) < $1Pd1Pt_{WI}$ (65%) < $1Pd3Pt_{WI}$ (68%).

The higher content of Pd in catalysts enhanced stability by suppressing C-C cleavage reactions, while, Pt promoted the same as observed from Figure 5.8b. As discussed earlier higher acidic nature of catalyst with more Pt content promoted cracking reaction thereby deactivating the catalyst. As observed above, the catalysts prepared by impregnation method suffered severe deactivation and lost their activity drastically after 10 h. The comparatively much lower deactivation and significantly improved stability in the bimetallic catalysts synthesized by deposition method may have resulted from stronger metal-support interaction and lower selectivity towards cracked product formation. It has been reported that the cracking and condensation reactions stimulate coke formation covering the active metal sites and ultimately leads to the deactivation of dehydrogenation catalysts. Thus, the catalytic stability profiles were well related with their corresponding product selectivity patterns and were influenced by the metal composition and preparation methodology adopted.

5.3.3 Analysis of spent catalysts

The spent deposited bimetallic catalysts were analysed using BET, TEM and TGA analysis. The obtained results were compared with the corresponding fresh catalysts to understand the variation in physicochemical properties of the catalysts after undergoing reaction. The properties of the spent bimetallic catalysts are summarized in Table 5.6. The surface area was found to decrease to 176, 179 and 178 m^2 g^{-1} for spent 3Pd1Pt$_{ED}$ 1Pd1Pt$_{ED}$ and 1Pd3Pt$_{ED}$ catalysts from 180, 181 and 183 m^2 g^{-1}, respectively of corresponding fresh catalyst. The decrease in surface area was thus nominal (1-3%) for all the spent catalysts. The loss of surface area was lowest for 1Pd1Pt$_{ED}$_spent catalyst and highest for 1Pd3Pt$_{ED}$_spent catalyst. The average pore size and pore volume of spent catalysts also reduced marginally compared to corresponding fresh catalysts (Table 5.6). A nominal decrease in surface area and pore volume suggested that there was no significant coke deposition or variation in support porous structure due to reaction.

Low coke deposition was also confirmed by the TGA analysis of samples in flow of air. In the TGA analysis, weight loss is expected owing to the combustion of deposited carbon in flow of air. The TGA profiles (Appendix H) of the spent catalysts showed the combustion around 100-200 °C with weight loss of 2.6, 4.8, and 6.7 wt% for 1Pd1Pt$_{ED}$_spent, 3Pd1Pt$_{ED}$_spent and 1Pd3Pt$_{ED}$_spent, respectively. The higher platinum content catalyst thus showed highest weight loss while 1Pd1PtED_spent showed lowest weight loss. This

suggested under similar reaction conditions, the highest coke deposition was observed for catalyst with higher Pt content that is 1Pd3PtED, while the lowest was observed for 1Pd1PtED. Along with the stability of the catalysts, the overall low coke deposition on the all the deposited catalyst might have also resulted from the presence of hydrogen in the feed which suppressed coke formation.

Table 5.6. Textural properties of spent bimetallic catalysts prepared by deposition method.

Catalysts	BET surface area (m^2 g^{-1})	Pore volume (cc g^{-1})	Average pore diameter (nm)
3Pd1Pt$_{ED}$_spent	176 (2.2)	0.300 (2.3)	5.8
1Pd1Pt$_{ED}$_spent	179 (1.1)	0.319 (2.4)	6.0
1Pd3Pt$_{ED}$_spent	178 (2.7)	0.297 (5.1)	5.7

Values in parenthesis correspond to percentage decrease with respect to corresponding fresh catalysts

The TEM images of spent catalysts are illustrated in Figure 5.10. The average cluster sizes were observed to increase to 5.2, 4.5 and 4.2 nm for spent catalysts from 4.9, 4.1 and 3.3 nm for 3Pd1Pt$_{ED}$_spent, 1Pd1Pt$_{ED}$_spent.and 1Pd3Pt$_{ED}$_spent, respectively. Though, there was a growth in average metal cluster size after the dehydrogenation reaction for all the compositions, the percentage growth was highest for the 1Pd3Pt$_{ED}$_spent catalyst having highest Pt content. The dispersion values also decreased to 21.7% (3Pd1Pt$_{ED}$_spent), 25.1% (1Pd1Pt$_{ED}$_spent) and 26.9% (1Pd3Pt$_{ED}$_spent) for corresponding spent catalysts, accordingly. The slight increase in average metal particle size and decrease in metal dispersion may be attributed to some structural modification of metal clusters. The sintering of the deposited metals under reaction conditions was the reason for the observed phenomenon.

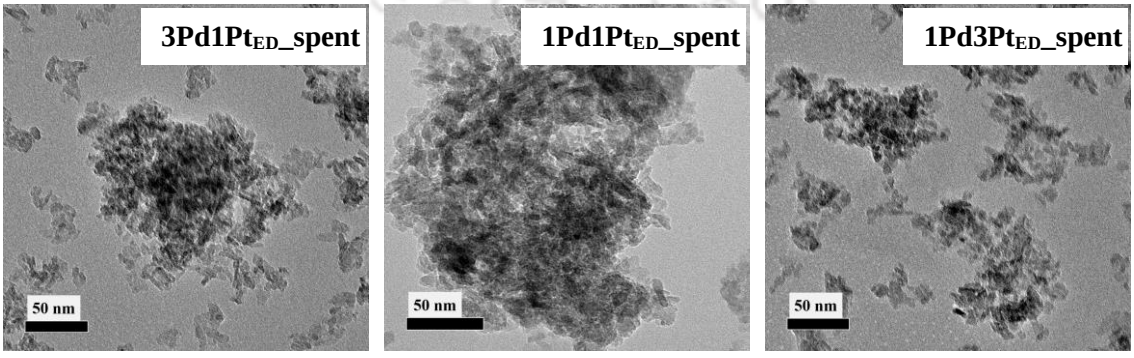

Figure 5.10. TEM images of spent bimetallic catalysts prepared by deposition method with different Pd-Pt compositions.

The analysis of the spent catalysts showed that overall coke deposition was low and catalyst structure was relatively stable for all the deposited bimetallic catalysts. The relatively higher deactivation observed for $1Pd3Pt_{ED}$ catalyst (high Pt content) at increased temperature of 600 °C agreed with relatively more deposition of carbon and modification of metal sites observed for this sample compared to other two deposited catalysts. The relatively higher coke deposition for $1Pd3Pt_{ED}$ catalyst suggested higher extent of cracking reaction over this catalyst that agreed with the lower butene selectivity observed for this sample at 600 °C. The lowering of activity at this temperature for $1Pd3Pt_{ED}$, as observed, also might be the result of slight coke deposition. The least coke deposition and structural modification led to highest activity and stability for $1Pd1Pt_{ED}$ catalyst.

5.4 Summary

The effects of metal composition and preparation were investigated on alumina supported Pd-Pt bimetallic catalysts employed for butane dehydrogenation. The Pd to Pt metal ratio was varied as 3:1, 1:1 and 1:3, while, preparation was done by electroless deposition and impregnation methods. Catalysts with higher Pd content exhibited lower acidity and highest selectivity while, higher Pt content led to improved metal dispersion and higher activity. Equimolar Pd and Pt ratio led to better metal-metal interaction as well as metal-support interaction. The deposited equimolar $1Pd1Pt_{ED}$ catalyst showed the highest butane conversion of 48.5% and butene yield of 42% at 550 ºC with lowest deactivation (15%) after 10 h process time. For all compositions, the deposited catalysts showed better catalytic performance than that of impregnated catalysts, which might be attributed to higher metal dispersion, stronger metal-metal and metal-support interactions and lower surface acidity observed in the former. The overall order for butene yield was $1Pd1Pt_{ED}$ (42%) > $1Pd3Pt_{ED}$ (41%) > $3Pd1Pt_{ED}$ (40.3%) > $3Pd1Pt_{WI}$ (18.7%) > $1Pd3Pt_{WI}$ (18.4%) > $1Pd1Pt_{WI}$ (15.8%), while for catalytic stability it was as follows: $1Pd1Pt_{ED}$ (15%) > $3Pd1Pt_{ED}$ (17%) > $1Pd3Pt_{ED}$ (34%) > $3Pd1Pt_{WI}$ (56%) > $1Pd1Pt_{WI}$ (65%) > $1Pd3Pt_{WI}$ (68%).

References

[1] E.L. Jablonski, A.A. Castro, O.A. Scelza, S.R. De Miguel, Effect of Ga addition to Pt/Al_2O_3 on the activity, selectivity and deactivation in the propane dehydrogenation, Appl. Catal. A Gen. 183 (1999) 189–198.

[2] S. Furukawa, M. Endo, T. Komatsu, Bifunctional catalytic system effective for oxidative

dehydrogenation of 1-butene and n -butane using Pd-based intermetallic compounds, ACS Catal. 4 (2014) 3533–3542.
[3] J. Silvestre-Albero, J.C. Serrano-Ruiz, A. Sepúlveda-Escribano, F. Rodríguez-Reinoso, Modification of the catalytic behaviour of platinum by zinc in crotonaldehyde hydrogenation and iso-butane dehydrogenation, Appl. Catal. A Gen. 292 (2005) 244–251.
[4] J. Wu, Z. Peng, P. Sun, A.T. Bell, n-Butane dehydrogenation over Pt/Mg(In)(Al)O, Appl. Catal. A Gen. 470 (2014) 208–214.
[5] M.H. Lee, B.M. Nagaraja, K.Y. Lee, K.D. Jung, Dehydrogenation of alkane to light olefin over PtSn/θ-Al_2O_3 catalyst: Effects of Sn loading, Catal. Today. 232 (2014) 53–62.
[6] B.M. Nagaraja, C.H. Shin, K.D. Jung, Selective and stable bimetallic PtSn/θ-Al_2O_3 catalyst for dehydrogenation of n-butane to n-butenes, Appl. Catal. A Gen. 467 (2013) 211–223.
[7] L. Deng, H. Miura, T. Ohkubo, T. Shishido, Z. Wang, S. Hosokawa, K. Teramura, T. Tanaka, The importance of direct reduction in the synthesis of highly active Pt-Sn/SBA-15 for: N-butane dehydrogenation, Catal. Sci. Technol. 9 (2019) 947–956.
[8] Z. Nawaz, W. Fei, Pt - Sn-based SAPO-34 supported novel catalyst for n-butane dehydrogenation, Ind. Eng. Chem. Res. 48 (2009) 7442–7447.
[9] P. Natarajan, H.A. Khan, S. Yoon, K.D. Jung, One-pot synthesis of Pt–Sn bimetallic mesoporous alumina catalysts with worm-like pore structure for n-butane dehydrogenation, J. Ind. Eng. Chem. 63 (2018) 380–390.
[10] V. Shashikala, H. Jung, C.H. Shin, H.L. Koh, K.D. Jung, N-butane dehydrogenation on PtSn/carbon modified MgO catalysts, Catal. Letters. 143 (2013) 651–656.
[11] S.A. Bocanegra, A.A. Castro, A. Guerrero-Ruíz, O.A. Scelza, S.R. de Miguel, Characteristics of the metallic phase of Pt/Al_2O_3 and Na-doped Pt/Al_2O_3 catalysts for light paraffins dehydrogenation, Chem. Eng. J. 118 (2006) 161–166.
[12] S.A. Bocanegra, A.A. Castro, O.A. Scelza, S.R. de Miguel, Characterization and catalytic behavior in the n-butane dehydrogenation of trimetallic InPtSn/$MgAl_2O_4$ catalysts, Appl. Catal. A Gen. 333 (2007) 49–56.
[13] S. Bocanegra, M.J. Yañez, O. Scelza, S. De Miguel, Effect of the synthesis method of $MgAl_2O_4$ and of Sn and Pb addition to platinum catalysts on the behavior in n -butane dehydrogenation, Ind. Eng. Chem. Res. 49 (2010) 4044–4054.
[14] A.D. Ballarini, P. Zgolicz, I.M.J. Vilella, S.R. de Miguel, A.A. Castro, O.A. Scelza, n-Butane dehydrogenation on Pt, PtSn and PtGe supported on γ-Al_2O_3 deposited on spheres of α-Al_2O_3 by washcoating, Appl. Catal. A Gen. 381 (2010) 83–91.
[15] C. Micheaud-Especel, D. Bazin, M. Guérin, P. Marécot, J. Barbier, Study of supported bimetallic Pd-Pt catalysts. Characterization and catalytic activity for toluene hydrogenation, React. Kinet. Catal. Lett. 69 (2000) 209-216.
[16] J.L. Rousset, L. Stievano, C.J. Santos Aires, C. Geantet, A.J. Renouprez, M. Pellarin, Hydrogenation of tetralin in the presence of sulfur over γ-Al_2O_3-supported Pt, Pd, and Pd–Pt model catalysts, J. Catal. 202 (2001) 163–168.
[17] Y. Lei, B. Liu, J. Lu, R.J. Lobo-Lapidus, T. Wu, H. Feng, X. Xia, A.U. Mane, J.A. Libera, J.P. Greeley, J.T. Miller, J.W. Elam, Synthesis of Pt-Pd core-shell nanostructures by atomic layer deposition: Application in propane oxidative dehydrogenation to propylene, Chem. Mater. 24 (2012) 3525–3533.
[18] J. Valecillos, D. Rodnguez, J. Méndez, R. Solano, C. González, T. Acosta, J. Sánchez, G. Arteaga, Propane dehydrogenation over alumina-supported palladium and palladium-tin catalysts, Ciencia (Special Number on Adsorption and Catalysis) 14 (2006) 125–134.
[19] L. Rodríguez, D. Romero, D. Rodríguez, J. Sánchez, F. Domínguez, G. Arteaga, Dehydrogenation of n-butane over Pd-Ga/Al_2O_3 catalysts, Appl. Catal. A Gen. 373 (2010) 66–70.
[20] D. Hu, H. Xu, Z. Yi, Z. Chen, C. Ye, Z. Wu, H.F. Garces, K. Yan, Green CO_2-Assisted Synthesis of Mono- And Bimetallic Pd/Pt Nanoparticles on Porous Carbon Fabricated from Sorghum for Highly Selective Hydrogenation of Furfural, ACS Sustain. Chem. Eng. 7 (2019) 15339–15345.
[21] M. Setnička, R. Bulánek, L. Čapek, P. Čičmanec, N-Butane oxidative dehydrogenation over VO_X-HMS catalyst, J. Mol. Catal. A Chem. 344 (2011) 1–10.
[22] M. Setnička, Z. Tišler, D. Kubička, R. Bulánek, Activity of Molybdenum Oxide Catalyst Supported on Al_2O_3, TiO_2, and SiO_2 Matrix in the Oxidative Dehydrogenation of n-Butane, Top. Catal. 58 (2015) 866–876.
[23] O.B. Bel'skaya, R.K. Karymova, D.I. Kochubey, V.K. Duplyakin, Genesis of the active-component precursor in the synthesis of Pt/Al_2O_3 catalysts: I. Transformation of the $[PtCl_6]^{2-}$ complex in the interaction between chloroplatinic acid and the γ-Al_2O_3 surface, Kinet. Catal. 49 (2008) 720–728.
[24] R. Venu, T.S. Ramulu, S. Anandakumar, V.S. Rani, C.G. Kim, Bio-directed synthesis of platinum

nanoparticles using aqueous honey solutions and their catalytic applications, Colloids Surfaces A Physicochem. Eng. Asp. 384 (2011) 733–738.

[25] J. Chen, Y. Wu, W. Hu, P. Qu, X. Liu, R. Yuan, L. Zhong, Y. Chen, Insights into the role of Pt on Pd catalyst stabilized by magnesia-alumina spinel on gama-alumina for lean methane combustion: Enhancement of hydrothermal stability, Mol. Catal. 496 (2020) 111185.

[26] D. Kubička, N. Kumar, T. Venäläinen, H. Karhu, I. Kubičková, H. Österholm, D.Y. Murzin, Metal-support interactions in zeolite-supported noble metals: Influence of metal crystallites on the support acidity, J. Phys. Chem. B. 110 (2006) 4937–4946.

[27] M. Skotak, Z. Karpiński, C_6-alkane conversion over γ-alumina supported palladium and platinum catalysts, Chem. Eng. J. 90 (2002) 89–96.

[28] J. Zhang, T. Chen, Y. Jiao, L. Wang, J. Wang, Y. Chen, Q. Zhu, X. Li, Role of acidity in catalytic cracking of n-decane over supported Pt-based catalysts, Appl. Surf. Sci. 507 (2020) 145113.

Chapter 6

SUPPORTED BIMETALLIC CATALYSTS: EFFECT OF METAL DEPOSITION SEQUENCE AND OTHER MODIFICATIONS

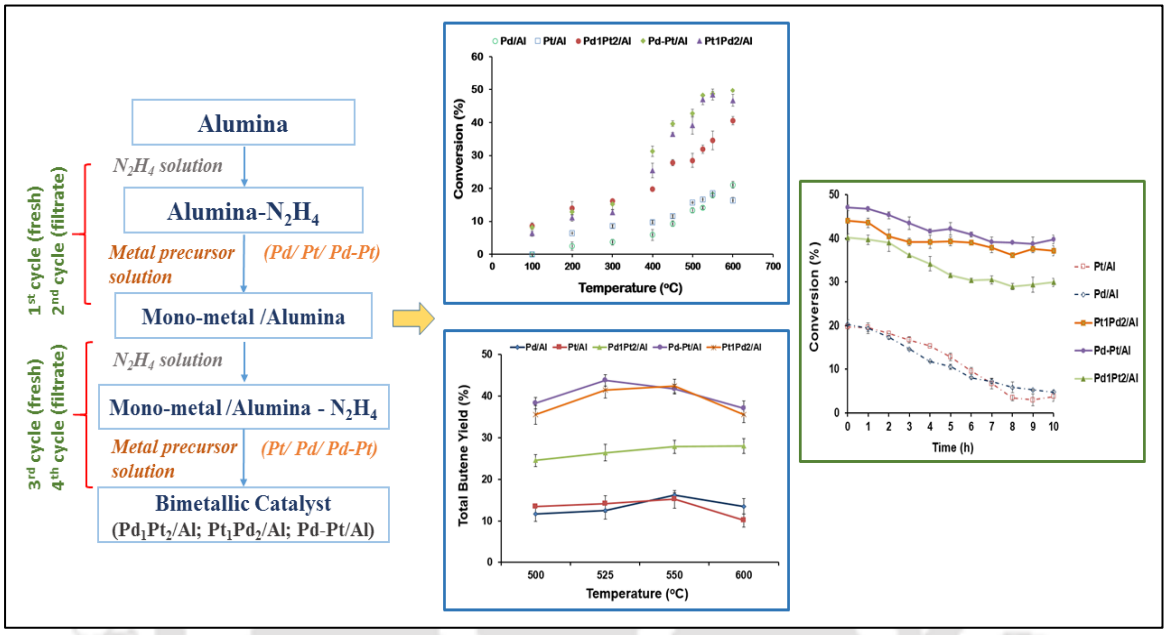

This chapter discusses the physicochemical properties and butane dehydrogenation activity of alumina supported Pd and Pt based bimetallic catalysts prepared by varying the sequence of metal deposition in modified electroless deposition method. The co-deposited Pd-Pt catalyst exhibited better activity for butane dehydrogenation in comparison to sequentially deposited catalysts. Effect of process parameters have been discussed for co-deposited Pd-Pt catalyst. The effects of addition of Cu as promoter and surfactant as dispersing agent to co-deposited Pd-Pt catalyst have also been discussed.

Keywords

Modified electroless deposition; palladium; platinum; bimetallic; butane dehydrogenation

Chapter 6

6.1 Introduction

In previous chapter, performance of Pd-Pt bimetallic catalysts was explored for dehydrogenation of butane by varying metal composition. The bimetallic catalyst having equal Pd and Pt ratio exhibited better catalytic activity in comparison to other two compositions. In this section, the effect of sequence of metal addition for equimolar Pd-Pt catalyst was investigated.

The change in deposition sequence is reported to control the interaction of metal with the support or metal-metal interaction itself. There are several literatures which reported the change in physicochemical properties and performance of the catalysts arising due to change in impregnation or deposition sequence. Feng et al. [1] studied the effect of deposition sequences on electro-catalytic properties of PtPd/C catalysts for formic acid electro-oxidation. The authors reported greater stability in Pt-Pd catalysts due to synergistic effects. Cai et al. [2] studied the metal deposition sequence in carbon supported Pd-Pt catalysts towards CO_2 electro-reduction to formate. The results showed that surface composition and coordination number of Pd and Pt were greatly influenced due to change in deposition sequence. Recently, Al-Awadi et al. [3] also reported the change in catalysts properties due to difference in addition sequence of precursor in Cr-MCM-41 catalysts used for ethane oxidative dehydrogenation. Similar results were also obtained by Jing et al. [4] on changing the metal precursor impregnation sequence, while investigating the structure and performance of Ni-Co/MgO catalysts.

In this chapter, the bimetallic catalysts were prepared by deposition of equal amount of Pd and Pt on alumina support and the effect of sequence of metal addition was investigated. Two catalysts were prepared by sequential deposition – depositing Pd prior to Pt and vice-versa and one was prepared by co-depositing both Pd and Pt simultaneously. The performance of these bimetallic catalysts was compared with that of corresponding monometallic catalysts. The effect of various process parameters on dehydrogenation reaction were investigated over best performing Pd-Pt/Al catalyst. The effect of addition of Cu as promoter and surfactant as dispersing agent to Pd-Pt bimetallic catalyst were also investigated.

6.2 Experimental

6.2.1 Preparation of bimetallic catalysts

All the catalysts were prepared with same total metal loading on molar basis. That is all the catalysts contained 112 μmoles of total metals per g of catalyst. For monometallic catalysts, this corresponded to 1.2 and 2.1 wt% of Pd and Pt metals, respectively. For bimetallic catalyst, each metal was 50% of total metal loading on molar basis and this corresponded to 1.1 wt% loading for platinum and 0.6 wt% loading for palladium.

The catalyst preparation by sequential deposition method involved passing of each metal precursor solution through the alumina support in a sequential manner. Thus, the Pt or Pd precursor solutions were prepared by dissolving 116.5 mg of H_2PtCl_6 and 40 mg of $PdCl_2$, respectively, in 40 mL of de-ionised water. Aqueous solution of hydrazine (reducing agent) was prepared by adding required volume of $N_2H_4.H_2O$ in distilled water. The molar ratio of reducing agent to metal precursor was maintained at 1:0.75 for $PdCl_2$ and 1:1.5 for H_2PtCl_6. The molar ratio of reducing agent was in 50% excess to that of metal precursor.

For preparation of sequentially deposited Pd_1Pt_2/Al bimetallic catalyst, 20 mL of hydrazine solution was passed through 2 g of alumina support and filtered after 10 min using vacuum. Then, Pd precursor solution (20 mL) was gradually poured through the filtered sample maintaining 10 min of interaction time. In the second cycle, filtrate collected for both hydrazine and Pd metal precursor (obtained after filtration of 1st cycle) were again passed through the support. In the third cycle, second metal i.e. Pt precursor solution (20 mL) was gradually poured on alumina after pouring 20 mL of fresh N_2H_4 solution and in the fourth cycle again the hydrazine filtrate (obtained from 3rd cycle) was passed followed by Pt precursor filtrate solution. In this manner, Pd metal was loaded prior to Pt metal for Pd_1Pt_2/Al catalyst as shown in Figure 6.1. The fresh and filtrate solutions were passed, respectively, to get sufficient deposition of metal (Pt or Pd) on aluminium oxide. The resulting wet catalyst was then dried in an oven at 110 °C for 12 h. Similarly, for Pt_1Pd_2/Al catalyst, the sequence was reversed, in which Pt precursor solution was poured in 1st and 2nd cycles followed by addition of Pd solution in 3rd and 4th cycles.

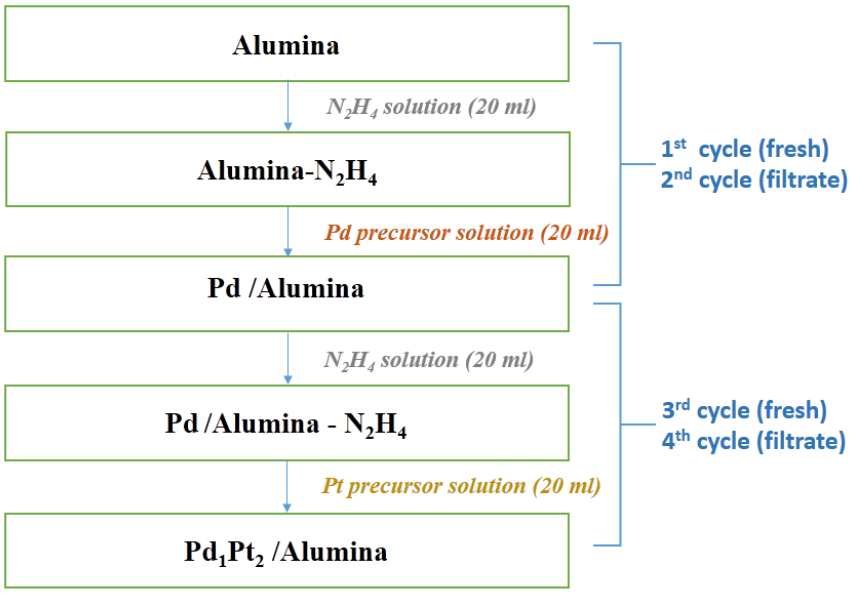

Figure 6.1. Preparation scheme of sequentially deposited bimetallic Pd_1Pt_2/Al catalyst.

For co-deposited bimetallic Pd-Pt/Al catalyst, 20 mL of each Pd and Pt precursor solution was mixed and stirred for 5 min. The resulting 40 mL solution contained both the metal precursors in required quantity. In the first cycle, 20 mL fresh solution of hydrazine was poured and filtered after 10 min. It was followed by passage of 20 mL Pd-Pt precursor solution prepared earlier. The respective filtrates of reducing agent and metal precursor solution were again passed through alumina in the second cycle. Similarly, third and fourth cycles were carried out with by pouring of fresh and filtrate solutions, respectively leading to co-deposition of Pd and Pt metal over the alumina support.

6.2.2 Preparation of surfactant modified bimetallic catalyst

To comprehend the effect of surfactant, the bimetallic catalyst having equal amount of Pd and Pt was prepared by electroless deposition method in presence of Tween 20 surfactant. The target loading of the surfactant modified catalyst was kept same to that prepared by ED method without surfactant. In this method, the required amount of surfactant corresponding to critical micelle concentration was first dissolved in 20 mL of de-ionized water and the resulting surfactant solution was added to 20 mL of solution containing precursors of both the metals. The final solution (40 mL) was mixed and stirred for 10 min to obtain the surfactant modified metal precursor solution. Then, the catalyst was prepared employing the reducing agent and surfactant modified metal precursor solution by

electroless deposition method as described in previous sections. The surfactant modified catalyst has been referred as Pd-Pt-T20 in the text.

6.2.3 Preparation of promoted bimetallic catalyst

The effect of copper promoter was investigated on monometallic Pt and bimetallic Pd-Pt catalysts prepared by modified deposition method and compared with Cu promoted Pd catalyst. In all catalysts the total metal loading was kept similar at 112.8 μmoles of metal per gram of catalyst. The promoted catalysts have been denoted as PtCu/Al, PdCu/Al and PdPtCu/Al in this section. The PtCu/Al catalyst had 90 mol% Pt loading and 10 mol% Cu, the PdCu/Al catalyst had 90 mol% Pd loading and 10 mol% Cu loading while, PdPtCu/Al had 45 mol% loading of Pd and Pt each with 10 mol% Cu loading. The preparation steps are same as discussed earlier.

6.2.4 Catalyst characterization

The physicochemical properties of Pd-Pt bimetallic catalysts were analysed using various characterization techniques such as EDX, BET surface area, XPS, TPR, XRD, TEM, NH_3-TPD and Pyr-FTIR spectroscopy. The details of the characterization methods employed are included in section 2.2.4 in Chapter 2.

6.2.5 Dehydrogenation tests

As mentioned in previous chapters, the n-butane dehydrogenation was carried out in a fixed-bed continuous down-flow reactor in the temperature range of 100–600 °C at atmospheric pressure using 0.25 g catalyst. The details are included in section 2.2.5 in Chapter 2.

6.3 Results and discussion

6.3.1 Effect on physicochemical properties

The metal loadings (Pd and/or Pt) of the prepared catalysts were determined by doing AAS analysis of initial solution and final solution after deposition. On molar basis, the metal (Pt and Pd) loadings were obtained almost in the same range as targeted. The Pt content was in the range of 93 - 99 μmoles (~1 wt%) while, Pd content was in the range of 85 - 99

μmoles (0.5 - 0.6 wt%) in bimetallic catalysts, as can be observed from Table 6.1. The composition of the catalysts was also determined by EDX (Table 6.2) and was comparable to that obtained through AAS analysis. The corresponding EDX spectra for the catalysts are shown in Appendix D.

Table 6.1. Elemental composition determined by AAS of bimetallic catalysts prepared by different metal deposition sequences.

Catalysts	Pt loading (wt%)	Pd loading (wt%)	Total loading (wt%)
Pd/Al	-	1.13 (106)	1.13 (106)
Pt/Al	2.08 (107)	-	2.08 (107)
Pd_1Pt_2/Al	1.0 (46.6)	0.60 (49.6)	1.60 (96.2)
Pd-Pt/Al	1.1 (49.3)	0.55 (45.4)	1.65 (94.7)
Pt_1Pd_2/Al	1.1 (49.5)	0.50 (42.9)	1.60 (92.4)

**Values in parenthesis represent the metal loading in μmoles g^{-1} of catalyst*

Table 6.2. Elemental composition determined by EDX of bimetallic catalysts prepared by different metal deposition sequences.

Catalysts	Pt loading (wt%)	Pd loading (wt%)	Total loading (wt%)
Pd/Al	-	1.1	1.1
Pt/Al	2.1	-	2.1
Pd_1Pt_2/Al	1.4	0.6	2.0
Pd-Pt/Al	1.5	0.7	2.2
Pt_1Pd_2/Al	1.4	0.7	2.1

The nitrogen adsorption-desorption isotherms and pore size distributions for all the catalysts are shown in Figure 6.2a and b, respectively. All the catalysts exhibited Type IV isotherms with H2-type hysteresis loop similar to that observed for the support. The BET surface area, pore volume and average pore size of the supported monometallic and bimetallic catalysts are summarized in Table 6.3. The surface area of all the catalysts reduced in comparison to the support. This decrease can be attributed to the deposition of metal species within the pores [5]. The monometallic catalysts showed only a slight decrease in surface area with respect to the support. The Pt/Al catalyst exhibited a surface area of 181 $m^2\ g^{-1}$ while it was 179 $m^2\ g^{-1}$ for Pd/Al catalyst. The surface area of the sequentially deposited bimetallic catalysts dropped significantly, irrespective of the sequence of metal addition. The Pd_1Pt_2/Al and Pt_1Pd_2/Al showed surface areas of 149 and 147 $m^2\ g^{-1}$, respectively. However, surface area of bimetallic catalyst prepared by co-

deposition was 181 $m^2 g^{-1}$, not showing any significant decrease with respect to that of alumina support. The significant decrease in the BET surface areas of the sequentially deposited bimetallic samples with respect to alumina support suggested that sequential incorporation of metal resulted in higher pore blockage.

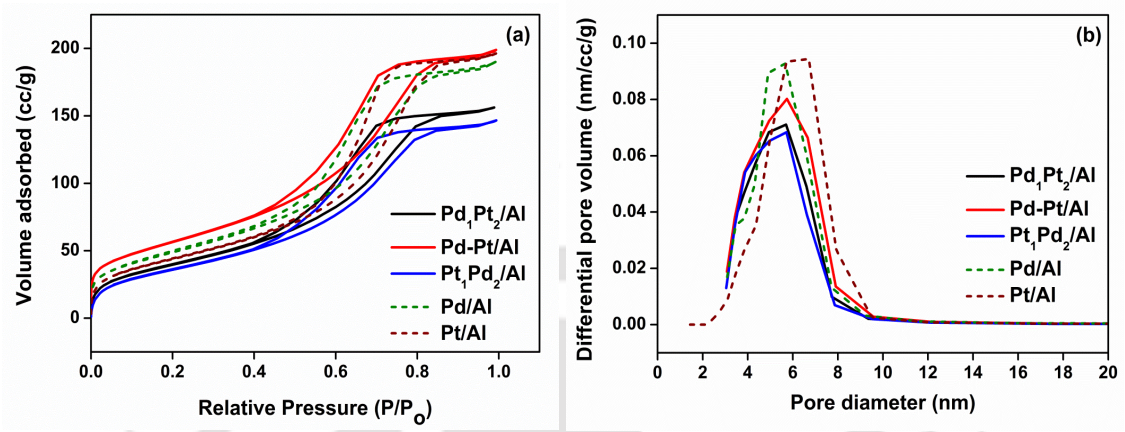

Figure 6.2. (a) Nitrogen adsorption-desorption isotherm and (b) pore size distribution of monometallic catalysts and bimetallic catalysts prepared by different metal deposition sequences.

Table 6.3. Physical properties of support and bimetallic catalysts prepared by different metal deposition sequences.

Catalysts	BET surface area ($m^2 g^{-1}$)	Pore volume (cc g^{-1})	Average pore diameter (nm)
Alumina	184	0.343	7.0
Pd/Al	179	0.315	6.0
Pt/Al	181	0.334	6.1
Pd_1Pt_2/Al	149	0.271	5.9
Pd-Pt/Al	181	0.327	6.0
Pt_1Pd_2/Al	147	0.277	5.9

Accordingly, the drop in pore volume was also significant for sequentially deposited catalysts as can be observed from Table 6.3. The pore volume of 0.343 cc g^{-1} observed for alumina support was reduced to 0.271 and 0.277 cc g^{-1} for sequentially deposited Pd_1Pt_2/Al and Pt_1Pd_2/Al catalysts, respectively. For co-deposited Pd-Pt/Al catalyst, the pore volume was reduced to only 0.327 cc g^{-1}. The average pore size was lower for all the catalysts and was in similar range of 5.9 - 6 nm, with respect to that of the support (7 nm). No micropores were observed in any of the catalysts (Figure 6.2b). From these results, it can be inferred

that variation in deposition sequence of metal strongly affected the physical properties of the synthesized bimetallic catalysts.

The core level XPS spectra of Pd (3d) and Pt (4f) region for monometallic and co-deposited bimetallic catalyst are shown in Figure 6.3. For Pd/Al catalyst, the Figure 6.3a shows two peaks at 335.1 and 336.3 eV in Pd $3d_{5/2}$ region corresponding to the presence of Pd^0 and Pd^{2+} species, respectively. The peaks were shifted to 335.0 (Pd^0) and 336.4 eV (Pd^{2+}) in the bimetallic Pd-Pt/Al catalyst as shown in Figure 6.3b. As per Figure 6.3c, the Pt/Al exhibited two peaks at 70.6 and 72.7 eV that corresponded to presence of metallic Pt^0 and oxidized Pt^{2+} species, respectively. The binding energy values increased significantly from 70.6 to 71.1 eV and from 72.7 to 72.9 eV for Pt^0 and Pt^{2+} states, respectively, in bimetallic Pd-Pt/Al catalyst (Table 6.4).

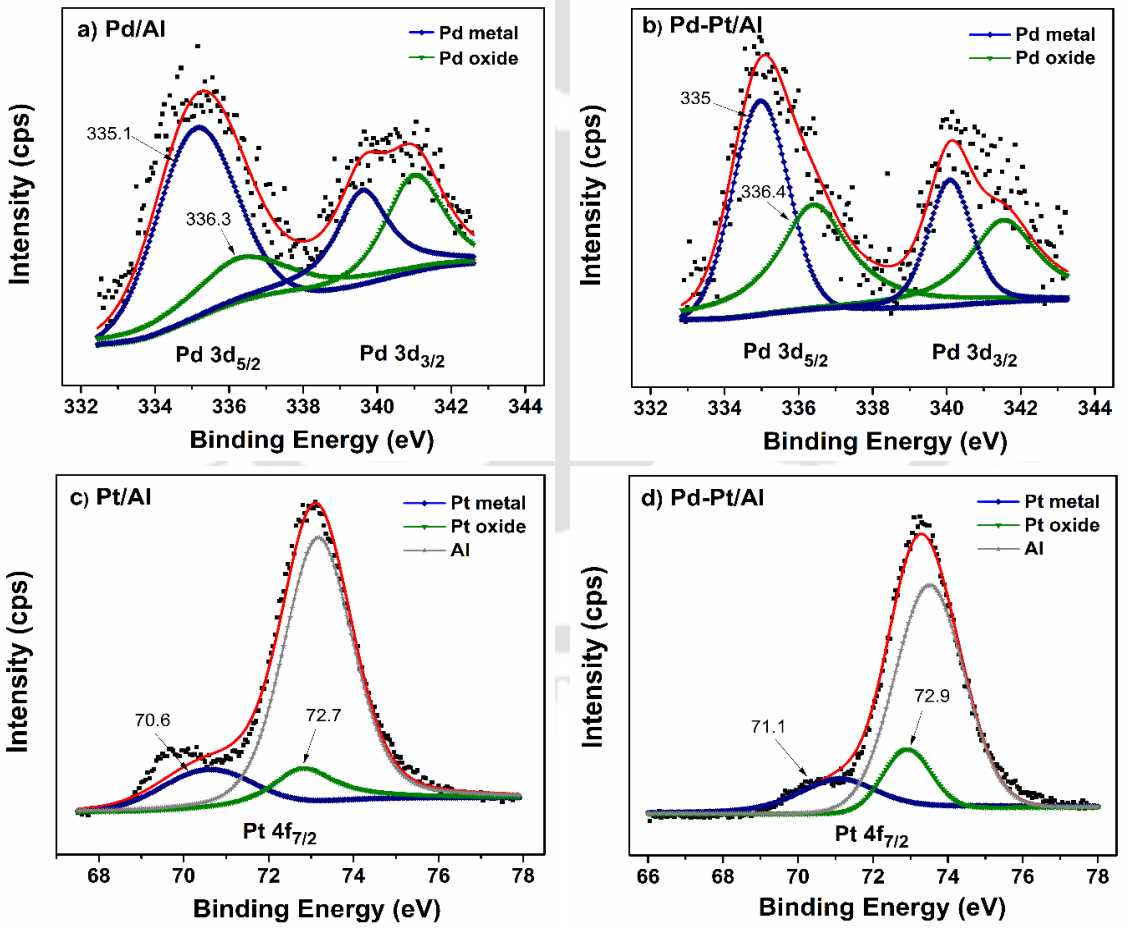

Figure 6.3. XPS spectra of Pd 3d region in (a) Pd/Al (b) Pd-Pt/Al and Pt 4f region in (c) Pt/Al (d) Pd-Pt/Al.

As already stated in chapter 2, binding energy values are generated due to the ejection of photoelectrons from metal particles and depends on their size. Smaller the metal particle, higher is the binding energy value. However, bimetallic Pd-Pt/Al catalyst exhibited almost similar average particle size to that of mono metallic as established by TEM analysis later. Hence, such a shift in binding energies observed for the metals in bimetallic catalyst compared to that of corresponding monometallic catalyst may be attributed to the modification in the electronic properties of Pd and Pt. These modifications might have caused by the electronic interactions between the metals resulting in the formation of Pd-Pt alloyed particles [6]. The significant 0.5 eV shift for Pt^0 in 4f region may be attributed to the transfer of electrons from Pd to Pt owing to higher electronegativity of the latter [7]. The Pd^0 accordingly underwent decrease in binding energy. Stronger metal-support interactions in bimetallic catalyst, as was also observed from TPR results discussed in next section, could be another reason for shift in BE values [8].

Table 6.4. Binding energy (B.E.) of Pd ($3d_{5/2}$) and Pt ($4f_{7/2}$), oxidation states and their relative contents.

Catalysts	Pd $3d_{5/2}$ B.E. (eV)	Pt $4f_{7/2}$ B.E. (eV)	Oxidation state	Relative content of respective metal (%)
Pd/Al	335.1	-	Pd^0	70
	336.3	-	Pd^{2+}	30
Pt/Al	-	70.6	Pt^0	64
	-	72.7	Pt^{2+}	36
Pd-Pt/Al	335.0	-	Pd^0	52
	336.4	-	Pd^{2+}	48
	-	71.1	Pt^0	53
	-	72.9	Pt^{2+}	47

The binding energies, oxidation states and their relative contents for both metals are compiled in Table 6.4. The relative concentration ratio of Pd^0/Pd^{2+} in Pd/Al and Pd-Pt/Al were 70/30 and 52/48, respectively. The ratio of Pt^0/Pt^{+2} were found to be 64/36 and 53/47 for Pt/Al and Pd-Pt/Al catalysts, respectively. The oxidized state might have resulted either from incomplete reduction during deposition or by subsequent oxidation on exposure to surroundings. Interestingly, the co-deposited bimetallic catalyst displayed presence of almost equal amount of metallic and oxidized states for both the metals. About 52-53 % of both the metals was observed in zero oxidation state in the co-deposited catalyst.

The TPR profiles of the catalysts with the de-convoluted peaks are shown in Figure 6.4. The presence of reduction peaks resulted from presence of oxidized metals on surface as observed in XPS analysis. The reduction peaks for the catalysts are summarized in Table 6.5. The monometallic catalyst, Pd/Al exhibited three peaks centered at 136 °C, 340 °C and 399 °C. The low temperature reduction peak at 136 °C corresponded to the reduction of the easily reducible palladium oxide crystallites, while the broad peaks at 340 and 399 °C were assigned to the reduction of relatively small and stable oxide species. The reduction peaks were located at similar positions for Pt/Al catalyst, 194, 345 and 390 °C. The assignments of the peaks are same as that for Pd/Al corresponding to reduction of bulk or weakly interacting oxide at 194 °C and strongly interacting platinum oxide clusters with support at temperature >300 °C.

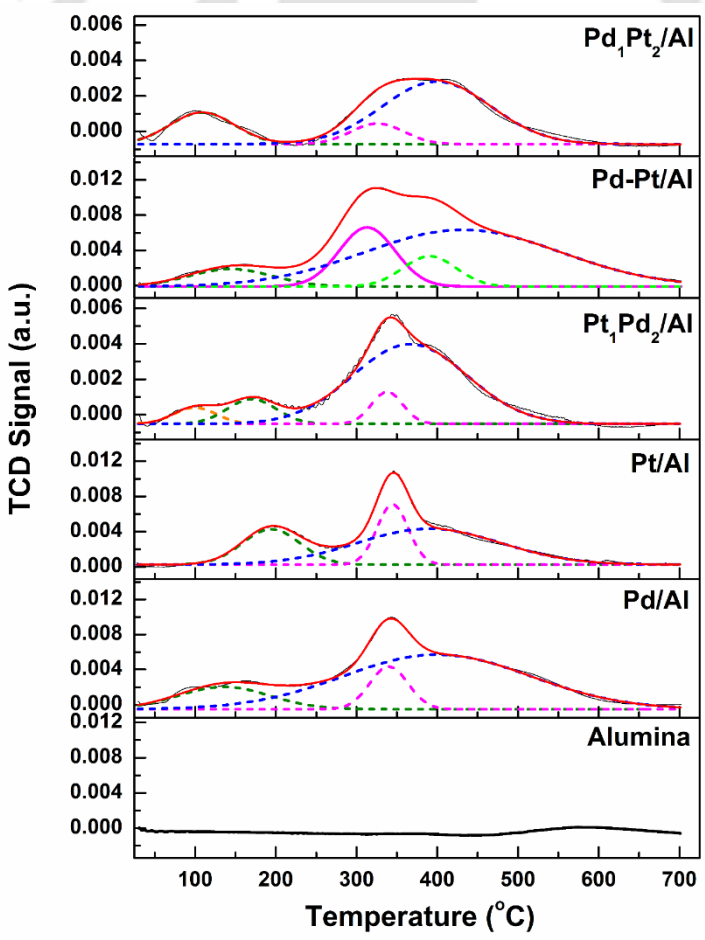

Figure 6.4. TPR patterns obtained for support, monometallic and bimetallic catalysts prepared by different metal deposition sequences.

In the sequential bimetallic catalysts, the low temperature reduction peaks appeared to have shifted to further lower temperature compared to the both the monometallic catalysts. The Pt_1Pd_2/Al catalyst exhibited two reduction peaks at 100 and 170 °C while, Pd_1Pt_2/Al showed peak at 109 °C. This suggested weakening of metal-support interaction in bimetallic catalysts in comparison to monometallic catalysts, with formation of metal oxide clusters having stronger metal-metal interactions. For both the sequentially prepared catalysts, the reduction peaks at higher temperature also experienced a shift to lower value in bimetallic catalysts compared to that in monometallic catalysts. The effect was more visible in Pt_1Pd_2/Al. The results agreed with the existence of strong metal-metal interaction and weakening of support-metal interaction.

Table 6.5. Reduction peaks as obtained in TPR profiles of monometallic and bimetallic catalysts prepared by different metal deposition sequences.

Catalysts	Reduction peak (°C)
Pd/Al	136, 340, 399
Pt/Al	194, 345, 390
Pd_1Pt_2/Al	109, 326, 399
Pd-Pt/Al	144, 313, 390, 432
Pt_1Pd_2/Al	100, 170, 338, 366

The strong metal-metal interaction in bimetallic catalysts indicated formation of alloys between Pt and Pd, resulting in shift in their reduction behavior compared to that observed for pure form in monometallic catalysts. For the co-deposited Pd-Pt/Al catalysts, similar strong metal-metal interaction was observed by shifting of reduction peaks. In co-deposited catalyst, appearance of a reduction peak at highest temperature of 432 °C suggested formation of nano-metal cluster existing in strongest interaction with the support. This peak was not observed for sequentially prepared bimetallic catalysts. The extent of reduction of co-deposited catalyst was similar to that of monometallic catalysts, however it was comparatively lower for sequentially deposited bimetallic samples. The TPR results suggested that the Pd-Pt interaction in bimetallic catalyst was stronger when metals were co-deposited.

The TEM images of the catalysts are shown in Figure 6.5. The average size of the metal clusters ranged from 3 to 5 nm. The monometallic Pd/Al and Pt/Al catalysts exhibited an average metal cluster size of 4.6 nm and 3.4 nm, respectively.

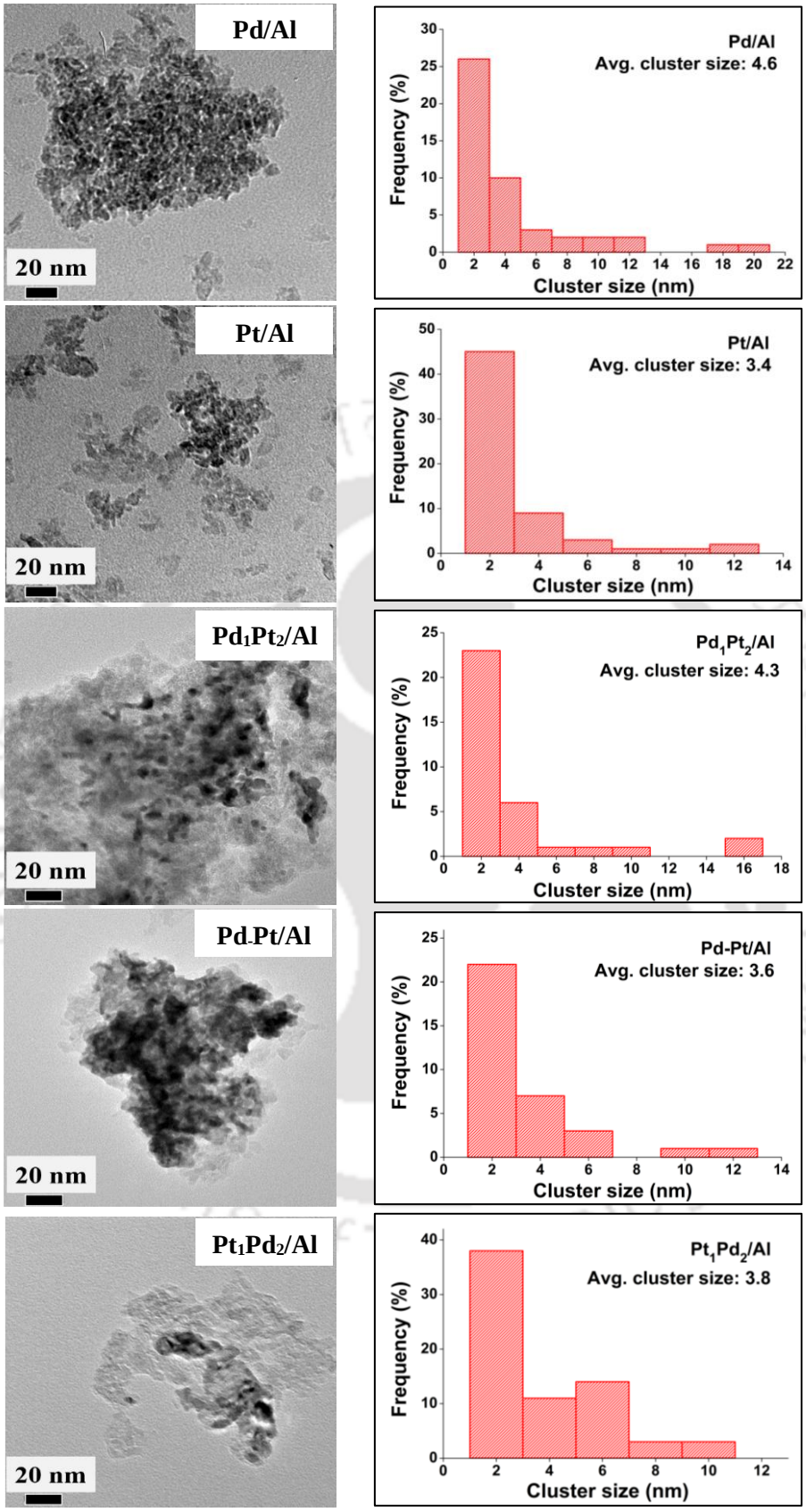

Figure 6.5. TEM images and particle size distribution of monometallic and bimetallic catalysts prepared by different metal deposition sequences.

Since the reduction potential of Pt is higher, Pt is expected to be reduced and deposited on the surface at a faster rate compared to that of Pd. This might have generated higher number of nucleation sites on surface in case of Pt deposition. Consequently, slightly lower growth of metal clusters was observed during deposition of Pt compared to that for Pd deposition. For bimetallic catalysts, where deposition of Pt was carried out prior to Pd as in Pt_1Pd_2/Al, the average cluster size was lower (3.8 nm) compared to that in Pd_1Pt_2/Al (4.3 nm). The synergistic effect of Pd-Pt in co-deposited catalysts may have resulted to a lowest average cluster size of 3.6 nm. The formation of lowest supported metal clusters on surface of the co-deposited catalyst was also confirmed by TPR profile which showed presence of reduction peak at highest temperature.

The metallic dispersion (D%) over the monometallic as well as the bimetallic catalysts was calculated using the equation: D = 1.13/d, where, d is the average particle size of deposited metals in nm as determined from TEM analysis [9]. The dispersion values obtained for Pd/Al, Pt/Al, Pd_1Pt_2/Al, Pd-Pt/Al and Pt_1Pd_2/Al were 24.5, 33.2, 26, 31.4 and 29.4%, respectively.

The structures of the bimetallic catalyst were also analysed using SAED (Selected Area Electron Diffraction) patterns obtained during HRTEM analysis as shown in Figure 6.6. The ring patterns obtained from the SAED analysis of Pt_1Pd_2/Al catalyst showed the presence of Pt predominantly in section of the clusters with Pd in the outer zone. The presence of inner platinum was also observed for Pd-Pt/Al where both the metals were co-deposited.

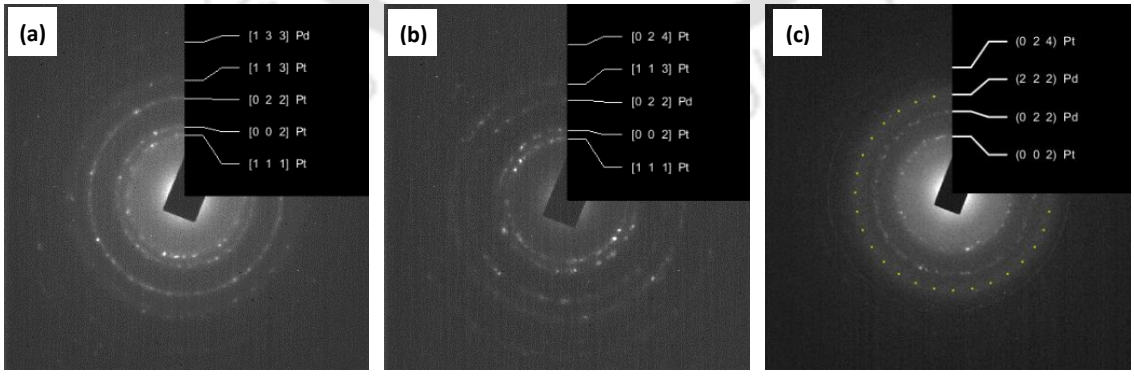

Figure 6.6. Electron diffraction patterns obtained during HRTEM analysis for bimetallic catalysts prepared by different metal deposition sequences: (a) Pt_1Pd_2/Al (b) Pd-Pt/Al (c) Pd_1Pt_2/Al.

As suggested earlier, the higher reduction rate of platinum might have resulted in its preferential deposition. Even for the Pd_1Pt_2/Al, where Pd was deposited prior to Pt, the appearance of some Pt in inner core suggested galvanic displacement of some of the initially deposited Pd by Pt. The higher reduction potential of Pt compared to that of Pd might have facilitated the galvanic displacement of later, when the sample was exposed to solution of Pt precursor. Pt was also observed in the exterior for Pd_1Pt_2/Al catalyst. In Pd-Pt/Al co-deposited catalyst, more uniform distribution of Pd and Pt was observed.

Figure 6.7 shows the XRD patterns for monometallic and bimetallic catalysts. The comparison of the profiles of alumina support with that of catalysts showed no significant variation in intensity of the alumina peaks. As discussed in earlier chapters, the results suggested the metals to be in dispersed state. The metal crystallites of sizes above 4 nm, if present on surface, were lower in concentration and hence difficult to detect by XRD. The TEM analysis, as discussed earlier, indeed confirmed the presence of larger particles (> 4 nm) to contribute only smaller fractions (9-15%) for all the catalysts. Lower loading of the metals might have also contributed to the non-detection of metal crystallites by XRD. It is reported that the XRD method is less sensitive for the detection of phases at low metal loading (<5%) [10].

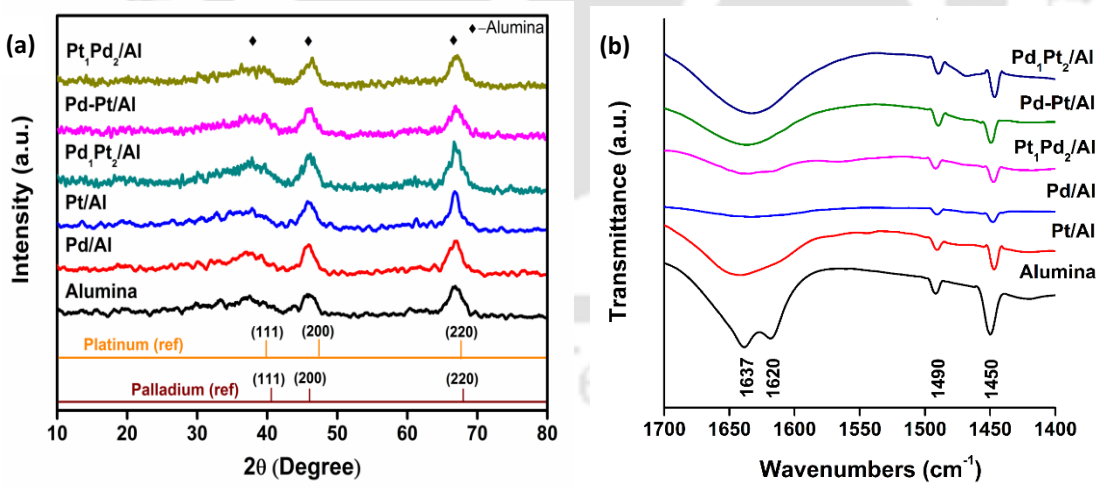

Figure 6.7. (a) XRD spectra and (b) FTIR spectra of chemisorbed pyridine for support, monometallic and bimetallic catalysts prepared by different metal deposition sequences.

The surface acidity was determined from IR spectra (Figure 6.7b) of the support and catalysts using pyridine as probe molecule. For alumina support, four peaks were observed at 1450, 1490, 1620 and 1637 cm^{-1}. The intensity of these peaks was highest for alumina

and decreased for catalysts after addition of metals. The decrease in the acidity for the metal catalysts may be attributed to the coverage or interactions of the support acidic sites with deposited metals. The acidity of Pt/Al was observed to be higher than that of Pd/Al as intensity of Lewis acid sites was lower and that of Brønsted acid sites was negligible for later. The disappearance of Brønsted acid sites for Pd/Al catalyst suggested that on deposition Pd preferentially interacted with these acidic sites involving OH groups. The higher interaction might have been caused by higher affinity of Pd for hydrogen thereby neutralizing all the Brønsted sites on the support surface. Pt also exhibited same tendency to interact with Brønsted sites OH but to lower extent, thus loss in Brønsted acid sites on Pt/Al catalyst was less. The decrease in intensity for Lewis acid sites can also be explained based on interaction of metals with these sites as discussed earlier in Chapter 5.

For bimetallic catalysts, the intensity of peaks with respect to support or monometallic catalysts depended of the sequence of metal deposition. The Pd_1Pt_2/Al catalyst showed acidic behaviour more like Pt/Al monometallic catalyst while Pt_1Pd_2/Al showed similar behaviour with that of Pd/Al catalyst. This behaviour can be explained based on distribution of Pd and Pt in metal clusters for bimetallic catalysts as discussed earlier. The Pd_1Pt_2/Al with presence of more Pt in outer zone of cluster showed behaviour similar to Pt/Al and Pt_1Pd_2/Al with more Pd in exterior part of cluster had acidic characteristic similar to that of Pd/Al catalyst. The co-deposited Pd-Pt/Al catalyst having more uniform metal distribution showed intermediate behaviour. The intensity of both the Lewis acid and Brønsted acid sites among bimetallic catalysts decreased in the following order: Pd_1Pt_2/Al > Pd-Pt/Al > Pt_1Pd_2/Al. The peak at 1490 cm^{-1} was also observed for all the catalysts and the intensity of this peak did not change significantly among the samples.

Figure 6.8 compares the NH_3-TPD profiles of the support and the catalysts. The corresponding total acidity in terms of ammonia uptake in mmol g^{-1} is summarized in Table 6.6. All the NH_3-TPD profiles were de-convoluted using Gaussian function to obtain the distribution of acidic strength of the samples. All the samples exhibited three types of peaks. The first peak (I) at 120-150 °C corresponds to weak acidic sites, the second peak (II) at 200-250 °C can be attributed to acidic sites of medium strength, and the third peak (III) at 350-400 °C can be considered as strong acidic sites [11]. The alumina support revealed the dominance of strong acidic sites with complete absence of weak acidic sites.

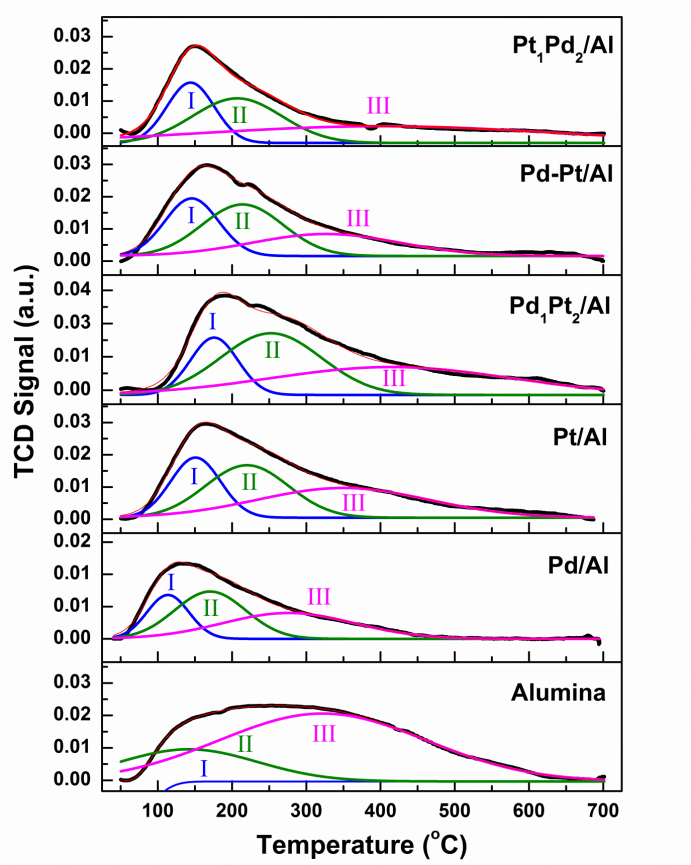

Figure 6.8. NH_3-TPD profiles for alumina support, monometallic and bimetallic catalysts prepared by different metal deposition sequences.

As shown in Table 6.6, the total acidity for the support alumina was highest with an ammonia uptake of 8.83 mmol g^{-1}. Both the monometallic catalysts exhibited lower acidity than alumina support. The acidity of Pd/Al was lower (5.24 mmol NH_3 g^{-1}) compared to that of Pt/Al catalyst (7.11 mmol NH_3 g^{-1}). The presence of all three types of acidic sites was observed in both the monometallic catalysts; Pt/Al showed slightly higher content of weaker sites while Pd/Al showed slightly higher content of sites of medium strength. Both showed similar quantity of stronger acidic sites. The result indicated that the incorporation of metals to the support decreased the acidic sites, which is well in agreement with the results obtained from FTIR analysis of adsorbed pyridine.

All the bimetallic catalysts also exhibited lower acidity compared to alumina support but higher than that of monometallic catalysts. Higher acidity in bimetallic catalysts may be a combined effect of presence of both the metals. The total acidity and relative distribution of acidic sites for bimetallic catalysts depended on the metal deposition sequence. The order of the total acidity (NH_3 uptakes) was Pd_1Pt_2/Al > Pd-Pt/Al > Pt_1Pd_2/Al, same as was

observed from pyridine adsorption study. Accordingly, Pd_1Pt_2/Al exhibited highest fraction of medium and strong acid sites followed by Pd-Pt/Al and Pt_1Pd_2/Al. The Pd_1Pt_2/Al catalyst, with presence more Pt in outer zone of metal clusters as discussed earlier, retained the highest acidity in comparison to other two bimetallic catalysts while in Pt_1Pd_2/Al with more Pd in outer section of metal clusters showed lowest acidity among bimetallic catalyst. The overall order of acidity in terms of total ammonia uptake was Alumina > Pd_1Pt_2/Al > Pd-Pt/Al > Pt/Al > Pt_1Pd_2/Al > Pd/Al. The acidity pattern obtained correlates well with the results of FTIR analysis of adsorbed pyridine.

Table 6.6. Acidity of support, monometallic and bimetallic catalysts prepared by different metal deposition sequences, in terms of mmol of NH_3 adsorbed per g of catalyst as obtained from NH_3-TPD profiles of samples.

Catalysts	Total acidity (mmol NH_3 g^{-1} cat)	Acid strength distribution Peak fraction (%)		
		I (weak)	II (medium)	III (strong)
Alumina	8.83	0	24	76
Pd/Al	5.24	21	39	40
Pt/Al	7.11	24	35	41
Pd_1Pt_2/Al	8.21	19	42	39
Pd-Pt/Al	7.35	25	37	38
Pt_1Pd_2/Al	6.76	27	39	34

6.3.2 Dehydrogenation study

Figure 6.9a illustrates the n-butane conversion in the temperature range of 100-600 °C for catalysts synthesized using electroless deposition. The conversion of n-butane steadily increased with increase in the reaction temperature for all the catalysts. At 100 °C, the monometallic Pd and Pt catalysts did not show any conversion. At 200 °C, the conversion was detected for both the monometallic catalysts but conversion of Pt/Al was higher than that of Pd/Al. This trend was observed up to temperature of 500 °C. As the temperature increased, difference in activity was decreased. At 550 °C, both the monometallic catalysts showed similar activity. Thereafter, the activity of Pt/Al started to decrease but that of Pd/Al continued to increase. The conversion was reduced from 18.4 at 550 °C to 16.3% at 600 °C for Pt/Al catalyst. In case of Pd/Al, the conversion of 17.9% at 550 °C increased to

21.1% at 600 °C. The results showed that the Pd/Al catalyst was more active at higher temperatures.

All the bimetallic catalysts showed better dehydrogenation activity in comparison to the monometallic catalysts. The dehydrogenation was observed even at 100 °C for bimetallic catalysts. The conversion was about 6-8% at 100 °C, which gradually increased with the increasing temperature. In the temperature range of 100-300 °C, the Pd_1Pt_2/Al catalyst, with more Pt in outer regions of metal clusters, showed highest activity while Pt_1Pd_2/Al with more Pd in outer zone showed the lowest activity. From 400 °C onwards, the activity of the Pd_1Pt_2/Al catalyst was quite lower compared to other two bimetallic catalysts, though the conversion still increased with temperature and was higher than both the monometallic catalysts. Between 100-300 °C, the co-deposited Pd-Pt/Al catalyst showed intermediate activity compared to other two sequentially deposited bimetallic catalysts.

However, beyond 400 °C the activity of co-deposited catalyst was highest closely followed by that of Pt_1Pd_2/Al catalyst. At higher temperature range of 400-600 °C the activity of bimetallic catalysts was much higher compared to monometallic catalysts and the order obtained was Pd-Pt/Al > Pt_1Pd_2/Al > Pd_1Pt_2/Al > Pd/Al > Pt/Al. The conversions of the catalysts at 550 °C are summarized in Table 6.7. The conversions for the Pd-Pt/Al and Pt_1Pd_2/Al catalysts were similar (~49%) and higher than the other catalysts at 550 °C.

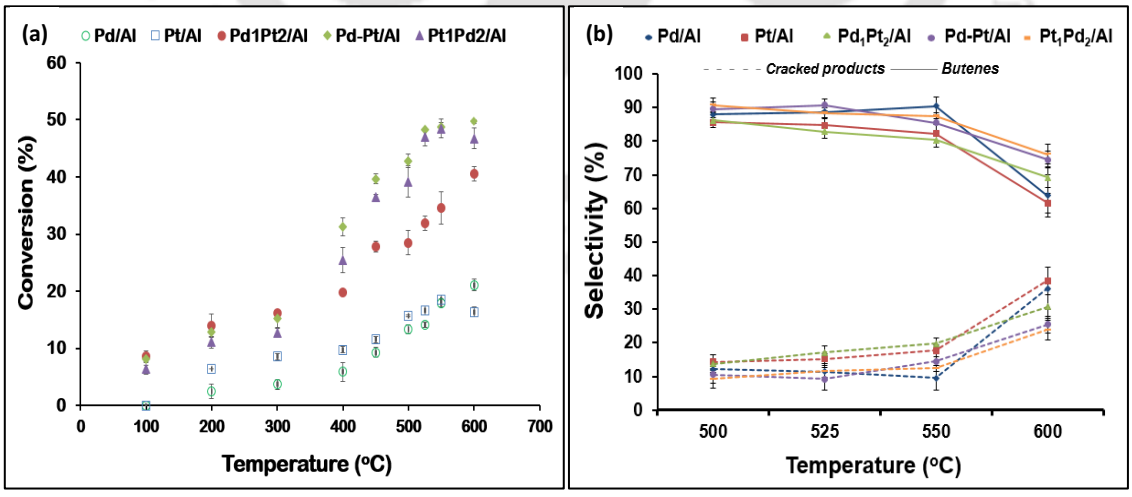

Figure 6.9. Catalytic performance of monometallic and bimetallic catalysts prepared by different metal deposition sequences, for butane dehydrogenation at different temperatures (a) conversion and (b) product selectivity.

The turnover frequencies (TOFs) of the catalysts were determined based on the total metal loading. Bimetallic catalysts exhibited higher TOFs than monometallic catalysts with Pd-Pt/Al showing highest TOF of 1.18 s^{-1} followed by Pt_1Pd_2/Al catalyst (1.15 s^{-1}). Both the monometallic catalysts exhibited similar TOFs of about 0.43 s^{-1} at 550 °C. The higher activity of bimetallic catalysts may be attributed to higher synergy between two deposited metals. The alloy formation was confirmed by TPR and XPS studies. Since, the dispersion of metallic cluster in bimetallic catalyst was almost in similar range to that of monometallic catalysts, the higher activity of the bimetallic catalysts must have resulted from higher activity of the alloys present.

The butenes along with C_1-C_3 hydrocarbons were the main products obtained during dehydrogenation of butane. The C_1–C_3 compounds included methane, ethane, ethylene, propane, and propylene (Appendix G). Both 1-butene and 2-butene were produced, while formation of butadiene was not observed as before. All the butene isomers were observed in the products. No higher hydrocarbons beyond butenes were detected. The overall selectivity trends for products in the temperature range of 500-600 °C for all the catalysts are shown in Figure 6.9b. The selectivity towards cracked products increased slowly with rising temperature up to 550 °C, but thereafter the increase was drastic at 600 °C as can be observed from the figure.

The selectivity towards butenes decreased from 85.6 to 82.3% for Pt/Al catalyst on increasing the temperature from 500 to 550 °C, while Pd/Al exhibited >90% selectivity in the similar temperature range. On increasing the temperature to 600 °C, butene selectivity dropped for both catalysts to ~63-65% due to increase in cracked product formation. The results are in agreement with reported works that observed enhanced cracking to lower hydrocarbons at higher process temperature, resulting in lower selectivity of butane. The product distributions at 550 °C for all catalysts are given in Table 6.7. Among monometallic catalysts, Pt/Al had slightly higher selectivity for cracked C_1-C_3 products (14-18%) compared to that shown by Pd/Al catalyst (about 9%).

At the reaction temperature of 550 °C, Pt/Al showed higher selectivity for 1-butene, while Pd/Al showed higher selectivity for 2-butenes. Pt/Al catalyst showed 22.7% and 19.6% selectivity for 1-butene and isobutene, respectively, and the corresponding values were 19.6 and 13.9% for Pd/Al. The Pd/Al catalyst exhibited 57% selectivity for 2 butenes (33%

trans-2-butene and 24% cis-2-butene) compared to 40% shown by Pt/Al catalyst (22% trans-2-butene and 18% cis-2-butene). In the temperature range of 500-525 °C, the bimetallic catalysts Pd-Pt/Al and Pt_1Pd_2/Al exhibited higher selectivity towards butenes in comparison to monometallic Pt/Al while it was more or less similar to that of Pd/Al catalyst. The bimetallic Pd_1Pt_2/Al catalyst exhibited lowest selectivity towards butenes in the same range. In contrast to monometallic catalysts, bimetallic catalysts retained higher butene selectivity (70-76%) even on raising the temperature to 600 °C.

The selectivity pattern for bimetallic catalysts depended on the metal deposition sequence. The bimetallic catalyst, Pd_1Pt_2/Al showed highest selectivity of 19.7% towards C_1-C_3 products, followed by co-deposited Pd-Pt/Al (14.5%). The lowest selectivity of 12.4% towards C_1-C_3 products was observed for Pt_1Pd_2/Al. Accordingly, at 550 °C, the total selectivity towards butene formation was highest for Pt_1Pd_2/Al (87.6%) followed by that of Pd-Pt/Al catalyst (85.5%), while it was lowest for Pd_1Pt_2/Al, 71.5%.

Table 6.7. Catalytic performance of monometallic and bimetallic catalysts prepared by different metal deposition sequences for n-butane dehydrogenation (reaction temp. = 550 °C; Feed composition - n-butane:hydrogen:nitrogen = 1:3:6).

Catalysts	Conversion (%)	TOF (s^{-1})	Selectivity (%)					
			Iso-butene	1-butene	Trans-2-butene	Cis-2-butene	Total Butene	C_1-C_3
Pd/Al	17.9	0.43	13.9	19.6	32.8	24.2	90.5	9.5
Pt/Al	18.4	0.44	19.6	22.7	22.1	17.9	82.3	17.7
Pt_1Pd_2/Al	48.5	1.15	24.6	17.7	25.8	19.5	87.6	12.4
Pd_1Pt_2/Al	34.6	0.83	23.0	22.5	20.0	14.8	80.3	19.7
Pd-Pt/Al	48.8	1.18	19.4	20.3	24.3	21.5	85.5	14.5

The lowest butene selectivity of Pd_1Pt_2/Al agreed with the fact that it had more Pt in outer zone of metal cluster and as noted earlier Pt/Al catalyst showed lower selectivity for butene. The higher selectivity of butene for Pt_1Pd_2/Al similarly can be explained by presence of higher percentage of Pd in outer shells of the metal clusters. Thus, the bimetallic catalyst Pd_1Pt_2/Al had similar product distribution that of Pt/Al while Pt_1Pd_2/Al showed similar selectivity trend as Pd/Al. The Pd-Pt/Al catalyst showed intermediate behaviour between the two catalysts. The higher surface acidity in Pt/Al and Pd_1Pt_2/Al catalysts, as apparent from the TPD and FTIR analysis, may have led to formation of cracked products. At higher temperature, more cracking resulted in blocking of the active sites and hence reduction in

activity was observed for these catalysts. The Pd/Al and Pt_1Pd_2/Al catalysts that exhibited least acidity showed lowest selectivity towards cracked products and highest selectivity to butenes.

Figure 6.10a shows the total butene yield over the catalysts in the temperature range of 500-600 °C. The yield was calculated as product of conversion and selectivity. Compared to monometallic catalysts, the yield of butenes was significantly higher for the bimetallic catalysts. The higher yield resulted from higher conversion as well as higher selectivity observed for bimetallic catalysts. The maximum butene yields were obtained at a reaction temperature of 525-550 °C. Among the bimetallic catalysts, the co-deposited Pd-Pt/Al exhibited highest yield (44%) for butenes followed by sequentially deposited Pt_1Pd_2/Al catalyst (42.4%). The yield of Pd_1Pt_2/Al (28%) was lowest among the bimetallic catalysts. The comparison of conversion and yield data of present catalysts with that of reported Pt based catalysts (Table 5.1) shows that the values were better for co-deposited Pd-Pt/Al catalyst at a similar temperature range.

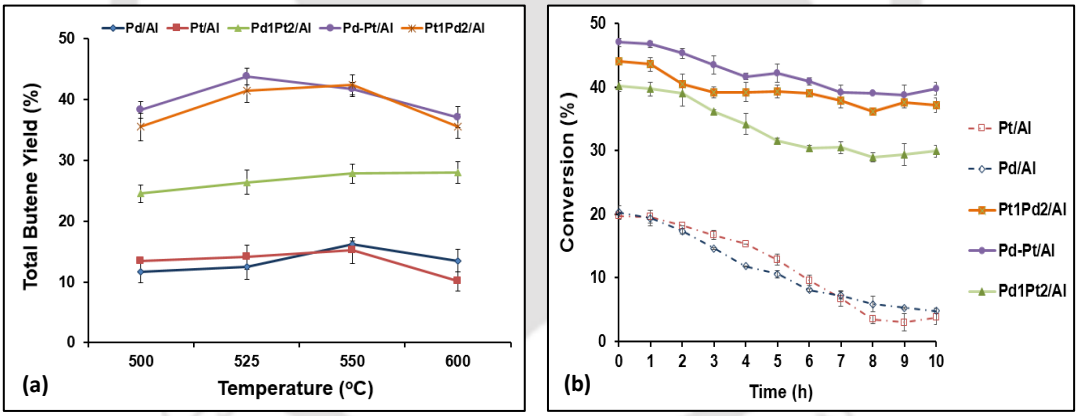

Figure 6.10. (a) Total butene yield at different temperatures and (b) Stability tests for 10 h time on stream at 550 °C for monometallic and bimetallic catalysts prepared by different metal deposition sequences.

Figure 6.10b shows the change in conversion of butane at 550 °C with time on stream for 10 h. The bimetallic catalysts were more stable compared to monometallic catalysts with time on stream. The catalytic activity of Pd-Pt/Al remained highest for entire range of time studied, closely followed by Pt_1Pd_2/Al. The Pd_1Pt_2/Al catalyst experienced a more severe deactivation after 2 h of study but gradually became stable in the later stage. On the other hand, both the monometallic catalysts, Pd/Al and Pt/Al, suffered continuous deactivation

and lost their activity significantly by the end of study after 10 h. The initial conversions of Pt/Al, Pd/Al, Pd_1Pt_2/Al, Pt_1Pd_2/Al and Pd-Pt/Al catalysts were 19.7, 20.3, 40.1, 44 and 47%, which after 10 h decreased to 3.8, 4.8, 29.9, 37.1 and 39.7% respectively. Thus, percent order of deactivation of the catalysts calculated after 10 h of reaction time was as follows: Pd-Pt/Al (15%) < Pt_1Pd_2/Al (16%) < Pd_1Pt_2/Al (25%) < Pd/Al (76%) < Pt/Al (81%). The lower deactivation for the bimetallic catalysts may have resulted from lower selectivity towards cracked products.

6.3.3 Reaction Mechanism

Based on the catalytic performance as discussed above, a mechanistic approach is shown in Figure 6.11. The scheme shows that the butane molecules get adsorbed on metal sites and undergoes C-H activation followed by hydrogen extraction to form butene. These butenes may get desorbed or undergo further secondary reactions to form lower hydrocarbons by C-C bond activation. The reaction results suggested that the butane dehydrogenation on prepared catalysts involved both primary and secondary reactions depending on the reaction conditions. The comparison of the conversion data of monometallic Pt/Al and Pd/Al suggested that at lower temperature Pt/Al was more active than that of Pd/Al. The Pd/Al showed similar or higher activity only at higher temperature beyond 450 °C. This suggested that the energy barrier for dehydrogenation was higher on Pd sites compared to that on Pt sites. The higher energy barrier for Pd sites might have resulted from the lower interaction tendency of Pd towards hydrocarbons [12]. Hence, for the co-deposited alloyed bimetallic catalyst with equal probability of exposure of Pd and Pt sites, the alkane is expected to interact preferentially with the Pt sites compared to that with Pd sites. As the temperature increased both platinum and palladium sites in alloyed metal contributed to the dehydrogenation reaction increasing the total activity significantly at higher temperature, as observed.

At lower temperature, mainly butenes were formed with negligible formation of C_1-C_3 hydrocarbons. This suggested absence of any secondary reactions of butene or C-C hydrogenolysis of butane at this low temperature condition. At higher temperature, appearance of lower hydrocarbons suggested contribution of these reactions. The higher activation energy of C-C cleavage compared to C-H activation agreed with this observations [13]. At higher temperature, simultaneous rupture of C–C bonds on the stronger support acidic sites may have also contributed significantly towards formation of

lighter hydrocarbons/cracked products [14,15]. The products of cracking reactions can further undergo oligomerization or polymerization leading to coke formation. The analysis of spent catalyst, as discussed later, showed negligible deposition of coke on catalyst surface under used reaction conditions. This suggested absence of coke generating reactions on the catalyst surface. This also agreed with the high selectivity observed for butene over co-deposited bimetallic catalyst. Since there was no major difference in metal size distribution and thereby, metal dispersion between bimetallic and monometallic catalysts hence, exposed support acidic sites can be assumed to be similar in all the catalysts. Therefore, the contribution of these support acidic sites to C-C cleavage reactions can be expected to be similar. The difference in selectivity pattern of the bimetallic and monometallic catalysts therefore might have resulted due to modification of electronic structure of alloyed metals in the former.

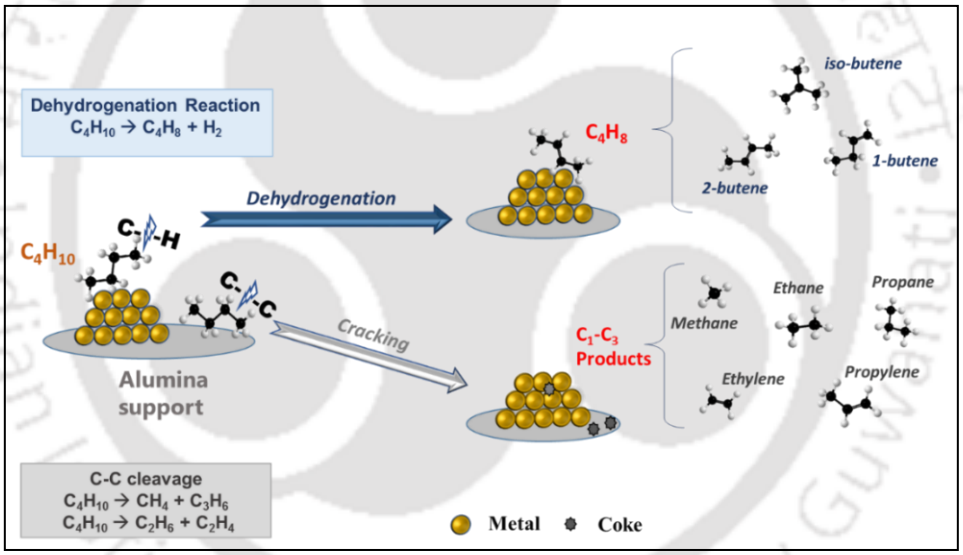

Figure 6.11. Reaction scheme observed for butane dehydrogenation over prepared catalysts.

The increase in electron density on Pt sites in alloyed metal clusters in bimetallic catalyst (as observed from XPS studies) allowed the product butene to desorb from the active sites more easily as compared to the monometallic metal sites. Faster butene desorption may be attributed to repulsive interaction between C=C and electron-rich Pt sites [12]. Faster desorption of product butene thereby generated vacant active metal sites, ready for further butane adsorption and subsequent dehydrogenation. This contributed to higher butane conversion over alloyed metal sites on bimetallic catalysts. The faster desorption also prevented butenes from undergoing deep dehydrogenation on alloyed metal sites

facilitating inhibition of undesired secondary reactions [15,16]. Consequently, butene selectivity and catalytic stability were improved as observed. The heat of adsorption for alkenes is reported to be lowered by alloyed formations [7]. The presence of Pd as the other metal in alloyed cluster which had inherently lower interaction tendency with hydrocarbons, as discussed above, only further improved the selectivity. The lower probability of formation C-C cleavage products might have inhibited the occurrence of coke generating reactions thereby increasing the stability of the bimetallic catalysts.

6.3.4 Analysis of spent catalyst

The detailed characterization studies of spent Pd-Pt/Al catalyst were done and the results were compared with that of fresh catalyst to understand the effect of reaction conditions on the physicochemical properties of the catalyst. The Pd-Pt/Al was selected as it gave the best performance among the studied catalysts. The spent catalyst was subjected to surface area and pore analysis, TGA, XPS, and TEM. All the results are shown in Figure 6.12.

The Figure 6.12a compares the nitrogen adsorption-desorption isotherm of spent and fresh Pd-Pt/Al catalyst. No significant change in nature of isotherm was observed for spent Pd-Pt/Al catalyst compared to that of the fresh one. Only a slight decrease in volume of adsorbed nitrogen was observed for the spent catalyst. Accordingly, the corresponding surface area of Pd-Pt/Al_spent was marginally lowered to 175 $m^2 g^{-1}$ compared to 181 $m^2 g^{-1}$ for the fresh Pd-Pt/Al catalyst (Table 6.8). The comparison of pore size distribution in Figure 6.12b shows that for Pd-Pt/Al_spent catalyst, the distribution was slightly broadened (2-11 nm) as compared to that of fresh Pd-Pt/Al catalyst (3-8 nm). The corresponding average pore size and pore volume for Pd-Pt/Al_spent catalyst were also slightly reduced as illustrated in Table 6.8. The slight decrease in surface area, pore volume and average pore size for Pd-Pt/Al_spent catalyst may be attributed to coke deposition or moderation of catalyst during reaction. However, only marginal decrease in the physical properties also suggested extent of carbon deposition or moderation to be very low.

Table 6.8. Physical properties of fresh and spent Pd-Pt/Al catalysts.

Catalysts	BET surface area ($m^2 g^{-1}$)	Pore volume (cc g^{-1})	Average pore diameter (nm)
Pd-Pt/Al_Fresh	181	0.327	6.0
Pd-Pt/Al_Spent	175	0.290	5.7

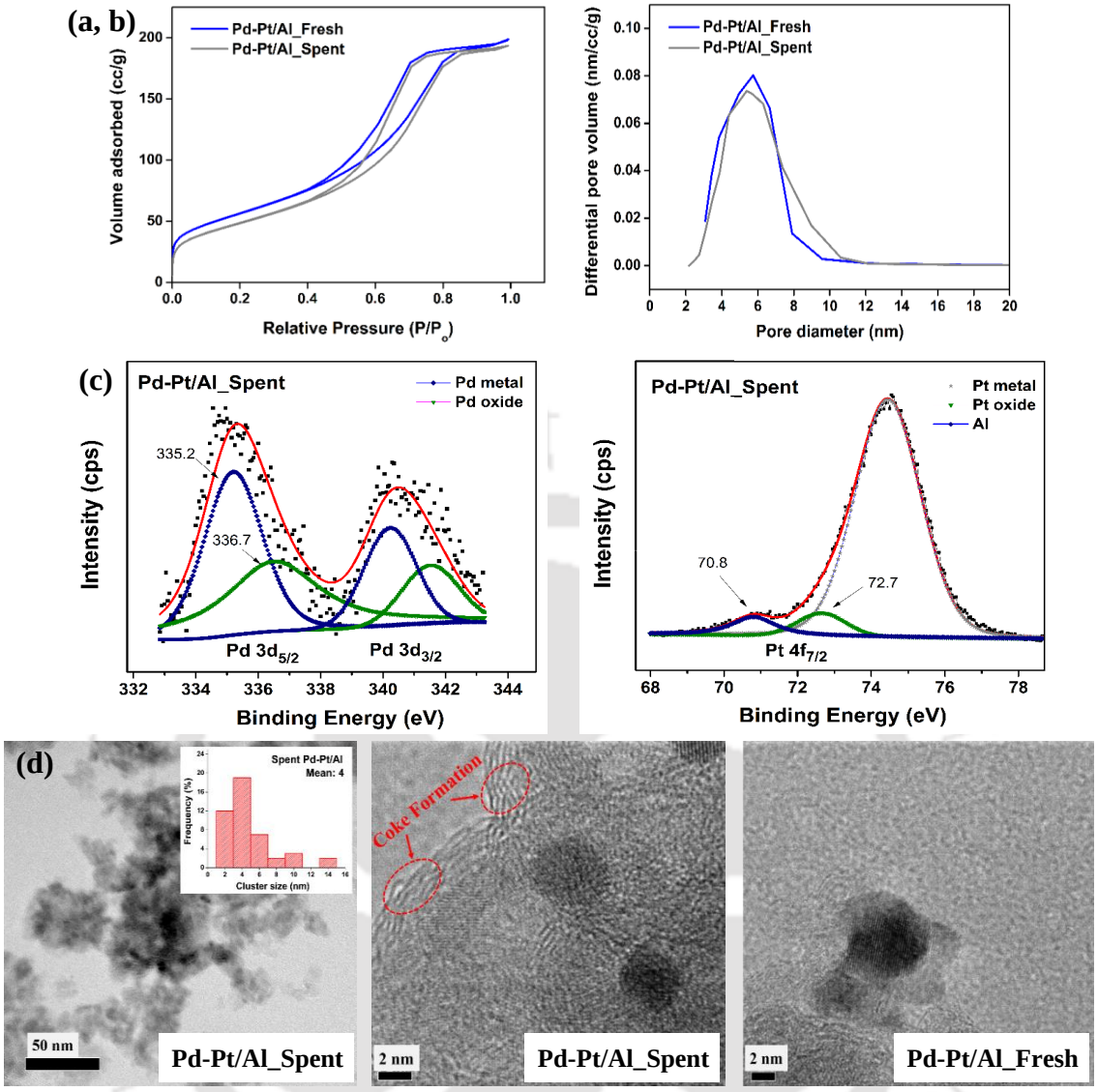

Figure 6.12. (a) Nitrogen adsorption desorption isotherm and (b) pore size distribution for fresh and spent Pd-Pt/Al catalyst; (c) XPS spectra of Pd 3d and Pt 4f region in spent Pd-Pt/Al catalyst; (d) HRTEM images and particle size distribution for spent Pd-Pt/Al catalyst.

The weight analysis of catalyst before and after reaction confirmed the coke deposition to be negligible, less than 0.5 wt%. The result was also confirmed by TGA analysis in flow of air that showed coke deposition to be less than 3 wt% (Appendix H). This low coke deposition may be accounted by two reasons. First is the presence of hydrogen in feed that suppressed the formation coke precursors. Secondly, it was observed and discussed in detail in earlier section how the alloyed metal sites in co-deposited bimetallic catalyst prevented secondary reactions, minimizing the formation of coke precursors.

The XPS analysis was carried out for Pd-Pt/Al_spent catalyst to investigate the modification in its electronic structure, if any, due to exposure to reaction conditions. The

corresponding profiles are included in Figure 6.12c. It was observed that the intensity of Pt 4f peak was reduced in spent catalyst in comparison to that in the fresh Pd-Pt/Al catalyst. The peaks were observed at 71.1 eV (for Pt^0), 72.9 eV (for Pt^{2+}), 335.0 eV (for Pd^0) and 336.4 eV (for Pd^{2+}) in the fresh Pd-Pt/Al catalyst. The corresponding peaks in monometallic catalysts were observed at 70.6 (Pt^0), 72.7 eV (Pt^{2+}), 335.1 (Pd^0) and 336.3 eV (Pd^{2+}), as already has been discussed in detail in earlier section.

The XPS profiles of the spent Pd-Pt/Al catalyst showed the peak positions of same metallic and oxidized species at 70.8 eV (Pt^0), 72.7 (for Pt^{2+}), 335.2 eV (Pd^0), and 336.5 (for Pd^{2+}), respectively. The comparison of binding energies of monometallic, fresh bimetallic and spent bimetallic suggested that there was slight redistribution of the electronic structure after the exposure of catalyst to reaction conditions. The lowering of electron density on alloyed Pt-sites for spent bimetallic catalysts compared to that in fresh bimetallic catalyst suggested some adverse effect on Pd-Pt interaction on the support by modification of structure during reaction. The ratio of Pd^0/Pd^{2+} and Pt^0/Pt^{+2} in Pd-Pt/Al_spent catalyst were 51/49 and 47/53, respectively. These values are mostly similar to that observed for fresh catalyst (Table 6.4).

TEM images of spent Pd-Pt/Al catalyst are illustrated in Figure 6.12d. The average metal size increased slightly from 3.6 nm for fresh Pd-Pt/Al to 4 nm for Pd-Pt/Al_spent catalyst. The corresponding dispersion value decreased to 28.2% for spent catalyst from 31.4 % obtained for fresh catalyst. The high resolution TEM images of Pd-Pt/Al_spent catalyst showed some distinct morphology that was not observed in fresh catalyst (Figure 6.12d). This new disordered morphology may be assigned to the presence of coke deposits on catalyst surface [16].

6.3.5 Effect of process parameters

This section discusses some additional effects of process parameters on butane conversion and butene selectivity for best performing bimetallic Pd-Pt/Al catalyst. The butane conversion and the product selectivity was determined by the Eq. 2.6 and 2.7 as described in chapter 2, section 2.2.5 (page no. 34).

The Figure 6.13a illustrates the effect of reaction temperature on selectivity of different butenes. The butane conversion increased from 39 to 48% with increase in temperature from 450 to 600 °C as discussed in earlier section. In this range, selectivity towards total

butenes decreased with the increasing reaction temperature. The decrease in butene selectivity from 91% at 450 °C to 75% at 600 °C was attributed to increased tendency towards cracking reaction at higher temperature. On increasing the reaction temperature from 450 to 600 °C, the selectivity towards trans-2-butene and cis-2-butene also decreased from 28 and 23% to 22.6 and 17.3%, respectively. Similar decrease in selectivity from 24 to 18.5% was also observed for 1-butene. However, the iso-butene selectivity increased from 16.2 to 19.4% with the increase in temperature up to 550 °C. This suggested that the isomerization reaction was more prominent at elevated temperature.

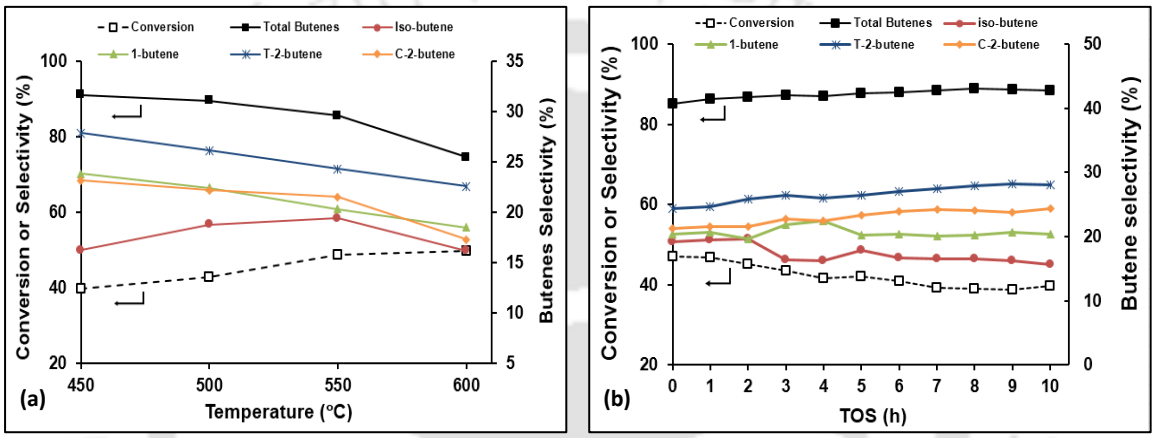

Figure 6.13. Selectivity of butenes: total butene (■), isobutene (●), 1-butene (Δ), trans-2-butene (×), cis-2-butene (♦) (a) as function of temperature and (b) as function of process time over Pd-Pt/Al catalyst. Reaction conditions: pressure = 1 atm, C_4H_{10}:H_2:N_2 = 1:3:6, catalyst mass (W) = 0.25 g.

Figure 6.13b shows the effect of process time of 10 h on selectivity of different butenes at 550 °C. The butane conversion decreased from 47 to 40% in the process time due to deactivation as discussed earlier. A gradual increase in total butene selectivity from 85 to 88.5% was observed over the process time. The selectivity towards 1 and 2-butene also increased with increase in process time. However, a decline in iso-butene selectivity was observed over the process time of 10 h. The selectivity trends suggested shift in reaction towards dehydrogenation from isomerization and cracking reactions over the time. The slight deactivation of the bimetallic catalyst over time might be the reason for the same.

Figure 6.14a illustrates the effects of hydrogen partial pressure on butane conversion and butene selectivity for Pd-Pt/Al catalyst at different temperatures. Previous studies have shown that catalyst deactivation can be inhibited by addition of H_2 to the feed [17]. Hence,

when no hydrogen was used in the reactant feed, butane conversion obtained was least. It increased gradually on introducing the hydrogen into the feed and raising the H_2 partial pressure from 10 to 30 kPa and decreased thereafter on further increasing the H_2 ratio. A similar effect has been observed previously during butane dehydrogenation over Pt/Mg(In)(Al)O catalyst by Wu et al. [18]. Thus, the maximum butane conversion was obtained at 30 kPa, and hence that was chosen as the optimal hydrogen to butane ratio for conducting butane dehydrogenation studies.

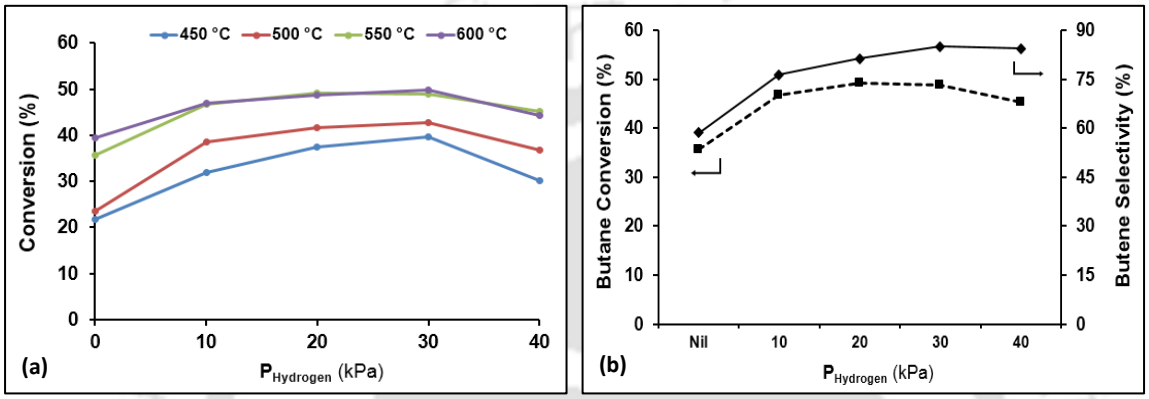

Figure 6.14. (a) Effect of H_2 partial pressure on butane conversion at different temperatures in dehydrogenation reaction using co-deposited Pd-Pt/Al catalyst and (b) Effect of H_2 partial pressure on catalytic performance of Pd-Pt/Al catalyst at 550 °C. Reaction conditions: C_4H_{10} = 10 mL min^{-1}, catalyst mass (W) = 0.25 g, W/Fa_o = 0.025 g min mL^{-1}.

Figure 6.14b illustrates the effect of H_2 partial pressure on butene selectivity at 550 °C. The butene selectivity of 58% was obtained without hydrogen that increased with the increase in hydrogen partial pressure. The maximum butene selectivity of 85% was obtained at 30 kPa. However, increasing the partial pressure above 30 kPa caused a little decrease in butene selectivity. Thus, in all the cases, the butane conversion and butene selectivity increased with increasing H_2/butane ratio and then decreased beyond 30 kPa. It has been reported that at optimal H_2 partial pressure, adsorbed hydrogen atoms on the catalyst surface contribute to the removal of the second H atom of the adsorbed alkyl species, thereby accelerating the rate of butene formation [19]. Increased butene production can also be attributed to hydrogen inhibiting deactivation by coke formation. However, at much higher hydrogen partial pressures, the conversion would decrease due to hydrogenation of the formed butene. For butane dehydrogenation over Pd-Pt/Al, the optimum hydrogen partial pressure was 30 kPa, at which considerable butane conversion was obtained and butene formation was maximized.

The Figure 6.15 shows the effect of residence time on butane conversion and total butene selectivity at higher temperature range of 500-600 °C over co-deposited Pd-Pt/Al catalyst. The conversion increased with residence time but plateaued off at higher residence time suggesting to approach steady-state conversion under the reaction condition used. This was observed in range of the temperatures studied. However, the change in butene selectivity with residence time was negligible, irrespective of reaction temperature.

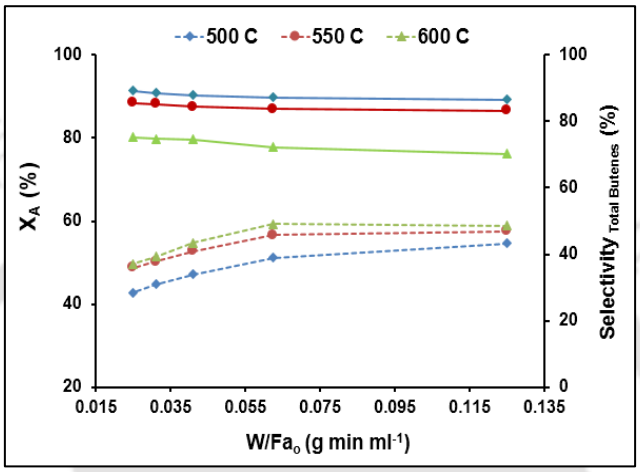

Figure 6.15. Effect of residence time (W/Fa$_o$) on butane conversion (dashed lines) and total butene selectivity (solid lines) at different reaction temperatures over co-deposited Pd-Pt/Al catalyst. W = 0.25 g; Fa$_o$ variation 2-10 kPa.

The effect of catalyst recycling on catalytic activity for dehydrogenation reaction was investigated by using the spent Pd-Pt/Al catalyst for subsequent runs. The butane dehydrogenation was repeated two times (Run 2 and Run 3) on the Pd-Pt/Al_spent catalyst under similar conditions. The corresponding butane conversion and total butene selectivity for all three runs are compared in Figure 6.16. Run 1 represents reaction over fresh catalyst, while, Run 2 and Run 3 were carried out over spent catalyst. It was observed that the catalytic activity obtained in Run 2 and 3 using the spent catalyst was quite close to that obtained using fresh catalyst (Run 1). The highest butane conversion of 48.8% at 550 °C on fresh catalyst was decreased to 45.2% for spent catalyst at same temperature on 2nd run. Later in 3rd run the conversion further dropped to 42.1% at 550 °C. The corresponding decrease in total butene selectivity, at 550 °C were also marginal: Run 1 (85.5%), Run 2 (82.4%) and Run 3 (81.3%). Thus, decrease in dehydrogenation performance, in terms of activity and selectivity was not significant for spent catalyst. The dehydrogenation results agreed with the characterization study of spent catalyst which showed only marginal

modification in physical and electronic structure along with very minor coke deposition. This suggested that alloyed nano-metals were mostly stable in the reaction condition used.

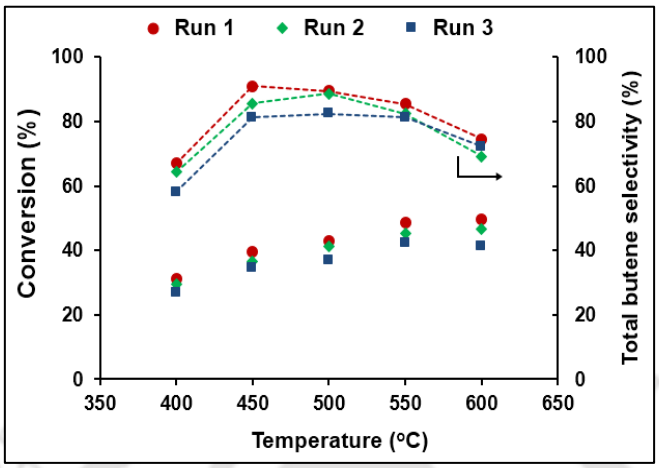

Figure 6.16. Effect of catalyst recycling on butane conversion and total butene selectivity over co-deposited Pd-Pt/Al catalyst. Reaction conditions: Temperature = 400 - 600 °C, pressure = 1 atm, flow rate = 100 mL min^{-1} (C_4H_{10}:H_2:N_2 = 1:3:6), catalyst mass (W) = 0.25 g.

The kinetic parameters, that is, order and activation energy of the butane dehydrogenation reaction was estimated for bimetallic Pd-Pt catalyst using a simple power law model by differential analysis. The contact time (W/Fa_o), where W is the weight of catalyst in grams and Fa_o is the molar flow rate of butane in mL min^{-1}. Individually, the Fa_o was varied in the range of 2 – 5 mL min^{-1}, while W was varied between 0.1 - 0.25 g. The W/Fa_o data were collected at conversion below 3% to maintain differential conditions. To calculate the activation energy, the data were collected at different temperatures between 100 - 150 °C. The total flow rate was maintained at 100 mL min^{-1}. At this condition, no mass transfer effects or deactivation was observed (Appendix A). The product distribution showed no presence of C_1-C_3 products. Hence, it can be assumed that under conditions mentioned, only dehydrogenation of butane had occurred. The apparent order and activation energy of butane dehydrogenation was obtained as ~1.2 and 103 kJ/mol. The Arrhenius plot is shown in Figure 6.17. In literature, for butane dehydrogenation the order of reaction has been reported as one, while the activation energies have been reported in range of 60 – 130 kJ/mol [20,21]. Curry and Thompson reported the apparent activation energy to be 117.5 kJ/mol for dehydrogenation of butane over Pt-Sn catalyst [20]. Wu et al. reported the activation energy for butane dehydrogenation to be 129.4 kJ/mol using Pt/Mg(In)(Al)O catalyst [18]. Natarajan et al. demonstrated that the apparent activation energies for n-

butane dehydrogenation reaction were obtained in the range of 60 – 75 kJ/mol over bimetallic Pt-Sn catalysts supported on mesoporous alumina [21].

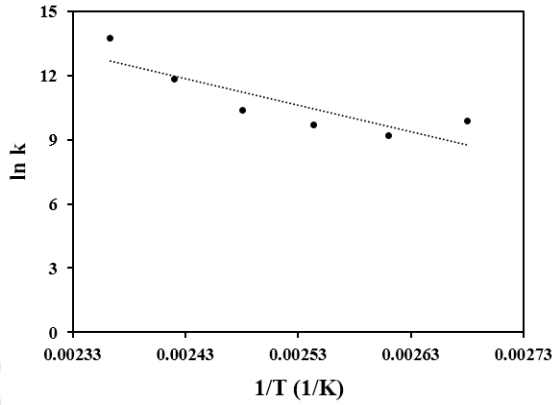

Figure 6.17. Arrhenius plot of butane dehydrogenation reaction over co-deposited Pd-Pt/Al catalyst.

6.3.6 Effect of surfactant on bimetallic Pd-Pt catalyst

In this section, the physicochemical properties and butane dehydrogenation performance of bimetallic Pd-Pt-T20 catalyst prepared in presence of surfactant were compared to that of the corresponding Pd-Pt/Al catalyst prepared without using surfactant. Both the catalysts were prepared by co-deposition method having equimolar Pd and Pt. The total metal loading was also kept similar in both the catalysts. The composition analysis by EDX confirmed that metal loading of the surfactant modified Pd-Pt-T20 catalyst was comparable to that of Pd-Pt/Al catalyst as shown in Table 6.9.

The nitrogen adsorption-desorption isotherms and pore size distributions of these catalysts are compared in Figure 6.18a and b, respectively. The nature of isotherm for both the catalysts was similar to that of alumina, but total volume of adsorbed nitrogen was lower for the catalysts compared to that of support. Pd-Pt-T20 catalyst exhibited higher surface area of 205 $m^2 g^{-1}$ than Pd-Pt/Al catalyst (181 $m^2 g^{-1}$). The Pd-Pt/Al catalyst exhibited a wider pore size distribution with an average pore size of 6 nm, while the average pore size was lowered to 5.1 nm in the surfactant modified Pd-Pt-T20 catalyst (Figure 6.18b). No micropores were observed in any of the catalysts. The pore volume observed for both the catalysts was also in similar range. All these physical properties are summarized in Table 6.9.

Table 6.9. Metal loadings, surface area and pore analysis for co-deposited bimetallic catalysts prepared with and without surfactant.

Catalysts	Loading[a] (wt %)		BET surface area (m^2 g^{-1})	Pore volume (cc g^{-1})	Average pore diameter (nm)
	Palladium	Platinum			
Pd-Pt/Al	0.55	1.10	181	0.327	6.0
Pd-Pt-T20	0.50	1.10	205	0.288	5.1

[a] *Metal loading determined by EDX analysis*

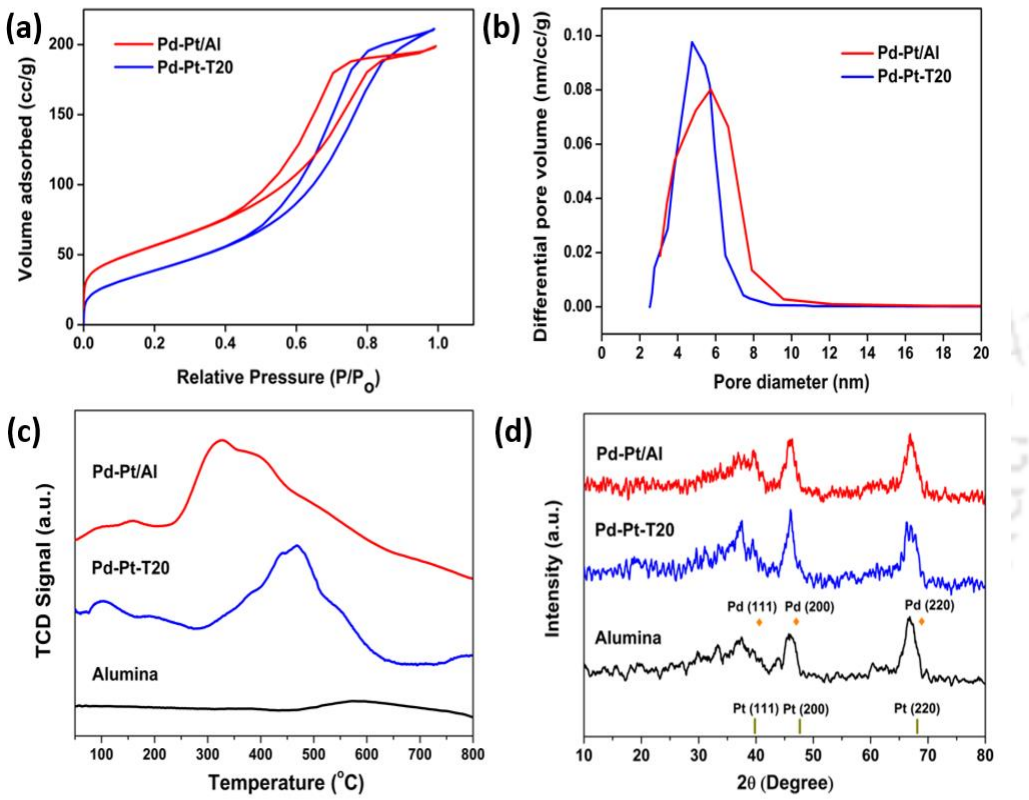

Figure 6.18. (a) Nitrogen adsorption-desorption isotherms, (b) BJH pore size distribution, (c) TPR profile and (d) XRD spectra of co-deposited bimetallic catalysts prepared with surfactant (Pd-Pt-T20) and without surfactant (Pd-Pt/Al).

The TPR profiles of Pd-Pt-T20 and Pd-Pt/Al catalysts are compared in Figure 6.18c. The Pd-Pt-T20 exhibited low temperature reduction peak at 100 °C corresponding to the presence of oxidized Pd particles that are in weak interaction with the support and hence easily reducible. This low temperature reduction peak was negligible in case of Pd-Pt/Al catalyst. The high intensity peak located at a temperature of 310 °C with a broad shoulder at 390 °C, as discussed earlier, assigned to the presence of Pd and Pt species in strong

interaction with the support for Pd-Pt/Al. Similar peak in Pd-Pt-T20 catalyst was observed at a much higher temperature of 480 °C. Such a shift for second reduction peak to a significantly higher temperature could be attributed to establishment of a much stronger metal-support interaction in the surfactant based catalyst.

The comparison of XRD profiles (Figure 6.18d) revealed that the crystalline structure of surfactant based catalyst was similar to that of catalyst prepared in absence of surfactant. Also, no characteristic peaks for Pd and Pt metals were observed in any catalysts as before.

From the TEM images (Figure 6.19), it can be observed that the metal particles were well distributed in both the catalysts. The average cluster size for Pd-Pt-T20 catalyst was 2.9 nm which was lower in comparison to that of Pd-Pt/Al catalyst (3.6 nm). The corresponding dispersion values were 39 and 31.4%, respectively.

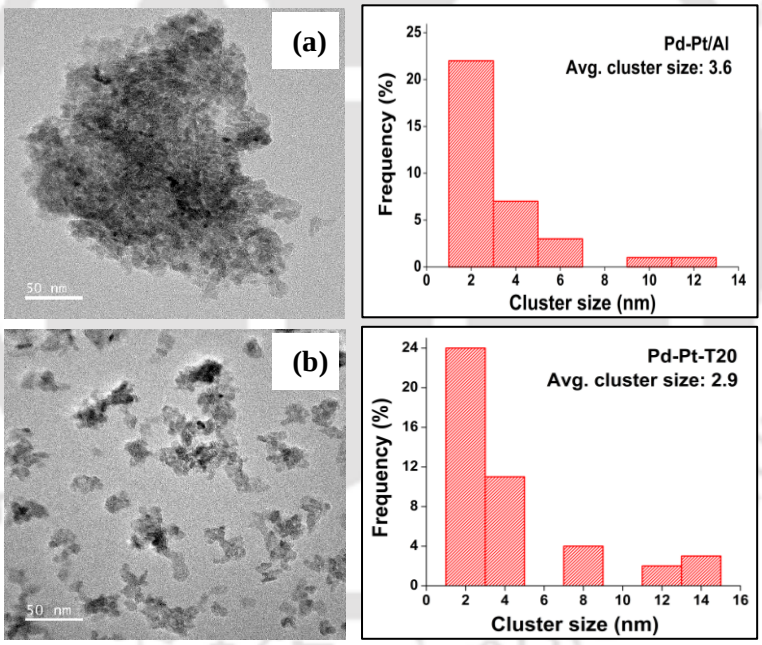

Figure 6.19. HRTEM images and particle size distribution of co-deposited bimetallic catalysts prepared without surfactant (a) Pd-Pt/Al and with surfactant (b) Pd-Pt-T20.

Figure 6.20a depicts the butane conversion obtained over the catalysts in the temperature range of 100 °C – 600 °C. In the low reaction temperature range of 100-300 °C, both the catalysts exhibited approximately similar conversion ranging from 8 to 15%. At all temperatures beyond 300 °C, the Pd-Pt/Al catalyst prepared without surfactant showed higher activity compared to that of Pd-Pt-T20 catalyst. The conversion picked up remarkably for Pd-Pt/Al catalyst on reaching 400 °C and thereafter. The conversion

increased gradually for Pd-Pt-T20 catalyst on raising the temperature, but it was considerably lower throughout than that observed for Pd-Pt/Al catalyst. At 550 °C, the Pd-Pt/Al catalyst exhibited higher conversion of 48.8% in comparison to Pd-Pt-T20 catalyst (42.7%). Thus, higher TOF value of 1.18 s^{-1} was attained by Pd-Pt/Al catalyst as compared to that of Pd-Pt-T20 (1.05 s^{-1}). The conversion increased to 49.7% and 44.6% at 600 °C for Pd-Pt/Al and Pd-Pt-T20 catalyst, respectively.

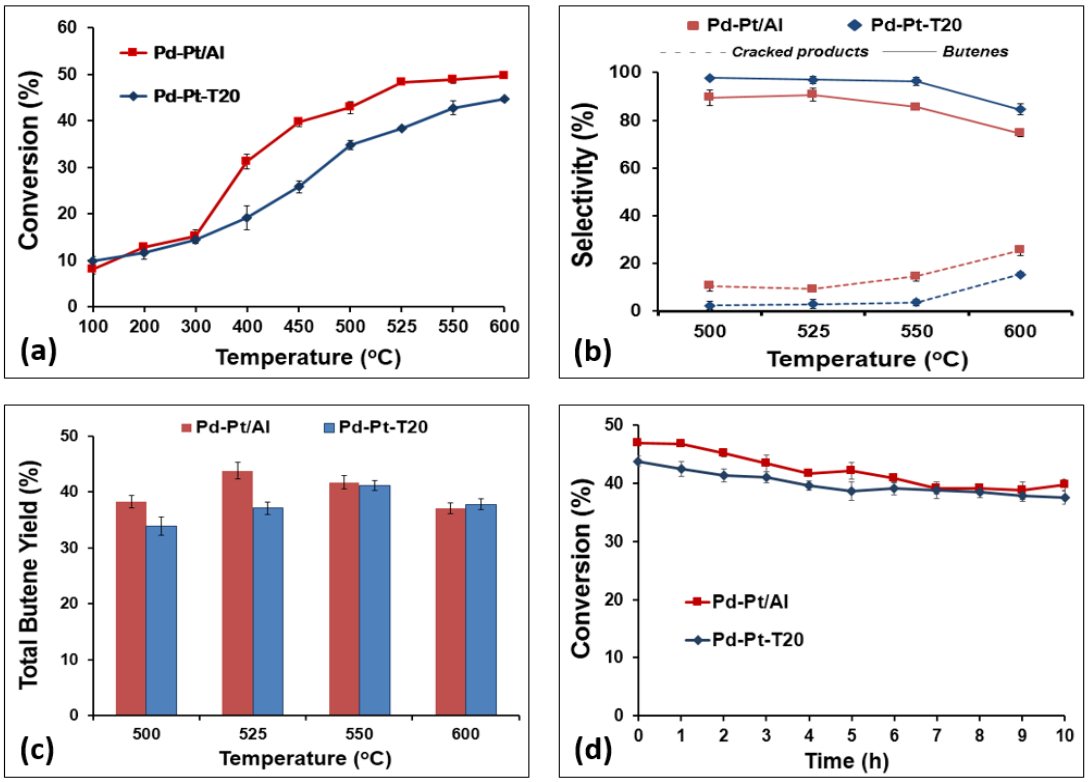

Figure 6.20. Catalytic activity of co-deposited Pd-Pt bimetallic catalysts prepared with and without surfactant (a) butane conversion profile, (b) product selectivity profile, (c) butene yield and (d) stability test at 550 °C.

Figure 6.20b compares the selectivity towards butene and cracked products at different temperatures. The selectivity towards butenes decreased gradually on raising the temperature from 500 °C to 600 °C, while selectivity for undesired C_1-C_3 products increased proportionally. The maximum butene selectivity of 97.7% was obtained by Pd-Pt-T20 catalyst at 500 °C that was significantly higher in comparison to Pd-Pt/Al catalyst which exhibited maximum selectivity of 90.7% towards butenes at 525 °C. The selectivity dropped to 84% and 75% for Pd-Pt-T20 and Pd-Pt/Al catalyst, respectively, on raising the temperature to 600 °C.

Table 6.10 depicts the selectivity towards different products at 550 °C by both the catalysts. The Pd-Pt-T20 catalyst exhibited highest selectivity towards trans-2-butene (36.8%) followed by cis-2-butene (27.5%) with a minimal selectivity towards cracked products (3.7%). On the other hand, Pd-Pt/Al exhibited about 14.5% selectivity towards cracked products and selectivity towards trans-2-butene and cis-2-butene decreased to 24.3% and 21.5%, respectively. Both the catalysts exhibited higher selectivity towards the formation of 1-butene in comparison to iso-butene. Hence, for catalyst synthesized using surfactant, the overall selectivity towards butenes was much higher in comparison to Pd-Pt/Al catalyst prepared without surfactant. The lower conversion in same temperature range resulted in higher butene selectivity for surfactant modified catalyst as observed.

Table 6.10. Catalytic performance of co-deposited bimetallic catalyst prepared with and without surfactant for n-butane dehydrogenation [reaction temp. = 550 °C, gas ratio (n-butane:hydrogen:nitrogen) = 1:3:6].

Catalysts	Conversion (%)	TOF (s^{-1})	Selectivity (%)					
			Iso-butene	1-butene	Trans-2-butene	Cis-2-butene	Total butene	C_1-C_3
Pd-Pt/Al	48.8	1.18	19.4	20.3	24.3	21.5	85.5	14.5
Pd-Pt-T20	42.7	1.05	14	18	36.8	27.5	96.3	3.7

Figure 6.20c illustrates the butene yield obtained at 550 °C for both the catalysts. The percentage yield for butenes was slightly higher in the temperature range of 500-525 °C for the Pd-Pt/Al catalyst prepared without surfactant. The highest yield of 44% was obtained at 525 °C for Pd-Pt/Al catalyst due to its higher conversion. At higher temperature of 550-600 °C, the yields obtained were approximately similar for both the catalysts. Pd-Pt/Al and Pd-Pt-T20 catalyst showed the butene yield in the range of 41-42% at 550 °C that dropped to 37-38% at 600 °C, due to the decrease in butene selectivity at elevated temperature.

Figure 6.20d shows a time-on-stream study comparing the butane conversion over Pd-Pt-T20 and Pd-Pt/Al catalysts for a duration of 10 h. The Pd-Pt-T20 catalyst exhibited lower conversion than Pd-Pt/Al catalyst over entire process time. However, the overall deactivation was slightly lower for the former. The Pd-Pt-T20 catalyst showed an initial conversion of 43.8%, which reduced to 37.6% after 10 h, exhibiting only 14% deactivation. The initial conversion of 47% obtained for Pd-Pt/Al catalyst decreased to 39.7% after 10 h, corresponding to 15% deactivation. A slightly lower deactivation in Pd-Pt-T20 catalyst

may be attributed to lower formation of cracked products leading to less coke deposition on active sites.

The results showed that use of surfactant during preparation of bimetallic catalyst by electroless co-deposition increased the metal dispersion. This resulted in less pore blockage and higher surface area of Pd-Pt-T20 compared to the catalyst that was prepared in absence of surfactant. However, the performance of the Pd-Pt-T20 catalyst was not improved significantly, with selectivity and yield for butene slightly increasing at higher temperature.

6.3.7 Effect of promoter on bimetallic Pd-Pt catalyst

In chapter 4, it was observed that addition of copper to monometallic supported palladium catalyst increased the catalytic performance of monometallic catalyst. Based on this, copper was also added to supported Pd-Pt bimetallic catalyst to investigate the effect. For comparison, two bimetallic catalysts PtCu/Al and PdCu/Al were prepared. Table 6.11 compares the metal loadings of Cu promoted monometallic and bimetallic catalysts. All the promoted catalysts were prepared keeping total metal loading constant to 112.8 µmoles. The Cu loading was maintained at 10 mol%. PtCu/Al, PdCu/Al and PdPtCu/Al catalysts exhibited a total metal loading of 1.97, 1.07 and 1.53 wt % respectively.

Table 6.11. Metal loading obtained for Cu promoted monometallic and bimetallic catalysts using AAS.

Catalysts	Cu loading (wt %)	Pd loading (wt %)	Pt loading (wt %)	Total loading (wt %)
PtCu/Al	0.073 (11.5)*	--	1.9 (97)	1.97 (108.5)
PdCu/Al	0.071 (11.5)	1.00 (94)	--	1.07 (105.5)
PdPtCu/Al	0.070 (11.0)	0.54 (51)	0.9 (46)	1.53 (108.0)

** Values in parenthesis denote metal loading in mol%*

The nitrogen adsorption-desorption isotherms and pore size distributions for the prepared catalysts are displayed in Figure 6.21a and b, respectively. All the catalysts exhibited Type IV isotherms with H2-type hysteresis loop. Table 6.12 illustrates that PtCu/Al and PdCu/Al catalyst exhibited almost similar surface area of 211 $m^2 g^{-1}$ and 208 $m^2 g^{-1}$, respectively. The surface area of tri-metallic PdPtCu/Al catalyst was significantly lower in comparison to that for Cu promoted Pd and Pt bimetallic catalyst. The decrease in BET surface areas of the tri-metallic sample with respect to other two catalysts may have resulted due to blockage of pores by higher cluster size of metal particles, also confirmed by TEM analysis.

Table 6.12. Surface area and pore analysis for Cu promoted monometallic and bimetallic catalysts.

Catalysts	BET surface area (m^2 g^{-1})	Pore volume (cc g^{-1})	Average pore diameter (nm)
PtCu/Al	211	0.327	5.2
PdCu/Al	208	0.320	5.2
PdPtCu/Al	197	0.302	6.0

All the three catalysts showed pores mainly in the range of 2-10 nm, with total peak intensity of PdPtCu/Al lower than that of bimetallic PtCu/Al and PdCu/Al catalysts. The PdCu/Al and PtCu/Al exhibited narrower pore size distribution with an average pore diameter of 5.2 nm in comparison to the PdPtCu/Al catalyst which had an average pore diameter of 5.8 nm. No micropores were observed in any of the catalysts. Among the catalysts examined, PtCu/Al catalyst retained highest surface area with higher pore volume.

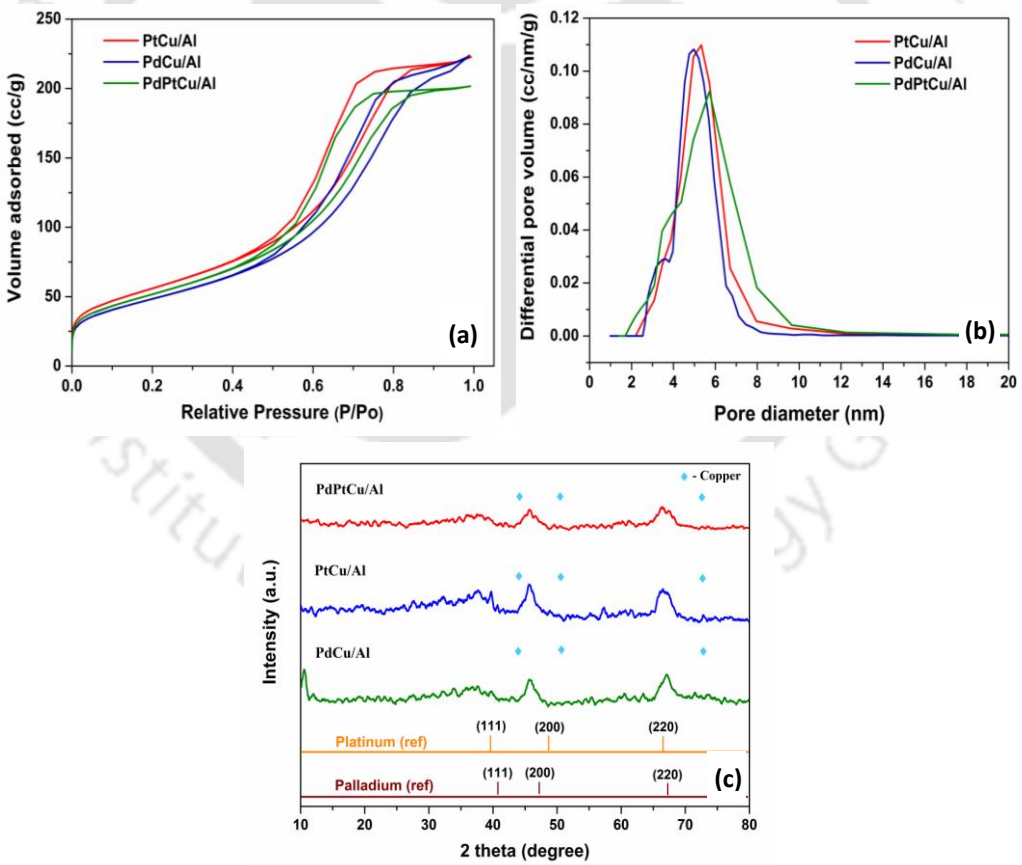

Figure 6.21. (a) Nitrogen adsorption-desorption isotherms, (b) BJH pore size distribution and (c) XRD spectra of Cu promoted monometallic and bimetallic catalysts.

The pore volume of all the three catalysts varied in the range of 0.30 to 0.33 cc g^{-1}. Figure 6.21c shows the XRD spectra for the Cu promoted catalysts. The peaks corresponding to copper, palladium and platinum phases were not present in any of the samples suggesting high dispersion of metals on the support.

The particle morphology for the copper promoted catalysts was studied using TEM for which the corresponding images are shown in Figure 6.22. Well dispersed metal particles were observed on the surface of all the catalysts. The average cluster size of the PtCu/Al, PdCu/Al and PdPtCu/Al catalysts were about 3.7, 3.8 and 4.2 nm, respectively. The trimetallic catalyst thus gave the largest metal clusters. Furthermore, the elemental composition of the promoted catalyst was confirmed through SAED patterns obtained during HRTEM analysis as shown in Figure 6.22. The SAED results of these catalysts confirmed the presence of Pt, Pd and Cu in the respective promoted catalysts.

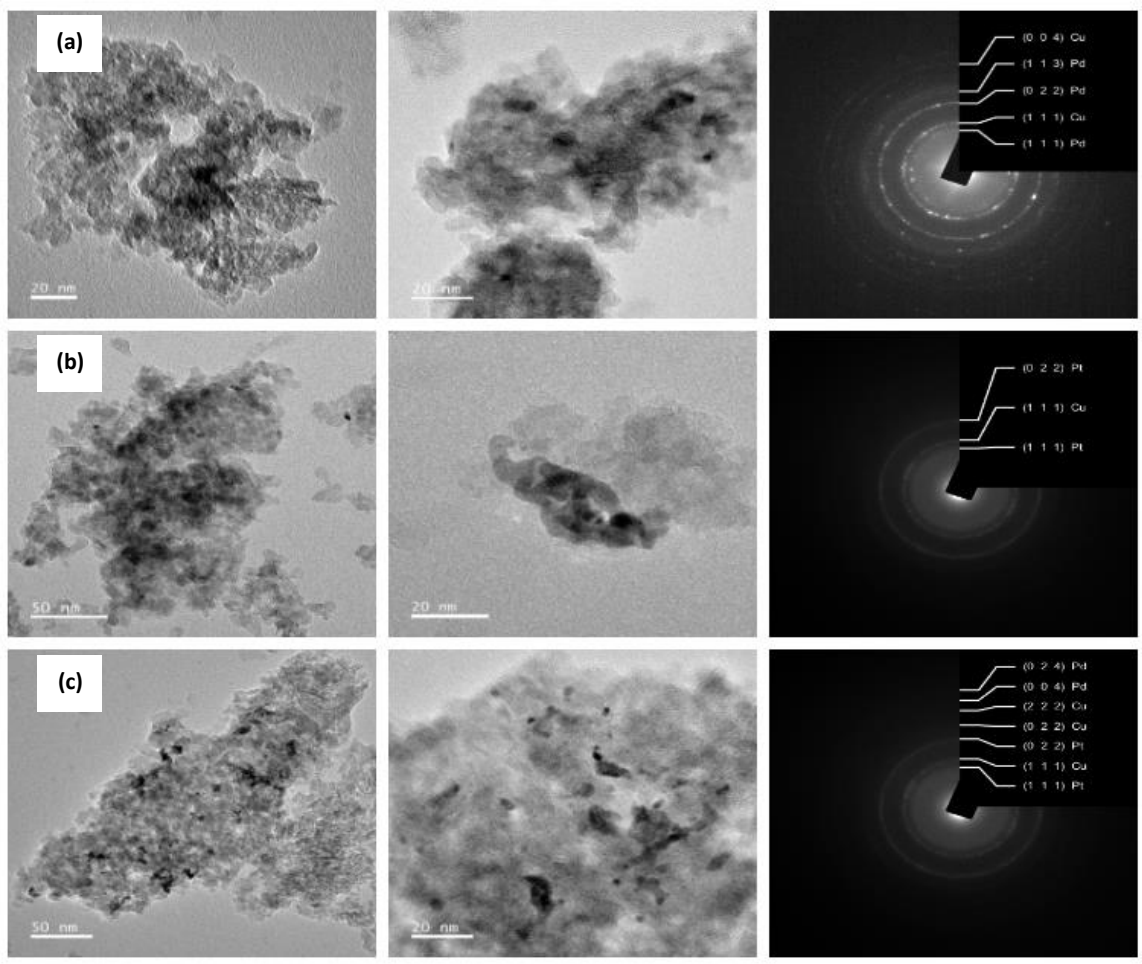

Figure 6.22. HRTEM images and corresponding SAED patterns of (a) PdCu/Al, (b) PtCu/Al and (c) PdPtCu/Al catalysts.

Figure 6.23a illustrates the n-butane conversion obtained in the temperature range of 100-600 °C over Cu promoted Pt and Pd catalysts prepared by electroless deposition method. It is apparent from the figure that the conversion of n-butane increased with an increase in the reaction temperature for all the catalysts. In the lower temperature range of 100-200 °C, PdCu/Al catalyst exhibited higher conversion than PtCu and PtPdCu catalysts. However, from 300 °C onwards, both the Pt based catalysts PtCu/Al and PdPtCu/Al outperformed PdCu catalyst. The PtCu/Al catalyst exhibited 38.4% butane conversion at 550 °C that increased to 39.6% at 600 °C. While PdPtCu/Al catalyst showed 39.4% conversion at 550 °C which decreased to 38.5% on further raising the temperature to 600 °C. Hence, tri-metallic PdPtCu/Al catalyst exhibited highest conversion at the reaction temperature of 550 °C followed by PtCu/Al (38.4%) and PdCu/Al catalyst (34.3%). However, in comparison to co-deposited bimetallic Pd-Pt/Al catalyst, the addition of Cu to Pd-Pt was inefficient in further enhancing the butane conversion.

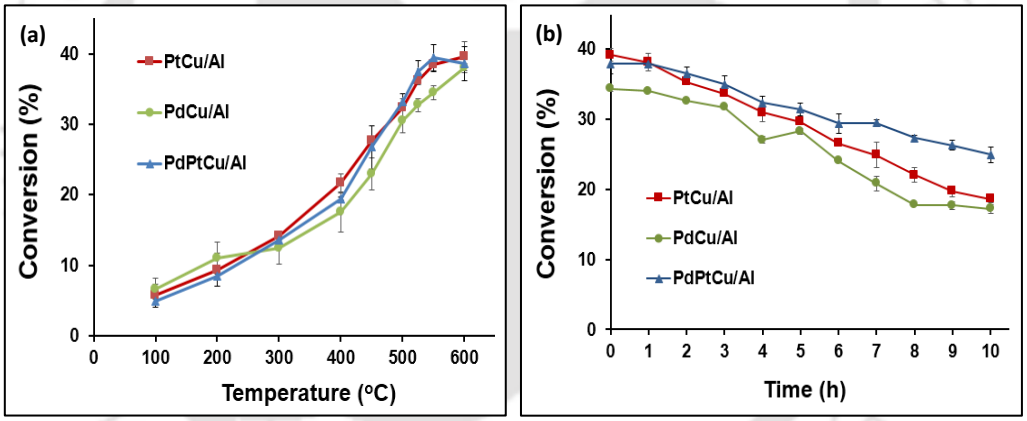

Figure 6.23. (a) Butane conversion profile and (b) stability tests for 10 h process time of Cu promoted monometallic and bimetallic catalysts.

Table 6.13 illustrates the selectivity towards the different products obtained for both Cu promoted Pd and Pt catalysts during n-butane dehydrogenation at 550 °C. The C_1-C_3 products and butenes were the main products obtained. It is evident from the table that the formation of C_1-C_3 products was inhibited to higher extent by Cu addition to PdPt while incorporation of Cu to Pt alone was least effective in suppressing the inhibition towards cracked products. The addition of Cu to bimetallic Pd-Pt catalyst led to an enhancement in the butene selectivity from 85.5 to 88%. It was followed by PdCu/Al (84%) and PtCu/Al (80%). The higher selectivity to butenes in tri-metallic catalyst may be attributed to the

alloying effect of Cu on Pd and Pt. The product distribution showed variation for three catalysts. The selectivity of iso-butenes was highest (16.3%) for PtCu/Al, whereas, PdCu/Al showed more preferable selectivity of 1-butene (17%). The PdPtCu/Al showed the highest selectivity for 1-butene. The selectivity of iso-butene was lowest (9.9%) for this trimetallic catalyst. There was no significant variation in selectivity of cis or trans-2-butene for the three catalysts. The PtCu/Al showed slightly lower value of 27.3% while PdPtCu/Al showed the highest value of 32.3%. All three samples showed cis-2-butene selectivity in the range of 23-24%.

Table 6.13 illustrates the total butene yield at 550 ^{o}C calculated as a product of conversion and selectivity. PtCu/Al catalyst showed a butene yield of ~31%, while, PdCu/Al had the lowest butene yield of 29.1%. The lower yield for Cu promoted Pd catalyst resulted from its lower conversion in spite of having higher butene selectivity than that of PtCu/Al. The highest percentage yield of butene (35.1%) was obtained for Cu promoted PdPt catalyst that resulted from high conversion and selectivity. The order of yield of butene obtained at 550 ^{o}C was PdPtCu/Al (35.1%) > PtCu/Al (30.9%) > PdCu/Al (29.1%). These yield values are considerably higher than that of monometallic Pt/Al (15.1%) and Pd/Al (16.2%) catalysts, which are discussed in chapter 2.

Table 6.13. Catalytic performance of Cu promoted monometallic and bimetallic catalysts for n-butane dehydrogenation [reaction temp. = 550 °C, gas ratio (n-butane:hydrogen:nitrogen) = 1:3:6].

Catalysts	Conversion (%)	Selectivity (%)						Yield (%)
		Iso-butene	1-butene	T-2-butene	Cis-2-butene	Total butenes	C_1-C_3	
PtCu/Al	38.4	16.3	12.6	27.3	24.4	80.6	19.4	30.9
PdCu/Al	34.3	12.3	17.1	31.9	23.7	85.0	15.0	29.1
PdPtCu/Al	39.9	9.9	21.7	32.3	24.0	87.9	12.1	35.1

The stability of these catalysts was then studied for butane dehydrogenation reactions for a process time of 10 h at 550 °C. Figure 6.23b shows the conversion of butane over Cu promoted Pd and Pt catalysts for a process time of 10 h. All the catalysts experienced a gradual deactivation over a process time of 10 h. The incorporation of Cu in bimetallic PdPt catalyst was observed to be most effective in enhancing the catalyst stability. PtCu/Al, PdCu/Al and PdPtCu/Al catalyst exhibited initial conversions of 39.2, 34.4 and 38% that

dropped to 18.6, 17.3 and 24.9, respectively, after 10 h. This corresponded to highest deactivation of 53% for PtCu catalyst followed by 50% deactivation for PdCu catalyst. In comparison, the time on stream activity was much steady for PdPtCu catalyst showing only 34% deactivation after 10 h. The deactivation behaviour can be correlated to product selectivity pattern of the catalysts. The PdPtCu catalyst exhibited least selectivity towards cracked product formation and experienced least deactivation. The PtCu/Al catalyst, with highest selectivity for C_1-C_3, was most deactivated during 10 h time on stream study. As discussed in earlier sections, higher selectivity for C_1-C_3 products causes higher coke formation tendency.

6.4 Summary

The alumina supported Pd and Pt based bimetallic catalysts were prepared by modified electroless deposition (ED) method and evaluated for performance for butane dehydrogenation reaction. The bimetallic Pd-Pt catalysts exhibited superior performance compared to that of either Pd or Pt based monometallic catalysts. The superior performance may be attributed to strong synergistic interaction between metals, stronger metal-support interaction and lower acidity of catalysts. The higher activity of alloyed Pd-Pt metal resulted in higher conversion for bimetallic catalysts. The lower acidity resulted in higher butene selectivity and stability for bimetallic catalysts by minimizing the cracking and secondary reactions. The metal deposition order of bimetallic catalysts also affected their performance. The co-deposited catalyst with more uniform distribution of Pd and Pt metals showed better performance than that of bimetallic catalysts prepared by sequential method. The co-deposited Pd-Pt/Al catalyst showed the highest butane conversion of 50% at 600 °C and maintained a high stability with only 15% deactivation after reaction time of 10 h. The same catalyst showed highest butene yield (~42%). Further, the analysis of spent Pd-Pt/Al catalyst showed that physical and electronic structure of the co-deposited bimetallic catalyst was mostly stable with very small modification by reaction condition. The coke deposition was also negligible. The activation energy was estimated to be 103 kJ/mol for butane dehydrogenation reaction over best performing Pd-Pt/Al catalyst.

The addition of surfactant did not show a considerable impact on the activity of co-deposited Pd-Pt/Al catalyst. However, it led to a significant enhancement in butene selectivity to 97.7% from 85% obtained over Pd-Pt/Al catalyst prepared without surfactant.

Also, incorporation of Cu to Pt/Al catalyst significantly increased butane conversion to 38.4% but with a drop in butene selectivity in comparison to Cu promoted Pd/Al catalyst. The addition of Cu to monometallic Pt/Al and Pd/Al as well as to bimetallic Pd-Pt led to a significant enhancement in butene yield. The order of yield of butene obtained at 550 ^{o}C was PdPtCu/Al (35.1%) > PtCu/Al (30.9%) > PdCu/Al (29.1%) > Pd/Al (16.2%) > Pt/Al (15.1%) catalysts. However, compared to Pd-Pt/Al catalyst, the improvement was observed only in terms of butene selectivity.

References

[1] L. Feng, F. Si, S. Yao, W. Cai, W. Xing, C. Liu, Effect of deposition sequences on electrocatalytic properties of PtPd/C catalysts for formic acid electrooxidation, Catal. Commun. 12 (2011) 772-775.

[2] F. Cai, D. Gao, R. Si, Y. Ye, T. He, S. Miao, G. Wang, X. Bao, Effect of metal deposition sequence in carbon-supported Pd-Pt catalysts on activity towards CO_2 electroreduction to formate, Electrochem. Commun. 76 (2017) 1-5.

[3] A.S. Al-Awadi, A.M. El-Toni, M. Alhoshan, A. Khan, J.P. Labis, A. Al-Fatesh, A.E. Abasaeed, S.M. Al-Zahrani, Impact of precursor sequence of addition for one-pot synthesis of Cr-MCM-41 catalyst nanoparticles to enhance ethane oxidative dehydrogenation with carbon dioxide, Ceram. Int. 45 (2019) 1125-1134.

[4] J. Jing, Z. Yang, J. Huo, H. Bai, W. Li, Metal precursor impregnation sequence effect on the structure and performance of Ni-Co/MgO catalyst, Int. J. Hydrog. Energy 44 (2019) 8089-8098.

[5] L. Čapek, J. Adam, T. Grygar, R. Bulánek, L. Vradman, G. Košová-Kučerová, P. Čičmanec, P. Knotek, Oxidative dehydrogenation of ethane over vanadium supported on mesoporous materials of M41S family, Appl. Catal. A Gen. 342 (2008) 99–106.

[6] K. Pattamakomsan, E. Ehret, F. Morfin, P. Gélin, Y. Jugnet, S. Prakash, J.C. Bertolini, J. Panpranot, F.J.C.S. Aires, Selective hydrogenation of 1,3-butadiene over Pd and Pd-Sn catalysts supported on different phases of alumina, Catal. Today. 164 (2011) 28–33.

[7] S.C. Purdy, P. Ghanekar, G. Mitchell, A.J. Kropf, D.Y. Zemlyanov, Y. Ren, F. Ribeiro, W.N. Delgass, J. Greeley, J.T. Miller, Origin of Electronic Modification of Platinum in a Pt3V Alloy and Its Consequences for Propane Dehydrogenation Catalysis, ACS Appl. Energy Mater. 3 (2020) 1410–1422.

[8] S. Bhogeswararao, D. Srinivas, Catalytic conversion of furfural to industrial chemicals over supported Pt and Pd catalysts, J. Catal. 327 (2015) 65–77.

[9] S.R. de Miguel, I.M.J. Vilella, P. Zgolicz, S.A. Bocanegra, Bimetallic catalysts supported on novel spherical $MgAl_2O_4$-coated supports for dehydrogenation processes, Appl. Catal. A Gen. 567 (2018) 36–44.

[10] V. V. Krishnan, V. V. Krishnan, A.N. Bhaskarwar, B. Bhargava, D. Parvatalu, S. Banerjee, Catalytic performance of bimetallic Ni-Pt nanoparticles supported on activated carbon, gamma-alumina, zirconia, and ceria for hydrogen production in sulfur-iodine thermochemical cycle, Int. J. Hydrogen Energy. 41 (2016) 10538–10546.

[11] B.M. Nagaraja, H. Jung, D.R. Yang, K.D. Jung, Effect of potassium addition on bimetallic PtSn supported θ-Al_2O_3 catalyst for n-butane dehydrogenation to olefins, Catal. Today. 232 (2014) 40–52.

[12] M. Skotak, Z. Karpiński, C_6-alkane conversion over γ-alumina supported palladium and platinum catalysts, Chem. Eng. J. 90 (2002) 89–96.

[13] J. Gascón, C. Téllez, J. Herguido, M. Menéndez, Propane dehydrogenation over a Cr_2O_3/Al_2O_3 catalyst: Transient kinetic modeling of propene and coke formation, Appl. Catal. A Gen. 248 (2003) 105–116.

[14] Q. Zhu, G. Wang, H. Zhang, X. Zhu, C. Li, n-Butane dehydrogenation over Ni-Sn/SiO_2: Adsorption modes and reaction paths of n-butane and 1-butene, Appl. Catal. A Gen. 566 (2018) 113–120.

[15] T. Srisakwattana, K. Suriye, P. Praserthdam, J. Panpranot, Preparation of aluminum magnesium oxide by different methods for use as PtSn catalyst supports in propane dehydrogenation, Catal. Today. 358 (2020) 90–99.

[16] F. Jiang, L. Zeng, S. Li, G. Liu, S. Wang, J. Gong, Propane Dehydrogenation over Pt/TiO_2-Al_2O_3 Catalysts, ACS Catal. 5 (2015) 438–447.
[17] S.B. Kogan, H. Schramm, M. Herskowitz, Dehydrogenation of propane on modified Pt/θ-alumina performance in hydogen and steam environment, Appl. Catal. A Gen 208 (2001) 185-191.
[18] J. Wu, Z. Peng, P. Sun, A.T. Bell, n-Butane dehydrogenation over Pt/Mg(In)(Al)O, Appl. Catal. A Gen 470 (2014) 208-214.
[19] G. Siddiqi, P. Sun, V. Galvita, A.T. Bell, Catalyst performance of novel Pt/Mg(Ga)(Al)O catalysts for alkane dehydrogenation, J. Catal. 274 (2010) 200-206.
[20] K.E. Curry, L.T. Thompson, Carbon-hydrogen bond activation over tungsten carbide catalysts, Catal. Today 21 (1994) 171-184.
[21] P. Natarajan, H.A. Khan, S. Yoon, K.D. Jung, One-pot synthesis of Pt–Sn bimetallic mesoporous alumina catalysts with worm-like pore structure for n-butane dehydrogenation, J. Ind. Eng. Chem. 63 (2018) 380–390.

Chapter 6

Chapter 7

CONCLUSIONS AND RECOMMENDATIONS

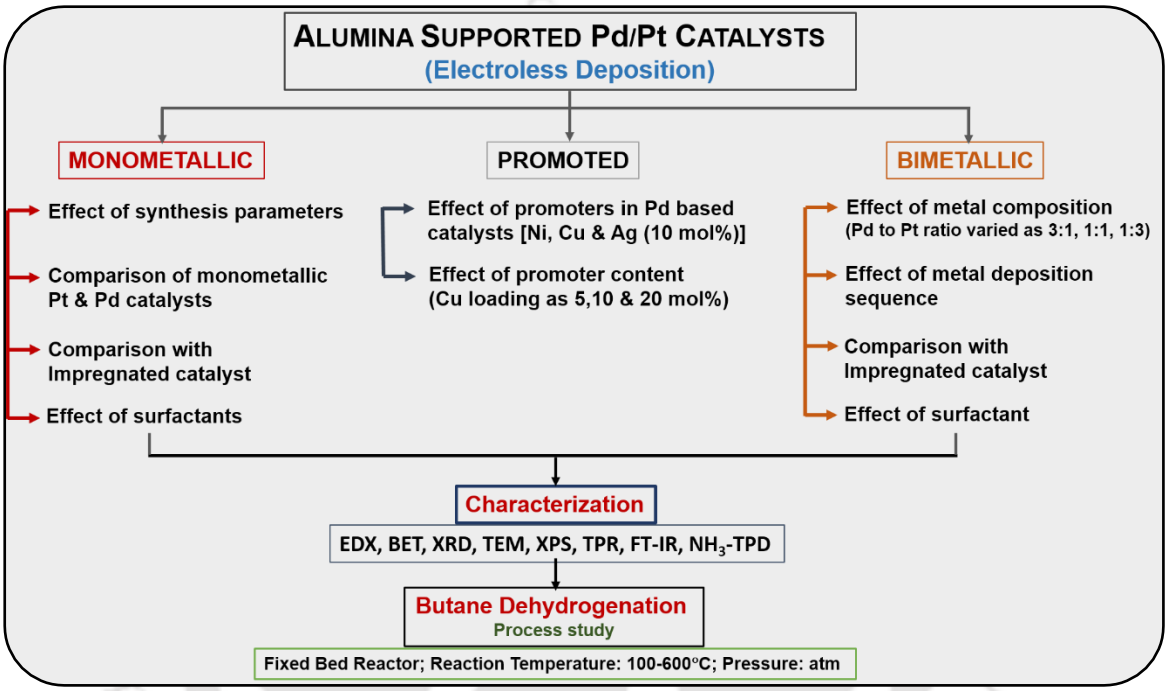

This chapter summarizes the major findings of the study and suggests recommendations for follow up work.

Chapter 7

7.1 Conclusions

In this work, the alumina supported palladium and platinum based catalysts were prepared by electroless deposition method and their physicochemical properties and catalytic performance for butane dehydrogenation were investigated. The effects of synthesis parameters as well as addition of surfactants and promoters were studied for monometallic catalysts. For alumina supported palladium and platinum bimetallic catalysts, the effects of composition and sequence of addition of metals, process parameters, addition of promoter and surfactant, were also investigated. The physicochemical properties and dehydrogenation performance for catalysts prepared by electroless deposition was compared with that prepared by conventional impregnation. The major findings of the study are discussed below.

1. The modified electroless deposition method was successfully employed for the preparation of highly dispersed alumina supported platinum and palladium based catalysts. The preparation parameters, such as metal precursor concentration, reducing agent concentration, reducing agent type etc., had significant effect not only on the metal loading but also on metal cluster size and hence on metal dispersion. The platinum loading and average metal cluster size increased with the increase in metal precursor concentration. The use of 50% excess reducing agent was observed to be sufficient to facilitate reduction as well as considerable metal deposition. It was also observed that it was advantageous to introduce reducing agent prior to the metal solution to alumina support. The average metal cluster size was higher on depositing platinum prior to hydrazine. The use of hydrazine as reducing agent gave higher metal deposition but lower metal cluster size compared to when formaldehyde was used as the reducing agent.

2. On comparing monometallic catalysts, it was observed that at lower temperature range alumina supported platinum catalyst, Pt/Al, showed the higher activity while, alumina supported palladium catalyst, Pd/Al, was more active at temperature above 550 ^{o}C. The overall conversion trend obtained at 550 °C was Pt/Al (18.4%) > Pd/Al (17.9%) > Pt/Al_WI (14.4%) > Pd/Al_WI (13.6%). The catalysts prepared by impregnation showed lower conversion. The higher activity of Pt/Al catalyst may be explained by its higher metal dispersion. The Pd/Al exhibited higher selectivity towards overall butene formation (>90%) compared to Pt/Al (82%). In comparison to deposited catalysts, impregnated catalysts exhibited higher selectivity (40-50 %) towards cracked product formation leading

to their faster deactivation. The percent deactivation order was Pd/Al (74%) < Pt/Al (75%) < Pd/Al_WI (79.5%) < Pt/Al_WI (81%). The preferential formation of cracked products at higher temperature might have caused greater deactivation of Pt/Al catalysts.

3. The effect of surfactant addition was investigated with alumina supported palladium catalyst, exhibiting almost similar activity to that of alumina supported platinum catalyst and with higher butene selectivity and stability. Both anionic (SDS) and non-ionic (Tween-20) surfactant were observed to be effective. Surfactant-assisted electroless deposition method facilitated the lowering of palladium cluster size to 1.2 nm from 4.6 nm and 11.9 nm obtained by deposition and impregnation method, respectively. The conversion and butene selectivity were observed to be function of deposited palladium cluster size. The catalyst, prepared in presence of anionic SDS surfactant with the highest metal dispersion and lowest metal size (1.2 nm), showed the best catalytic performance with a conversion of 33% and 99.7% selectivity towards butenes. It was followed by catalyst prepared in presence of non-ionic Tween 20 surfactant, showing 25% conversion and over 99% butene selectivity. The catalyst prepared by impregnation with the highest metal particle size (11.89 nm) exhibited the least activity and selectivity for butene.

4. The efficiency of alumina supported palladium catalyst was modified by addition of Ni, Cu and Ag as promoter. The co-deposition of copper or silver with palladium increased activity and yield of butene. The copper promoted sample showed highest conversion of 34% at 550 °C that further increased to 38% on increasing the temperature to 600 °C. The silver promoted catalyst possessed highest selectivity towards butenes (>90% at 550 °C). The order of yield of butene was Pd-Cu/Al (29%) > Pd-Ag/Al (23%) > Pd/Al (16%) > Pd-Ni/Al (13%) at 550 °C. Further increase in copper content increased yield of butene and highest yield of 32% was observed for Pd-Cu_{20}/Al with 20 mol% copper. The palladium metal was in strong interaction with the promoter metals forming alloys. Higher activity of these alloys enhanced performance of the promoted catalysts. The sintering tendency of nickel lowered the performance of Pd-Ni/Al. The addition of promoters also led to enhancement in stability of the catalysts. The stability order was Pd-Ag/Al (27%) > Pd-Cu/Al (34%) > Pd-Ni/Al (61%) > Pd/Al (76%).

5. The variation in metal composition in alumina supported palladium and platinum bimetallic catalysts affected the physiochemical properties and thereby their catalytic performance. Catalysts with higher palladium content exhibited lower acidity while higher

platinum content led to improved metal dispersion. The deposited bimetallic catalysts, $1Pd1Pt_{ED}$, having equimolar palladium and platinum showed the highest butane conversion of 48.5% and butene yield of 42% at 550 °C. The same catalyst was also most stable showing only 15% deactivation after reaction time of 10 h. The $3Pd1Pt_{ED}$ catalyst with higher palladium content showed higher butene selectivity (91%) and stability (17% deactivation) in comparison to $1Pd3Pt_{ED}$ catalyst with higher platinum content (84.7 % butene selectivity; 34% deactivation). The $3Pd1Pt_{ED}$ catalyst, having less acidic sites, suppressed C-C cleavage. The catalysts prepared by electroless deposition method gave higher product yield and stability, compared to that prepared by conventional impregnation method. The overall order for butene yield was $1Pd1Pt_{ED}$ (42%) > $1Pd3Pt_{ED}$ (41%) > $3Pd1Pt_{ED}$ (40.3%) > $3Pd1Pt_{WI}$ (18.7%) > $1Pd3Pt_{WI}$ (18.4%) > $1Pd1Pt_{WI}$ (15.8%).

6. The physicochemical properties and catalytic performance of alumina supported bimetallic palladium and platinum catalyst was also affected by sequence of metal deposition. The co-deposited catalyst with more uniform distribution of palladium and platinum metals showed better performance than that of bimetallic catalysts prepared by sequential deposition. The co-deposited Pd-Pt/Al catalyst showed the highest butane conversion of 50% at 600 °C and butene yield (~42%). The addition of surfactant to co-deposited Pd-Pt/Al catalyst improved butene selectivity to 97.7% from 85% obtained for bimetallic catalyst prepared without surfactant. The addition of copper to monometallic and bimetallic catalysts led to significant enhancement in butene yield. The apparent activation energy for butane dehydrogenation was 103 kJ/mol over co-deposited bimetallic catalyst.

7.2 Recommendations for future work

In continuation to present studies, few other areas can also be explored. The effect of total metal loading and different supports can also be explored. The effect of surfactant modification can be further investigated on promoted Pd catalysts. In-situ study of the dehydrogenation reaction on active sites can be performed to gain better insights to the underlying mechanisms. Detail kinetic study for the bimetallic catalyst can be done. Furthermore, the application of electroless deposition method can be investigated for other catalytic systems as well.

APPENDICES

Appendix A: Mass transfer effects

The effect of external mass transfer in dehydrogenation reactions was investigated with a catalyst loading of 0.25 g by varying the total flow rate from 20 to 120 mL min^{-1}. Figure A1a shows the effect of variation of feed flow rate on butane conversion at different temperatures. At lower reaction temperatures of 100 and 150 °C, the butane conversion kept increasing until 100 mL min^{-1} but became constant thereafter. However, at higher reaction temperature, the butane conversion of 48% was achieved at a feed flow rate of 80 mL min^{-1} that did not change significantly with further increment in flow rate. The results suggested that at all temperature studied, the effect of external mass transfer was negligible at total flow rate of 100 mL min^{-1}. All the catalytic performance was measured at total flow rate of 100 mL min^{-1} ensuring that all the observations were only due to surface kinetics. Internal mass transfer was considered to be negligible since the catalyst was used in a powder form in all the dehydrogenation experiments.

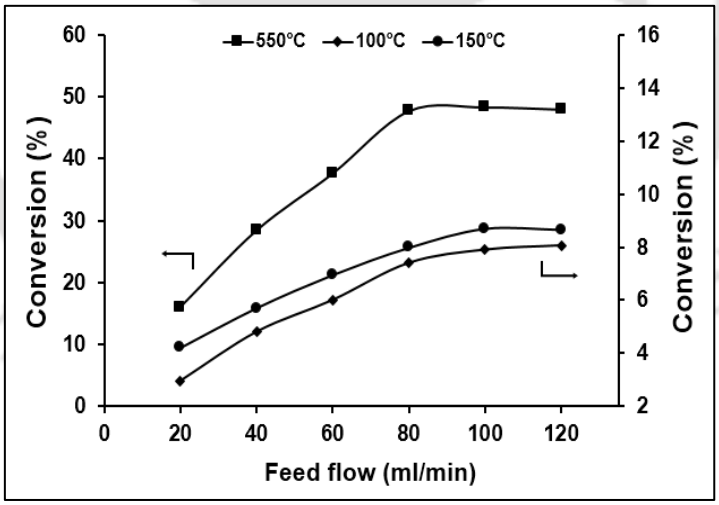

Figure A1. Butane conversion over Pd-Pt/Al catalyst at different feed flow rates. Reaction conditions: pressure = 1 atm, C_4H_{10}:H_2:N_2 = 1:3:6, catalyst mass (W) = 0.25 g.

Appendix B: Experimental setup and procedure

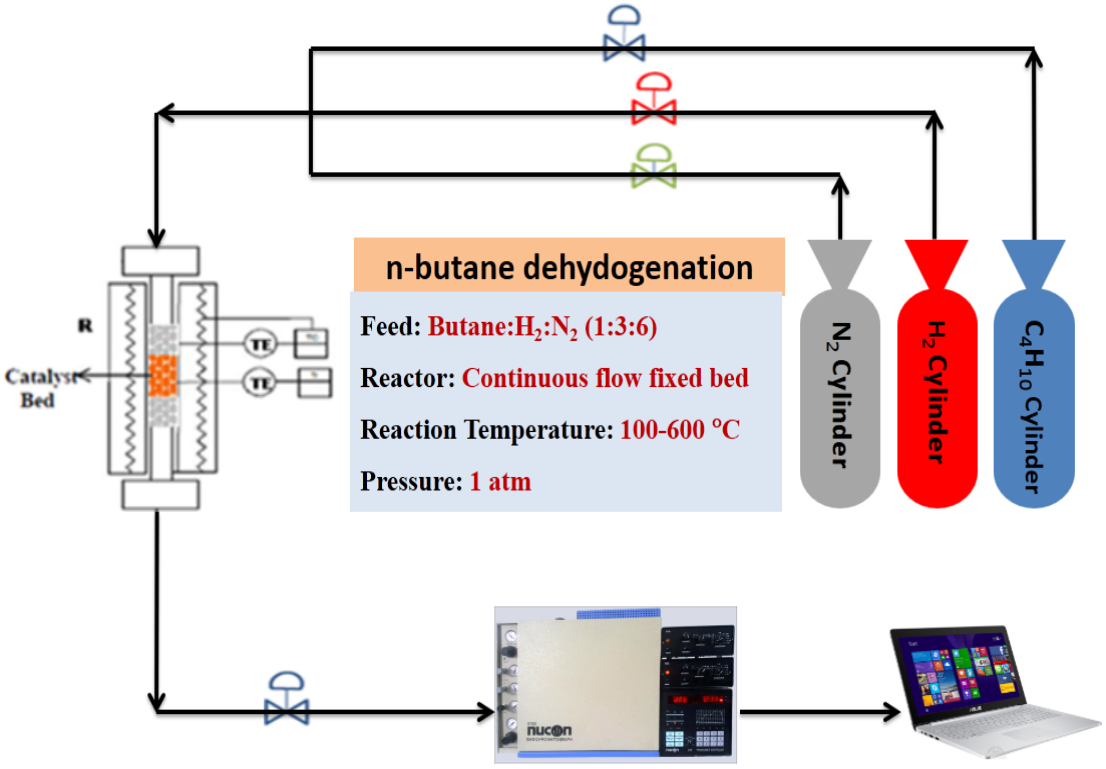

Figure A2: Schematic of experimental setup used for conducting butane dehydrogenation.

The feed composition was decided by optimizing the required flow of butane and hydrogen gas. The butane flow was varied in the range from 2 to 14 mL min^{-1} and was fixed at 10 mL min^{-1}. This ensured enough product formation with coke formation being tolerable. Then, the hydrogen gas was fed in the ratio of 1:1, 1:2, 1:3 and 1:4 to further study the coke inhibition pattern. The ratio of 1:3 was observed to give minimum coke formation without affecting the butene yield. Hence, the butane and hydrogen flow rate was maintained at 10 and 30 mL min^{-1}, respectively. The total flow rate was maintained at 100 mL min^{-1}, by using inert nitrogen as the balance gas (60 mL min^{-1}), to avoid external mass transfer limitations. This feed gas composition agreed well with that reported in literature for butane dehydrogenation.

For a particular catalyst, temperature was gradually increased and data was collected at a definite temperature interval ranging from 100-600 °C. The time to achieve the steady state was around 8-10 min and total data collection time was approximately 150 min for procuring one data set of each catalyst.

Appendix C: Properties and interaction of surfactants

Table A1. Properties of different surfactants.

Surfactant	Molecular formula	Molecular weight (g/mol)	CMC (mM)	HLB value
SDS	$NaC_{12}H_{25}SO_4$	288.37	8.2	40
TWEEN 20	$C_{58}H_{114}O_{26}$	1,227.54	0.049	16.7
CTAB	$C_{19}H_{42}BrN$	364.45	1	10

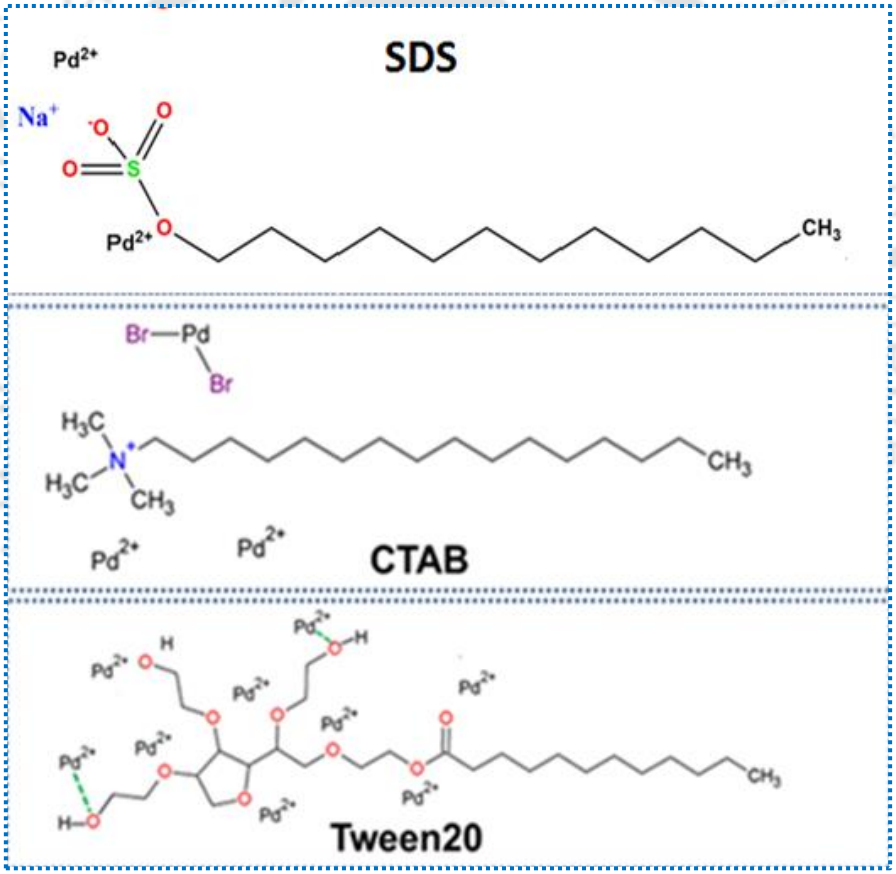

Figure A3. Structure of different surfactants and probable surfactant–palladium cation interactions: For SDS and Tween20, interactions are attractive with positively charged Pd ions but it is repulsive in nature for CTAB.

Appendix D: EDX spectra of different catalysts

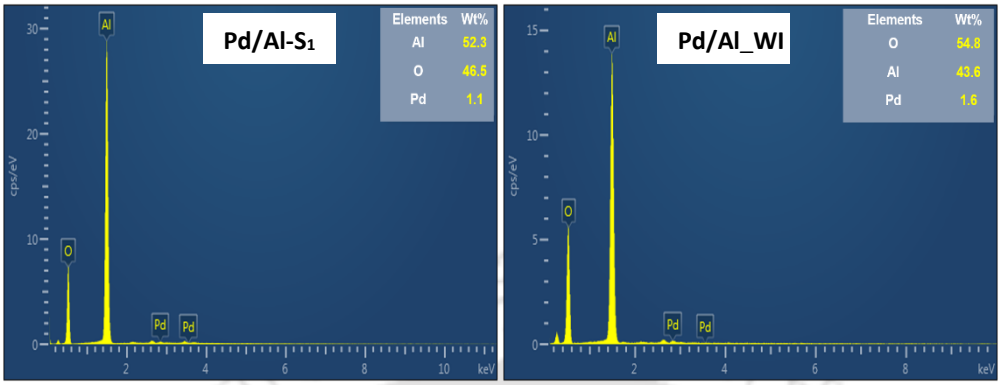

Figure A4. EDX spectra of alumina supported palladium catalysts prepared by (a) SDS surfactant assisted deposition and (b) impregnation.

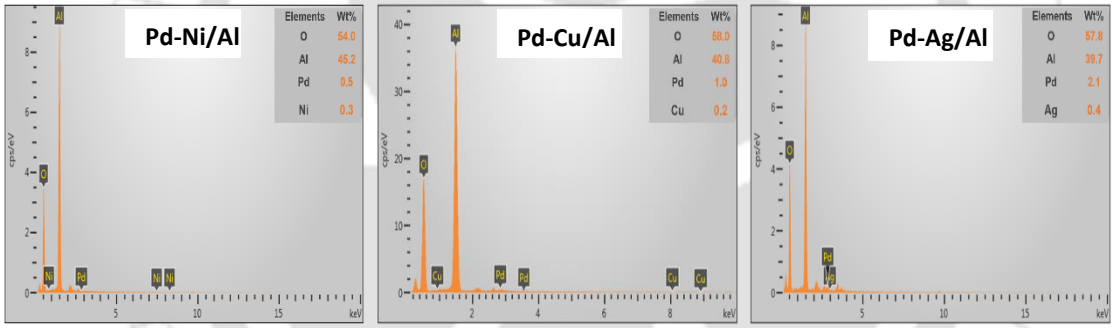

Figure A5. EDX spectra of Ni, Cu and Ag promoted Pd catalysts.

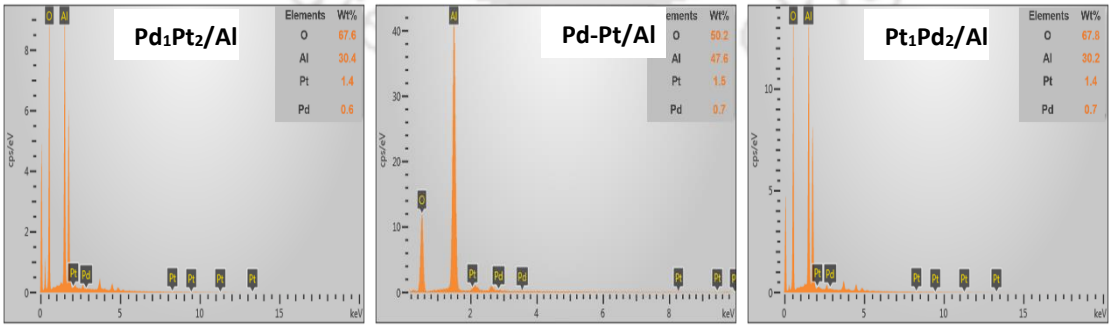

Figure A6. EDX spectra of Pd-Pt bimetallic catalysts prepared by different deposition sequences.

Appendix E: EDX mapping images of different catalysts

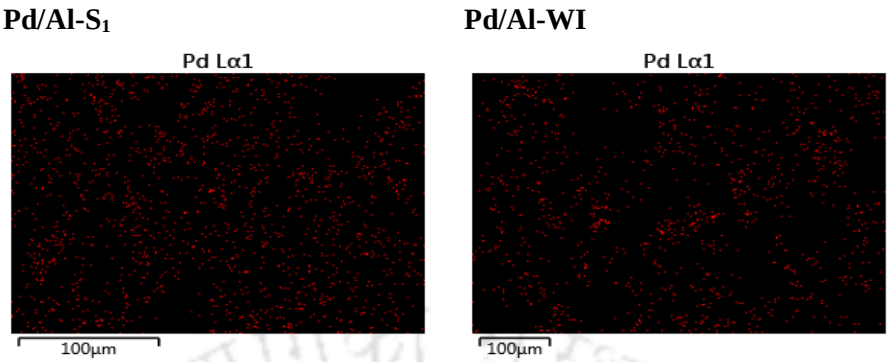

Figure A7. EDX mapping images of alumina supported palladium catalysts prepared by (a) SDS surfactant assisted deposition and (b) impregnation.

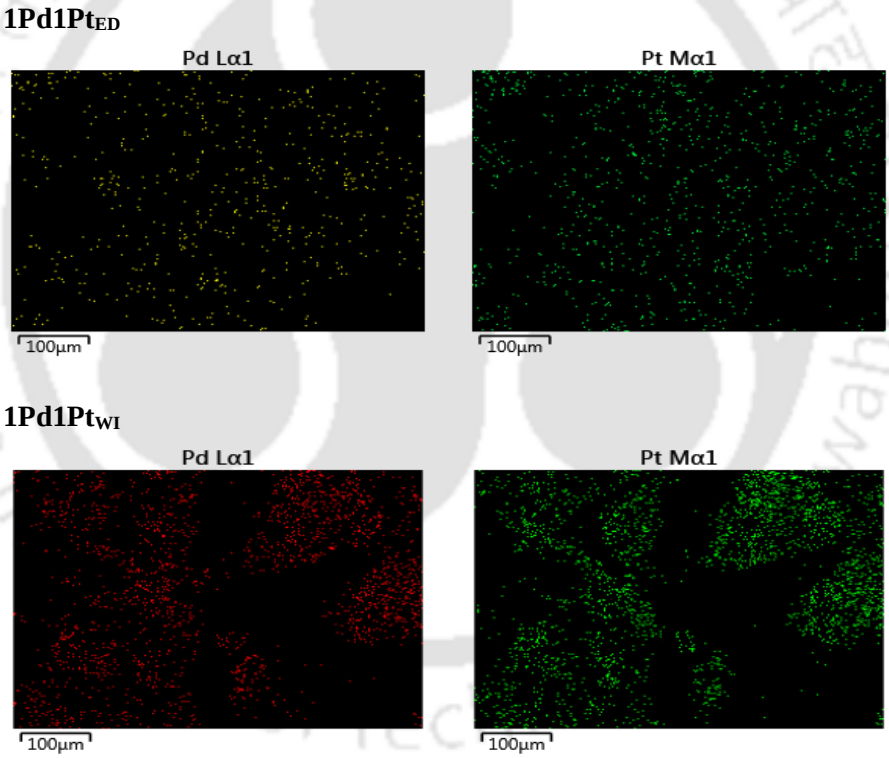

Figure A8. EDX mapping images of Pd-Pt bimetallic catalysts prepared by co-deposition and co-impregnation.

Appendix F: Product Chromatogram

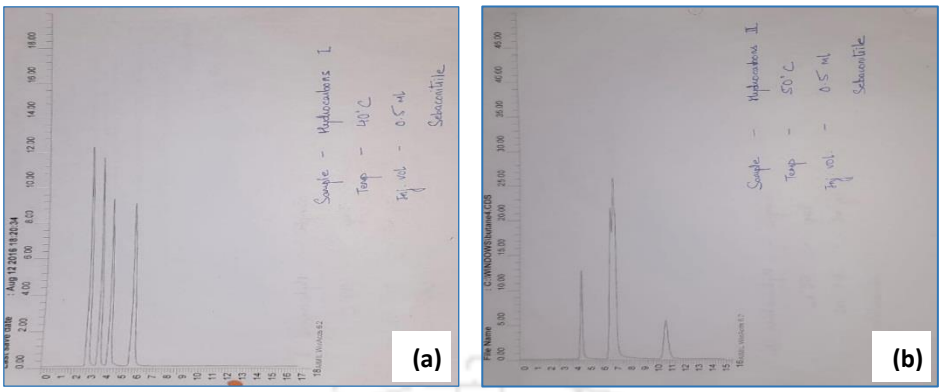

Figure A9. Chromatogram obtained for calibration gas mixtures (a) Hydrocarbon mixture I containing ethane (5.2%), ethylene (5.17%), propane (5.12%) and propylene (5.2%) in sequence from left to right; (b) Hydrocarbon mixture II containing iso-butane (4.91%), 1-butene (9.85%), iso-butene (14.33%) and 1,3-butadiene (4.91%) in sequence from left to right.

Appendix G: Distribution of C_1-C_3 products

Table A2. C_1-C_3 products selectivity obtained at 550 °C for different catalysts.

Catalysts	Selectivity (%)				
	Methane	Ethane	Ethylene	Propane	Propylene
Pt/Al	4.0	1.9	2.7	3.1	6.0
Pd/Al	4.5	1.1	0.9	0.8	2.2
Pt/Al_WI	16.2	2.7	2.9	6.3	21.4
Pd/Al_WI	25.1	5.8	2.9	1.7	8.2
Pd/Al-S_1	0.3	--	--	--	0.1
Pd/Al-T_1	0.4	0.2	--	--	0.1
Pd-Ni/Al	7.8	7.4	8.1	4.6	10.7
Pd-Cu/Al	5.6	2.3	--	3.5	3.6
Pd-Ag/Al	2.6	0.7	1.2	2.2	1.4
Ni/Al	9.7	8.9	10.3	7.4	13.0
Cu/Al	7.6	11.6	--	23.6	4.6
Ag/Al	8.1	5.6	4.3	7.6	4.1
$3Pd1Pt_{ED}$	3.3	1.2	0.7	0.9	2.8
$1Pd1Pt_{ED}$	3.2	2.8	1.2	2.0	5.3
$1Pd3Pt_{ED}$	5.4	0.9	1.2	1.6	6.2
$3Pd1Pt_{WI}$	17.4	4.6	2.8	2.1	11.3
$1Pd1Pt_{WI}$	19.0	6.1	5.4	6.6	8.6
$1Pd3Pt_{WI}$	14.4	3.1	4.2	5.7	20.5
Pt_1Pd_2/Al	2	2.3	1.7	1.2	5.2
Pd_1Pt_2/Al	4.4	2.8	3.3	3.7	5.5
Pd-Pt/Al	3.2	2.8	1.2	2.0	5.3
Pd-Pt-T20	1.8	0.7	--	0.4	0.8
PdPtCu/Al	5.3	1.5	0.2	0.5	4.6

Appendix H: Thermogravimetric plots of spent catalysts

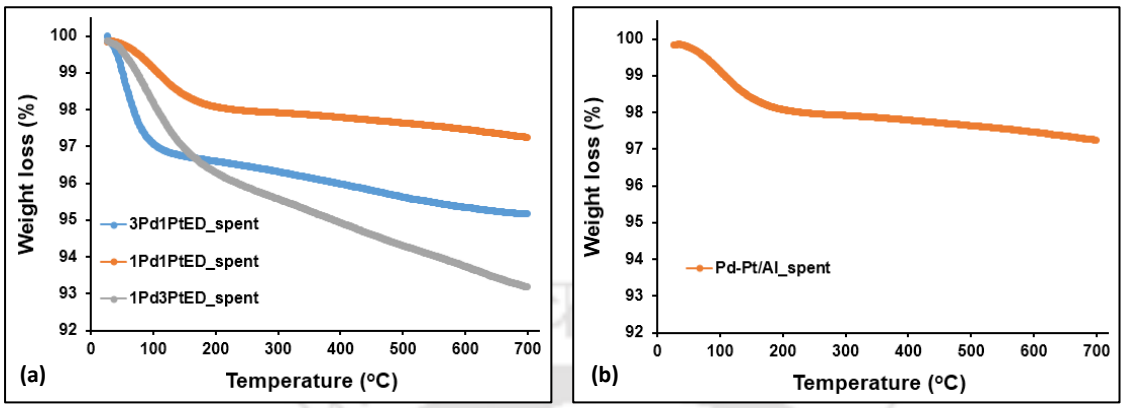

Figure A10. Thermogravimetric plots of (a) spent bimetallic catalysts prepared by deposition method with different Pd-Pt compositions; (b) Pd-Pt/Al_spent catalyst.